Conversion of Cellulosic Biomass into Chemicals using Heterogeneous and Electrochemical Catalysis

vorgelegt von

MS (Research) in Chemical Engineering

Koteswara Rao Vuyyuru

aus Andhra Pradesh (Indien)

Von der Fakultät II –Mathematik und Naturwissenschaften

der Technischen Universität Berlin

zur Erlangung des akademischen Grades

Doktor der Ingenieurwissenschaften

Dr. Ing.

genehmigte Dissertation

Promotionsausschuss:

Vorsitzender: Prof. Dr. Arne Thomas

Berichter: Prof. Dr. Peter Strasser

Berichter: Prof. Dr. Robert Schlögl

Tag der wissenschaftlichen Aussprache: 27. November 2012

Berlin 2012

D83

Zusammenfassung

Regenerative Elektrizität aus Wind und Sonne einerseits und Biomasse andererseits sind 2 fundamentale Grundpfeiler einer zukünftigen nachhaltigen Versorgung mit Energie und Chemikalien. Diese beiden Bereiche existieren und entwickeln sich im Moment weitgehend unabhängig voneinander. Diese Dissertation unternimmt den konzeptionellen Versuch, durch eine Untersuchung der elektrochemischen Umwandlung von Biomasse und einem Vergleich zu herkömmlichen thermisch katalysierten Prozessen diese beiden Technologiebereiche naeher zusammen zu rücken. Uebergeordnetes Ziel der Arbeit ist ein Verstaendnis dafuer zu entwickeln, inwieweit sich anhand eines ausgewaehlten Modellreaktionssystem zwischen der elektrochemischen Katalyse, also durch elektrisches Potential aktivierte Oberflaechenprozesse, und der heterogenen chemischen Fluessigphasenkatalysen, die durch thermische Aktivierung kontrollierbar ist, Gemeinsamkeiten und Unterschiede in ihrem jeweiligen Zusammenhang von Reaktivitaet/Selektivitaet und externen Kontrollparametern identifizieren lassen.

Die Arbeit präsentiert einen Vergleich von chemisch und elektrochemisch katalysierten Oxidationen und Reduktionsprozessen eines der wichtigsten Plattformmolekülen, des 5-Hydroxymethylfurfurals. Die Arbeit widmet sich darüberhinaus auch seiner katalytischen Herstellung aus Fruktose.

Zunächst beschäftigt sich diese Arbeit mit der Flüssigphasen säurekatalysierten Dehydratation von Fruktose zu HMF. Dazu wurde die katalytische Aktivitaet verschiedenster fester Saeuren untersucht und zu der Aktivitaet von konventionellen Mineralsaeuren und Loesungsmittel in Beziehunggesetzt; insbesondere wurden polymere Ionenaustauschermaterialien sowie auch sulfonierte anorganische Metalloxide (SiO_2, ZrO_4, TiO_2) betrachtet, die durch kovalente Verankerung von Sulfongruppen auf der Oxidoberflaeche hergestellt wurden.

Anschliessend stellt diese Arbeit eine umfangreiche vergleichende Untersuchung der katalytischen Oxidations und Reduktionsverhalten von HMF auf metallischen und metalloxidischen Oberflaechen vor. Die Verwendung von freien Elektronen zur katalytischen Umwandlung von Biomasse ist ein bisher noch nicht bearbeitetes Forschungsfeld. Thermisch- katalytische Studien (heterogene Fluessigphasenkatalyse) zur Aktivitaet und Selektivitaet der HMF oxidation zur Furandicarbonsaeure und ihren Intermediaten werden als erste betrachtet. Dazu werden verschiedene Metallkatalysatoren (Pt, Au, Ru, Rh, Pd) und der Einfluss verschiedener

Kontrollparameter wie pH, Temperatur, Druck untersucht. Danach wird die thermisch chemische Katalyse von HMF zu Dimethylfuran, einem Brennstoffzusatz, in gleicher Weise untersucht.

Schliesslich wird die katalytische Aktivitaet und Selektivitaet derselben Metallkatalysatoren untersucht, wenn sie als Elektroden in einer elektrochemischen Umgebung unter Anlegen eines elektrischen Potentials eingesetzt werden. Diese Reaktionsfuehrung erspart den Einsatz von molekularen Sauerstoff oder Wasserstoff als Reaktanten, da Teilreaktionen der Wasserspaltung in waessrigen Loesungen co-katalysiert werden. Ausserdem existieren 2 zusaetzlich Kontrollparameter, die fliessende Elektrische Stromdichte sowie das angelegte Elektrodenpotential. Es wurde untersucht, inwieweit sich diese einfach einzustellenden Kontrollparameter auch im Zusammenspiel mit anderen konventrionellen Reaktionsparametern wie pH oder Temperatur zur Steuerung von Aktivitaet und Selektivitaet einsetzten lassen. Tatsaechlich ist die angelegte Stromdichte und ebenso das daraus folgende Elektrodenpotential sehr gut geeignet, die Selektivitaet der entstehenden Oxidations und Reduktionsprodukte zu steuern. Pt und Ni zeigen dabei zum Beispiel exzellente Aktivitaet fuer die kontrollierte Herstellung des Intermediates Furandicarbaldehyd, das sich in der konventionellen thermischen Katalyse nicht einfach stabilisieren laesst. Mit Ni Elektrokatalysatoren laesst sich HMF zu Brennstoffaehnlichen Produktmolekuelen bis hin zum Dimethylfuran reduzieren.

Abstract

Renewable solar/wind electricity and renewable biomass conversion represent two fundamental pillars for a future sustainable supply of energy and chemicals. Both areas are currently developing independently. This thesis investigates ways to bring the two areas together by using electrical energy to convert biomass into chemicals; it offers a comparative perspective of biomass-based chemical processes using heterogeneous and electrochemical catalysis. The key platform molecule of interest here is 5-hydroxymethylfurfural (HMF) obtained from glucose/fructose. This work considers its formation from fructose and its subsequent chemical and electrochemical transformations into oxidized and reduced products.

First, the liquid-phase acid catalyzed dehydration of fructose to HMF is addressed. Sulfonated metal oxides (SiO_2, ZrO_4, TiO_2) are synthesised by covalent anchoring strategies with various sulfonic acid groups. The activities of these novel heterogeneous solid acid catalysts were explored for the dehydration of fructose into HMF. Activity of these catalysts were compared with commercially available solid and liquid acid catalysts.

Subsequently, this thesis addresses the oxidation and reduction of HMF using chemical and electrochemical catalysis. While thermally activated catalytic HMF transformations are intensively investigated and in part well documented, the catalytic activation of HMF conversion reactions using an electrical interfacial potential (electrocatalysis) is new and poorly explored to date. A comparative study of HMF catalysis using thermal heterogeneous and electrocatalysis of HMF in liquid-phase is reported and discussed. Catalytic reactivity/selectivity studies were carried out using aqueous-phase heterogeneous catalysis under mild temperature ($50^{o}C$) and pressure (max. 10 bar) conditions. The catalytic activity of Pt/C catalyst and compared with Au/TiO_2, Ru/C, Rh/C and Pd/C. The important reaction parameters such as influence of pH, effect of pressure and type of catalytic metal surface were explored. HMF degradation mechanism was discussed using *in-situ* NMR study.

Electrochemical catalysis offers the added advantage by providing the electrode potential and the faradaic current as two additional external control parameters. These are helpful to tune the thermodynamic driving force, activation energy and thus the reaction rate and selectivity of complex reaction processes. Activity and selectivity of HMF oxidation and reduction was investigated as function of thermal and electrical

external parameters is reported and compared to the thermally activated conditions. The study suggests that the electrical potential can serve as an effective parameter for controlling the product selectivity in HMF conversion reactions.

Acknowledgements

Table of Contents

Chapter 1   Introduction and Aim of the Research

Chapter 2   Experimental Details and Materials

Chapter 3   Conversion of Lignocellulosic Biomass into HMF

Chapter 4   Heterogeneous Catalytic Oxidation of HMF

Chapter 5   Heterogeneous Catalytic Hydrogenation of HMF

Chapter 6   Electrocatalytic Oxidation of HMF

Chapter 7   Electrocatalytic Reduction of HMF

List of Figures

List of Tables

List of Abbreviations

BHMF	2,5 (bis)hydroxymethylfuran
BHMTHF	2,5 (bis)hydroxymethyltrtrahydrofuran
C	Conversion
CE	Counter electrode
CP	Chronopotentiometry
CV	Cyclic voltammetry
DMA	Dimethylacetamide
DMF	2,5-Dimethylfuran
DMSO	Dimethyl sulfoxide
DMTHF	2,5-Dimethyltrtrahydrofuran
E	Potential
FDC	2,5-Furandicarbaldehye
FDCA	2,5-Furandicarboxylic acid
F_{eff}	Faradaic efficiency
FFCA	5-Formyl furan-2-carboxylic acid
geo.	Geometrical
HMF	5-Hydroxymethyl-2-furfural
HMFC	5- Hydroxymethyl-2-carboxylic acid
LA	Levulinic acid
MF	5-Methylfuran
MPTMS	3-Mercaptopropyl)trimethoxysilane
OCP	Open circuit potential
RE	Reference electrode
RHE	Reversible hydrogen electrode
S	Selectivity
TESAS	(3-((3-(trimethoxysilyl)propyl)thio)-propane-1-sulfonic acid)
V	Voltage
WE	Working electrode
Y	Yield
ΔG_r	Gibbs free energy of reaction

Chapter 1

Introduction and aim of research

1.1 Introduction

Human civilization has started in the 19th century towards the comfort life by converting earth's resources into energy. Resources such as coal, oil and natural gas are being used traditionally to produce electricity, heat, and transportation fuels[3]. Chemistry constantly thrives towards fulfilling new and existing demands from consumers and end users[4]. This has been the case for at least a century, where medicines, pesticides, high-performance materials and many other products have been developed and integrated into our society. A significant industrial revolution stepped into unbelievable and sophisticated life style in terms of transportation, communication and medicine. During the 20th century, the amount of natural resources such as coal and oil were drastically converted into energy[5] (e.g. electricity, heating, transportation fuels) and chemicals (e.g. plastics, pharmaceuticals, basic chemicals). The consumption of different fossil resources are shown in the fig. 1.1
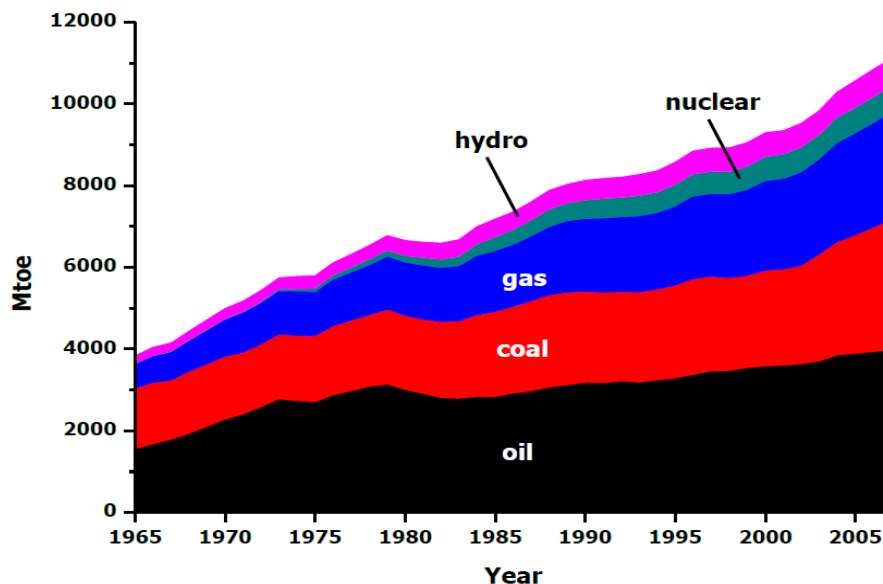
Fig. 1. 1 Development in the global energy consumption measured in million tonnes of oil equivalents (Mtoe). (IEA world energy statistics 2010).

So far, petroleum is the largest source (exceeding coal, natural gas, nuclear, or hydroelectric for energy and chemical needs and consumed about 4.8

barrel/year/person [6, 7]). Crude oil is a product, formed from the various remains of plants and animals that lived and died millions of years ago. Hence, fossil fuels are considered nonrenewable, i.e., they are not replaced as fast as consumed. Crude oil is one of the primary raw materials in the petroleum refining industry to produce many types of chemicals and fuels [8].
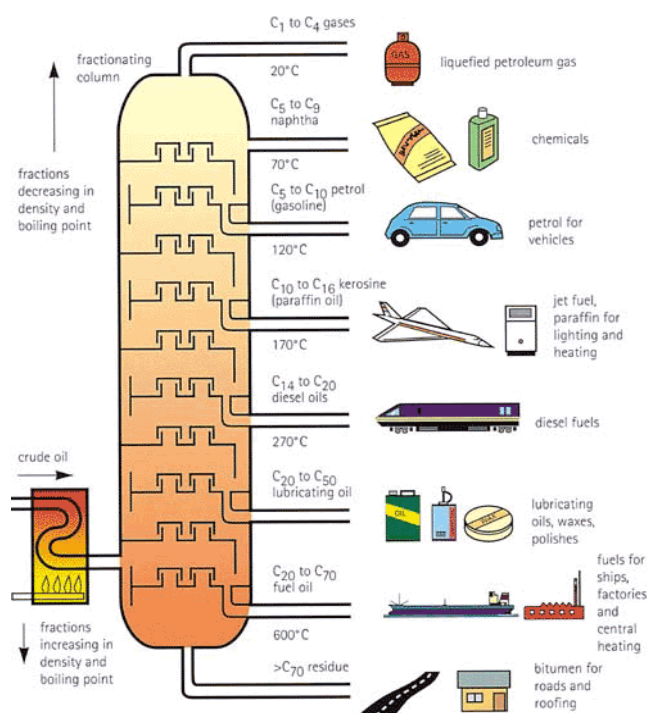
Fig. 1. 2 A variety of products from petroleum refining industry (source: handbook of petroleum refining processes).

Fig. 1. 2 shows the transformation of crude oil into various fuels in a petroleum refinery ranging from C_1-C_{70} hydrocarbons. An important nonfuel use of petroleum is to produce chemical raw materials. The two main classes of petrochemical raw materials are olefins (ethylene and propylene) and aromatics (benzene and xylene), both of which are produced in large quantities. All these molecules contain carbon with different compositions of hydrogen and oxygen [9, 10].

The petroleum reserves can be classified into three categories: proven, probable, and possible reserves. Proven reserves are those fields from which petroleum can be produced using current technology at the current prices. Probable reserves are those fields from which petroleum can be produced using the near-future technology at current prices.
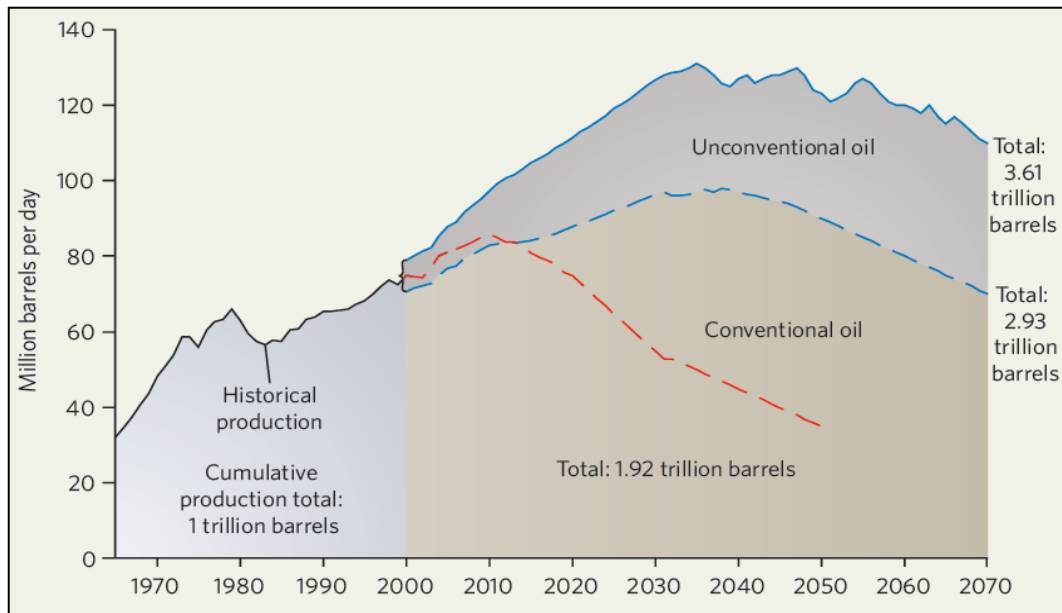
Fig. 1. 3 Crude oil production scenario. Twin peaks: peak-oil supporters think we have already reached or will soon reach a historical maximum of oil production; others argue that oil production will not peak until at least 2030 (adopted Witze, 2007[11]).

As per the present rate of petroleum production, the smaller petroleum reserves are on the verge of depletion, and the larger reserves are estimated to be depleted in less than 50 years. Hence, the world is facing a bleak future of petroleum short supply. Fig 1. 3 illustrates the global crude oil production scenarios based on today's production. According to one estimate, peak in global oil production is likely to occur by 2012, and thereafter the production will start to decline at a rate of several percent per year. By 2030, the global petroleum supply will be dramatically lower, which will create a supply gap that may be hard to fill by growing contributions from other fossil, nuclear, or alternative energy sources in that time frame. However, there are other estimates that the peak production will occur beyond 2030 [11]. The chemical industry will face tremendous challenges in terms of raw material, if present technology not modified [12, 13].

1.2 History of crude oil price

Current industrial economics are mainly dependant on the price of crude oil. As it shown in the fig. 1.2, a variety of chemicals and fuels are delivering only from crude oil.
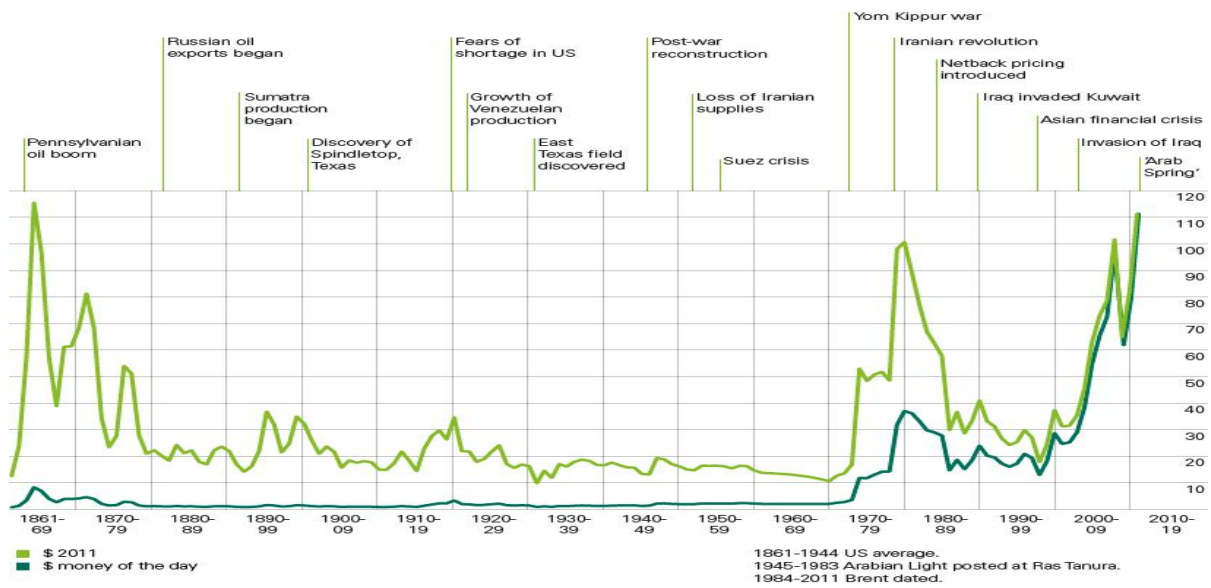
Fig. 1. 4 Historical crude oil prices from 1861 to Present [14].

Fig. 1. 4 presents the history of crude oil price and availability in different countries. The oil price is continuously growing and highly influenced by the demand and supply (both current and perceived future supplies), which in turn are highly dependent on global macroeconomic and political conditions. It is often claimed that OPEC sets a high crude oil price and the true cost of crude oil production is only $2/barrel in the Middle East. The peak crude oil price in 2008 of $145/barrel put a severe strain on many world economies, which in part contributed to the recession that followed. It was already expected that the rate of crude oil even increases to further in the near future due to demand precedes the supply. The economics of chemical industry always fluctuates based on the oil price.

1.3 Effect of unbalanced carbon cycle

Upon combustion of long chain carbon in the liquid form of petroleum with the oxygen, gaseous form of carbon dioxide is released. In fact, these carbon molecules were not existed in the atmosphere but brought from the original source of solid (coal) or liquid (petroleum) on or beneath the earth. Over the past century, human activities have released large amounts of carbon dioxide and other greenhouse gases into the atmosphere by converting fossil fuels. The majority of the greenhouse gases come from burning fossil fuels to produce energy during the industrial processes. Greenhouse gases act like a blanket around the earth, trapping the sun radiation in the

atmosphere and causing it to warm. This phenomenon is called the greenhouse effect and is natural and necessary to support life on earth. However, the buildup of the greenhouse gases can change earth's climate and result in dangerous effects to human health and welfare and to the ecosystems [15].
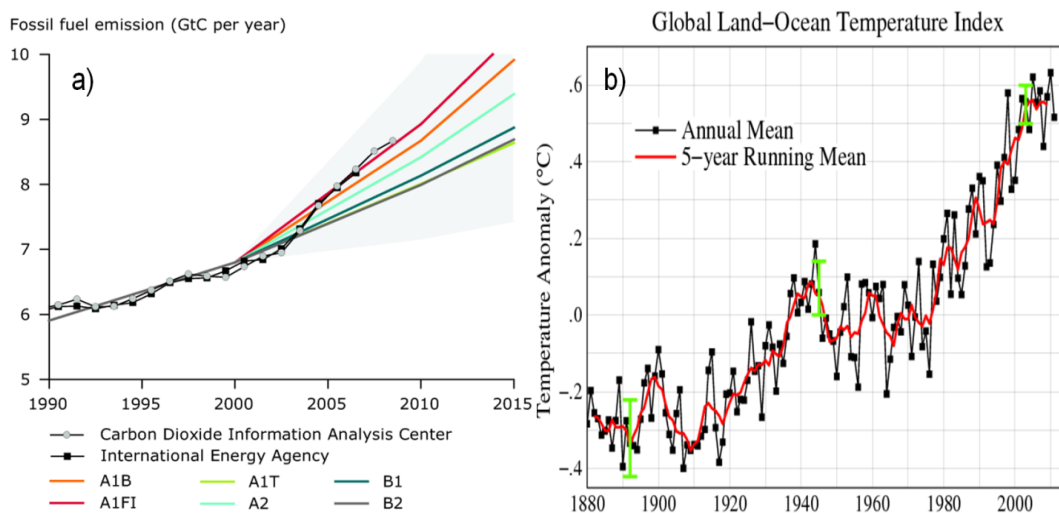
Fig. 1. 5 Effect of greenhouse gases in worldwide, a) carbon dioxide release from fossil fuel; b) change in the surface temperature is due to global warming (adopted Goddard Institute for Space Studies, 2009).

Fig 1. 5a shows the increase of carbon dioxide released into the atmosphere since 1990 and expected the trend to increase further if our emissions continue. About 98% of global carbon dioxide emissions results from the fossil fuel combustion. Since the start of the industrialization, the CO2 level has increased from 280 ppm to a current level of 384 ppm, growing around 2-3 ppm annually [16]. Although still up for debate, most climatologists believe that these elevated levels will result in an increased average global temperature as shown in the fig. 1. 5b. Over the last century, average global temperature has increased by 0.56°C. Due to an increase in the carbon dioxide emissions and the auto feedback mechanism of heating, the increase in the temperature for the next century is estimated to be anywhere between 1.5°C to 5.8°C[17]. If it is the case, then we have to face drastic changes on the surface such as displacement of agricultural zones, melting of polar ice caps and glaciers, rise in the sea level from 9 to 88 cm, etc[16]. Therefore, greenhouse gas reduction has received tremendous attention, both scientifically and politically [18, 19].

1.4 Environmental regulations

Since chemical processes create waste, management of this waste is an important issue. Generation of waste can be viewed as an inefficient use of resources that will consequently result in a less economically attractive process. The most attractive way to manage waste is to prevent it rather than to clean it up. In 1997, Kyoto Protocol was passed to address such issues. According to the Kyoto Protocol, OECD member countries and those with transition economies must reduce their emissions of six GHGs by at least 5.2% compared to 1990 levels. The emission reduction should take place from 2008 to 2012 [20]. This is really a great challenge for chemical industry to update their current technology in order to meet the environmental regulations.

1.5 National energy security policies

Another key issue is national energy security. A major problem with petroleum fuels is their uneven distribution in the world; for example, about 2% of the world population in the Middle East has 63% of the global reserves and is the dominant supplier of petroleum [21]. Political decisions aiming to reduce dependency on the fossil resources. Among other actors, European Union (EU) has announced an ambitious goal of reaching 20% renewable energy share by 2020 [22]. Germany's new energy policy includes far more than just phasing out nuclear power by 2022. The expansion of the renewables like wind and solar power (80% of the energy mix by 2050) and the reduction of greenhouse gases (80% by 2050) planned by the German government will require a wide range of measures. Chemical industries are required at to play a creative role in order to achieve the goal of energy security policies.

1.6 Raw material change in chemical industry

The resource challenge is a result of the global population boom of the 20th century, where the population has almost quadrupled to over 6 billion people by the year 2000 and expected to 9 billion by 2050 [23]. This combined with the fact that more and more people enjoy the benefits of a high living standards, has put strain on the resources needed to fuel this population and consumption boom. Chemistry has made a vast array of materials, medicines, fertilizers and fuels available at low cost. However, the chemical industry is based almost entirely on processes that convert petroleum derived resources into these highly valued products. During 20th century, cheap and abundant petroleum feedstocks have been readily available; however it has become shockingly

clear that these feedstocks will be priced very differently in the 21st century, as the dwindling supplies can no longer keep pace with an ever increasing demand [2]. This event will undoubtedly impact the chemical industry of the 21st century. In the chemical industry profound changes took place in the 1980's influencing research and process development today. As shown in the fig. 1. 6 , petroleum is the main raw material for the chemical industry with a share of more than 75% [24]. In many cases this has led to a redefinition of the objectives in the
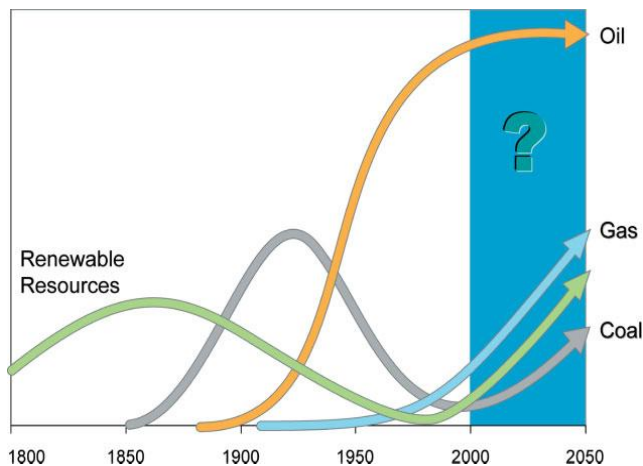
Fig. 1. 6 Trend of raw material usage and window of uncertainty[2].

chemical industry. After past oil crisis, a great improvement was made in terms of energy conversation. At present, less economic improvements were left and energy costs have been stabilized at a moderate level. Due to the foreseeable worldwide shortage of fossil resources and the resulting increase in their prices, it becomes necessary to think about alternative raw materials. In the future, natural gas, carbon dioxide and biomass should supplement increasingly to crude oil as raw materials in chemical production [25].

Herein, we explore the prospects for using renewable resources, namely biomass, as an alternative to the fossil resources as a feedstock for the chemical industry [26]. In an attempt to start identifying promising opportunities, it is instructive to establish a simple value chain that illustrates how the petrochemical industry transforms fossil resources into desirable products by a series of chemical transformations.

The value chain in the fig. 1. 7 qualitatively illustrates the value of various important commodity chemicals relative to that of the fossil raw materials, that is, coal, natural gas, and crude oil. This is certainly a very simplistic illustration as the value of the fossil resources varies considerably, not only according to the geographic origin and quality but also over time for complex socio-economic reasons. Nonetheless, this fossil value chain for the chemical industry emphasizes that crude oil is transformed into transportation fuels by relatively simple, efficient, and inexpensive operations. Thus, transportation fuels are among the least expensive chemicals available. In these considerations biomass plays a key role. Although for energetic purposes biomass has

a lower potential than other alternatives like photovoltaic. It is the only renewable carbon source.
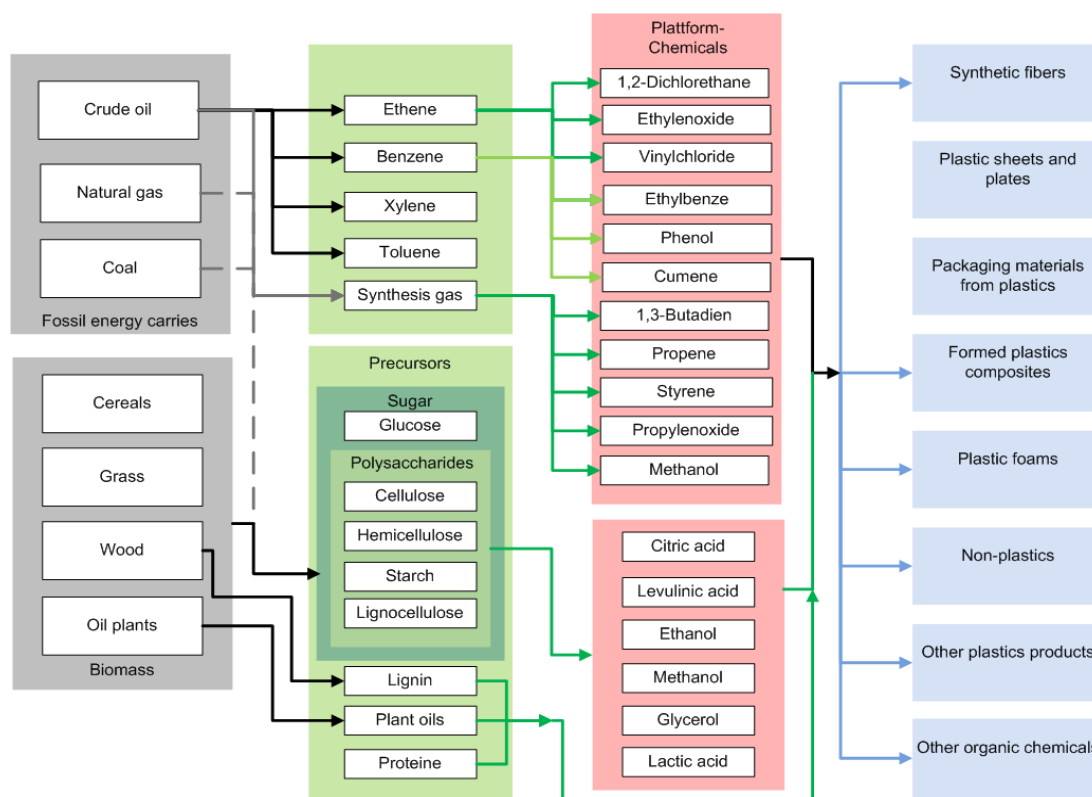
Fig. 1. 7 Options for raw material change in the chemical industry.

For substituting oil by biomass a main challenge of the near future is the systematic development of new production concepts. Different approaches for the raw material change in the chemical industry are distinguished. In one approach biomass is converted to synthetic gas and all other products are built up from the so-called C_1 building blocks [10, 26]. Natural gas and coal can be used for this route as well. In other approaches more complex molecular structures like glucose, lignin, plant oil etc., which are produced by plants, are used as intermediates, and all final products are obtained from these platform chemicals

1.7 Biomass conversion technologies

1.7.1 Thermo-chemical conversion:

In thermo-chemical conversion, biomass is converted into gas & liquid intermediates that can be used for fuels and chemical synthesis. The term Biomass to Liquid (BtL) is

applied to synthetic fuels produced from biomass via thermo-chemical route [27]. The objective is to produce fuel components that are similar to those of current fossil-derived petrol (gasoline) and diesel fuels and hence can be used in the existing fuel distribution systems and with standard engines. They are also known as synfuels. The intermediate products include clean syngas ($CO+H_2$), bio-oil (pyrolysis or hydrothermal product), and gases rich in methane or hydrogen. These intermediates can further be synthesized to gasoline, diesel, alcohols, ethers, synthetic natural gas etc. and also high purity hydrogen, which can be used as fuels in electric power generation. Gasification at higher temperatures of $1200^{o}C - 1600^{o}C$ leads to few hydrocarbons in the product gas and a higher proportion of CO & H_2.
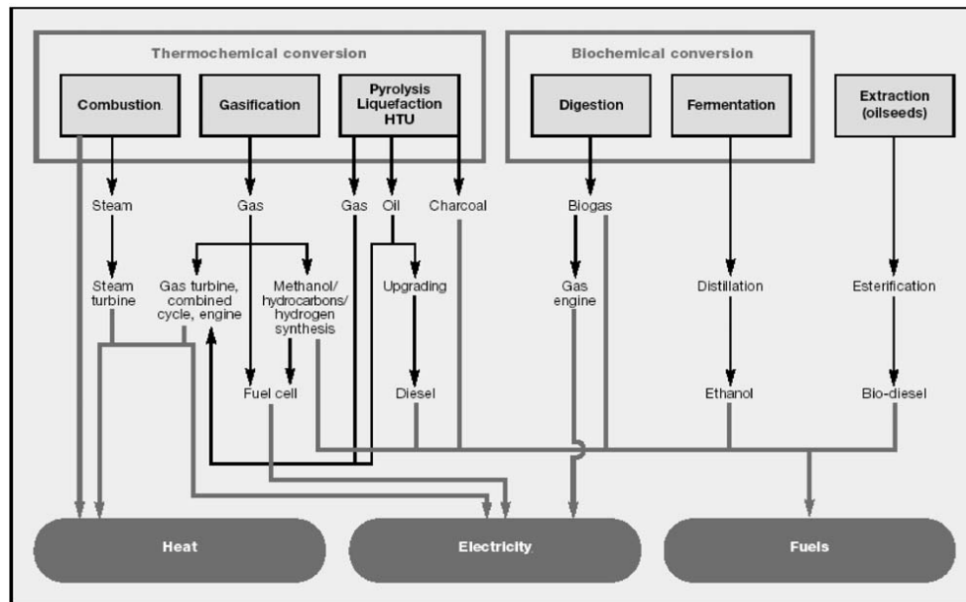
Fig. 1. 8 Main conversion options for biomass and end applications (adopted Faaij, 2006[13]).

If the ratio of H_2 to CO is 2:1 then Fischer-Tropsch synthesis is an option to convert syngas into high quality synthetic biofuels which are compatible with conventional fossil fuel engines. Pyrolysis is the thermal de-polymerization of biomass at modest temperatures in the absence of added oxygen. The products of fast pyrolysis include gases, bio-oil, and char which depend on the process temperature, pressure, and residence time of the liberated pyrolysis vapors. The production of bio-products is maximized by fast pyrolysis, typically performed at temperatures (~450-500°C) at atmospheric pressure, high heating rates (i.e., 500°C/sec) and short residence times (1-2 sec). Slow pyrolysis reaction occurs at 300 - 500°C and the heating rates are slow i.e. around 20 - 30°C/sec and the residence time allowed is more. In this case, the yield

of gaseous product and solid residue is more as compared to fast pyrolysis. But the quality of liquid product is better [13, 27-30].

1.7.2 Bio-Chemical Conversion Process

The bio-chemical conversion process deals with agricultural residues, energy crops and to some extent paper & pulp mill residues. It is a combination of pretreatment, enzymatic hydrolysis, and fermentation [27, 31, 32].

1.8 Bottlenecks of renewable biomass conversion technologies

The biomass thermo-chemical conversion processes are endothermic, and heat is required during the operation of the process. Biomass conversion has a variety of process heating needs depending on the conversion route adopted (fig.1. 9). Drying of biomass can put a heavy heat load on the process. For example, the external heating needs are about 3000–4000 kJ/kg of water removed. The electrical (or mechanical) energy needs of the process are for conveying, grinding, and
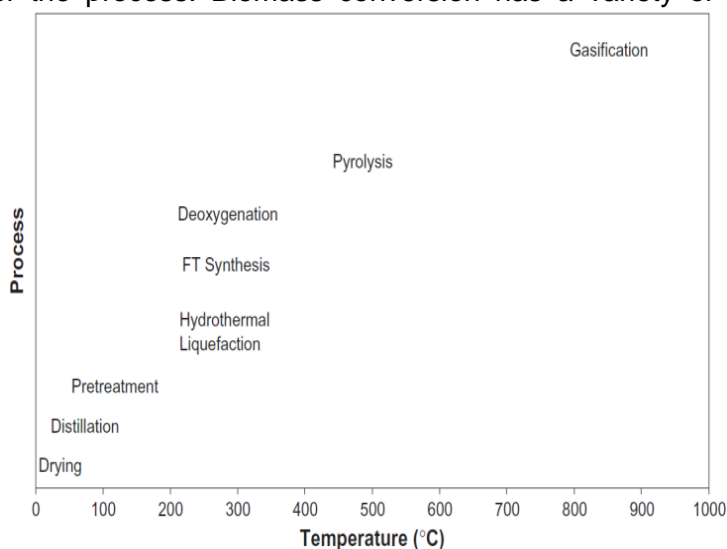
Fig. 1. 9 Thermal energy needs for biofuel production processes.

pumping. In total, 20–27% of the energy content of biomass is required simply to run the process (e.g gasification, pyrolysis). The generation of heat by combustion of biomass releases harmful carbon dioxide [33]. In addition, pure oxygen and hydrogen are required for oxidation and hydrodeoxygenation of bio-oil and biocrude, and for conditioning of syngas to produce chemicals and fuels [34]. The source of hydrogen is also under debate to decide whether the process is renewable or not. If pure oxygen is used instead of air, the input costs are high.

In order to claim biomass conversion technologies are renewable and zero carbon foot-print, one should address the source of heating, pure oxygen and hydrogen required for the process. These bottlenecks will be serious issues in the next 20 -30 years. Burning of biomass via gasification and pyrolysis to get the C1-C20 molecules

increases the complexity of the process [29]. To address such issues, we believe that use of direct sun energy in different forms will be the ultimate solution to answer all these issues. Sun energy is tremendous and readily available at all places in different forms. The challenge is to convert unlimited sun energy into required applications.

1.9 Renewable energy from Sun

The unlimited Sun energy has tremendous effect on this creation. The sun energy in the form of solar radiation reaches the Earth about 174×10^{12} KW[35], in which 30% of energy is reflected back. The total solar energy absorbed by clouds, oceans and land masses is approximately 3.85×10^{24} joules per year [36]. The advantage of this energy is 'spread throughout the world' (available in all countries). The disadvantage of this energy is 'in the diffused form' (not concentrated as in coal mine or petroleum well). In general words, one hour utilization of this energy is more than sufficient to our world's energy needs in one year[1]. Fig. 1. 10 shows a small part of Sahara desert that would be enough to provide sufficient
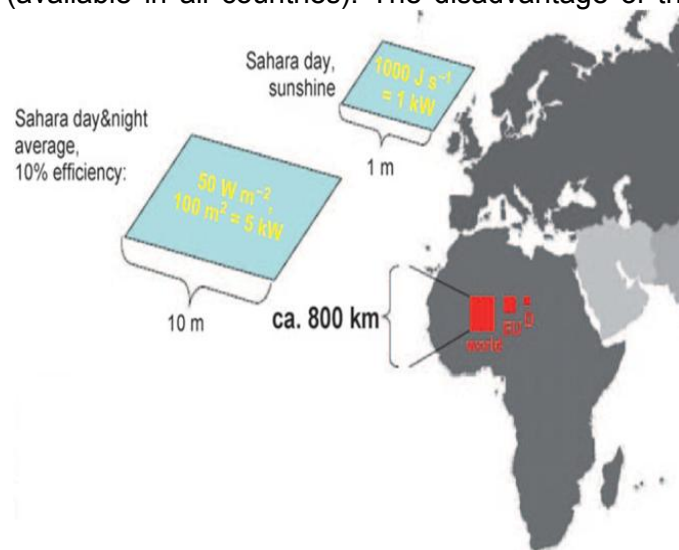
energy to the world with 10% conversion efficiency according to the consumption

Fig. 1. 10. Small desert area (11 40000 km^2) is sufficient to lift 6.4 billion people to EU energy standard with respect to the use of primary energy. (Schüth, 2010) [1].

of a European citizen (5 kW power per person) [37]. Unfortunately, no technology was developed to convert the solar radiation directly into other energy form. But this solar radiation is helpful to harvest different types of energies such as sunlight, wind, hydrothermal, planned growth (biomass), tides, geothermal heat [38]. Sunlight absorbed by the oceans and land masses keeps the surface at an average temperature of 14 °C[39]. By photosynthesis green plants convert sunlight into chemical energy, which produces food, wood and the biomass from which fossil fuels were derived million years ago. Photosynthesis captures approximately 3,000 EJ per year in biomass. The plant material uses less than 0.1% of total sun energy received by earth.

Fig. 1. 12 Schematic and simplified network of different pathways to capture solar radiation (Schüth, 2010 [34]).

Almost any conversion of energy from one form into another involves a chemical transformation. And understanding the fundamental nature of these reactions is a key for the development of new materials and energy transformation pathways. Chemistry plays a pivotal role in most technological options. Fig.1. 12 illustrate schematically the conversion pathways of solar radiation to chemical storage molecules or to electrical energy[40]. All renewable resources are based on solar radiation to produce electricity, but in our opinion, it could not serve the problem completely. Because current chemical industrial technology is mainly based on "carbon" related molecules and it is not possible to get carbon directly from electricity.

Therefore, it is clear that biomass is the only renewable resource to get "carbon" based molecules. New technologies are required to transform "carbon" in the biomass to substituted molecules derived from petroleum.

1.10 Concept of biorefineries based on chemical conversion

A biorefinery is a facility that integrates biomass conversion processes and equipment to produce fuels, power, heat, and value-added chemicals from biomass [34]. The biorefinery concept is analogous to today's petroleum refinery, which produce multiple fuels and products from petroleum. In the process of selective chemical transformation in a biorefinery, HMF should be originated from abundant renewable carbohydrates in high yield with low process energy consumption [41]. Current processes to produce HMF involve the use of acid catalysts and are mainly limited to fructose as a feed [42-44]. A drawback with acid catalysts is that they cause various side reactions, significantly increasing the cost of product purification. For example, in water under acidic conditions, HMF decomposes to levulinic acid and formic acid. Levulinic acid is particularly difficult to separate from HMF. Substituting glucose as a feed substantially reduces HMF yields and produces additional byproducts. Therefore we selected very promising route to convert cheap carbohydrate-derived sugars into high-value chemicals and fuels by simple hydration, dehydration, oxidation, and hydrogenation and are aldol condensation reactions. Fig. 1. 13 shows the possible chemical conversion of cellulosic biomass into various chemicals and fuel type molecules. The proposed concept will be viable only when the source of external elements likes heat, oxygen and hydrogen are generated from renewable sources.

In order to face the future energy challenge, we propose a new and innovative idea to produce sustainable chemicals and fuels from biomass using renewable free electrons from the sun. Finding the way to integrate renewable electricity directly with renewable biomass conversion is the main subject of this PhD thesis. To achieve this goal we adapted electrochemical catalysis to get required hydrogen or oxygen by simply using a small amount of electrons from wind, solar and hydropower (to electrify the surface of the catalyst) at mild reaction conditions [45].

The idea is illustrated in the fig. 1. 14**.** Therefore, the aim is to use the free electrons from sun to convert sun-derived biomass into required chemicals and fuels. The challenge for scientists/researchers is to capture this energy in an efficient way to reduce our dependency on fossil resources. We need a catalyst with structural and electronic modifiers, which can be used acrobatically to produce chemicals by combining plant biomass and electrons from renewable resources. Then we can see sustainable future of chemical industry with renewable raw material to produce chemicals, transportation fuels and polymers.
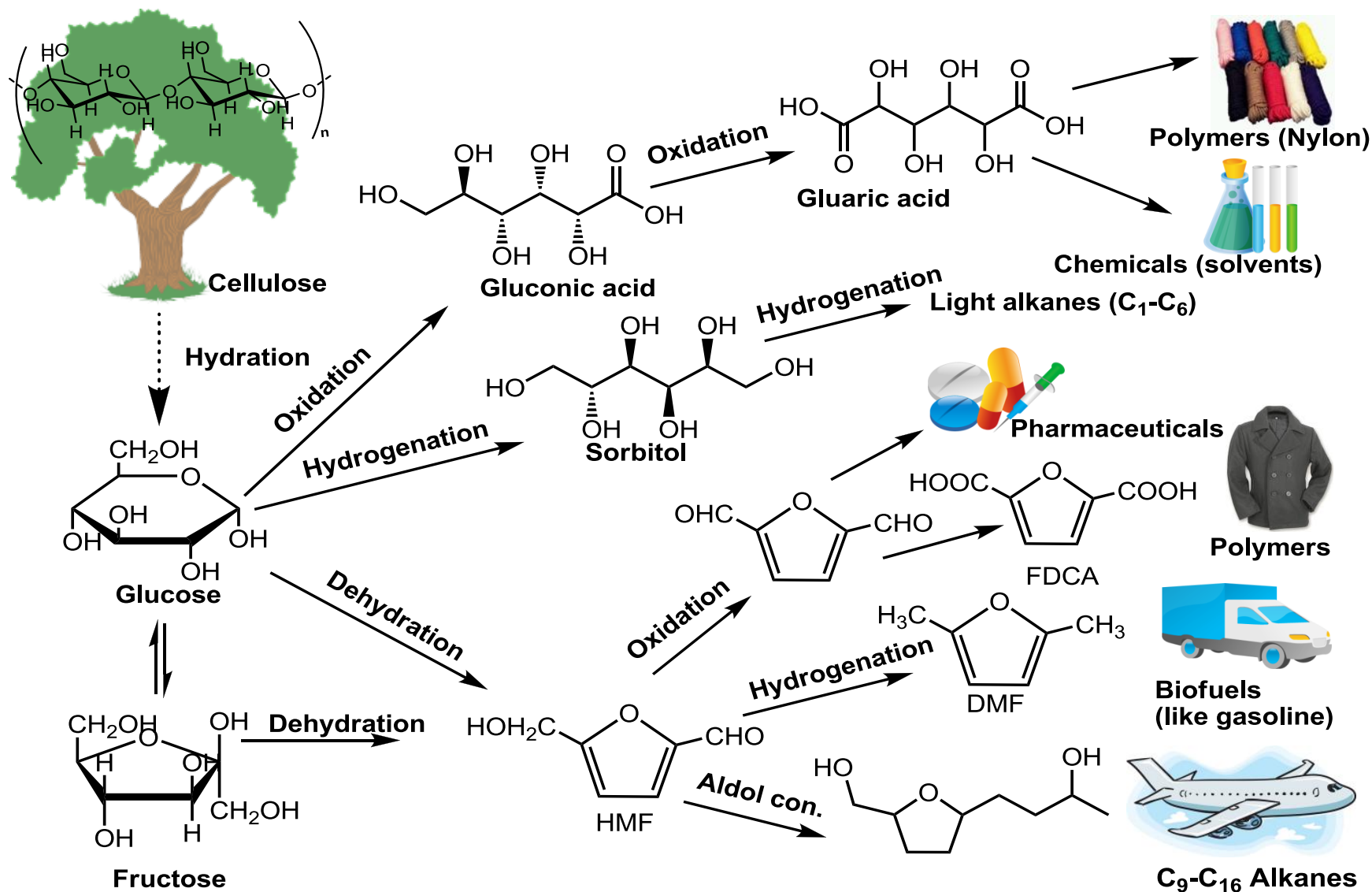
Fig. 1. 13 Concept of biorefinery to produce high-value chemicals and fuels based on selective chemical conversion.
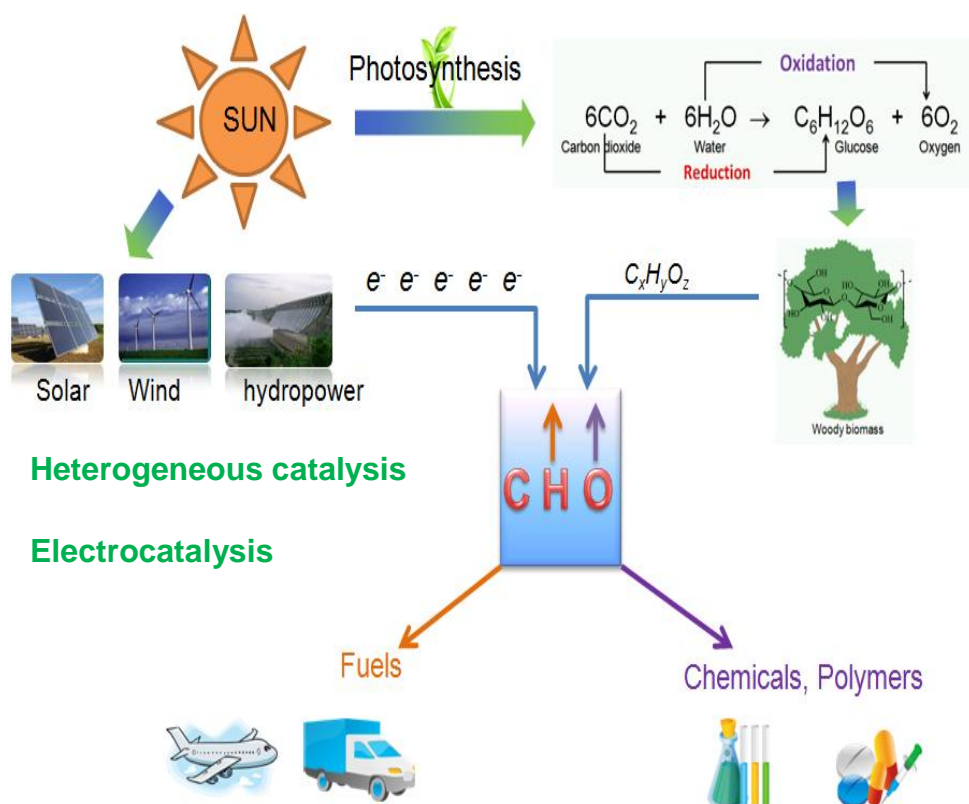
Fig. 1. 14 Utilization of Sun-derive biomass and free electrons to produce sustainable chemicals.

1.11 Aim and objectives of PhD thesis

The aim of this PhD thesis is a comparative study of the electrocatalytic and heterogeneous catalytic conversion of biomass derived oxygenated compounds into useful commodity chemicals. In particular, we investigate the dehydration, oxidative and reduction reactions of sugar-based biomass compounds into chemical/fuel type molecules under heterogeneously catalyzed and electrochemically catalyzed conditions. The simplified reaction pathway was shown in the fig. 1. 15 .
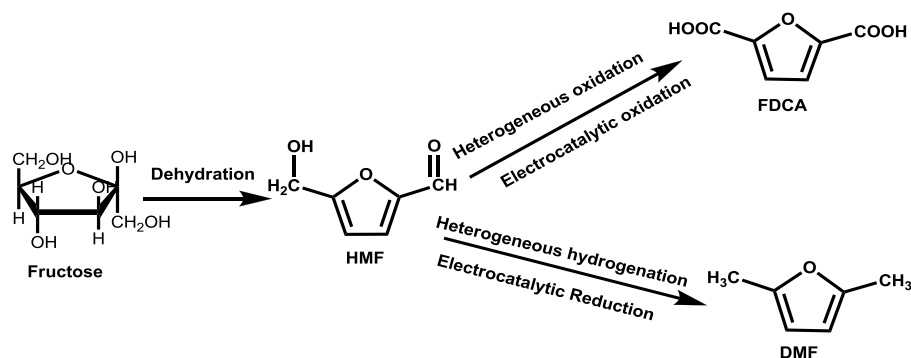
Fig. 1. 15 Selected reaction pathway for Ph.D thesis research.

The work packages of this thesis include:

1. Synthesis of a novel solid acid catalyst for the heterogeneous catalytic dehydration of fructose. Investigating the effect of different operating conditions (temperature, solvent, support material, etc.) on catalyst activity in terms of conversion and selectivity. Comparative studies between self prepared and commercial solid acid catalysts.

2. Synthesis and characterization of a supported metal catalyst and testing for HMF oxidation in liquid-phase at mild conditions. Insights into HMF oxidative pathways under different reaction conditions along with mechanistic details. Comparing the catalytic activities of different supported heterogeneous catalysts. Optimization of important operating parameters to increase process viability.

3. Testing of different metal catalysts for hydrogenation reactions. Selection of suitable reaction conditions and effect of different solvents on catalytic activity.

4. Understanding of electrochemical characteristics of HMF and its oxidative/ hydrogenative derivatives on different metal electrodes under different conditions. Investigating the anodic oxidation and cathodic reduction powers of electrodes for HMF conversion with qualitative and qualitative analytics. Exploring the influence of different parameters (temperature, pH, current densities, etc) on catalytic activities of electrodes for HMF conversion into valuable chemicals.

5. Finally, comparing electrochemical catalysis and heterogeneous catalysis for HMF conversion in terms of conversion, yield and selectivity to explore unifying or contrasting principles.

1.12 References

1.   Morton, Oliver, Solar Energy: A New Day Dawning?: Silicon Valley Sunrise. *Nature*, 2006. 443(7107): p. 19-22.
2.   Diercks, R., Arndt, J. D., Freyer, S., Geier, R., Machhammer, O., Schwartze, J., and Volland, M., Raw Material Changes in the Chemical Industry. *Chemical Engineering & Technology*, 2008. 31(5): p. 631-637.
3.   Kamm, B., Production of Platform Chemicals and Synthesis Gas from Biomass. *Angewandte Chemie International Edition*, 2007. 46(27): p. 5056-5058.
4.   Binder, Joseph B. and Raines, Ronald T., Simple Chemical Transformation of Lignocellulosic Biomass into Furans for Fuels and Chemicals. *Journal of the American Chemical Society*, 2009. 131(5): p. 1979-1985.
5.   Shakun, Jeremy D., Clark, Peter U., He, Feng, Marcott, Shaun A., Mix, Alan C., Liu, Zhengyu, Otto-Bliesner, Bette, Schmittner, Andreas, and Bard, Edouard, Global Warming Preceded by

Increasing Carbon Dioxide Concentrations During the Last Deglaciation. *Nature*, 2012. 484(7392): p. 49-54.

6. *www.eia.doe.gov*.

7. *BP statistical review of world energy*, 2010.

8. Behr, A., Westfechtel, A. and Pérez Gomes, J., Catalytic Processes for the Technical Use of Natural Fats and Oils. *Chemical Engineering & Technology*, 2008. 31(5): p. 700-714.

9. Meyers, Robert, *Handbook of Petroleum Refining Processes* 2003.

10. Groenendaal, B.J. and Gielen, D.J., *The Future of the Petrochemical Industry* 1999.

11. Witze, Alexandra, Energy: That's Oil, Folks. *Nature*, 2007. 445(7123): p. 14-17.

12. Vogel, G. H., Change in Raw Material Base in the Chemical Industry. *Chemical Engineering & Technology*, 2008. 31(5): p. 730-735.

13. Diercks, R., Arndt, J.-D., Freyer, S., Geier, R., Machhammer, O., Schwartze, J., & Volland, M. , Raw Material Changes in the Chemical Industry. *Chemical Engineering & Technology*, 31(5), 631–637. Doi:10.1002/Ceat.200800061. 2008.

14. *Statistical Review of World Energy 2012, www.bp.com/statisticalreview*.

15. Sokolov, A.P., *Probabilistic Forecast for 21st Century Climate Based on Uncertainties in Emissions (without Policy) and Climate Parameters*. 2009.

16. Meehl, Gerald A., Washington, Warren M., Collins, William D., Arblaster, Julie M., Hu, Aixue, Buja, Lawrence E., Strand, Warren G., and Teng, Haiyan, How Much More Global Warming and Sea Level Rise *Science*, 2005. 307(5716): p. 1769-1772.

17. Http://Www.Telegraph.Co.Uk/Science/Science-News/3302874/Global-Warming-Forecast-Predicts-Rise-in-2014.Html

18. Weaver, Andrew J. and Hillaire-Marcel, Claude, Global Warming and the Next Ice Age. *Science*, 2004. 304(5669): p. 400-402.

19. http://data.giss.nasa.gov/gistemp/ and http://www.epa.gov/climatechange/basics/.

20. Group, Igbp Terrestrial Carbon Working, The Terrestrial Carbon Cycle: Implications for the Kyoto Protocol. *Science*, 1998. 280(5368): p. 1393-1394.

21. Faaij, Andr. P. C., Bio-Energy in Europe: Changing Technology Choices. *Energy Policy*, 2006. 34(3): p. 322-342.

22. Birol, F. , World Energy Outlook 2010, International Energy Agency, Paris, France 2010.

23. Blaschek, H. P., & Ezeji, T. C., Science of Alternative Feedstocks Introduction, 112–128. 2010.

24. Arndt, J. D., Freyer, S., Geier, R., Machhammer, O., Schwartze, J., Volland, M., and Diercks, R., Rohstoffwandel in Der Chemischen Industrie. *Chemie Ingenieur Technik*, 2007. 79(5): p. 521-528.

25. Röper, Harald, Renewable Raw Materials in Europe — Industrial Utilisation of Starch and Sugar [1]. *Starch - Stärke*, 2002. 54(3-4): p. 89-99.

26. Muffler, K. and Ulber, R., Use of Renewable Raw Materials in the Chemical Industry – Beyond Sugar and Starch. *Chemical Engineering & Technology*, 2008. 31(5): p. 638-646.

27. Demirbas, M. F., Current Technologies for Biomass Conversion into Chemicals and Fuels. Energy Sources, Part A: Recovery, Utilization, and Environmental Effects, 28(13), 1181–1188. Doi:10.1080/00908310500434556. 2006.

28. Palkovits, Regina, von Malotki, Christian, Baumgarten, Martin, Müllen, Klaus, Baltes, Christian, Antonietti, Markus, Kuhn, Pierre, Weber, Jens, Thomas, Arne, and Schüth, Ferdi, Development of Molecular and Solid Catalysts for the Direct Low-Temperature Oxidation of Methane to Methanol. *ChemSusChem*. 3(2): p. 277-282.

29. Yaman, S., Pyrolysis of Biomass to Produce Fuels and Chemical Feedstocks. *Energy Conversion and Management*, 45(5), 651–671. Doi:10.1016/S0196-8904(03)00177-8. 2004.

30. Meine, Niklas, Rinaldi, Roberto and Schüth, Ferdi, Solvent-Free Catalytic Depolymerization of Cellulose to Water-Soluble Oligosaccharides. *ChemSusChem*. 5(8): p. 1449-1454.

31. Sánchez, O. J., & Cardona, C. , Trends in Biotechnological Production of Fuel Ethanol from Different Feedstocks. *Bioresource Technology*, 99(13), 5270–95. Doi:10.1016/J.Biortech.2007.11.013. 2008.

32. Rinaldi, Roberto, Engel, Philip, Büchs, Jochen, Spiess, Antje C. and Schüth, Ferdi, An Integrated Catalytic Approach to Fermentable Sugars from Cellulose. *ChemSusChem*. 3(10): p. 1151-1153.

33. Barth, T. and Kleinert, M., Motor Fuels from Biomass Pyrolysis. *Chemical Engineering & Technology*, 2008. 31(5): p. 773-781.

34. Goyal, G. C., Tan, Z., Yin, C., Marsolan, N., & Amidon, T., *Biorefinery – an Overview.*

35. Smil, V., *General Energetics Energy in the Biosphere and Civilization*. 1991: John Wiley, New York.

36. Smil, V., *Transforming the Twentieth Century: Technical Innovations and Their Consequences.* . 2006. : Oxford University Press, New York.

37. Schüth, Ferdi, Guest Editorial: Paving the Way to New Energy Systems: The Key Role of the Chemical Sciences. *ChemSusChem*, 2010. 3(1): p. 6-8.

38. Iea Renewable Energy Working Party (2002).

39. Somerville, Richard. , "Historical Overview of Climate Change Science". *Intergovernmental Panel on Climate Change. http://www.ipcc.ch/pdf/assessment-report/ar4/wg1/ar4-wg1-chapter1.pdf.*

40. Schüth, Ferdi, Chemistry Paves the Road to Novel Energy Systems. *ChemSusChem*, 2008. 1(1-2): p. 155-156.

41. Holladay, J. E., White, J. F., Bozell, J. J., & Johnson, Biorefinery Lignin. Evaluation, II(October). Top Value-Added Chemicals from Biomass Volume Ii — Results of Screening for Potential Candidates from Biorefinery Lignin. Evaluation, (October). 2007.

42. Roman-Leshkov, Yuriy, Chheda, Juben N. and Dumesic, James A., Phase Modifiers Promote Efficient Production of Hydroxymethylfurfural from Fructose. *Science*, 2006. 312(5782): p. 1933-1937.

43. Tyrlik, Stanisaw K., Szersze„, Dorota, Olejnik, Marian and Danikiewicz, Witold, Selective Dehydration of Glucose to Hydroxymethylfurfural and a One-Pot Synthesis of a 4-Acetylbutyrolactone from Glucose and Trioxane in Solutions of Aluminium Salts. *Carbohydrate Research*, 1999. 315(34): p. 268-272.

44. Watanabe, Masaru, Aizawa, Yuichi, Iida, Toru, Aida, Taku M., Levy, Caroline, Sue, Kiwamu, and Inomata, Hiroshi, Glucose Reactions with Acid and Base Catalysts in Hot Compressed Water at 473K. *Carbohydrate Research*, 2005. 340(12): p. 1925-1930.

45. Lyko, H., Deerberg, G., & Weidner, E. (2009). Coupled Production in Biorefineries--Combined Use of Biomass as a Source of Energy, Fuels and Materials. *Journal of Biotechnology*, 142(1), 78–86. Doi:10.1016/J.Jbiotec.2009.03.016. 2009.

Chapter 2

Experimental Details and Materials

2.1 Chemicals and materials

The chemicals (reagent grade) and materials were procured from different sources as follows.

Chemicals from sigma aldrich:

Furan, 99+%, d-fructose, d-glucose anhydrous, d-gluconic acid, 49-53 wt.%, d-glutamic acid, 5-(hydroxymethyl)furfural, 99+%, 2,5-furandicarboxylic acid, levulinic acid, 2-methylfuran, 99%, 2,5-dimethylfuran, 99%, tetrahydrofuran, anhydrous, >=99.9%, 2-furaldehyde, >=98%, furfuryl alcohol, >=98%, 5-acetoxymethyl-2-furaldehyde, 99%, dimethyl succinate, 98%, tetrabutylammonium perchlorate, sodium acetate anhydrous, sodium bicarbonate, sodium phosphate dibasic: anhydrous, sodium phosphate 96%, sodium phosphate monobasic monohydrate, titanium dioxide, mangan(iv)-oxid, chrom(vi)-oxid, 4-methyl-2-pentanon>=98,5%, blei(iv)-acetat 95%, pyridin wasserfrei 99.8%, kaliumdichromat 99 +%, sodium hypochlorite solution, wasserstoffperoxid 30%, zirconium(iv) hydroxide, 97%, furan-2-carbonsaeure 98%, 5-methylfurfural 99%, 2-acetylfuran 99%, natriumdeuteroxid 40% in D_2O, indium tin oxide coated glass slide, natronlauge 1 mol/l, a-cellulose, lignin alkali, niederer sulfon-gehalt, staerke loeslich nach zulkowsky aus, chlorsulfonsaeure, 4-chlorbenzolsulfonsaeure techn. 90%, montmorillonit k 10, pulver, chrom(iii)-chlorid hexahydrat, (3-mercaptopropyl)-trimethoxysilan 95%, silica, zirconium(iv) oxide, powder, <5 micron, p-toluenesulfonic acid, polymer-bound, m, schwefelkohlenstoff 99.9%, 4-(brommethyl)-benzolsulfonsaeurechlorid, 3-bromopropanesulfonic acid sodium, copper, foil, 0.25mm thick, 99.98% metal, nickel, folie 0,125 mm 99,9 +%, nickel, foil, 0.5mm thick, 99.98% metals, gold(III) chloride trihydrate, 99.9+%, polyvinylalkohol, 99+% hydrolysiert, d-(+)-glucose monohydrate, polyvinylpyrrolidone mol.wt. 40,000, natriumborhydrid, gold folie, 0,1 mm 99.99%, 2,5-dimethyltetrahydrofuran 96%, 1,2,6-hexanetriol 96%.

Chemicals from alfa aesar:

N-dimethylacetamide 99%, furfuryl alcohol 98%, 4-methyl-2-pentanone 99%, 5-hydroxymethyl-2-furaldehyde 98+%, furan 99% stab. with ca 250ppm bht, n-

dimethylformamide 99%, sodium 2-chloroethanesulfonate hydrate 98+% (dry wt.) water <10%, p-toluenesulfonic acid polymer-supported 1.0-2.0 mmol/g on polystyrene, platinum foil 0.1mm (0.004in) thick 99.99% (metals basis), palladium foil 0.1mm (0.004in) thick 99.9% (metals basis), palladium 5% on gamma alumina powder reduced, platinum 1% on gamma alumina powder reduced, gold wire 1.0mm (0.04in) dia 99.95% (metals basis), nickel on silica-alumina catalyst, 2-furaldehyde acs 98% min, ethyl acetate acs 99.5+%, acetaldehyde 98.5%, sodium hydroxide 0.01n standardized solution, sodium hydroxide 1.0n standardized solution, dihydrogen hexachloroplatinate(iv) hexahydrate acs 99.95% (metals basis) Pt 37.5% min, d-sorbitol 98%, glassy carbon plate 1mm (0.04in) thick type 1, diethyl ether hplc grade 99% stab. with ethanol, nickel wire 1.0mm (0.04in) dia hard 99.5% (metals basis), platinum wire 1.0mm (0.04in) dia annealed 99.95% (metals basis), nickel wire 0.5mm (0.02in) dia puratronic® 99.999% (metals basis), zirconium oxide catalyst support, cerium(iv) oxide 99.9% (metals basis), aluminum oxide gamma-phase catalyst support high surface area bimodal, titanium(iv) oxide catalyst support, silicon oxide catalyst support high surface area, nickel foil 2.0mm (0.08in) thick 99.5% (metals basis), copper based methanol synthesis catalyst, zinc oxide 99.99% (metals basis), amberlyst-15 ion exchange resin.

Sulfuric acid (98%), dichlormethan (99,5%), n-hexan (99%) were received from ROTH. Zinc chloride (anhydrous, 98 %) was stored in a glove box and used as received from ABCR GmbH. 2,5-furandicarbaldehyde (TCI GmbH, 98%), 5-hydroxymethyl-2-furancarboxylic acid (Interchim), 5-formyl-2-furancarboxylic acid (Chemos GmbH), 20wt.% and 46.8wt.% Pt/ Vulcan were received from research unit, BASF. 1wt.% Au/TiO$_2$, 5wt.% Ru/C, 5wt.% Rh/C and 5wt.% Pd/C from strem chemical Ltd.

2.2 Equipment details

2.2.1 Semi-batch reactor (Autoclave)

Heterogeneous catalysts were tested in semi-batch reactor. Premex autoclave reactor was custom made with hastelloy C-22 material, which contains pitched blade stirrer (0-2000rpm), temperature controller, pressure controller (Maas flow controller), provision for sample in/out and pressure release valve as shown in
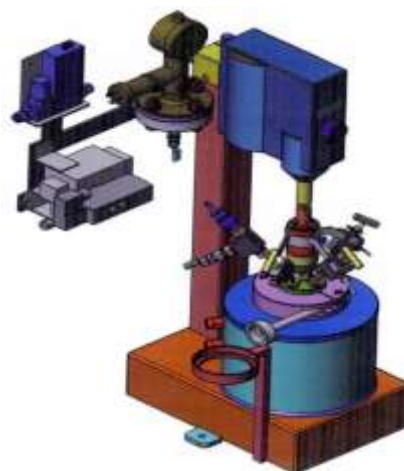
Fig. 2. 1 Schematic view of semi-batch reactor.

fig. 2. 1. The maximum operating temperature and pressure are 240oC and 40 bar respectively. Hastelloy material shows good resistance against acid or base corrosion. The reactor vessel was made with stainless steel with the thicker wall and it can withstand the 40 bar pressure. The reactor was inserted with a special custom made Teflon liner, which was mixed with carbon to avoid the temperature gradients as shown in the fig. 2. 2a. The reactor was heated or cooled with an external source using Huber thermostat as shown in the fig. 2. 2c. and the dramatic view of inside the reactor and head of the reactor was shown in fig.2. 2b and fig.2. 2c respectively.
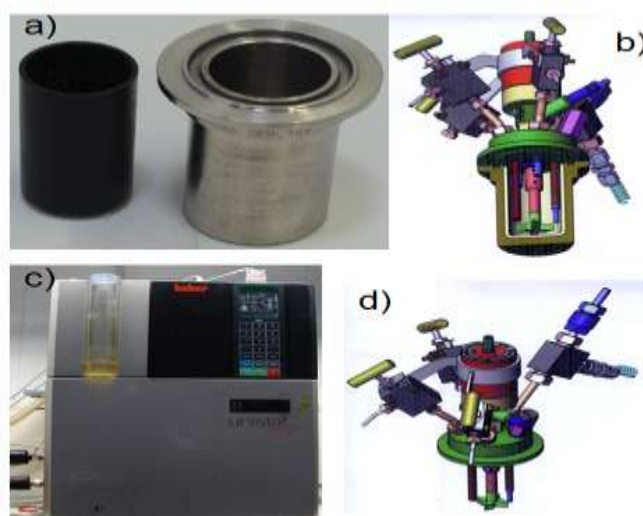
Fig. 2. 2 Different components of semi-batch reactor. a) reactor vessel and Teflon liner; b) schematic view of reactor inside with stirrer, temperature sensor, gas inlet, sample in/out provision, pressure release provision; c) thermostat with oil circulation; d) schematic view of head part of reactor.

The reactor was completely closed with leak proof fitting (o-ring) during the time of reaction. The reactor was controlled and operated by computer using a custom software from Ordino CS 350 from Pro-Control Ltd as shown in the fig. 2. 3. The Control panel provides the window to see the stirrer speed, to set the desired temperature and pressure (set point, SP) along with present value (PV). This software automatically provides the MFC calibration for hydrogen oxygen or hydrogen gases. User-defined reaction temperature profile can be created before the start of the reaction as a function of time. This software also shows the profiles of different operating parameters such as temperature, pressure, flow of oxygen, stirring speed with respect to reaction time.
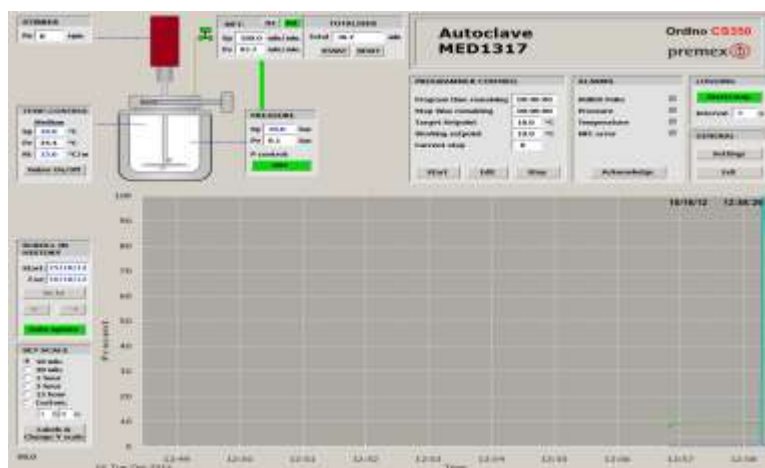
Fig. 2. 3 Control panel to operate semi-batch reactor.

2.2.2 Reflux condenser reactor setup

Fig. 2. 4 shows schematic view of reflux condenser reactor setup. The reactor contains katydid controller, magnetic stirrer controller, oil bath, round bottom flask with three provisions for condenser, temperature sensor, nitrogen gas from balloon. The reactants were added to the reactor, when it is heated to the desired temperature. The condenser was connected to water circulation to cool the vapors of reaction mixture. The temperature of the reaction was controlled with auto-cut of heating. The samples were collected at regular intervals of time using syringe with 120mm needle.
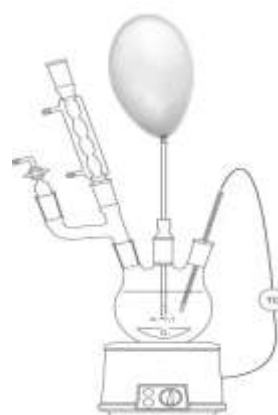
Fig. 2. 4 Schematic view of reflux condenser reactor setup.

2.2.3 Electrocatalytic cell setup

Electrocatalytic studies were conducted in two types of electrochemical cell setup.

2.2.3.1 Batch-type cell with three electrodes

Liquid phase electrochemical reactions were conducted in a batch type three electrode electrochemical cell. The cell was made up of glass with water circulation jacket and a closed head with five provisions as shown in fig. 2. 5 : 1) lugging capillary for reference electrode, 2) working electrode, 3) counter electrode, 4) gas bubbling and 5) gas outlet or blanketing or sampling. The electrolyte was stirred using controllable magnetic stirrer. The whole setup was kept on magnetic stirrer assembly. Fig. 2. 5 shows hot water circulation pump to the water jacket of the cell to heat the electrolyte at a desire temperature. Gamry reference potentiostat 600 series has been used for variation of potential and current during electrochemical reaction as shown in fig. 2. 5 . The working

electrode, reference electrode and counter electrodes are properly connected to potentiostat to regulate current density or voltage. The data was recorded using Gamry framework and analyzed by Gamry Echem Analyst software.

Fig. 2. 5 Three electrode electrochemical cell setup; a) Gamry reference potentiostat 600 series; b) electrochemical cell with five provisions on magnetic stirrer; c) hot water circulation for heating the cell.

2.2.3.2 Continues flow-type cell with two electrodes.

Fig. 2. 6a shows continuous flow-type cell with liquid pump, gamry potentiostat and electrode assembly. The setup contains anode, cathode sandwiched with catalyst coated membrane. The electrolyte was pumped through micro-channels of the anode and collected at the exit side. Constant current was applied using gamry potentiostat to maintain the potential at catalyst interface. The cell was under leak proof conditions.
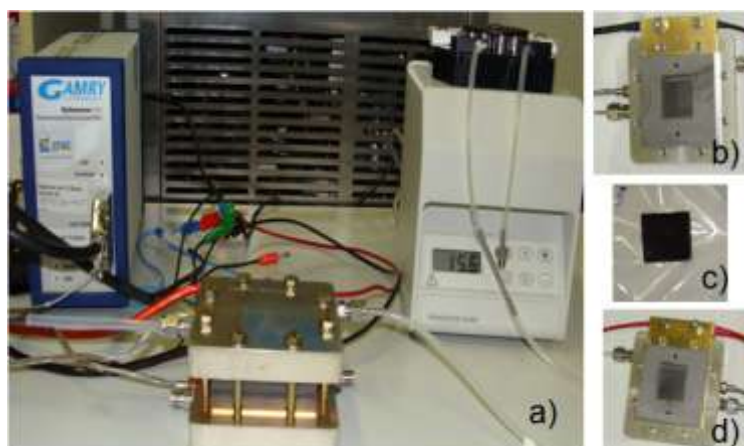
Fig. 2. 6 Continues flow-type cell; a) cell setup with pump and potentiostat; b) anode side flow channel; c) catalyst coated membrane; c) cathode side flow channel.

2.2.4 NMR

NMR spectra were recorded on a Bruker AC 500 (^{1}H, 500 MHz; ^{13}C, 125 MHz). NMR samples were prepared by dissolving solid compounds (e.g. 5mM HMF) into D_2O, $CDCl_3$ and 1M NaOD solvents. The required pH was obtained by mixing NaOD in D_2O. For *in-situ* NMR studies, the sample was purged with N_2 gas about 10 min and sealed. Throughout (kinetic) the measurement, the sample probe was maintained at 50°C. NMR scanning was recorded for every 1 hour over 10 hours.

2.2.5 HPLC-MS

High pressure liquid chromatography–mass spectrometry (LC-MS) was brought from Agilent technologies 6120 series. The equipment contains 1) degasser 2) binary pump 3) auto-sampler 4) thermostat 5) UV detector 6) RI detector 7) MS detector 8) chemstation software interface. Aglent's (1200 series) HPLC has been used to pump the solvent

Fig. 2. 7 HPLC coupled with MS (LC-MS).

and to inject the sample using an auto-sampler. The separation of compounds was achieved by using an 'Organic Acid' column (8mm x 300mm) from Klaus Zeimer GmbH (part# 7.528 980 30), solvent (0.1% formic acid in millipore water), flow rate 1 ml/min using isocratic pump and column temperature is 60°C. The calibration chart was prepared using pure chemicals. The Agilent's single quadrupole mass spectrometer (6120 series) was equipped with multimode ionization (electrospray ionization (ESI) + atmospheric pressure chemical ionization (APCI)) source. The following operating conditions were used. Drying gas flow: 12l/min; nebulizer pressure 40 psig; drying gas temperature 350°C; vaporizer temperature 250°C; capillary voltage + 1000V & -2500V; corona current +2μA & -4μA; charging voltage +2000V & -2000V. The organic molecules are ionized in multimode source and mass (m/z) of the species scanned from 50 to 800 in both positive and negative polarity to identify the specific molecule.

2.2.6 GC

Samples were periodically withdrawn from the reaction mixture to analyze the concentrations product distribution. Quantitative analysis of the reaction species was carried out by the gas chromatography (GC) on Shimadzu 2010 plus instrument equipped with a HP-5 (30m, 0.25 mm, $1\mu m$) column using helium as the carrier gas, with the ame ionization detector set at 250^oC and injector set at 250^oC. The oven temperature was

Fig. 2. 8 Gas chromatography (GC) equipped with auto-sampler.

maintained at 60^oC for 5 min to start with and then ramped to 120^oC at 10^oC min^{-1} and finally to 250^oC at 20^oC min^{-1} where it was held for 10 min.

2.2.7 XRD

XRD profiles were measured with a D8 Advanced X-ray diffractometer (Bruker AXS) equipped with a position sensitive LynxEye detector (PSD) and a Cu Kα source, operated at 40 kV / 40 mA. The following scan parameters were used: $2\Theta = 15^o–80^o$, step size = 0.01^o, holding time per step = 10s, variable divergence slit = 4 mm, PSD Iris = 13 and

Fig. 2. 9 XRD.

sample rotation = 15 rpm. The crystal phase Rietveld quantification and crystallite size were established with TOPAS (Bruker AXS, Version 4-2).

2.2.8 TEM

The morphology of Pt/C was observed through the transmission electron microscopy (TEM), FEI TECNAI G² 20 S-TWIN equipped with energy dispersive X-ray spectroscopy (EDS) and GATAN MS794 P CCD-Camera. TEM was operated by the accelerating voltage of 200 kV. The optimal resolution of this microscopy is 0.24 nm in Bright field. An aliquot of catalyst in ethanol was pipette on a Cu grid with holey carbon film (PLANO, Germany) and dried in air. The analysis of the TEM images was carried out with imageJ software to determine the particle size distribution by counting more than 200 particles of carbon supported platinum nanoparticles.

2.2.9   BET

The surface areas of different supported metal catalyst were determined by nitrogen adsorption and desorption measurements at liquid nitrogen temperature using Quantachrome Autosorb-1-C. Prior to adsorption, the samples were degassed in vacuum at 200°C for 4h. Specific surface areas were calculated from the Brunauer_Emmett_Teller (BET) method.

2.3 Synthesis of heterogeneous catalyst

2.3.1   Solid acid catalyst (SAC) using chlorosulfuric acid

In order to attach the SO_3H-group covalently to the surface, an excess of chlorosulfuric acid was added (mole ratio 4:1) to hydroxysilane (4.542 ml/g Si-OH), hydroxy titanium (3.32 ml/g Ti-OH) and zirconium hydroxide (1.69 ml /g $Zr(OH)_4$) independently. The suspension was stirred at room temperature for about 8 hours. Milli-Q water was added to the suspension to stop the reaction. The suspension was filtered and washed thoroughly with the Milli-Q water and dried in a freeze dryer (Labconco) [1].

$$SiH_3\text{-}OH + Cl\text{-}SO_3H \longrightarrow Si\text{-}O\text{-}SO_3H + HCl$$

$$Ti\text{-}OH + Cl\text{-}SO_3H \longrightarrow Ti\text{-}O\text{-}SO3H + HCl$$

$$Zr(OH)_4 + 4\ Cl\text{-}SO_3H \longrightarrow Zr\text{-}O\text{-}(SO_3H)_4 + HCl$$
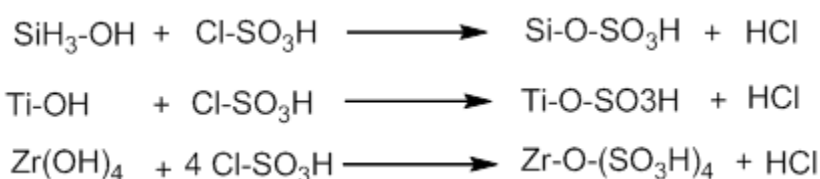
Fig. 2. 10 Sulfonation using chloro-sulfonic acid.

2.3.2   SAC using 4-chlorobenzenesulfuric acid

4-Chlorobenzenesulfuric acid is solid at room temperature. 4-chlorobenzenesulfuric acid was melted at 115°C in order to react with solid support. 6.4 g, 4.85 g and 4.89 g of 4-chlorobenzenesulfuric acid were added to 1g SiH_3-OH (molar ratio 2:1), 1 g Ti-OH (molar ratio 2:1) and 1g $Zr(OH)_4$ (molar ratio 4:1) respectively. They were stirred for about 8 hours at 115 °C. Then suspension was washed thoroughly with Milli-Q water and dried with a freeze dryer.

Fig. 2. 11 Preparation of chlorobenzenesulfuric acid functionalized catalyst. M= Si-OH, Ti-OH, $Zr(OH)_4.$

2.3.3 SAC using 3-mercaptopropyl)trimethoxysilane (MPTMS)

The suspension of silicondioxide (5 g), titaniumdioxide (5 g) and zirconiate-trahydroxide (5 g) are prepared using dry Toluene (320 ml). 0.47 ml of MPTMS was added to the suspension and stirred with magnetic stirrer. It was heated to 110 °C under reflux for 18 hours. The last 30 minutes of the suspension was heated to 120 °C. The suspension was filtered and washed with 30 ml toluene and dried over night at 110 °C. H_2O_2 (30%, 25 ml) and one drop of a solution of H_2SO_4 in 25 ml Methanol were added to the dried powder. The suspension was stirred at room temperature for another 12 hours. After that it was filtered and washed three times with Milli-Q water (50 ml). The solid was dissolved in a 10 wt% H_2SO_4 solution (30 ml) for 4 hours. The solid was filtered and dried at 120 °C over night [2].

A second batch was prepared using MPTMS (1,86 ml) and
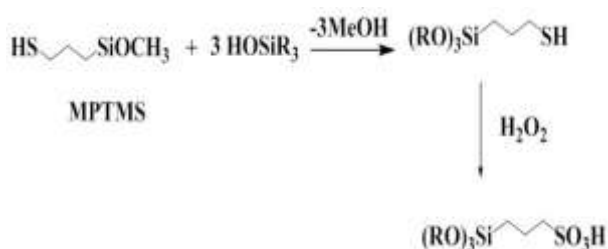
Fig. 2. 12 Preparation of MPTMS-SBA-15.

Zirconiatetrahydroxide (5 g) in dry Toluene (150 ml) at similar conditions. For the oxidation H_2O_2 (30%, 43 ml) was used and for the protonation two drops of of H_2SO_4 in Methanol (15 ml). After the preparation the catalyst was washed successively with toluene (5 ml), acetone (5 ml), ethanol (5 ml), ethanol/water (1:1,v/v) (5 ml), water (5 ml), ethanol (5 ml), acetone (5 ml) and pentane (5 ml) [3]. The reaction proceeds similar for $Zr(OH)_4$ and TiO_2.

2.3.4 TESAS-SBA-15

Pluronic P123 (2.00 g) was dissolved in a mixture of distilled water (30 g) and a 2 M aqueous HCl (60 g) with continuous stirring and heated to 35 °C. After P123 was fully dissolved, a freshly prepared 1 wt % aqueous poly(vinyl alcohol) (PVA; Mav = 130 000) was added in different amounts. To this solution tetraethoxysilane (1.05 g) was added and the resulting mixture was kept at 35 °C for 24 h, subsequently poured into a Teflon-lined autoclave, and aged at 80-150 °C for another 24 h. After 30 min, NaCl (425 mg, 7.33 mmol) was added to the reaction mixture, to produce a 0.10 M solution. After 1 h, solid NaTESAS (700 mg, 2.06 mmol) was added in 44 mg increments every 15 min for 4 h. Twenty hours later, the reaction mixture was divided equally among three Parr bombs (30 mL) fitted with Teflon liners. Each was heated at 100 °C for 24 h.

27

The resulting suspensions were filtered, washed with water, and air-dried. The surfactant was removed by refluxing TESAS-SBA-15 (1.30 g) in slightly acidified ethanol (500 ml) for 15 h. The solid was recovered by vacuum filtration and washed with ethanol (200 ml). The extraction process was performed once more on the filtrate. The resulting solid was washed with water and suspended in HCl (2M,100 ml). After 3 h, the solid was collected and washed with water until the pH of the water was neutral. The solid was dried at 60 °C in air overnight, then at 150 °C under vacuum (0.1 mTorr) for 12 h.
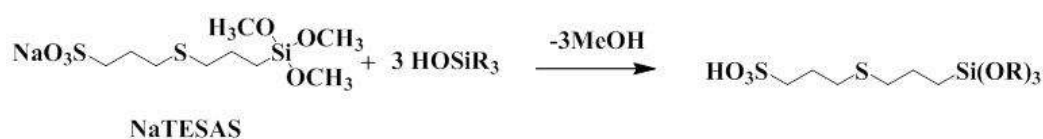
Fig. 2. 13 Preparation of TESAS-SBA15.

2.3.5 Synthesis of Covalent Triazine Frameworks (CTFs)

The respective monomer and the metal salt were transferred into a quartz ampoule (3x12cm) under an inert atmosphere. The ampoules were evacuated, sealed and heated to 400°C for 20h (CTF-1) while 400°C & 600°C for 20h & 20h (CTF-HSA). The ampoule was then cooled down to room temperature and opened. The reaction mixture was subsequently grounded and then washed thoroughly with water to remove most of the $ZnCl_2$. Further stirring in diluted HCl for 15 h was carried out to remove the residual salt. After this purification step, the resulting black powder was filtered, washed successively with water and THF and dried in vacuum at 150 °C.

The sulfonation of the CTF (0.3 g) was carried out in a Teflon container set in a Teflon-lined autoclave where the powders were contacted with the vapor from 4 ml 60% SO3/H2SO4 at 333 K for 24 h. The sulfonated samples were stirred and filtered 2 times with hot distilled water (>353 K), then with HCl (1N) and finally washed with water and dried at 373 K overnight in air.
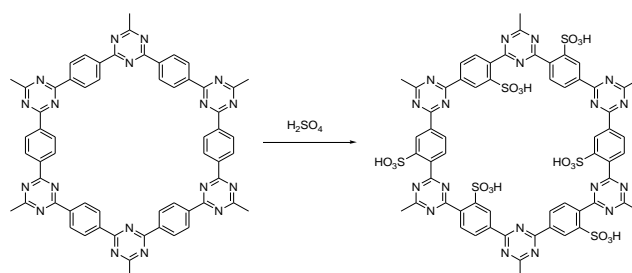
Fig. 2. 14 Sulfonation of the CTFs.

2.4 Electrodes preparation

2.4.1 Metal foil electrode

The working electrode is made-up of pure Pt, Pd, Ni, Cu foil (4.5 cm^2)$_{geo}$ and connected by pure Pt, Pd, Ni, Cu metal wire respectively. The working electrode is cleaned after each experiment by staying few seconds at over potential (2.5 V/RHE) to oxidize the adsorbed organic species. After that the working electrode is cleaned using nitric acid, acetone, ethanol under ultrasonification and rinsed with milli-Q water after each cleaning step [4, 5].

2.4.2 High surface area electrode

Measured catalyst powder (46.7% Pt/vulcan) between 0.1–0.15g was added to 0.5ml DI water to avoid catalyst burning. The slurry was mixed with iso-propanol (10–15 min refrigeration), the amount is 33 vol.% (in L) of the catalyst weight. The solution is stirred continuously for 15 min with a magnetic stirrer. Thereafter the solution is sonicated for 1 h, followed by addition of 33 wt% Nafion (5 wt%, DE 521) with further sonication of 1 h. An ethyele tetrafluroethylene (ETFE) film of size 33×33 was used to coat the ink. About 10 ml of ink is poured in a straight line, and the mayer rod is dragged through the ink with a gentle vertical pressure quickly without letting the ink dry. This coating was allowed for 15 min to dry in the air. After drying, required amount of electrode was carefully cut off with sharp blade. Anode an cathode were prepared separately by sandwich assembly with the ink coating film, gylcon pads, krpton films and nafion membrane. This assembly was arranged in between aluminum plates abd pressed ay 145°C with 5000lb load for 4min. After that system was cooled to room temperature and collected anode or cathode on nafion membrane to test for their electrocatalytic activity.

2.4.3 Reference and counter electrodes

The reference electrode used in electrochemical experiments is Reversible hydrogen electrode (RHE). It is a commercial one. It was brought from Gaskatel GmbH (HydroFlex, http://www.gaskatel.de/). The US patent number is 5407555. This reference electrode (RHE) is constructed by using small sheet of Pt mesh, PTFE (Polytetrafluoroethylene) tube with diameter of approx. 8 mm and hydrogen cartridge. This is liquid free electrode and hydrogen gas is always circulated on Pt mesh. There is no fluid electrolyte inside reference electrode. We can use it without an additional electrolyte bridge. Counter electrode is pure Pt gaze (100 mesh) connected by pure Pt

wire. Counter electrode is also cleaned after each experiment using nitric acid, acetone, ethanol and subsequent rinsing with water.

2.5 Preparation of active metal catalyst

Heterogeneous catalyst has been used in order to study the HMF oxidation and hydrogenation. Supported metal catalysts were synthesized by adding metal precursor into weighted amount of commercial support (activated carbon, vulcan, etc. Slurry is made with the support powder and metal precursor mixture. The mixture is then freeze-dried and annealed.   For the synthesis of supported catalysts, the precursor for Pt is dihydrogen hexachloroplatinate(IV) hydrate ($H_2PtCl_6.6H_2O$, 99.999%), Ru is $RuCl_3.3H_2O$, Ni is $Ni(NO_3)_2.6H_2O$, Pd is $N_2O_6Pd.2H_2O$, Rh is $Rh_2(OOCCH_3)_4$.

2.5.1 Synthesis Methodology

The required amount of metal precursor combined in 20 ml isopropanol vials. 5 ml of de-ionized water is then pipetted into the vials. The mixture is sonicated for 5 min to produce thick and shiny slurry. The slurry is frozen by partially submerging the vials into a cryo-tray of liquid nitrogen for at least 15 min. After at least 5 min and when the liquid nitrogen has stopped bubbling vigorously (liquid nitrogen in contact with the vial walls will boil-off upon submerging the vials due to the great disparity of temperature between the vials and liquid nitrogen), the cryo-tray is brought to the freeze-drier (LABCONCO). The vials are then transferred into the Bulk Tray Drier. A thermostat is put in contact with one of the vials so that the temperature of the vials can be monitored over the period of the freezedrying process. The Bulk Tray Drier's door is then sealed and the freeze-drier is evacuated to 50 mTorr. The set-up is left overnight for the slow freeze-drying to complete. The process is completed when the temperature of the vials have reached room temperature
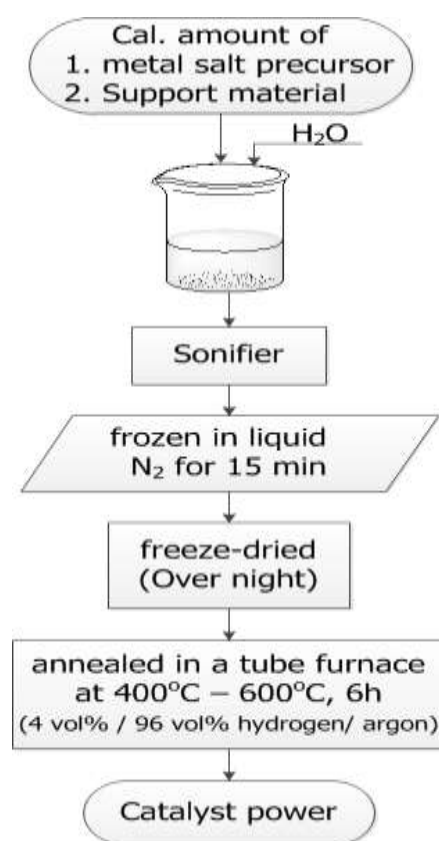
Fig.   2. 15 Synthesis procedure for supported metal catalyst.

again. When the freeze-drying process is complete, the samples look like cakes of black powder that crumbles on contact. The samples are transferred into the individual

rectangular alumina boats and covered partially with an alumina lid, leaving about 5 – 10% opening for gas flow, before being inserted into the quartz tube of the flow furnace. The annealing protocol is then set up on the temperature control console. The "Start" button is then clicked to start the protocol. Regardless of the annealing conditions, the hydrogen gas (6% hydrogen and Argon mix, laboratory certified grade, from Matheson Tri-gas) flowed at room temperature in the first hour is to de-aerate the quartz tube of oxygen. The presence of oxygen will result in the burning off of the carbon support. After the first hour, the temperature is increased to $250^{0}C$ at a rate of $10^{0}C/min$ and held at the high temperature for 2 hours. This is to decompose the anions that are present in the metal precursor or other impurities contamination of the samples. After the 2 hours temperature hold at $250^{0}C$, the temperature is raised again to the respective annealing temperature ($450^{0}C$ or $600^{0}C$) for the required amount of time 6 h. During this period, the samples are annealed at the chosen conditions.

Depending on the temperature and duration of the annealing process, the particle size distributions, final catalyst compositions (dependent on how complete the alloying process is) and catalytic activities are fixed. When the annealing process ends, the furnace is left to cool down to the room temperature via natural convection. Once the furnace reaches room temperature, the gas flow is stopped and the quartz tube is opened to allow air to enter. The catalysts are left in the quartz tube, exposed to air for at least half an hour before they were taken out of the quartz tube and transferred into glass vials where they will be stored under desiccated environment. Fine platinum particles are very much prone to sparks especially when exposed to friction, heat source or sudden contact with oxidizer. The exposure to air inside the quartz tube is to allow the catalysts to reach equilibrium in air (20% oxygen) so as to prevent sparks from occurring when the catalysts are removed from the furnace. The graphical representation of synthesis procedure is as shown in fig. 2. 15.

2.6 Analytical method development

Analytical methods were developed to separate different molecules in the reaction mixture and to estimate percentage of product distribution. HPLC-MS equipped with UV, RI and mass detector have been used for quantification & qualification of product distribution.

2.6.1. Fructose
Fructose was separated from the reaction mixture by using Organic acid column from Klaus Ziemer GmbH [300×8 mm], injection volume is 10 μL, column temperature $60^{o}C$,

flow rate is 1mL/min and mobile phase is 0.1% formic acid in water. Fructose was the detected using refractive index detector.

2.6.2. HMF, HMFC,FDC, FFCA, FDCA

HMF and its oxidative products such as HMFC, FFCA, FDC, FDCA were separated and analyzed using ion exchange column from Klaus Ziemer GmbH [300×8 mm], injection volume is 10 µL, column temperature 60°C, flow rate is 1mL/min and mobile phase is 0.1 (vol).% formic acid in water. All products were detected at 265nm wavelength of UV-Vis. Separation of all products were shown in the fig.2. 16

1) 2,5 furandicarboxylic acid (FDCA)
2) 5-formyl furan 2-carboxylic acid (FFCA)
3) 5- hydroxymethyl 2-carboxylic acid (HMFC)
4) 5-hydroxymethyl-2-furfural (HMF)
5) 2,5 furandicarbaldehye (FDC)
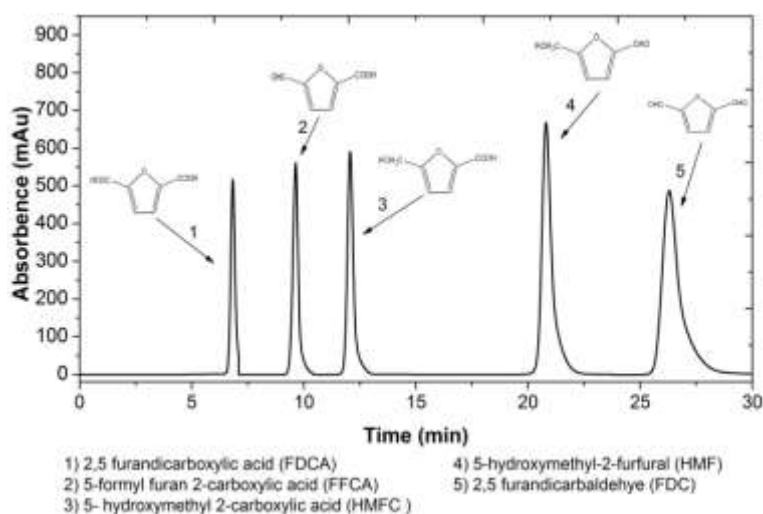
Fig. 2. 16 HPLC spectrum of HMF oxidative derivatives.

2.6.3. DMF, BHMTHF, BHMF, BHMTHF

HMF hydrogenation products were separated and analysed using Agilent Zorbax XDB C-18 from Agilent technologies. Conditions were injection volume was 10 µL, column temperature 40°C, flow rate is 0.8mL/min and mobile phase was 50% (vol) acetonitrile in water. The compounds were detected at 221nm wavelength of UV and refractive index detector (35°C) as shown fig. 2. 17. GC was also used to confirm the products.

2.6.4. MS detector

The Agilent's single quadrupole mass spectrometer (6120 series) was equipped with the multimode ionization (electrospray ionization (ESI) + Atmospheric pressure chemical ionization (*APCl*)) source. The following operating conditions were used. Drying gas flow: 12l/min; nebulizer pressure 40psig; drying gas temperature 350°C; vaporizer temperature 250°C; capillary voltage + 1000V & -2500V; Corona current +2µA & -4µA; Charging voltage +2000V & -2000V.

The organic molecules are ionized in the multimode source and mass (m/z) of the species was scanned from 50 to 800 in both positive and negative polarity to identify the specific compound. Mass spectrum of some important species are shown in fig. 2. 16 .
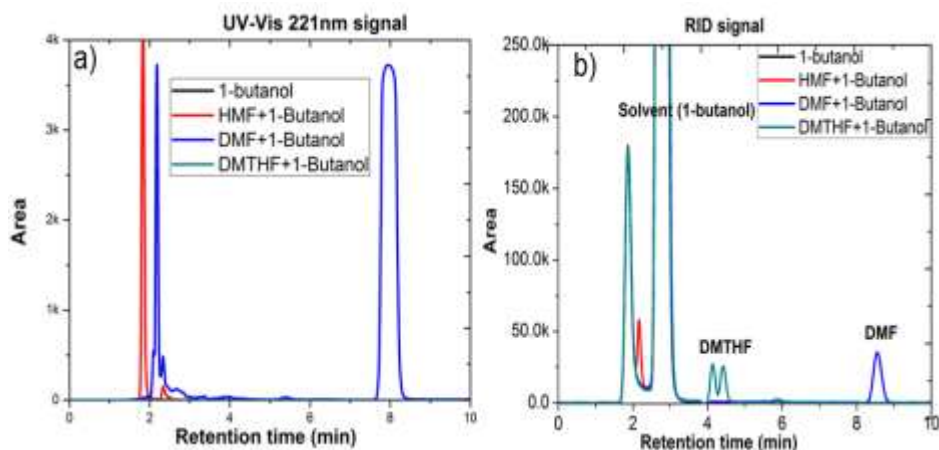
Fig. 2. 17 HMF hydrogenation products separation and detection; a)UV-Vis signals; b)RID signals.
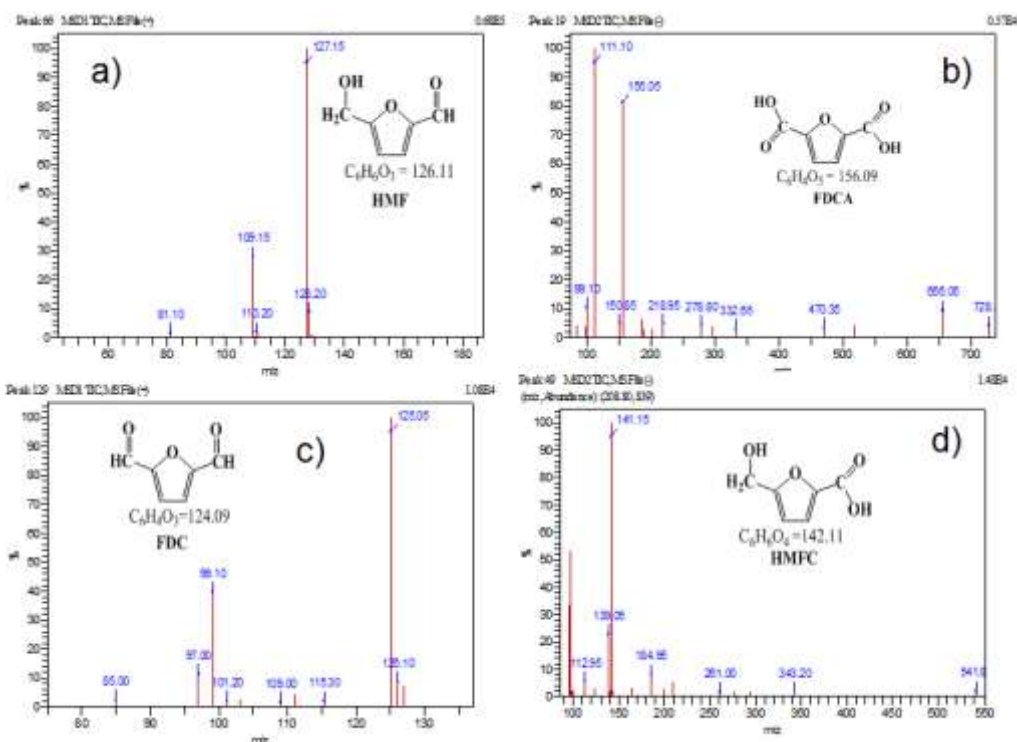
Fig. 2. 18 Qualitative to information of HMF and its derivatives. a) Mass spectrum of HMF; m/z =127 (M+H). Where M = molecule; H = proton; b) Mass spectrum of FDCA; m/z =155 (M-H); Fragmented ion = loss of CO_2 (44) = (m/z)111; c) Mass spectrum of FDC; m/z =125 (M+H); d) Mass spectrum of HMFC; m/z =142 (M-H); Fragmented ion = loss of CO_2 (44) = (m/z).

2.7 Dehydration of fructose

The dehydration reactions were carried out in a 100 ml two neck glass-reactor with a reflux condenser at a range of temperature between 40 °C and 140 °C depending on the solvent. The reactor was submerged in stirred silicon oil bath to maintain uniform temperature during the reaction. A magnetic stirrer was used at 1000 rpm. The starting concentration of fructose was 10, 25 or 50 mM. The condenser was sealed with a N_2 balloon. The reaction time was between 3 and 6 hours, however 4 h results were used for comparison. The fructose conversion was calculated as moles of fructose reacted per moles of fructose fed. The HMF selectivity was calculated as moles of HMF produced per mole of fructose reacted. The reaction mixture was separated using organic acid HPLC column and the detected by UV, RID detectors. The calibration chart was prepared using pure standards. Unknowns were estimated using the prepared calibration chart (see appendix). Conversion of reactant, yield and selectivity of product were calculated using equations 2.1, 2.2 and 2.3 [6].

.

$$\text{Conversion of "Bio"(\%)} = \frac{\text{Moles of "Bio" disappeared}}{\text{Moles of "Bio" initial}} \times 100 \dots\dots\dots\dots (2.1)$$

$$\text{Yield of product } x(\%) = \frac{\text{Moles of } x \text{ formed}}{\text{Moles of "Bio" intial}} \times 100 \dots\dots\dots\dots\dots\dots (2.2)$$

$$\text{Selectivity of product } x (\%) = \frac{\text{Moles of } x \text{ formed}}{\text{Moles of "Bio" disappeared}} \times 100 \dots (2.3)$$

2.8 Heterogeneous catalytic oxidation of HMF

5mM (0.25mmol) HMF was dissolved in 50ml of aqueous solution. Required amount of NaOH was added to 50ml of an aqueous solvent, e.g. pH 13 aqueous solvent contains 5mmol (0.1M) NaOH. Then, a calculated amount of supported metal catalyst was added to the above aqueous solution. The reactant mixture was charged to semi-batch autoclave reactor (see section 2.2). The reactor was closed and stirred at 1000 rpm to mix all the reactants and catalyst. At the same time reactor was pressurized 3 times to 2 bars with O_2 gas and released to provide purely O_2 reacting environment, and then pressurized to the required pressure. Throughout this paper, pressure is referred as gauge pressure. The reactor was heated or cooled to a desired temperature by oil circulation using Huber thermostat. After regular intervals of time, the reactor was cooled to 30^oC to take 50μl of reaction mixture using syringe. The reaction mixture was

filtered using micro filters (13 mm HPLC Syringe Filter, PTFE, 0,2µm). 10µl sample was injected in LC-MS for quantification and qualification of unknown compounds (see appendix). The conversion of reactant (HMF), yield and selectivity of product (FDCA, FDC, etc) were calculated using equations 2.1, 2.2 and 2.3.

2.9 Heterogeneous catalytic hydrogenation of HMF

Hydrogenation of HMF was carried out using semi-batch reactor. 20ml of aqueous or organic solvents was used to mix 0.1M HMF with supported metal catalyst. The reaction mixture was stirred at 1000rpm and stated stepwise to 175°C. Different hydrogen and pressures were used. Over the reaction time, the sample was cooled to the room temperature using water circulation and analyzed using LC-MS or GC. The unknowns of reaction mixture were identified using calibration chart of standard compounds (see appendix). Conversion of reactant, yield and selectivity of product were calculated using equations 2.1, 2.2 and 2.3.

2.10   Electrocatalytic oxidation of HMF

0.3M $NaClO_4$+0.1mM NaOH (pH10) was chosen as electrolyte where HMF is stable and $NaClO_4$ makes the electrolyte more conductive. Working electrode, counter electrode and reference electrode were connected to the potentiostat. 5mM HMF was added to the electrolyte and stirred with magnetic stirrer. The electrolyte was purged with nitrogen gas and then blanketed. Desired potential or current was applied using potentostat. Reaction mixture was drawn at regular intervals of time and analyzed. The qualitative and quantitative information obtained by analysis of reaction mixture was conducted using   Agilent's (6120 series) LC-MS equipped with UV/Vis and MS detectors. The separation of compounds was achieved by using 'Organic Acid' column (8mm x 300mm) from Klaus Zeimer GmbH, solvent (0.1% formic acid in Millipore water), flow rate 1 ml/min using isocratic pump and column temperature 60°C. The calibration chart was prepared using pure standard chemicals (see appendix). Conversion of reactant, yield and selectivity of product were calculated using equations 2.1, 2.2 and 2.3.

Faradaic efficiency for formation of FDC from HMF oxidation was calculated using Faraday's 1st law of electrolysis (The mass of a substance altered at an electrode

during electrolysis is directly proportional to the quantity of electrical charge (coulomb) at that electrode) as shown in equation 2.4.

$$\text{Faradaic efficiency } (F_{eff}) \text{ for FDC yield } (\%) = \frac{\text{Mass of FDC from HPLC (experiment t)}}{I \times t} \times 100 \quad ......(2.4)$$

Where I = current in A, t = time in sec.

2.11   Electrocatalytic hydrogenation of HMF

Biphasic system and contains 50ml of aqueous conducting electrolyte (0.3M $NaClO_4$+0.1mM NaOH) and 20ml of 1-butanol. 5mM HMF was added to three electrode electrochemical cell and applied constant current of -10mA. Different metal foil electrodes were used to test the HMF hydrogenation. Reactions were carried out at room temperature under N_2 atmosphere. After the reaction, organic phase and aqueous phase were separated using separating funnel and analysed separately using HPLC. The unknown amount of products in the reaction mixture were estimated using standard calibration chart (see appendix). Conversion of reactant, yield and selectivity of product were calculated using equations 2.1, 2.2 and 2.3.

2.12   Electrochemical methods

2.12.1. Cyclic voltammetry

The electrochemical behavior of a metal can be obtained through a series of steps to different potentials by recording current-time curves. Cyclic voltammetry (CV) or potentiodynamic cycling is an electrochemical technique in which potential of the polarized electrode is scanned between two potential windows and the current response of the electrochemical system is measured to obtain different surface reactions taking place on the electrode. The relationship between the passage of the charge and the applied potentials yields information about the processes occurring as a function of the relative free energy changes in the system. Potential sweep technique such as CV has been applied to understand the potential at which the process occurs with the type of adsorption, state of oxidation of the molecule and degree of purity of the system. These preliminary studies are also helpful to choose the oxidation potentials of a particular compound.

2.12.2. Chronopotentiometry

A particular constant current density is applied to the electrode, and the potential variation is followed as a function of time. When there is no electrode reaction, the entire current is a nonfaradaic charging current. As shown in fig. 2.20 E vs. t curve is represents chronopotentiometry behavior.
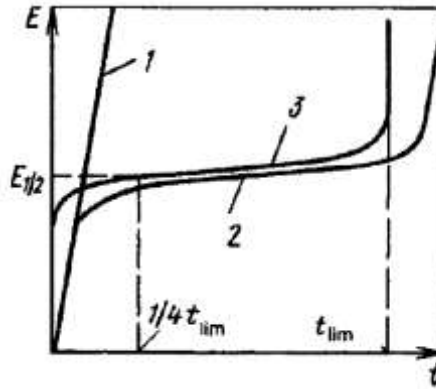
Fig. 2. 19 Galvanostatic curves: (1) without a reaction; (2) with a reaction; (3) corrected.

When an electrode reaction takes place, the applied current is divided between the non-faradaic components and a faradaic component. Because of the latter, there is a gradual decrease in surface concentration of the reactant. When the time, t, required for diffusion to change from transient to steady is large compared to the transition time t_{lim}, the reactant's surface concentration will fall to zero within the time t_{lim} Consider the shape of the E vs. t relation for the cathodic reaction $Ox + ne^- \rightarrow$ Red, and assume that the initial product concentration $C_v=0$. Assume further that the share of non-faradcaic current is small and that all the applied current can be regarded as faradaic. In reversible reactions the electrode potential is determined by the values of C_s, ox and $C_{s,red}$. Prior to current flow the potential is highly positive since $C_{s,red}=C_{v,red}=0$. When the current has been turned on, the changes in surface concentrations are determined by equation 2.5

$$C_s = C_v \left[1 - \left(\frac{t}{t_{lim}} \right)^{1/2} \right] \qquad \ldots\ldots\ldots\ldots (2.5)$$

Substituting these values into the Nernst equation, we obtain equation (2.6)

$$E = E_{1/4} + \frac{RT}{nF} \ln \frac{t_{lim}^{1/2} - t^{1/2}}{t^{1/2}} \qquad \ldots\ldots\ldots (2.6)$$

The relation between E and t is S-shaped (curve 2 in fig. 2.20). In the initial part we see the non-faradaic charging current. The faradaic process starts when certain values of potential are attained, and a typical potential "arrest" arises in the curve. When zero reactant concentration is approached, the potential again moves strongly in the negative direction (toward potentials where a new electrode reaction will start, e.g., cathodic hydrogen evolution). It thus becomes possible to determine the transition time t_{lim} precisely. When the non-faradaic current is not small enough, the appropriate correction must be included when constructing the curves. At constant current, the charge consumed is proportional to time; therefore, we can graphically correct by subtracting at each potential the time t spent for charging of the electrode (or actually, the charge) from the current value of time t (curve 3).

2.13 References

1. Salehi, Peyman, Dabiri, Minoo, Zolfigol, Mohammad Ali and Fard, Mohammad Ali Bodaghi, Silica Sulfuric Acid: An Efficient and Reusable Catalyst for the One-Pot Synthesis of 3,4-Dihydropyrimidin-2(1h)-Ones. *ChemInform*, 2003. 34(27): p. no-no.
2. Karimi, Babak and Khalkhali, Maryam, Silica Functionalized Sulfonic Acid as a Recyclable Interphase Catalyst for Chemoselective Thioacetalization of Carbonyl Compounds in Water. *Journal of Molecular Catalysis A: Chemical*, 2007. 271(1-2): p. 75-79.
3. Kailasam, K, Natile, MM, Glisenti, A and Müller, K, Fourier Transform Infrared Spectroscopy and Solid-State Nuclear Magnetic Resonance Studies of Octadecyl Modified Metal Oxides Obtained from Different Silane Precursors. *Journal of Chromatography A*, 2009. 20(1216 (12)): p. 12345-12354.
4. Jaksic, M. M., Johansen, B. and Tunold, R., Electrochemical Behaviour of Platinum in Alkaline and Acidic Solutions of Heavy and Regular Water. *International Journal of Hydrogen Energy*, 1993. 18(10): p. 817-837.
5. Ohta, K., Kawamoto, M., Mizuno, T. and Lowy, D. A., Electrochemical Reduction of Carbon Dioxide in Methanol at Ambient Temperature and Pressure. *Journal of Applied Electrochemistry*, 1998. 28(7): p. 717-724.
6. Levenspiel, Octave, Chemical Reaction Engineering. 1999. Third edition.

Chapter 3

Conversion of Lignocellulosic Biomass into HMF

3. 1.   Introduction

The era of 1st generation of biomass conversion, datable to 1996-2006, called as golden age of biofuels, when bio-ethanol from the corn and sugarcane, and bio-diesel from the lipid biomass were rapidly expended [1-3]. But, within less span of time, public cited a wide spectrum of problems like adverse effect on global food supply, collapse of environmental credibility and deforestation with bio-energy crops [4-8]. To overcome such critics, researchers and technologists focused on alternative biomass source (non-food competition). The immediate answer at the hand was woody biomass [1, 9]. This is called 2nd generation biomass conversion or advanced biomass conversion technology [10]. The uncontroversial woody plants were enormous and are highly attractive for both commercial and environmental reasons. Lignocellulosic biomass has a tremendous applications as a renewable resource for the production of fuels and chemicals [11-15]. This is very promising because it is inexpensive and readily available from crop residues and forests. From the beginning of 2006, there is an immense research attention towards conversion of lignocellulosic biomass [11-15].

3.1.1   Lignocellulosic biomass

Lignocellulosic biomass refers to the plant biomass that is mainly composed of cellulose, hemicellulose, and lignin as shown in the fig. 3.1. Lignin (15%–25%) is complex aromatic structure with p-hydroxyphenyl-propene building blocks. The average molecular weight distribution may be less than 10,000 [16, 17]. Lignin binds hemicellulose and cellulose together in plant cell walls and shields them from enzymic and chemical degradation. Lignin is an amorphous polymer composed of methoxylated phenylpropane structures such as coniferyl alcohol, sinapyl alcohol, and coumaryl alcohol [18, 19]. This compound provides plants with strength and structural rigidity as well as a hydrophobic vascular system for the transportation of water and solutes [20]. The hemicellulose and cellulose fractions are surrounded by lignin, when desired can be first depolymerized by a pretreatment step so that the cellulose and hemicellulose portions can be easily accessed for further upgrading [21]. Although lignin can be isolated, it is

not readily amenable to upgrading strategies. One option for lignin utilization is to burn it directly to produce heat and electricity. Required heat and power for the process are obtained from burning lignin and other residual solids and are sufficient to drive the biofuel production process [22, 23]. In addition, lignin can serve as a feedstock in the production of phenolic resins [24]. Pyrolysis strategies for lignin have been reported for the production of bio-oils and aromatics [25-28].
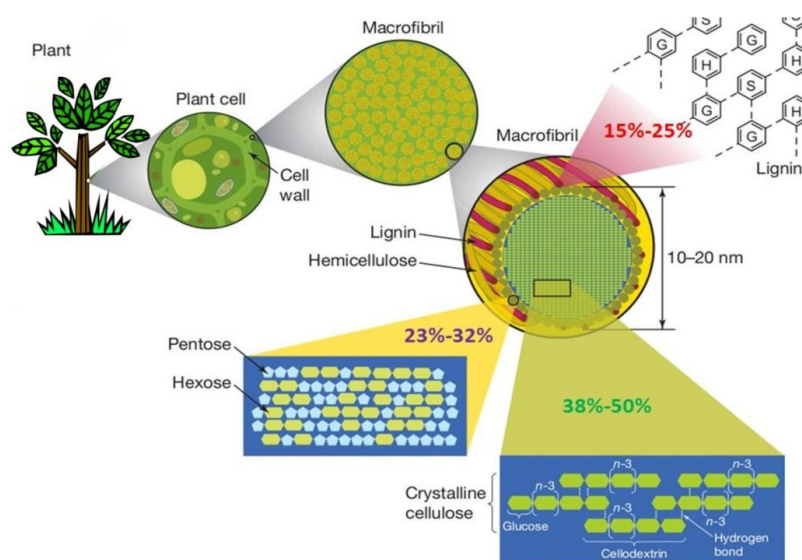
Fig. 3. 1 Composition of woody biomass and structure of cellulose.

Hemicellulose (23%–32%) is a polymer of 5- & 6-carbon sugars. It is a complex, branched and heterogeneous polymeric network, based on pentoses such as xylose and arabinose, hexoses such as glucose, mannose and galactose, and sugar acids [29]. Xylose is the second most abundant sugar in the biosphere. It has a lower molecular weight (50,000) than cellulose and its role is to connect lignin and cellulose fibers [17, 30]. If separate processing of cellulose is desired to increase the effectiveness of the hydrolysis step in the production of glucose, the hemicellulose fraction of biomass can be removed during pretreatment. The pretreatment process helps to preserve the xylose obtained from hemicellulose and inhibits the formation of degradation and dehydration products [31]. Compared to hydrolysis of crystalline cellulose, hemicellulose extraction/hydrolysis is an easier process and allows for high yields of sugar.

Cellulose (38%–50%) is most abundant form of carbon in the biosphere and polymer of glucose. Its synthesis rate is estimated approx.10^{10}-10^{11} metric tonnes per annum [32]. Cellulose is a linear polymer of high molecular weight (500,000-1,500,000) that is over-

lapped and aggregated into macroscopic fibers [30]. Cellulose is a polymer composed of glucose units linked via β-glycosidic bonds, providing the structure with a rigid crystallinity that inhibits hydrolysis [33]. Cellulose is more accessible to hydrolysis in untreated biomass before the removal of lignin and hemicellulose [34]. High yields of glucose (>90% of theoretical maximum) can be achieved by enzymatic.

Plants produce carbohydrates such as starch, cellulose, and hemicellulose and fix C, H, and O in the form of C_5 and C_6 sugar molecules. Cellulose, hemicellulose, and lignin (lignocelluloses) are constituents of wood and are nonfood materials. Therefore cellulose appears as a valuable feed stock for future biomass conversion technologies/biorefinaries [35].

Table 3.1 Composition of common lignocellulosic raw materials (wt % on dry biomass) [36].

Lignocellulosic materials	Cellulose(%)	Hemicellulose(%)	Lignin(%)
Hardwoods stems	40–55	24–40	18–25
Softwood stems	45–50	25-35	25–35
Nut shells	25–30	25–30	30–40
Corn cobs	45	35	15
Grasses	25–40	35–50	10–30
Paper	85–99	0	0–15
Wheat straw	30	50	15
Sorted refuse	60	20	20
Leaves	15–20	80–85	0
Cotton seed hairs	80–95	5–20	0
Newspaper	40–55	25–40	18–30
Waste papers from chemical pulps	60–70	10–20	5–10
Primary wastewater solids	8–15	NA	24–29
Swine waste	6	28	NA
Solid cattle manure	1.6–4.7	1.4–3.3	2.7–5.7
Coastal Bermuda grass	25	35.7	6.4
Switchgrass	45	31.4	12

3.1.2 Conversion of cellulosic biomass into sugars

As shown in the fig. 3.1, hydrogen bonds (dashed) keep all D-glucose together as polymer within and between cellulose molecules [35, 37, 38]. Breaking of these hydrogen bonds can be done by both chemical and biological methods to get sugars[35, 39, 40]. Depending on the pretreatment process used, lignin and/or hemicelluloses are removed and cellulose crystallinity is disrupted. Cellulose is hydrolyzed using cellulase

enzyme to produce sugars needed for fermentation. Due to the high cost of enzyme, focus has been on improving cellulases and decreasing the costs associated with the enzymatic hydrolysis of cellulose. Hydrolysis of cellulose requires the cooperation of three classes of cellulolytic enzymes: (1) cellobiohydrolases, (2) endo-β-1,4-glucanases, and (3) β-glucosidases. In this process, the pH is adjusted and enzymes are added to initiate cellulose hydrolysis to fermentable sugars. If hemicelluloses are also present, then additional hemicellulase enzymes are added. Hydrolysis is typically performed at pH 5 and 50°C for 24–120 h. The challenges with enzymatic hydrolysis of lignocellulose include enzyme cost, product inhibition, loss of enzyme due to binding with lignin, and denaturation or degradation. The amount and types of enzymes required strongly depend on the biomass being hydrolyzed and the type and severity of pretreatment used. In this connection, Corma et al. Dumesic and coworkers in 2007, have reviewed the possible chemical routes for the transformation of sugars into chemicals and fuels [19].
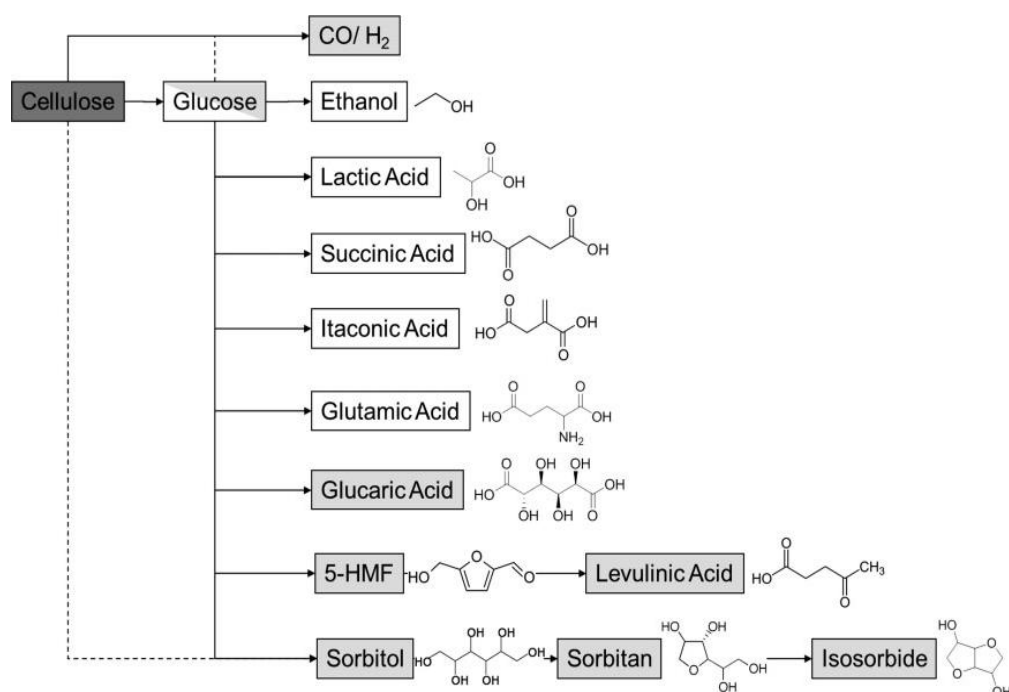
Fig. 3. 2 Value chain of cellulose to produce different platform chemicals [41].

One of the derivative of sugars is 5-hydroxymethylfurfural (HMF). Therefore we focused on catalytic chemical transformation of sugars into HMF and its derivatives.

3.1.3   HMF as a building block for the sustainable chemicals

For the sustainable future of the chemical industry requires renewable feedstocks rather than steadily depleting sources. Glucose and fructose, two abundant six-carbon sugar molecules, are potential feedstocks for this purpose, and recent efforts have focused on converting them to HMF [42]. It is a versatile intermediate between biomass-based carbohydrate chemistry and petroleum-based industrial organic chemistry [43]. HMF and its derivatives could potentially replace voluminously consumed petroleum-based building blocks, which are currently used to make plastics and fine chemicals. Recently, Dumesic and co-workers introduced the idea of using HMF as a key intermediate to produce liquid alkanes from renewable biomass resources [44]. It is a good starting point for the synthesis of precursors of pharmaceuticals, thermo-resistant polymers, and macrocyclic compounds, and particularly for the synthesis of di-aldehydes, ethers, amino alcohols, and other organic intermediates [41]. These may lead to the possibility of numerous chemical products such as solvents, surface-active agents, phytosanitary products, and resin [45]. High production cost, purity currently limits the availability and use of HMF industrially.

3.1.4   Review of technology for conversion of sugars into HMF

HMF can be obtained by the acid-catalyzed dehydration of fructose, glucose, sucrose and even cellulose [19, 46]. It was first separated with 20% yield from the reaction mixture of fructose and sucrose in the presence of oxalic acid [47]. Recently, a tandem process combining an isomerase enzyme and an acid dehydration catalyst was employed to produce HMF from glucose [48]. For these systems, the dehydration reaction is complicated by competing pathways, including reversion, fragmentation and polymerization [49]. Mineral acid catalysts such as HCl, H_2SO_4, and H_3PO_4 have been employed at temperatures ranging from 80 to 350 $^{\circ}$C [41] and a variety of chlorides & bromides of ionic liquids & metals have been used [50]. Using HCl in water, a typical selectivity for HMF from fructose is 50% at 50% conversion [49, 51], but HCl is very corrosive and handling is difficult. There are proposed mechanisms involving either acyclic or cyclic intermediates, however, isotope-labeling studies suggest that HMF is produced via three consecutive losses of water from the cyclic furanose tautomer [52]. Temperature and the presence of co-solvents play an important role in the selectivity of acid-catalyzed fructose dehydration, due to their effects on the furanose-pyranose tautomer equilibrium [53]. Cottier et al. showed that both aqueous and non-aqueous pro-

cesses lead to around 37% yield of 5-HMF; they found that the reactions performed in the aqueous solution provoke the degradation of 5-HMF and that its polymerization occurs in both aqueous and non-aqueous media [54]. Antal et al. proved that 5-HMF was formed from hexoses through removing three water molecules in the acid-catalyzed dehydration reaction [55]. The catalysts used generally for the dehydration reactions are classified as, mineral acid, organic acid, solid acid catalysts and metal-containing catalysts. Zaho et al. studied the effect of different metal chlorides such as $CrCl2$, $CrCl_3$, $FeCl_2$, $FeCl_3$, $CuCl$, $CuCl_2$, VCl_3, $MoCl_3$, $PdCl_2$, $PtCl_2$, $PtCl_4$, $RuCl_3$, $RhCl_3$ in 1-alkyl-3-methylimidazolium chloride ([AMIM]Cl) solvent and achieved HMF yields ranging from 63% to 83% from dehydration of fructose at 80°C [46].

It is easy to understand the chemical and mechanistic aspects of fructose dehydration using homogeneous liquid acid catalysts. However, there are some hidden drawbacks such as difficult to separate the products from reaction mixture, catalyst deactivation, difficult to recycle the catalyst, catalyst degradation at higher temperature, not suitable for continuous and industrial applications and difficult to control number of active sites and their effects (catalyst tuning) [56-58].

As per our observations, usage of solid acid catalysts for the fructose dehydration studies were not well focused [59, 60]. This type of studies are essential to estimate the relative performance of new materials as they become developed, which in turn helps to gain insight in to future direction. Solid acid catalysts have several advantages over metal chlorides, bromides and liquid acid catalysts in terms of handling of catalyst, recycle, operation at high temperatures and shortening the reaction time to avoid HMF degradation[60, 61], less humins formation with less reaction time, easy to adjust the surface acidity to improve the selectivity, and easy to use as support for as bi-functional catalyst synthesis [57, 58, 61-65].

Therefore, solid acid catalysts were chosen to understand the dehydration of fructose. We also aimed to select suitable support for bi-functional catalyst, which contains both acidic sites and metallic sites in order to perform both dehydration of fructose and oxidation/reduction reaction of HMF in a single reactor / process. In order to carry out these studies, variety of novel catalysts were developed and tested. Few commercial catalysts were also tested for comparative purpose.

3.1.5 Objective of this chapter

The primary goal of this chapter is to study the dehydration of fructose into HMF using heterogeneous solid acid catalysis. The objectives include finding the suitable solvent and operating conditions using homogeneous acid catalyst, synthesis of a novel solid acid catalyst by covalently bonded acid groups, optimizing the reaction conditions and testing recyclability. Finally, screening and selecting the effective support material for the development of bi-functional catalyst to carry both dehydration and oxidation/reduction reactions in a single run.

3. 2.   Dehydration reaction of fructose

Dehydration of fructose reaction is not very new in the literature. First time, in 1986 van Dam et al. [66] studied the formation of HMF by fructose dehydration using acid catalyst. The reaction was tested in different operating conditions to improve the product selectivity. More research attention was gained in the recent 8 -10 years because of its importance [42].

3.2. 1. Mechanism of fructose dehydration

The mechanism of fructose dehydration to HMF has been studied by several groups during the 20th century. The debate concerning the mechanism divided chemists into two groups, those in favor of an open chain mechanism and those advocating a mechanism involving only cyclic species. A study by Antal et al. suggested that HMF is formed from dehydration of fructose in its furanose form and occurs through a series of cyclic furan intermediates [55]. Others have suggested that HMF is formed through an acyclic mechanism proceeding through an enediol pathway [55, 67-69]. The enediol is proposed as an intermediate in the isomerization of glucose to fructose. Glucose has competing reaction pathways that lead to formation of by-products. In one pathway, dehydration forms non-furan cyclic ethers; in another, C-C bond scission occurs through reverse aldol condensation [69]. To obtain high HMF yields from glucose, effective methods for selective in situ isomerization to fructose are required.

Dehydration reactions are a subset of elimination reactions. Because the hydroxyl group (–OH) is a poor leaving group, having a brønsted acid catalyst often helps by protonating the hydroxyl group to give the better leaving group, $-OH_2^+$. Fructose is a 6-

carbon polyhydroxyketone. It is an isomer of glucose, i.e. both have the same molecular formula ($C_6H_{12}O_6$) but they differ structurally. According to Antal Jr et al., the literature contains two alternative hypotheses for the mechanism of dehydration of fructose to HMF, namely (I) a sequence of reactions commencing with and retaining the fructofuranose ring intact, and (2) a succession of reactions proceeding mainly via open-chain intermediates. The existing evidence for hypotheses (I) and (2) is reviewed and found to favor (1) as shown in fig. 3. 3 [55].
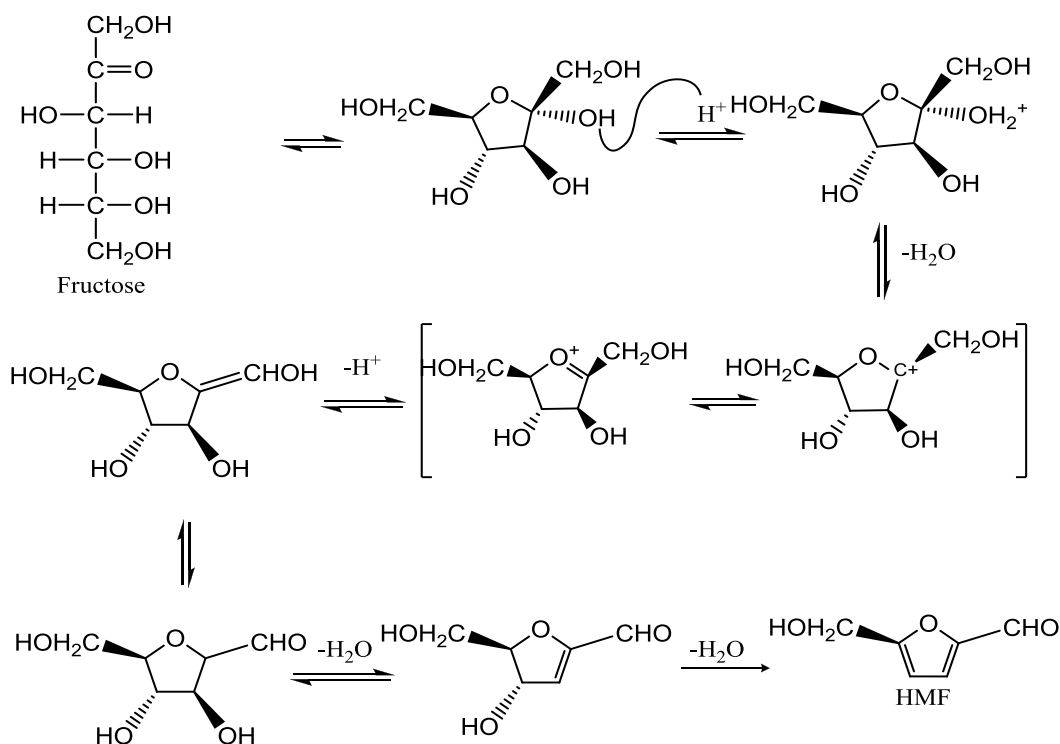
Fig. 3. 3 Proposed mechanism for fructose dehydration into HMF.

3. 3.   Results and Discussions

Initially we repeated dehydration reaction in our experimental conditions using liquid acid as a catalyst to understand the influence of different operating conditions. After that studies were continued with self prepared and commercial solid acid catalyst.

3. 3.1. Dehydration of fructose with liquid acid catalyst

The dehydration reaction of fructose into HMF was studied under homogeneous conditions using liquid acids such as CH_3COOH, HCHO, H_2SO_4 and COOH-COOH as a catalyst in order to determine better proton donor to accelerate dehydration reaction of

fructose in aqueous solvent at 100°C in stirred batch reactor. Compared to other liquid acids, H_2SO_4 shows better performance for HMF yield.

3.3.1.1. Selection of suitable solvent

In an aqueous solvent the dehydration reaction was not selective and leads to many side reactions, especially formation of colored soluble polymers and insoluble brown to black humins by cross polymerization, and further hydrolysis of HMF into levulinic acid. On the other hand, non-aqueous solvents allow getting more selective dehydration reactions of fructose and suppressing further hydration of formed HMF.
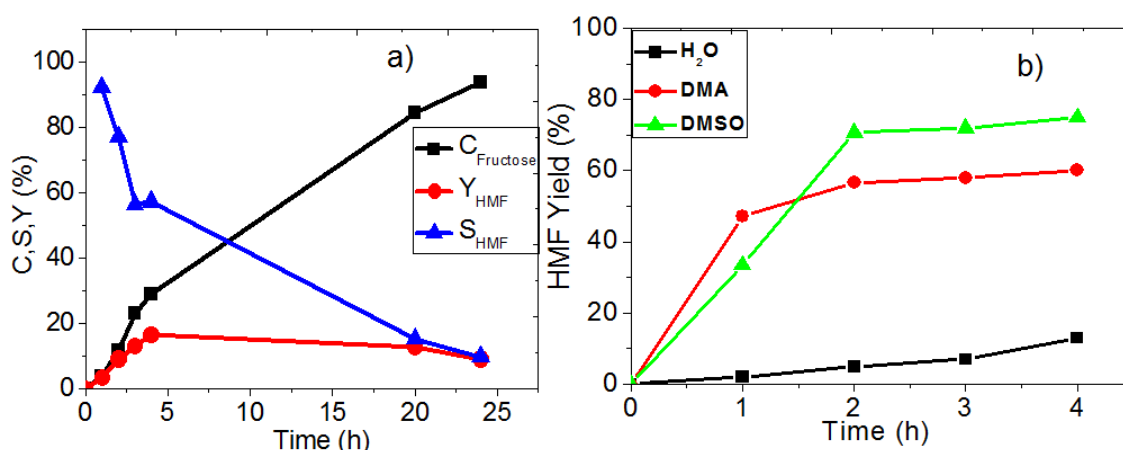
Fig. 3. 4 Fructose dehydration using liquid acid catalysts; a) in water; b) effect of solvent on dehydration of fructose using the liquid acid catalyst in different solvents. Reaction conditions: 50mM fructose in 20 ml of different solvents, 5mM H_2SO_4, 100 °C, magnetic stirrer, N_2 atmosphere.

Fig.3. 4 illustrates the effect of solvent on dehydration of fructose. The rate of formation of HMF was more in the early reaction time as shown in the fig. 3. 4a. The HMF selectivity decreased with longer (24h) reaction time and this confirms the inadequate nature of water for fructose dehydration as noticed in the literature [66, 70, 71]. Water is a bad solvent for the dehydration of fructose reaction because of cross polymerization and leads to formation of humins. Also, further hydration of HMF leads to formation of levulinic acid and formic acid in 1:1 ratio. On the other hand, non-aqueous solvents allow to get more selective dehydration reactions of fructose and suppress further hydration of formed HMF [38]. As cited in the literature [72], DMSO showed highest yield of HMF than DMA and H_2O as shown in the fig.3. 4b. The advantage of using DMSO

as solvent is that it avoids the formation of levulinic and humic acids. However, the dis-advantages of DMSO are: it is difficult to separate product from DMSO and the possi-bility to form toxic sulfur containing by-products. Another interesting solvent apart from DMSO is DMA. Fructose is stable in DMA without self-degradation even at higher tem-peratures. It is a good solvent for selective dehydration of fructose into HMF [73]. An-other non-aqueous solvent 2-butanol was also tested [49] [74], but solubility of fructose is less.

Blank reactions (in the absence of acid catalyst) were studied in order to find the stabil-ity of fructose at given reaction conditions. Fig. 3. 5 demonstrates the formation of HMF in a "blank" condition using different solvents. The stability of fructose at 100°C was constant (no conversion) in both aqueous solvent (H_2O) and non-aqueous solvent DMA, where as significant amount of HMF is observed in blank conditions [72]. DMSO alone acted as catalyst and without addition H_2SO_4 and acti ve for 35% HMF yield [71]. Therefore, the total yield of HMF in fig. 3. 4b was a combine effect of H_2SO_4 acid catalyst and DMSO solvent. As our aim is to study the effect of solid acid cata-lyst, DMSO was discarded as sol-vent for further studies.
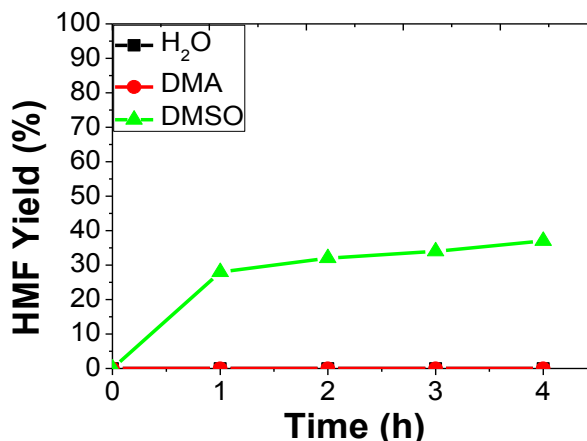
Fig. 3. 5 Fructose dehydration in "blank" conditions. Conditions: 50mM fructose, 50 ml of solven,100 °C, magnetic stirring under reflux conditions.

Amarasekara et al. explained the effect of DMSO solvent for dehydration of fructose using NMR study and proposed a mechanism as presented in fig. 3. 6 [75].

According to Amarasekara et al. [75], at a given temperature, the nucleophile of sulfur in DMSO pulls the lone pair of electrons and triggers the dehydration reaction by form-ing reactive radical species. The DMSO radical further reacts with the hydroxymethyl group and forms the unstable intermediates 2 & 3 by removing one H_2O molecule and then further dehydrates to form the dihydrofuran-2- aldehyde intermediate 4. Finally the compound reacts with another DMSO radical and forms HMF by leaving another H_2O molecule.

The NMR studies indicate that the compounds 2 & 3 are very unstable and difficult to analyze by NMR, where as the concentration of 4 increases and decreases with time and results in the increase of HMF yield. The total study suggests that DMSO alone acts as a catalyst and dehydrates fructose into HMF. The advantage of DMSO as solvent is that it is a dipolar aprotic solvent and prevents the formation of levulinic acid and humins [76].
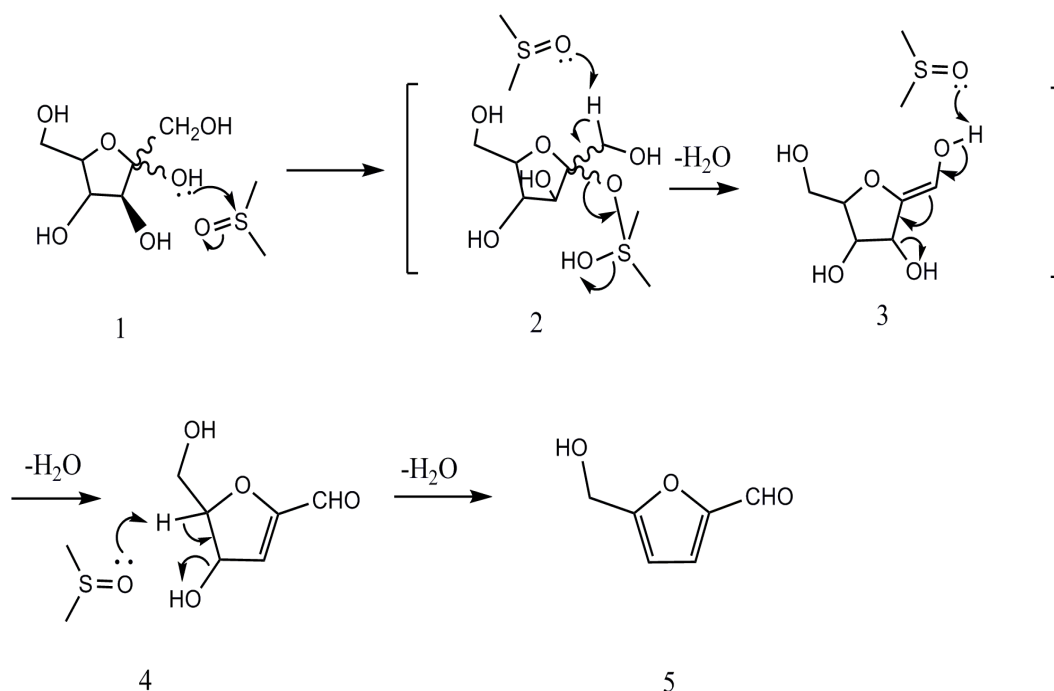
Fig. 3. 6 Mechanism of fructose dehydration reaction with DMSO.

Therefore, for all screening experiments, DMA has been chosen as the suitable solvent due to its ability to dissolve fructose at room temperature, stability (no reaction with reactants or products) at high temperature, not being a catalyst itself for dehydration reaction, cheap solvent, higher boiling point than HMF and ease of separation of products.

3.3.1.2. Effect of acid concentration on fructose dehydration

The effect of H_2SO_4 acid concentration was studied for fructose dehydration using different acid concentrations H_2SO_4 (1mM, 10 mM, and 50 mM) in DMA solvent.

Fig. 3. 7 explains that increase of acid concentration increases the fructose conversion and HMF yield. This indicates that the reaction is more favorable for HMF formation under excess acid, which means that the increase of concentration of protons increases the rate of reaction and leads to the formation of more products in less time. It was

also observed that formation of undesired soluble & non-soluble colored polymer stuff like humins were suppressed.
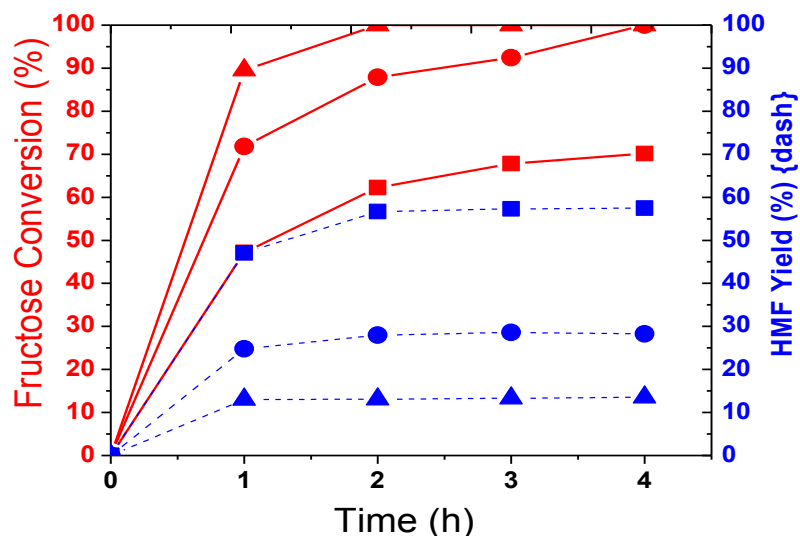
Fig. 3. 7 Effect of acid concentration in DMA solvent (where —■—1mM H_2SO_4, —●—10mM H_2SO_4, —▲—50mM H_2SO_4). Conditions: 50mM fructose, 20 ml of DMA solvent, 100°C, magnetic stirring under reflux conditions, N_2 atmosphere.

It was realized that the type of solvent and the amount of acidity have influence on dehydration of fructose. So, further studies were focused on to study the surface acidity of heterogeneous catalyst by synthesizing them from different acid sources.

3.3.2 Dehydration of fructose with solid acid catalyst

Metal oxides such as SiO_2, ZrO_4 & TiO_2 were sulfonated with different acid sources (see section 2.3) and tested for the fructose dehydration.

3.3.2.1 Sulfonated SiO_2, ZrO_4 & TiO_2 using chlorosulfonic acid

From table 3. 2 , sulfonated TiO_2 was relatively not active for fructose conversion. Whereas sulfonated SiO_2 and ZrO_4 were active for conversion of fructose. In case of sulfonated SiO_2 (surface area 30m^2/g), the reaction was not very selective for HMF formation. We assume that the activities of these catalysts were differed due to different amount of hydroxyl groups present on the surface. In case of TiO_2, the amount of available hydroxyl groups were very less (surface area <10m^2/g) to make covalent bond with sulfonic acid groups.

Table 3. 2 Dehydration of fructose using sulfonated SiO_2, ZrO_4 & TiO_2 in DMA solvent. Reaction conditions: 50 mM fructose, 100mg of catalyst, 20 ml DMA as a solvent, 6h, 100°C temperature, N_2 atmosphere, 600 rpm magnetic stirring under reflex conditions. (C= conversion, Y= yield, S= selectivity).

Catalyst	$C_{Fructose}$ (%)	Y_{HMF} (%)	S_{HMF} (%)
SiO_2-SO_3H	54.40	6.22	11.45
TiO_2-SO_3H	8.50	≤1	≤1
ZrO_4-SO_3H	100	38.51	38.51

In case of zirconia, the surface area of unfuntionalized $Zr(OH)_4$ is about 160m^2/g. Our assumption is that more surface area was covered with hydroxyl groups. This means $Zr(OH)_4$ has more hydroxyl (–OH) functional groups on its surface to form covalent bond with sulfonic acid group (-SO_3H) than TiO_2 and SiO_2. Therefore, higher –OH on the surface leads to a higher acid loading. The $Zr(O-SO_3H)_4$ catalyst showed the highest activity and selectivity, which was comparable to the homogeneous catalysis in the range of 10 and 50 mM H_2SO_4 (fig.3. 7). Qi et al. observed similar type of trend in DMSO–acetone (30 : 70 w/w) mixture using ZrO_4-SO_3H and achieved 72.8% yield of HMF and 93% of fructose at 180°C [61].
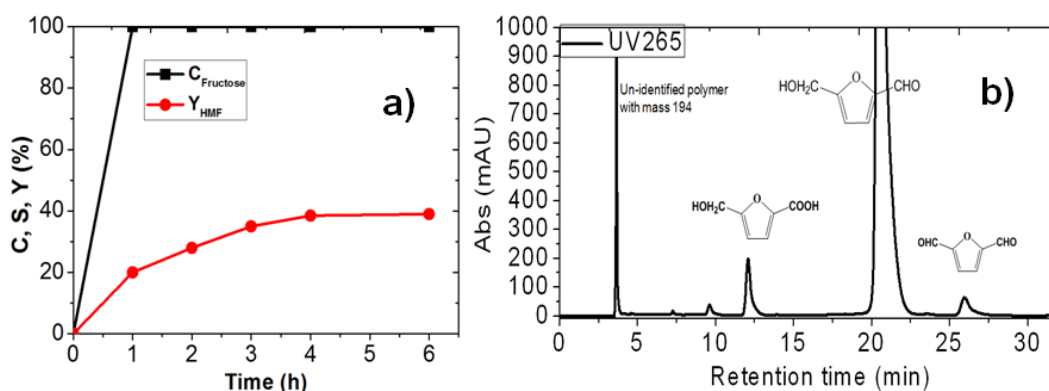
Fig. 3. 8 Dehydration of fructose using sulfonated zirconia; a) kinetics of fructose conversion and HMF formation, b) HPLC chromatogram for product distribution. Conditions: 50mM fructose, 100mg of solid acid catalyst, 20 ml of solven,100 °C, magnetic stirring under reflux conditions.

Fig. 3. 8 shows 38.51% formation of HMF at 6h of reaction time with 100% conversion of fructose in less than 1h. Corresponding HPLC chromatogram was shown in the fig

.3. 8 . ZrO$_4$ support was active for conversion of products (HMF) into some other in-
termediates.

3.3.2.2 Sulfonated SiO$_2$, ZrO$_4$ & TiO$_2$ using chlorobenzenesulfonic acid

Similar type of sulfonated SiO$_2$, TiO$_2$ and ZrO$_4$ were prepared using
chlorobenzensulfuric acid and tested. The reactions showed totally different results and
indicated that the prepared catalysts were not active for dehydration of fructose. Our
interpretation for insignificant catalytic activity is that the formation of covalent bond
was not successful or leached during wash. The synthesis procedures need to be im-
proved or modified in order to prepare active catalyst. Therefore, more research focus
is required to identify the problems associated with these linkers to form covalent bond.

3.3.2.3 p-Toluenesulfonic acid polymer-bound

p-Toluenesulfonic acid (fig. 3. 9a b) acid is a commercially available catalyst and tested
for comparative purpose. It has similar functionality as benzenesufuric acid, but has a
polymer support.
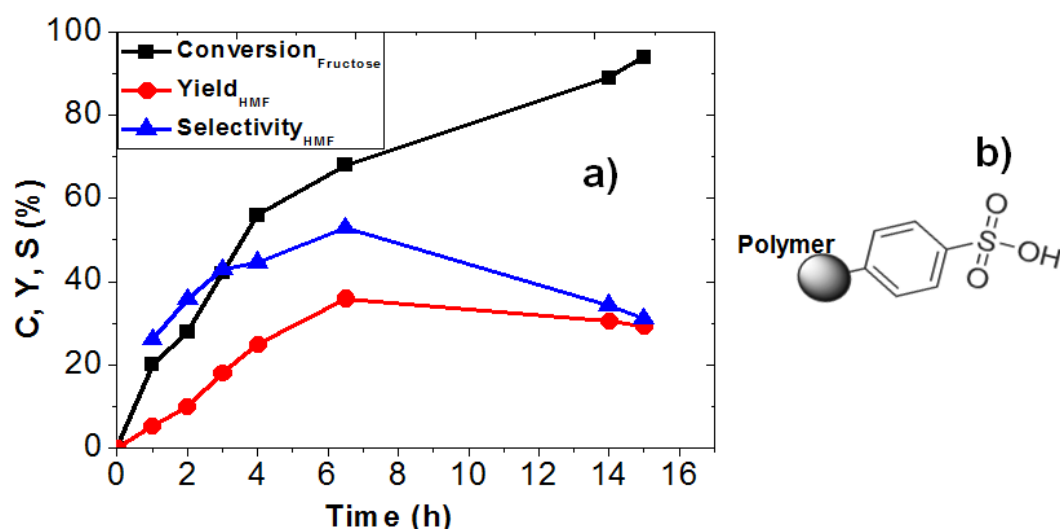
Fig. 3. 9a Dehydration reaction of fructose using p-toluenesulfonic acid. Reaction conditions:
50 mM fructose, 100mg of catalyst, 20 ml DMA as a solvent, 100°C temperature, N$_2$ atmos-
phere, 600 rpm magnetic stirring under reflex conditions.

Fig. 3. 9a shows activity of p-toluenesulfonic acid for dehydration of fructose into HMF.
It exhibited higher activity for fructose conversion with 32% of FDC yield. Inspite of its
catalytic activity for fructose dehydration, it has a disadvantage in terms of its support
source. It is difficult to use as a support for bi-functional catalyst to impregnate active
metal surface. Under similar conditions, this material showed better catalytic activity for

dehydration of fructose into HMF than sulfonated SiO_2 and TiO_2. It suggests that the proposed materials in section 3.3.2.1 and 3.3.2.2 are possible to use as dehydration catalyst, but needed to improve the catalyst synthesis procedure. Therefore, the proposed sulfonated ZrO_4 has a strong potential for dehydration reactions as well as to use as a support for bi-functional catalyst synthesis.

3.3.2.4 Nafion membrane

Nafion is a sulfonated tetrafluoroethylene based fluoropolymer as shown the in fig. 3. 10b. Nowadays nafion has received a considerable amount of attention as a proton conductor (fuel cell application). This material was tested for fructose dehydration to understand influence of different supports.
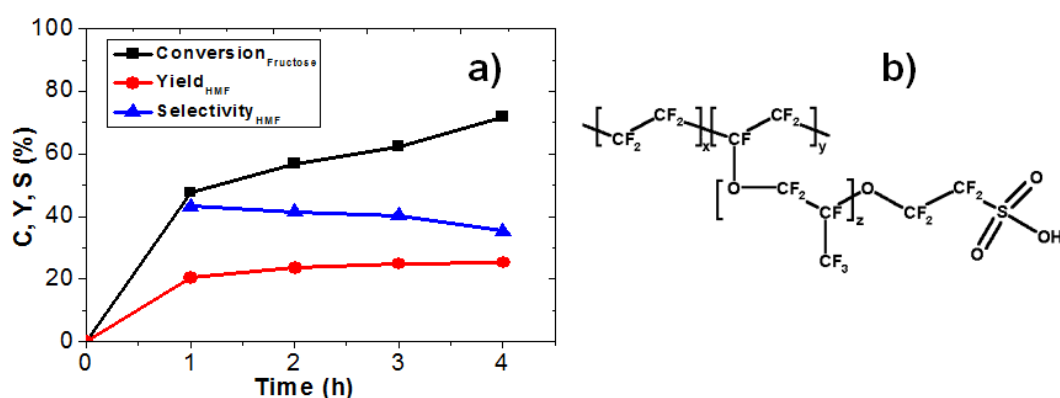
Fig. 3. 10 a) Dehydration of fructose into HMF using nafion; b) chemical structure of nafion. Reaction conditions: 50 mM fructose, 20 ml DMA as a solvent, 5 cm^2 nafion membrane, 100°C temperature,N_2 atmosphere, 600 rpm magnetic stirring under reflex conditions.

The tested nafion membrane is catalytically active for dehydration reaction and converts fructose into HMF. The rate of formation of HMF is more in early reaction till 1h as shown in fig. 3. 10a. Nafion membrane was active for fructose dehydration, but the disadvantage was its instability to reuse. At 100°C, nafion was slowly dissolving into DMA solvent and it loses its catalytic activity. At the same time, this material was also not advisable as a support for development of bi-functional solid acid catalyst.

3.3.2.5 Covalent triazine frameworks (CTFs)

CTFs are new class of covalent organic frameworks (COFs) that are formed by the trimerization of aromatic nitriles in molten $ZnCl_2$ [77, 78 , 79]. CTFs exhibit very high surface areas and high amounts of nitrogen functionalities in the networks [80]. Because of the fully covalent structure, they possess an increased thermal and chemical

stability. These are interesting candidates as new catalyst supports for impregnation of acid sites and metallic sites for liquid phase reactions [80].

Different types of CTFs have been prepared (see section 2.3) and tested for their catalytic activity. Unfortunately, neither the pure CTF (without sulfonation) nor the sulfonated CTFs have showed activity for the dehydration reaction. The fructose conversion was less than 2 % in all the experiments. This indicates that the sulfonation was not successful or this may be because of the basic effect of the superposed by nitrogen (incorporated on CTF surface).

CTF material will be a promising support material for a variety of bi-functional catalyst support once its sulfonation step was improved. This material has many attractive properties as a novel support material from organic metals, strong chemical and mechanical properties. This material is more useful as a new catalyst support material for different metals to carry further oxidation and hydrogenation reactions of HMF. More research attention is required in order to improve the sulfonation of these materials by performing more characterization studies.

3.3.2.6 SiO_2, TiO_2, ZrO_4 with 3-(mercaptopropyl)trimethoxysilane (MPTMS) linker

In line to exploring new solid acid materials, another class of linker such as MPTMS was selected. This linker was chemically anchored to high surface area inorganic solid carriers to create new organic/inorganic hybrid (interphase) catalyst [81]. The reactive centers of these linker were supported on solids and were more flexible similar to homogeneous catalysts (fig. 3. 11). The advantage of this material was recyclability like heterogeneous catalysts [63]. Selected metal oxide supports such as SiO_2, TiO_2 and ZrO_4 were anchored with MPTMS linker (see section 2.3) .
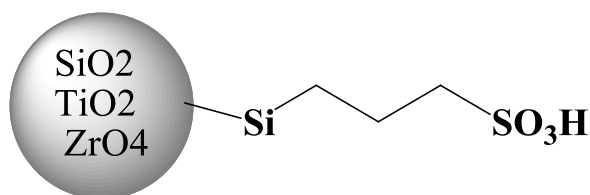
Fig. 3. 11 Surface modification with MPTMS on SiO_2, TiO_2 and $Zr(OH)_4$.

Sulfonation of MPTMS and attachment to functionalized solid support opens the door for new applications. Unfortunately, this material shows less catalytic activity for dehydration reactions of fructose. The main drawback of this synthesis is non-functionalized support material. We believe that the used materials contain less hy-

droxyl groups and were difficult to anchor these MPTMS linkers to the support material. In summary more functionalized porous materials are required in order to develop a successful solid acid material.

3.3.2.7 Sulfonated SBA-15 with TESAS linker

The TESAS-linker has a similar structure as MPTMS besides its longer chain and the thioether group. The structure is designed to ensure accessibility of fructose to the catalytic sites and it is used as advancement to imitate the structure of DMSO on a heterogeneous catalyst. The sulfur atom in the thioether group should promote the same or similar type of effect as the sulfur atom in DMSO itself as described by Amarasekara et al. [75]. The performance of the catalyst was improved without the problem of the separation/diffusion of formed HMF. This catalyst was prepared by the reaction of 3-((3-(trimethoxysilyl)propyl)thio)-propane-1-sulfonic acid with hydroxyl groups on SBA-15 (fig. 3. 12). SBA-15 is mesoporous silica materials with high surface area (see section 2.3). This is another type of novel supporting material and is useful to prepare bifunctional catalyst.
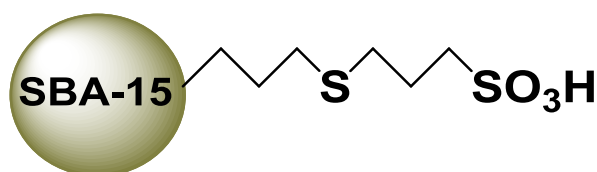
Fig. 3. 12 Sulfonated SBA-15 with TESAS (3-((3-(trimethoxysilyl)propyl)thio)-propane-1-sulfonic acid) linker.

3.3.2.7.1 Characterization of SBA-15-TESAS

The ^{13}C and ^{29}Si NMR spectra of the pure silane TESAS and the catalyst SBA-15-TESAS are shown in fig. 3. 13a and fig. 3. 13b respectively [75]. In the ^{13}C spectrum of the pure TESAS, the signal at 10 ppm shows the carbon which is directly next to the Si ($-SiCH_2$). The signals for the $CH_2CH_2SCH_2CH_2$ methylene groups appear at 23.5 ppm and the signals for the methylenes next to the thioether CH_2SCH_2 appear at 31.5 and 35 ppm. The signal at 49.5 ppm represents both the methoxy groups $-OCH_3$ groups from the organosilane and the CH_2SO_3H groups.

After the grafting of the TESAS on SBA-15, all the signals of the methylene groups remain the same (fig.3. 13b). The relative intensity of signal at 50.5 ppm is lower compared to the signal in the pure TESAS sample which explains the grafting of TESAS through the methoxy groups on the SBA-15 surface.

The ^{29}Si spectrum (fig.3. 13c) shows peaks at -92, -100 and -110 which represent the two hydroxyl group on silicon atom grafted on the surface, one hydroxyl group on silicon and siloxane bond with no OH groups of the silica framework in SBA-15 respectively.
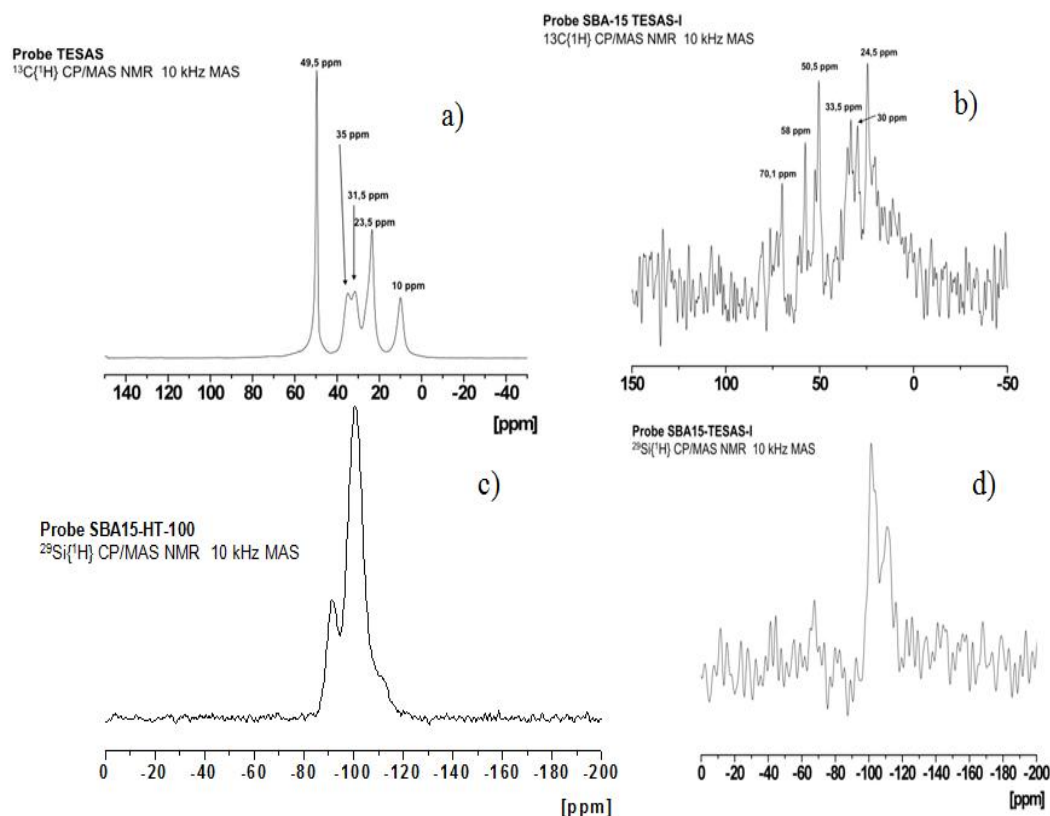
Fig. 3. 13 a) ^{13}C-NMR of TESAS, b) ^{13}C (^{1}H)-NMR of TESAS-SBA15, c) ^{29}Si(^{1}H)-NMR of SBA-15, d) ^{29}Si(^{1}H)-NMR of TESAS-SBA-15.

^{29}Si spectrum (fig. 3. 13d) of the TESAS grafted on SBA-15 shows the decrease in amount of the hydroxyl group on silicon groups and increase in amount of the siloxane bond with no OH groups compared to bare SBA-15 which indicates the TESAS group attached to the surface silanol groups of the SBA-15 material. The signal (at -65 ppm) of the silicon which is attached to the surface indicates the complete attachment of the silane through all the three methoxy groups to the silanols of the silica framework.

3.3.2.7.2 Activity of SBA-15-TESAS

The SBA-15 itself showed a negligible activity towards HMF but a low conversion of the fructose.

Table 3. Comparison of solid acid catalyst supported on SBA-15 for fructose dehydration over 4 h reaction time. Reaction conditions: 50 mM fructose, 20 ml DMA as a solvent, 100°C temperature,N_2 atmosphere, 600 rpm magnetic stirring under reflex conditions.

Catalyst	Conversion in %	Yield in %	Selectivity in %
SBA-15 (blank)	11.74	1.14	≤ 1
SBA-15-MPTMS	28.14	15.82	56.21
SBA-15-TESAS	48.46	34.27	70.71

Table 3 shows the testing of SBA-15 for fructose dehydration in blank conditions and with sulfonated SBA-15 with MPTMS and TESAS linkers. Un-functionalized SBA-15 performed insignificant activity for HMF formation in blank conditions. Basically SBA-15 is acidic material, but this acidity is not sufficient to catalyze dehydration reaction. MPTMS on SBA-15 exhibited activity for fructose conversion with 28% selectivity of HMF. Unlike other catalysts, TESAS on SBA-15 showed very promising catalytic activity for dehydration of fructose into HMF reaction with 48.46% fructose conversion, 34% HMF yield and 70% of HMF selectivity. This material showed higher selectivity compared to other self prepared solid acid catalysts. These results underline the great influence of the structure of the linker and its mobility, which confirms that structure is more important than the loading of acid. Therefore, improvement of SBA-15 with TESAS linker looks very promising for future dehydration reactions in heterogeneous catalysis.

3.3.2.7.3 Recycling of SBA-15-TESAS

So far, the most promising catalyst TESAS on SBA-15 was tested for its recyclability, which is very important in order to develop an industrial grade catalyst. After each cycle the catalyst was filtered and washed four times with fresh DMA (5 ml) and once with MiliQ water (10 ml) and then dried over night at 55°C.

Fig. 3. 14 shows the catalytic activity of TESAS on SBA-15. The activity of the catalyst was reproducible over 4 recycle studies with a loss of 10% HMF yield. This selectivity was comparable with insignificant amount of loss in fructose conversion.
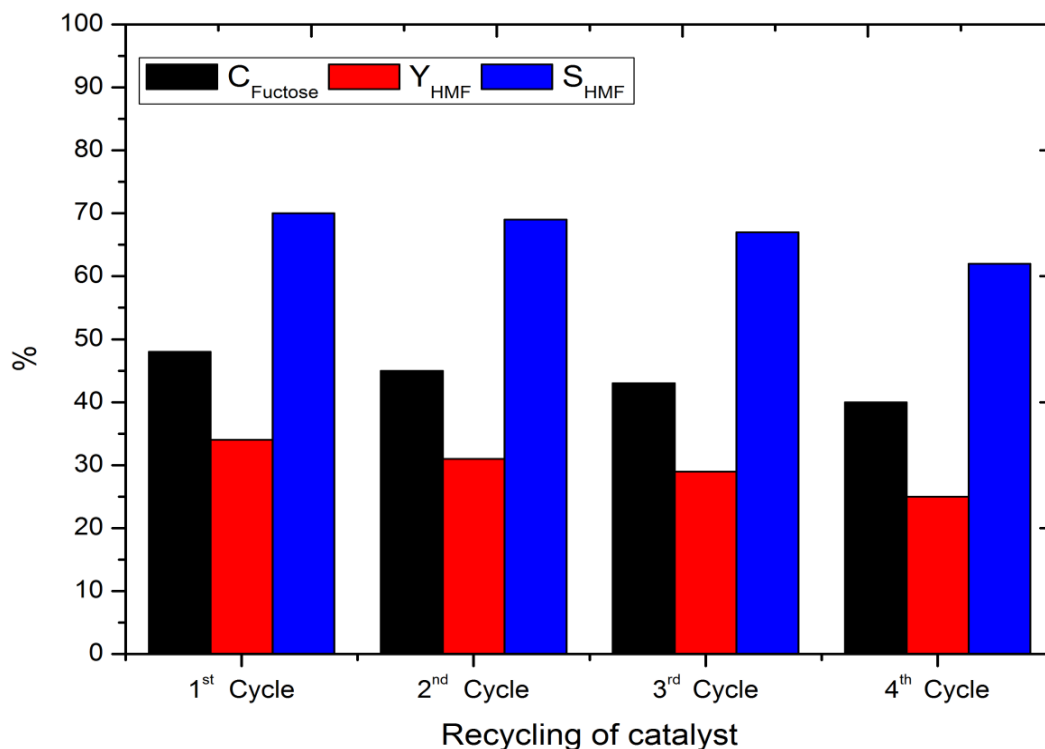
Fig. 3. 14 Recyclability of TESAS on SBA-15 for dehydration of fructose. Reaction conditions: 50 mM fructose, 20 ml DMA as a solvent, 10 h,100°C temperature,N_2 atmosphere, 600 rpm magnetic stirring under reflex conditions.

3.3.3 Testing with commercial solid acid catalyst

Amberlyst-15 is an ion-exchange resin or ion-exchange polymer. It is an insoluble matrix normally in the form of small (1–2 mm diameter) beads. The material has highly developed pore structure on the surface, which is easily trapped and released ions. This material was tested for fructose dehydration.

3.3.3 1 Amberlyst-15 with different solvents

Fig.3. 15   present the dehydration of fructose into HMF in different solvents using Amberlyst-15 solid acid catalyst. Due to the auto-catalytic activity of DMSO, it showed highest yield of HMF followed by DMA. Acetone: water mixture was used because of the structural similarities between DMSO and Acetone. Acetone has added advantage due to its lower boiling point, which makes products separation process more favourable. Qi et Al. reported positive effects of the addition of acetone on the HMF yields in DMSO:acetone mixtures[61].
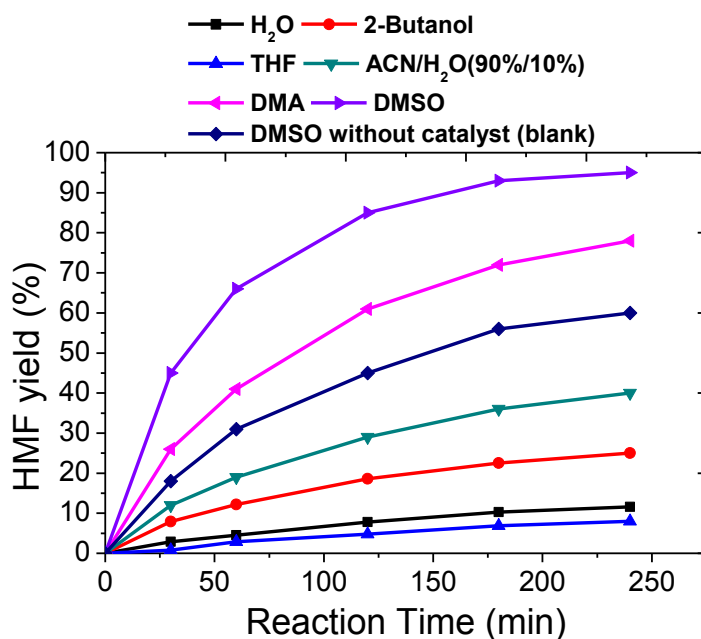
Fig. 3. 15 Effect of solvent for dehydration of fructose into HMF using Amberlyst-15. Reaction conditions: 50 mM fructose,100mg of catalyst, 20 ml of solvent, 4 h, 100°C temperature, N_2 atmosphere, 600 rpm magnetic stirring under reflex conditions.

3.3.3 2 Effect of temperature

So far, Amberlyst-15 showed better activity for dehydration of fructose into HMF. In continuation, the effect of temperature on dehydration of fructose was studied using amberlyst-15.
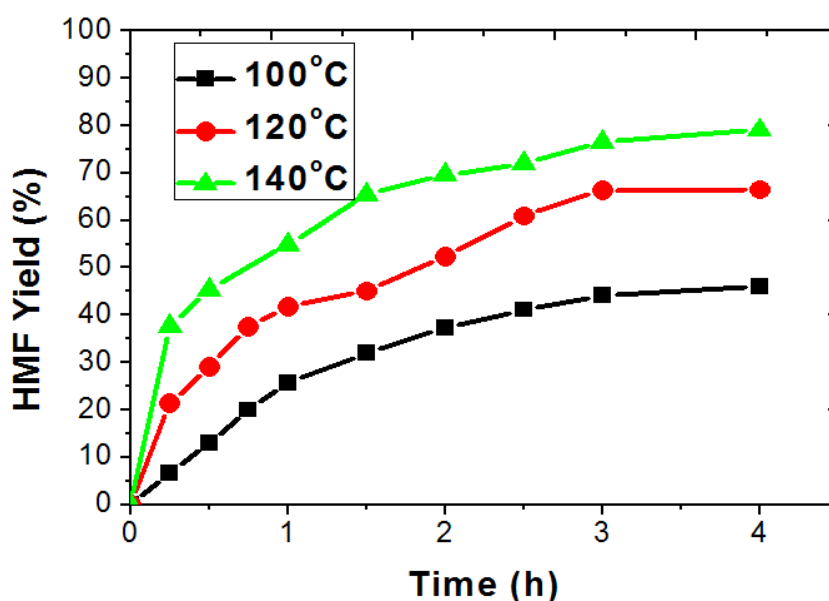
Fig. 3. 16 Effect of temperature on fructose dehydration reaction using Amberlyst-15. Conditions: 50 mM fructose,100mg of catalyst, 20 ml of solvent, 4 h, N_2 atmosphere, 600 rpm magnetic stirring under reflex conditions.

Fig. 3. 16 shows the effect of temperature on dehydration of fructose into HMF. A significant effect of temperature on dehydration reaction was observed under given conditions using amberlyst-15 material. Catalytic activity is higher with increase of temperature. Higher temperatures are more favorable to increase the rate of the reaction and it is less likely to undergo rehydration or polymerization.

3.4 Conclusion

The use of sugars such as fructose for the production of multi-functional furan chemicals like HMF is a vital alternative to fossil-based energy resource; such use is of real significance in the sustainable chemistry. In this study, we presented the preliminary results of heterogeneous solid acid catalyst activity for dehydration of fructose into HMF.

Aqueous solvents are not recommended for dehydration of fructose because of their undesired reaction that leads to the formation of soluble or insoluble colored polymer (humins) type compounds. Cheap organic solvent, DMA was selected to study the fructose dehydration because of its selective nature for HMF formation with reduced cross-polymerization/humins formation. Sulfonated zirconia exhibited relatively higher activity for HMF formation than sulfonated silica and titania. Based on our observations, we believe that surface functional groups such as hydroxyl groups influence the catalyst activity. Therefore, functionalization of material surface is a crucial step to attach sulfonic acid groups covalently.

The acidic centers of MPTMS and TESAS linkers supported on solids have more advantage in terms of limited mass transfer effects. The sulfonated arms of MPTMS and TESAS can move freely during reaction like homogeneous catalysts and at the same time these have the advantage of recyclability like heterogeneous catalysts. MPTMS and TESAS linkers on SBA-15 appeared as the potential candidates in order to develop a bi-functional novel catalyst. Effect of temperature on dehydration of fructose into HMF influenced catalytic activity significantly.

Outlook

More efforts are required to achieve the goal of stable solid acid catalyst. Further research is required to carry out characterization of solid acid material in order to use them in the continuous process. To find out the exact amount of acid sites on surface of solid acid materials, the characterization techniques like ammonia-TPD and CO-TPD

need to be performed. These studies help to tune catalyst with required amount of acidity. Systematic mechanistic investigations are required in order to understand and control the influence of surface acidity and effect of support to maximize the selectivity of HMF from fructose.

3. 4.   References

1.   Dugar, D. and G. Stephanopoulos, *Relative potential of biosynthetic pathways for biofuels and bio-based products.* Nat Biotech, 2011. 29(12): p. 1074-1078.
2.   Ragauskas, *The Path Forward for Biofuels and Biomaterials.* Science, 2006. 311(5760): p. 484-489.
3.   Naik, S.N., et al., *Production of first and second generation biofuels: A comprehensive review.* Renewable and Sustainable Energy Reviews, 2010. 14(2): p. 578-597.
4.   Fargione, *Land Clearing and the Biofuel Carbon Debt.* Science, 2008. 319(5867): p. 1235-1238.
5.   Scharlemann, Laurance, *How Green Are Biofuels?* Science, 2008. 319(5859): p. 43-44.
6.   Righelato, R. and D.V. Spracklen, *Carbon Mitigation by Biofuels or by Saving and Restoring Forests?* Science, 2007. 317(5840): p. 902.
7.   Melillo, *Indirect Emissions from Biofuels: How Important?* Science, 2009. 326(5958): p. 1397-1399.
8.   Havlik, *Global land-use implications of first and second generation biofuel targets.* Energy Policy, 2010. 39(10): p. 5690-5702.
9.   Wenner, M., *The Next Generation of Biofuels.* Scientific American 2009. 19: p. 46-51.
10.   Sims, *An overview of second generation biofuel technologies.* Bioresource Technology, 2010. 101(6): p. 1570-1580.
11.   Dodds, R.A. Gross, *Chemicals from Biomass.* Science, 2007. 318(5854): p. 1250-1251.
12.   Lipinsky, *Chemicals from Biomass: Petrochemical Substitution Options.* Science, 1981. 212(4502): p. 1465-1471.
13.   Ng, T.K., *Production of Feedstock Chemicals.* Science, 1983. 219(4585): p. 733-740.
14.   Somerville, *Feedstocks for Lignocellulosic Biofuels.* Science. 329(5993): p. 790-792.
15.   Vispute, *Renewable Chemical Commodity Feedstocks from Integrated Catalytic Processing of Pyrolysis Oils.* Science. 330(6008): p. 1222-1227.
16.   Froment, F. Pla, *Determinations of Average Molecular Weights and Molecular Weight Distributions of Lignin*, in *Lignin.* 1989, American Chemical Society. p. 134-143.
17.   Reid, *Determining molecular weight distributions of lignins and their biodegradation products by gel filtration on a high-performance acarose column with a mixed ethanol-aqueous alkali solvent.* Biotechnology Techniques, 1991. 5(3): p. 215-218.
18.   Chakar, A.J. Ragauskas, *Review of current and future softwood kraft lignin process chemistry.* Industrial Crops and Products, 2004. 20: p. 131-141.
19.   Chheda, G.W. Huber, and J.A. Dumesic, *Liquid-Phase Catalytic Processing of Biomass-Derived Oxygenated Hydrocarbons to Fuels and Chemicals.* Angewandte Chemie International Edition, 2007. 46(38): p. 7164-7183.
20.   Demirba, *Relationships between lignin contents and fixed carbon contents of biomass samples.* Energy Conversion and Management, 2003. 44(9): p. 1481-1486.
21.   Mohamad Ibrahim, *Chemical and thermal properties of lignins from oil palm biomass as a substitute for phenol in a phenol formaldehyde resin production.* Carbohydrate Polymers. 86(1): p. 112-119.
22.   Chakar and A.J. Ragauskas, *Review of current and future softwood kraft lignin process chemistry.* Industrial Crops and Products, 2004. 20(2): p. 131-141.

23. Pandey and C.S. Kim, *Lignin Depolymerization and Conversion: A Review of Thermo-chemical Methods.* Chemical Engineering & Technology. 34(1): p. 29-41.

24. Simmons, D. Loqua, and J. Ralph, *Advances in modifying lignin for enhanced biofuel production.* Current Opinion in Plant Biology. 13(3): p. 312-319.

25. Mihai brebu, *pyrolysis of lignin – a potential method for obtaining chemicals and/or fuels.* Cellulose chemistry and technology, 2010.

26. Pandey and C.S. Kim, *Lignin Depolymerization and Conversion: A Review of Thermo-chemical Methods.* Chemical Engineering & Technology, 2010. 34(1): p. 29-41.

27. Demirba, A., *Effect of lignin content on aqueous liquefaction products of biomass.* Energy Conversion and Management, 2000. 41(15): p. 1601-1607.

28. Gani, A. and I. Naruse, *Effect of cellulose and lignin content on pyrolysis and combustion characteristics for several types of biomass.* Renewable Energy, 2007. 32(4): p. 649-661.

29. Ma, M.G., *Isolation and characterization of hemicelluloses extracted by hydrothermal pretreatment.* Bioresource Technology. 114(0): p. 677-683.

30. Ajay, S. and M. Prashant, *5 Microbial metabolism of pentoses*, in *Progress in Industrial Microbiology*. 1995, Elsevier. p. 119-145.

31. Zhang, *Pretreatment of partially delignified hybrid poplar for biofuels production: Characterization of organosolv hemicelluloses.* Industrial Crops and Products. 33(2): p. 310-316.

32. Zhao, X., L. Zhang, and D. Liu, *Biomass recalcitrance. Part I: the chemical compositions and physical structures affecting the enzymatic hydrolysis of lignocellulose.* Biofuels, Bioproducts and Biorefining. 6(4): p. 465-482.

33. Abdul Khalil, H.P.S., A.H. Bhat, and A.F. Ireana Yusra, *Green composites from sustainable cellulose nanofibrils: A review.* Carbohydrate Polymers. 87(2): p. 963-979.

34. Huber, G.W., S. Iborra, and A. Corma, *Synthesis of Transportation Fuels from Biomass: Chemistry, Catalysts, and Engineering.* Chemical Reviews, 2006. 106(9): p. 4044-4098.

35. Klemm, *Cellulose: Fascinating Biopolymer and Sustainable Raw Material.* Angewandte Chemie International Edition, 2005. 44(22): p. 3358-3393.

36. Sun, Y.a.J.C., *Hydrolysis of lignocellulosic materials for ethanol production: A review.* Bioresource Technology 2002. 83(1): p. 1-11.

37. Lange, *Valeric Biofuels: A Platform of Cellulosic Transportation Fuels.* Angewandte Chemie International Edition. 49(26): p. 4479-4483.

38. Dhepe, P.L. and A. Fukuoka, *Cellulose Conversion under Heterogeneous Catalysis.* ChemSusChem, 2008. 1(12): p. 969-975.

39. Moreau, C., M.N. Belgacem, and A. Gandini, *Recent Catalytic Advances in the Chemistry of Substituted Furans from Carbohydrates and in the Ensuing Polymers.* Topics in Catalysis, 2004. 27(1): p. 11-30.

40. Jiang, N., *Effect of Formic Acid on Conversion of Fructose to 5-Hydroxymethylfurfural in Aqueous/Butanol Media.* BioEnergy Research: p. 1-7.

41. Rosatella, A., *5-Hydroxymethylfurfural (HMF) as a building block platform: Biological properties, synthesis and synthetic applications.* Green Chemistry, 2011. 13(4): p. 754-793.

42. T. Werpy and G. Petersen, *Top Value Added Chemicals From Biomass Volume I: Results of Screening for Potential Candidates from Sugars and Synthesis Gas* Pacific Northwest National Laboratory (PNNL) and the National Renewable Energy Laboratory (NREL), 2004.

43. Kamm, B., *Production of Platform Chemicals and Synthesis Gas from Biomass.* Angewandte Chemie International Edition, 2007. 46(27): p. 5056-5058.

44. Huber, G.W., *Production of Liquid Alkanes by Aqueous-Phase Processing of Biomass-Derived Carbohydrates.* Science, 2005. 308(5727): p. 1446-1450.

45. Casanova, O., S. Iborra, and A. Corma, *Biomass into Chemicals: Aerobic Oxidation of 5-Hydroxymethyl-2-furfural into 2,5-Furandicarboxylic Acid with Gold Nanoparticle Catalysts.* ChemSusChem, 2009. 2(12): p. 1138-1144.

46. Zhao, H., *Metal Chlorides in Ionic Liquid Solvents Convert Sugars to 5-Hydroxymethylfurfural.* Science, 2007. 316(5831): p. 1597-1600.

47. Kiermayer, J., Chemiker-Zeitung, 1895. 19: p. 1003–1006.

48. Huang, R., *Integrating enzymatic and acid catalysis to convert glucose into 5-hydroxymethylfurfural.* Chemical Communications. 46(7): p. 1115-1117.

49. Chheda, J.N., Y. Roman-Leshkov, and J.A. Dumesic, *Production of 5-hydroxymethylfurfural and furfural by dehydration of biomass-derived mono- and poly-saccharides.* Green Chemistry, 2007. 9(4): p. 342-350.

50. Binder, J.B., *Mechanistic insights on the conversion of sugars into 5-hydroxymethylfurfural.* Energy & Environmental Science, 2009. 3(6): p. 765-771.

51. Kuster, B.F.M., *5-Hydroxymethylfurfural (HMF). A Review Focussing on its Manufacture.* Starch - Stärke, 1990. 42(8): p. 314-321.

52. Nikolov, P.Y., and V.A. Yaylayan, *Reversible and Covalent Binding of 5-(Hydroxymethyl)-2-furaldehyde (HMF) with Lysine and Selected Amino Acids.* Journal of Agricultural and Food Chemistry. 59(11): p. 6099-6107.

53. Lichtenthaler, F.W. and S. Ronninger, *[small alpha]-D-Glucopyranosyl-D-fructoses: distribution of furanoid and pyranoid tautomers in water, dimethyl sulphoxide, and pyridine. Studies on ketoses. Part 4.* Journal of the Chemical Society, Perkin Transactions 2, 1990(8): p. 1489-1497.

54. Cottier, L., Ind. Alim. Agricol. , 1989: p. 567–570.

55. Antal Jr, M.J., W.S.L. Mok, and G.N. Richards, *Mechanism of formation of 5-(hydroxymethyl)-2-furaldehyde from d-fructose and sucrose.* Carbohydrate Research, 1990. 199(1): p. 91-109.

56. Suganuma, S., *Hydrolysis of Cellulose by Amorphous Carbon Bearing SO3H, COOH, and OH Groups.* Journal of the American Chemical Society, 2008. 130(38): p. 12787-12793.

57. Shimizu, K.-i., R. Uozumi, and A. Satsuma, *Enhanced production of hydroxymethylfurfural from fructose with solid acid catalysts by simple water removal methods.* Catalysis Communications, 2009. 10(14): p. 1849-1853.

58. Takagaki, A., *A one-pot reaction for biorefinery: combination of solid acid and base catalysts for direct production of 5-hydroxymethylfurfural from saccharides.* Chemical Communications, 2009(41): p. 6276-6278.

59. Yang, F., *Conversion of biomass into 5-hydroxymethylfurfural using solid acid catalyst.* Bioresource Technology, 2011. 102(3): p. 3424-3429.

60. Wang, J., *Efficient catalytic conversion of fructose into hydroxymethylfurfural by a novel carbon-based solid acid.* Green Chemistry. 13(10): p. 2678-2681.

61. Qi, X., *Sulfated zirconia as a solid acid catalyst for the dehydration of fructose to 5-hydroxymethylfurfural.* Catalysis Communications, 2009. 10(13): p. 1771-1775.

62. Wilson, K. and J.H. Clark, *Solid acids and their use as environmentally friendly catalysts in organic synthesis.* Pure and applied chemistry, 2000. 72: p. 1313–1319.

63. Karimi, B. and M. Khalkhali, *Silica functionalized sulfonic acid as a recyclable interphase catalyst for chemoselective thioacetalization of carbonyl compounds in water.* Journal of Molecular Catalysis A: Chemical, 2007. 271(1-2): p. 75-79.

64. Barbaro, P., *Heterogeneous Bifunctional Metal/Acid Catalysts for Selective Chemical Processes.* European Journal of Inorganic Chemistry, 2012. 2012(24): p. 3807-3823.

65. Climent, M.J., A. Corma, and S. Iborra, *Converting carbohydrates to bulk chemicals and fine chemicals over heterogeneous catalysts.* Green Chemistry, 2011. 13(3): p. 520-540.

66. van Dam, H.E., A.P.G. Kieboom, and H. van Bekkum, *The Conversion of Fructose and Glucose in Acidic Media: Formation of Hydroxymethylfurfural.* Starch - Stärke, 1986. 38(3): p. 95-101.

67. Kabyemela, B.M., *Glucose and Fructose Decomposition in Subcritical and Supercritical Water: Detailed Reaction Pathway, Mechanisms, and Kinetics.* Industrial & Engineering Chemistry Research, 1999. 38(8): p. 2888-2895.

68. Srokol, Z., *Hydrothermal upgrading of biomass to biofuel; studies on some monosaccharide model compounds.* Carbohydrate Research, 2004. 339(10): p. 1717-1726.

69. Kabyemela, B.M., *Kinetics of Glucose Epimerization and Decomposition in Subcritical and Supercritical Water.* Industrial & Engineering Chemistry Research, 1997. 36(5): p. 1552-1558.

70. Mushrif, S.H., S. Caratzoulas, and D.G. Vlachos, *Understanding solvent effects in the selective conversion of fructose to 5-hydroxymethyl-furfural: a molecular dynamics investigation.* Physical Chemistry Chemical Physics, 2012. 14(8): p. 2637-2644.

71. Qi, X., *Selective Conversion of D-Fructose to 5-Hydroxymethylfurfural by Ion-Exchange Resin in Acetone/Dimethyl sulfoxide Solvent Mixtures.* Industrial & Engineering Chemistry Research, 2008. 47(23): p. 9234-9239.

72. Musau, R.M. and R.M. Munavu, *The preparation of 5-hydroxymethyl-2-furaldehyde (HMF) from d-fructose in the presence of DMSO.* Biomass, 1987. 13(1): p. 67-74.

73. Binder, J.B. and R.T. Raines, *Simple Chemical Transformation of Lignocellulosic Biomass into Furans for Fuels and Chemicals.* Journal of the American Chemical Society, 2009. 131(5): p. 1979-1985.

74. Verendela, J.J., T.L. Churcha, and P.G. Andersson, *Catalytic One-Pot Production of Small Organics from Polysaccharides.* Synthesis 2011(11): 1649-1677, 2011. 11: p. 1649-1677

75. Amarasekara, A.S., L.D. Williams, and C.C. Ebede, *Mechanism of the dehydration of d-fructose to 5-hydroxymethylfurfural in dimethyl sulfoxide at 150°C: an NMR study.* Carbohydrate Research, 2008. 343(18): p. 3021-3024.

76. Qi, X., *Catalytic dehydration of fructose into 5-hydroxymethylfurfural by ion-exchange resin in mixed-aqueous system by microwave heating.* Green Chemistry, 2008. 10(7): p. 799-805.

77. Thomas, A., *Functional Materials: From Hard to Soft Porous Frameworks.* Angewandte Chemie International Edition. 49(45): p. 8328-8344.

78. Kuhn, P., M. Antonietti, and A. Thomas, *Porous, Covalent Triazine-Based Frameworks Prepared by Ionothermal Synthesis.* Angewandte Chemie International Edition, 2008. 47(18): p. 3450-3453.

79. Palkovits, R., *Development of Molecular and Solid Catalysts for the Direct Low-Temperature Oxidation of Methane to Methanol.* ChemSusChem. 3(2): p. 277-282.

80. Chan-Thaw, C.E., *Covalent Triazine Framework as Catalytic Support for Liquid Phase Reaction.* Nano Letters, 2010. 10(2): p. 537-541.

81. Crisci, A.J., *Acid-Functionalized SBA-15-Type Silica Catalysts for Carbohydrate Dehydration.* ACS Catalysis. 1(7): p. 719-728.

Chapter 4

Heterogeneous Catalytic Oxidation of HMF

4. 1.   Introduction

The low functionality of the petroleum (e.g., -OH, -C=O, -COOH) increases the difficulty to produce commodity and fine chemicals directly [1]. Therefore, the concept of selective oxidation was developed to increase the functionality of the petroleum to get chemicals in the presence of heterogeneous catalyst [2, 3]. In contrast to petroleum, biomass-derived carbohydrates contain excess functionality to be used as fuels and chemicals, and the challenge in this field is to develop methods to reduce the functionality in the final product [4-6]. HMF is one of the promising molecules originated from the renewable cellulosic biomass via sugars dehydration (see chapter 3) [7]. In the open literature HMF is referred to as "sleeping giant", because of its diverse applications [8-10]. HMF is a valuable platform molecule for the future chemical industry/biorefinery and expected to play a major role in the new generation renewable based chemicals [11,12]. HMF and its derivatives could potentially replace or substitute petroleum-based building blocks [13], which are currently used to make plastics and fine chemicals [14]. Surprisingly, no technical process has been constructed until now, even though their potential is very well understood [15, 16].

4. 1. 1. Chemicals and polymers from HMF

The molecular formula of HMF is $C_6H_6O_3$. The ratio of C:H is 1:1 and C:O is 2:1. In order to produce non-flammable or less inflammable chemicals and fire resistant polymer, the ratio of C:H should be decreased to a minimum level and C:O ratio need to be increased relatively. Apart from the selective oxidation, the powerful functional groups of HMF will play an active role in the condensation reactions to produce a wide range of products as shown in the fig. 4. 1 . The success of this new task will require an intelligent use of the intrinsic functionality already present in HMF. The functionalities of these intermediates are the –OH group, C=O group and the five membered heterocyclic aromatic ring system. The alcohols of HMF and carboxylic acids of the HMF derivatives are condensed into alkoxylmethylfurfural ethers and

esters. These molecules have good oxidation stability [17]. HMF can undergo cross-condensation with acetone (and other aldehydes and ketones with at least an acidic α-proton [18-20]. In a similar carbanion reaction with malonic acid, can activate methylene compound to form a coupling partner with HMF. It can link HMF by C–C bond formation via a Knoevenagel reaction to form more flexible intermediates. This increases the –OH functionality to ease the polymerization process.

The other potential reaction routes for achieving this goal include the benzoin reaction, the hetero Diels–Alder reaction, condensation and ketonisation reactions. However, the complimentary feedstocks (ethanol, acetone, ethanoic acid, malonic acid etc.) engaged in these processes may not be exclusively from renewable sources or they may suffer from energy balance limitations inherent in their production methods.

The need for complimentary feedstocks can be avoided if there are efficient reaction routes for the oxidation of HMF through the use of available oxygen. This can be possible by adding molecular oxygen to the HMF by oxidation reactions [21]. Selective oxidation of the hydroxymethyl group of HMF is an attractive route to produce 2,5-furandicarbaldehyde (FDA, $C_6H_4O_3$) [22]. FDC has potential applications in the synthesis of drugs [23], fungicides, various applications as monomer, pharmaceuticals and antifungal agents [24]. Hui et. al reported the synthesis of polymeric schiff bases bearing furan moieties by condensation of DFF with a number of diamines. These compounds exhibited thermal stabilities up to about $260^{o}C$ and fully conjugated polymers displayed semiconductivity after doping with iodine [25].

Terephthalic acid (PTA) is an important oil-based aromatic dicarboxylic acid for producing high purity polyethylene terephthalate (PET) [26-28], a polymer commonly used in consumer goods for thousands of applications [29, 30]. The biomass-derived 2,5-furandicarboxylic acid (FDCA) is a desirable replacement for oil-based terephthalic acid for the polyester production[16]. The referred route of FDCA synthesis is the catalytic oxidation of HMF, which is derived from fructose, glucose and cellulose substrates. FDCA can also be used for the preparation of polyamides and polyurethane [11, 31]. Because of the multiple applications, FDCA has been identified as one of the twelve biomass derived chemicals by the U.S. department of energy (DOE) [8]. FDCA is further converted into polyamides, polyesters, polyurethane, etc. using urea or difunctional aromatic diamines. These derivatives have enhanced curative properties when used as curatives for hybrid epoxy-urethanes, hybrid urea-urethanes,

chainextenders for polyurethane, polyurea elastomers and reaction injection molding products [32].
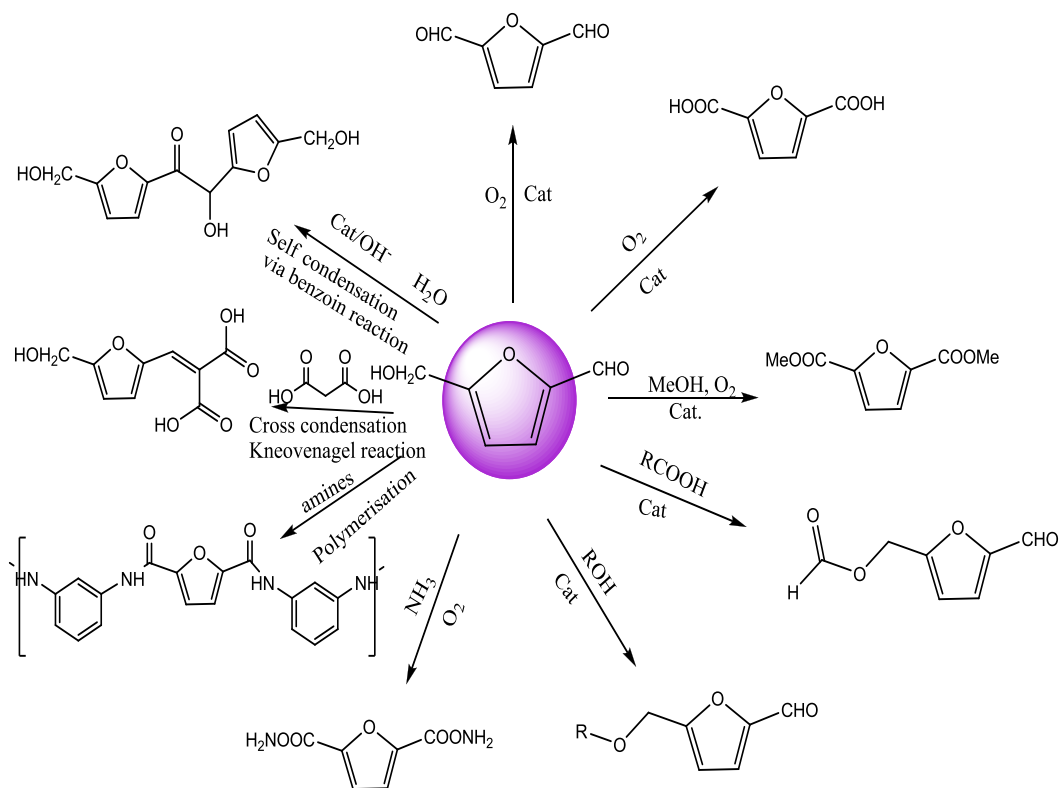
Fig. 4. 1 Chemicals and polymers from HMF.

4. 1. 2. Catalytic Oxidation of HMF

As outlined in the section 4.1.1, a variety of valuable products are possible from HMF oxidation. The type and the purity of the final product totally depends on the depends on the process temperature, pH, partial pressure of oxygen, the nature of the solvent and more importantly the nature of the reactive surface (catalyst). The HMF oxidation reaction can be influenced by the type of oxidant used. Classical oxidants such as BaMnO4, pyridinium chlorochromate (PCC), NaOCl, and 2,2,6,6-tetramethylpiperidine-1-oxide (TEMPO) free radicals with co-oxidants has been used for the HMF oxidation [33-35]. Reijendam et al. reported that the reaction of HMF with lead tetracetate in pyridine gave FDC (37% yield) [36]. The oxidation of HMF has been reported for stoichiometric oxidants (e.g. KMnO4) [34] highly polluting metal catalysts (e.g. Pb) [37] and homogeneous metal salts comprising transition-metal acetates and a bromide source, $Co(OAc)_2/HBr/Mn(OAc)_2$, commonly known as the amoco mid-century (MC)

catalyst [38]. Cottier et al. performed the oxidation of HMF with DMSO-potassium dichromate oxidative complex. 75% FDC was observed with ultrasonic irradiation[39]. Cottier et al. tested a variety of co-oxidants such as calcium hypochlorite, sodium hypochlorite-potassium bromide, copper (I) chloride-oxygen pair, p-toluenesulfonic acid, iodine in alkaline conditions. Yields varied from 20% to 80% depending on the nature of 4-substituent and of the co-oxidant [40]. Saha et al. studied HMF oxidation using homogeneous catalyst (Co(OAc)2/Zn(OAc)$_2$/Br) in acetic acid solvent and achieved 60% of FDCA yield [41]. But homogenous catalysis suffers due to the handling and recycling problems. However, drastic development in the field of green chemistry could realize the selective oxidation using the molecular oxygen as a powerful oxidant and affording to a more environmentally friendly.

Du et. al oxidized HMF into maleic anhydride (52% yield) with the molecular oxygen using VO(acac)$_2$ as the catalyst in the liquid phase [42]. Van Bekkum et. al have developed methods of the selective oxidation of a hydroxymethyl group with noble metal catalysts such as platinum, palladium or ruthenium, that gave excellent yields and selectivities [43]. HMF is highly soluble in water and most of the organic solvents. Moureau et al. [7, 8] have reported the HMF oxidation in organic solvents, such as toluene, benzene, methyl isobutyl ketone (MIBK) in the range of 75–200°C at 10 bar air pressure with heterogeneous catalysts based on different metal oxides (Ti/Zr/Cr/V/Nb/Cr). For instance, with V_2O_5 supported on TiO_2 and toluene as a solvent, HMF conversion reached 91% with 93% selectivity at 90°C and 10bar after 4h reaction time. However, high catalyst-to-substrate ratio (2/1 wt/wt) was necessary for obtaining such result.

Gold is supported on different supports and used for the oxidation with molecular oxygen. Casanova et al. found that HMF was selectively converted into FDCA (99% yield) in highly basic conditions under temperature and pressure (65–130°C, 10bar air) with Au/CeO$_2$ catalyst [44, 45]. Gorbanev et al. studied the oxidation of HMF to FDCA on an Au/TiO$_2$ catalyst and with NaOH as an additive at ambient temperature. A 71% yield of FDCA at 100% of HMF conversion was obtained after 18h at 30°C under 20bar oxygen pressure [46]. Biosen et al. studied the process integration for FDCA production [46]. Taarning et al. reported other applications of HMF conversion like oxidative esterification of HMF to furan-2,5-dimethyldicarboxylate, over Au/TiO$_2$ catalyst with oxygen as the oxidant using sodium methoxide as a promoter at 130°C under 4 bar pressure. They obtained 98% selectivity and 60% yield of furan- 2,5-dimethyldicarboxylate [47]. So far, researchers are exploring different metal options

and conditions in laboratory scale to maximize the desired product [39, 46, 48-52]. However, for the conversion of HMF into FDCA, high process temperature, pressure, and unknown reaction pathway throw challenges to make process viable. Therefore, we focused on understanding of HMF oxidation pathways and the role of heterogeneous catalysts for HMF oxidation at mild conditions.

4. 1. 3. Objective of this chapter

The main objective of this chapter is to study the oxidation of the HMF into valuable products (FDC, FDCA) using heterogeneous catalysis in the liquid phase. This includes synthesis and characterization of different supported solid metal catalysts and testing them for oxidation reactions with quantitative and qualitative product distribution.

4. 2.   Catalyst Characterization

4. 2. 1. BET

The BET surface area studies were carried out to know the available surface area of given solid catalyst. The BET surface area is shown in table 4. 1 along its source information.

Table 4. 1 BET Surface area of supported metal catalyst.

Catalyst type	BET surface area $(m^2/g_{Cat.})$	Source
5% Pt/ activated carbon	1075	Self prepared
5% Ru/ activated carbon	1125	Strem Chem.Ltd
5% Rh/ activated carbon	1100	Strem Chem.Ltd
1% Au/TiO$_2$	50	Strem Chem.Ltd
20% Pt/vulcan	150	BASF
5% Ni/vulcan	180	Self prepared
5% Ru/vulcan	160	Self prepared
5% Pd/activated carbon	980	Self prepared
1% Pt/Al$_2$O$_3$	300	Alfa Aesar
5% Pd/Al$_2$O$_3$	250	Alfa Aesar
5% Pt/CTF	25	Self prepared

4. 2. 2. XRD

The XRD patterns were studied to get the information about the phase of the respective supported material and crystalline properties.

Fig. 4. 4a shows XRD patterns of 20% Pt/vulcan. Pt (111), (200) and (220) reflections are consistent with a face centered cubic. The crystallite size of Pt was calculated from the complete XRD pattern using integral breadth method via TOPAS 4–2 (Bruker AXS). The integral breadth method is independent of the distribution in size and shape. The average Pt crystallite size is noticed as 2.3 ± 0.6 nm. Similarly XRD patterns of other metals are also shown in fig. 4. 4b, c, d, e, f, g and h.

4. 2. 3. Particle size analysis
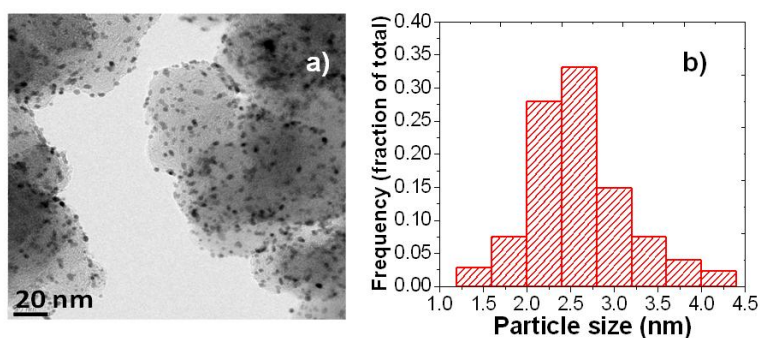
Fig. 4. 2 a) TEM of 20% Pt/vulcan b) Particle size distribution of 20% Pt/Vulcan.

Fig. 4. 2a shows the TEM image of well dispersed Pt nanoparticles on the carbon support. Size of about 200 Pt particles were calculated and shown as histogram in fig. 4. 2b. The average Pt particle size using TEM was calculated to be 2.6 ±1.3 nm. The TEM particle size results are consistent to crystallite size from the XRD data.
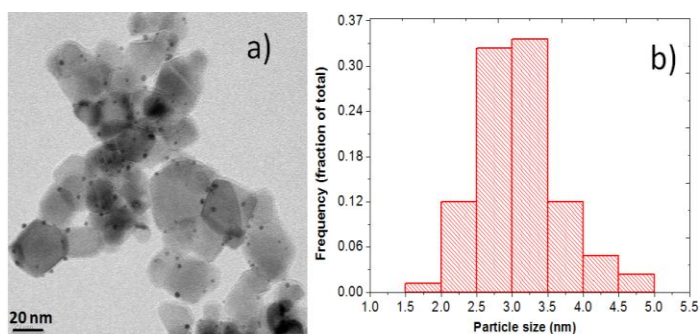
Fig. 4. 3 Characterization of 1wt.% Au/TiO2 catalyst using. a) TEM; b) particle size distribution.
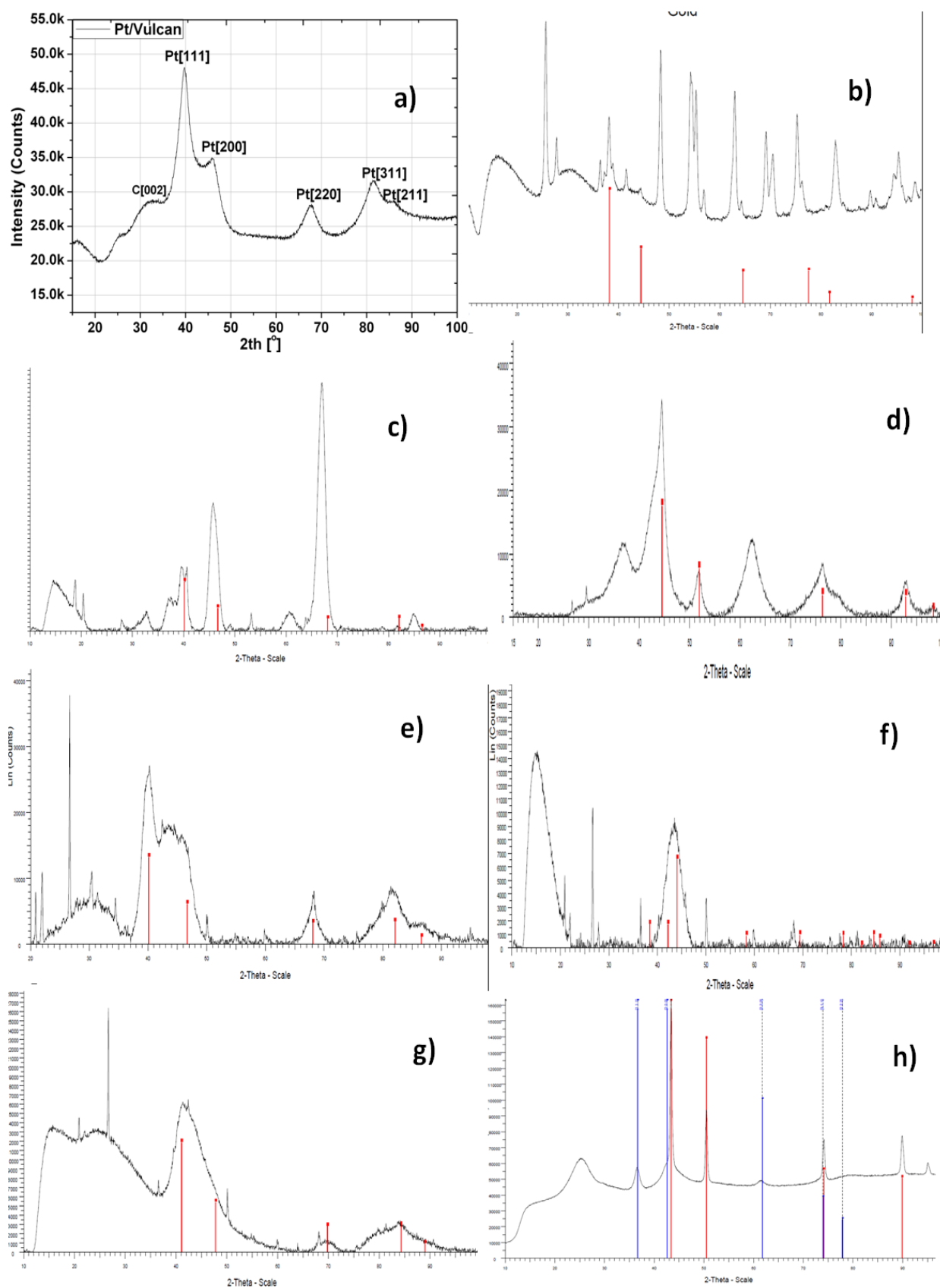
Fig. 4. 4 XRD patterns of selected catalysts a) 20% Pt/vulcan; b) 1% Au/TiO2; c) 5% Pd/Al$_2$O$_3$; d) Ni/SiO$_2$; e) 5%Pd/C; f) 5% Ru/C; g) 5% Rh/C; h) 10% Cu/C.

In the same way, Au/TiO$_2$, Ru/C, and Rh/C were also characterized. The particle size distribution and TEM image of each catalyst are shown below fig. 4. 4, fig. 4. 5and fig. 4. 6.

Fig. 4. 4 shows the well dispersed gold nanoparticle on TiO$_2$ support. The average Au particle size using TEM was calculated to be 3.25 ±1.6 nm
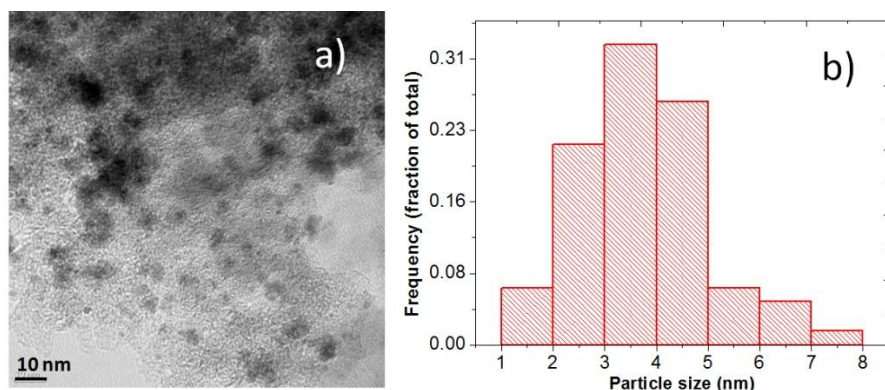
Fig. 4. 5 Characterization of 5wt.% Ru/C catalyst using a) TEM; b) particle size distribution.

Fig. 4. 5a shows the TEM image of carbon supported Ru. Fig. 4. 5b gives average Ru particle size distribution 3.5 ±1.2 nm.
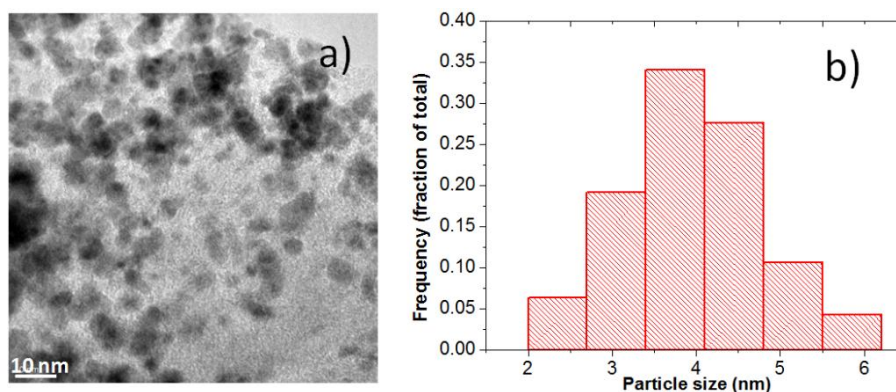
Fig. 4. 6 Characterization of 5wt.% Rh/C catalyst using a) TEM; b) particle size distribution.

Fig. 4. 6a shows TEM image and particle size distribution of Rh supported on carbon are shown in fig. 4. 6b. The particles are well dispersed. The average Rh particle size was calculated to be 3.6 ±1.4 nm using TEM image.

4. 3.   Results and Discussions

Alcohol, aldehyde functional groups of HMF and furan ring of HMF are the chemically reactive sites. HMF may undergo different reactions and forms different desired and undesired products. The distribution of reaction products mainly depends upon the catalyst surface and the reaction conditions. So far, no single unambiguous reaction mechanism of the HMF oxidation was put forward and proved in previous work. Only few researchers proposed a model pathway based on their catalyst surface and conditions [44, 45, 48, 49]. Fig. 4.3.1 summarizes the possible HMF oxidative derivatives with and without intact furan ring system (side products).

Partial or complete oxidation of the functional groups of HMF (solid arrows in fig. 4. 7) occurs on suitable catalyst surfaces and reaction conditions. If C-C bond splitting occurs, HMF may also form many undesired products (dotted arrows in fig. 4.7) by opening furan ring or losing armed functional groups. Before testing the catalytic activity, the stability of HMF functional groups has been tested in the control experiments. Reactions are conducted under different pH conditions in the absence of di-oxygen and metal catalyst (blank reactions).
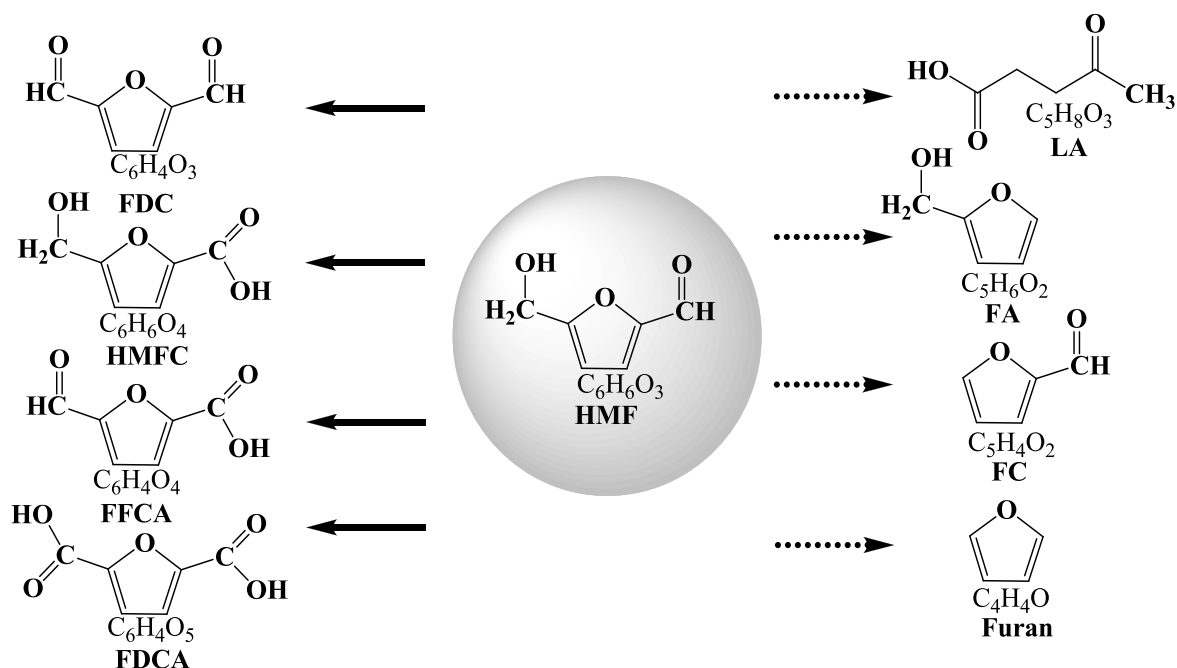
Fig. 4. 7 The major HMF oxidation products (solid arrows) and side reaction products undergoing C-C bond splitting (dotted lines). (Where HMF: 5-hydroxymethyl-2-furfural; FDC: 2,5 furandicarbaldehye; HMFC: 5- hydroxymethyl 2-carboxylic acid; FFCA: 5-formyl furan 2-carboxylic acid; FDCA: 2,5 furandicarboxylic acid; LA: levulinic acid; FA: furfuryl alcohol ; FC: furan carbaldehyde).

4. 3. 1. Selection of solvent

Initially oxidations of reactions were conducted in the organic solvent, because fructose conversion is effective in organic solvents than aqueous solvents (see chapter 3). Pt, Pd and Ni catalysts were tested in the batch reactor for oxidation of HMF in different organic solvents as shown in the table 4. 2

Table 4. 2 Oxidation of HMF in different organic solvents at $25^{\circ}C$, 1bar O_2, metal/HMF is 0.01, 8 h reaction time.

Catalyst	Solvent	C_{HMF} (%)	Y_{FDC} (%)	Y_{FDCA} (%)
Pt/Al_2O_3	DMA	45.00	28.45	4.28
	DMSO	37.85	19.31	10.51
	THF	15.64	8.73	8.43
	CH_2Cl_2	32.14	25.75	≤ 1
Pd/Al_2O_3	DMA	14.26	10.39	1.84
	DMSO	12.79	8.91	2.18
	THF	9.46	4.37	≤ 1
	CH_2Cl_2	11.95	6.82	≤ 1
Ni/SiO_2	DMA	24.81	12.78	6.17
	DMSO	19.46	5.98	4.81
	THF	28.16	7.25	7.19
	CH_2Cl_2	26.49	9.47	3.7

Table 4. 2 shows the conversion of HMF in different organic solvents and using different supported metal catalyst. Overall, less than 50% of HMF conversion was observed at 8h of reaction time. The converted HMF was mainly forming intermediates. Compared to other metals, Pt/ Al_2O_3 surface shows more activity for HMF conversion followed by Ni/SiO_2 and than Pd/ Al_2O_3. The FDC appears as major product rather than FDCA. It is observed that the tested catalysts were active for intermediates formation and less active for complete oxidation. We suspect that desorption of FDCA from catalyst surface is the rate limiting step in this reaction, because the solubility of FDCA is limited in these organic solvents.

Solubility tests were conducted for FDCA in different solvents and found that aqueous solvent under basic conditions is a suitable solvent to study the performance of catalyst

activity for the HMF oxidation into FDCA. Therefore, furthers studies were continued in the aqueous solvents.

4. 3. 2. Blank test for HMF stability under inert atmosphere

Before testing the catalytic activity of catalyst, "blank" reactions were carried out to check the stability/conversion of HMF in the absence of heterogeneous catalyst. HMF is added to the aqueous solvent at pH 1 (0.2M H_2SO_4 in H_2O), pH 6 (H_2O), pH 10 (0.1mM NaOH in H_2O) and pH 13 (0.1M NaOH in H_2O). Blank runs were carried out at selected temperatures ($25^{o}C$, $50^{o}C$), under the inert atmosphere (1bar N_2) and stirred at 1000 rpm. At $50^{o}C$, insignificant amount of HMF conversion was observed at pH 1 and pH 6. About 2% of HMF conversion was noticed at pH 10. Surprisingly, significant amount of HMF conversion was observed at pH 13 as shown in the fig. 4. 8. In our context, we have defined the meaning of degradation as the change of reactant into less-value product (undesired or waste) and conversion is the change of reactant into high-value product (desired or value-added).
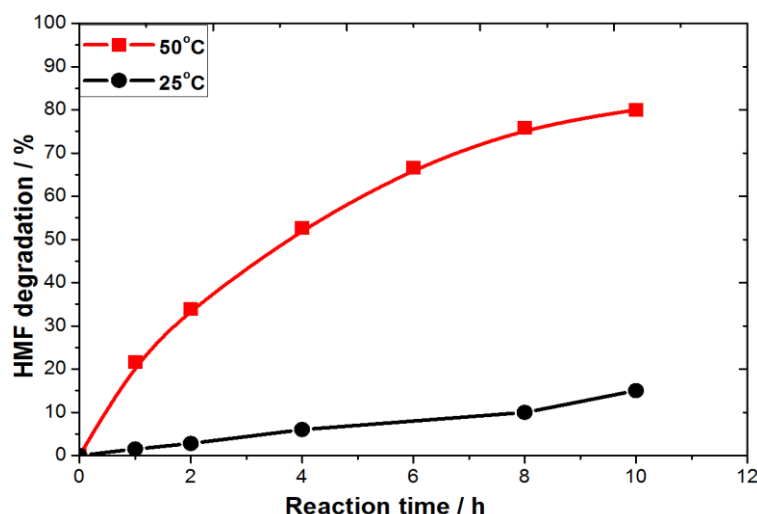
Fig. 4. 8 shows 80% of HMF degradation at $50^{o}C$ and 18% of HMF degradation at $25^{o}C$
Fig. 4. 8 HMF degradation in absence of catalyst in pH 13 solvent under inert (N_2) atmosphere at $25^{o}C$, $50^{o}C$ temperature and ambient pressure.

without any significant desired product (i.e. FDCA) formation over 10h. These observations are agreed with Pasini et al. [48]. HMF was degraded into undesired or waste products and difficult to identify using HPLC. The color of the reaction mixture was turning from colorless to brown and then into dark brown with reaction time as shown in the fig.4. 9
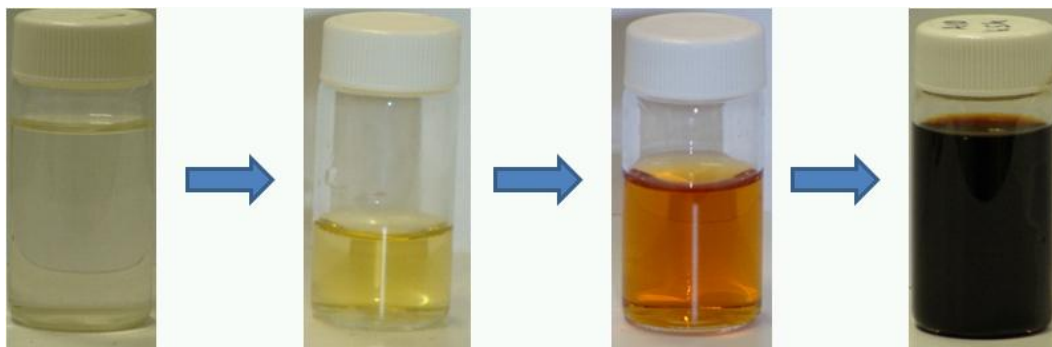
Fig. 4. 9 Degradation of HMF into dark brown products (unknown).

Mass spectroscopy (MS) was used to identify product from dark brown aqueous solution, but without success. To probe more insight information about the loss of HMF, in-situ ^{1}H NMR (500Hz) kinetic studies were conducted under inert (N$_2$ sealed) atmosphere at pH 6 and pH 13 as show in fig. 4. 10 .
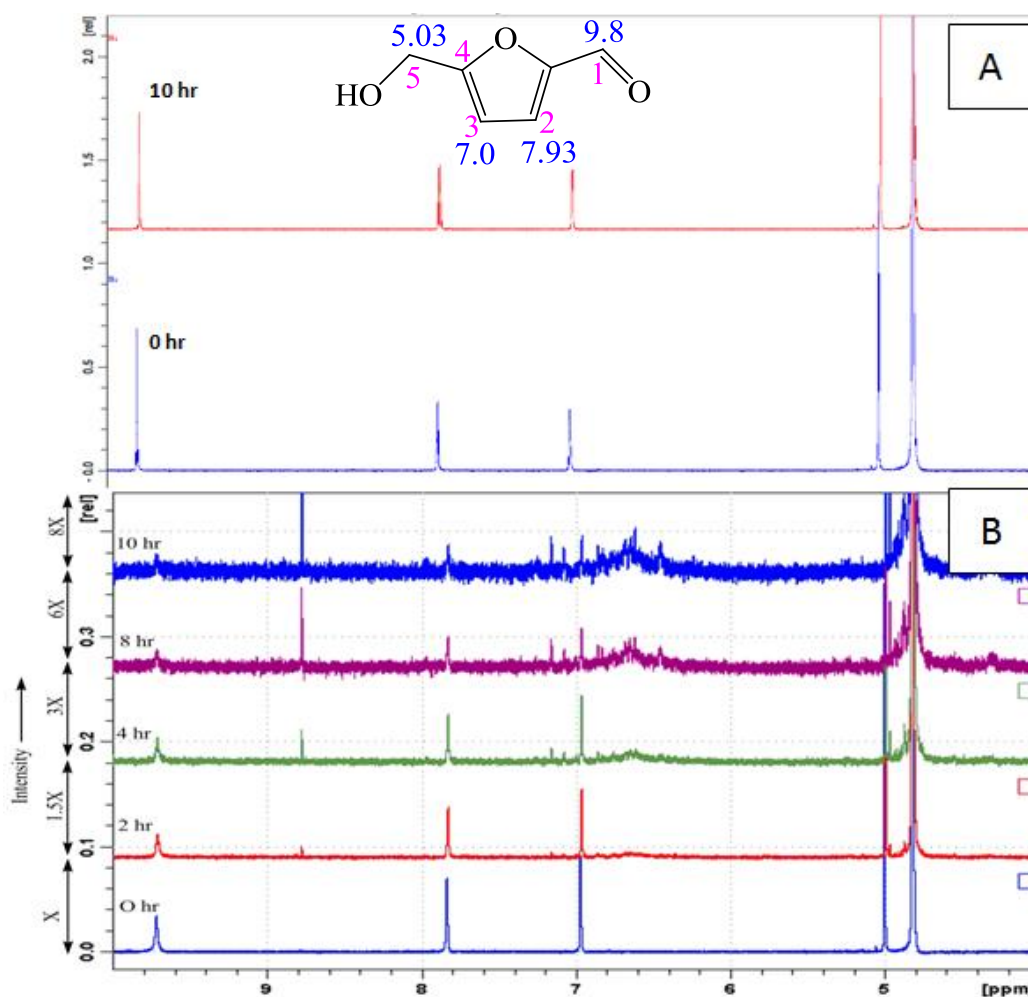
Fig. 4. 10 In-situ kinetic study of 5mM HMF using 1H NMR at a) pH 13 (0.1M NaOD), b) in pH 6 (D$_2$O) at 50°C under N$_2$. Where CHO=9.8ppm; CH=7.93 & 7ppm; D$_2$O=4.94ppm.

In ^{1}H NMR, the two protons of furan ring C-H were shown at 7 ppm and 7.93 ppm, proton of CHO was at 9.8 ppm and proton of CH_2OH group is at 5.03 ppm. The proton of alcohol was difficult to show in specified NMR equipment. Fig. 4. 10 a shows ^{1}H NMR of 5mM HMF at pH 6 for 0h and 10h, where there was no change in any protons peak intensity. It indicates that HMF was stable at pH 6 at 50°C conditions. Fig. 4. 10 b shows ^{1}H NMR at higher pH 13, the intensity of all protons has decreased slowly along with time from 0h to 10h and finally disappeared. The scale of y-axis was zoomed to several times to see small peaks at higher reaction times for the new product formation, if any. From Fig. 4. 10 b, it is very clear that there are no furan ring contained products, which indicates cross polymerization of HMF at C-H by replacing protons. The intensity of CH_2OH and CHO has also disappeared at 10h of reaction time. So we are interpreting that at higher pH (pH 13 or more) HMF is not stable and undergoing polymerization by open-up of furan ring. Finally the HMF is turning into dark brown colored, insoluble solid compound (humins). This information supports the degradation of HMF in fig 4. 8.

4. 3. 3. Testing of supported metal catalyst for HMF oxidation

As shown in the section 4.3.1, HMF is not stable at higher pH (≤13) in the absence of a catalyst. Surprisingly in the presence of a carbon-supported Pt nanoparticle catalyst (Pt/C), a different reaction pathway was observed for the HMF oxidation. HMF was added to pH 13 aqueous solvent. The reaction was carried out with Pt/HMF molar ratio 0.1 at 50°C and 10 bar O_2.
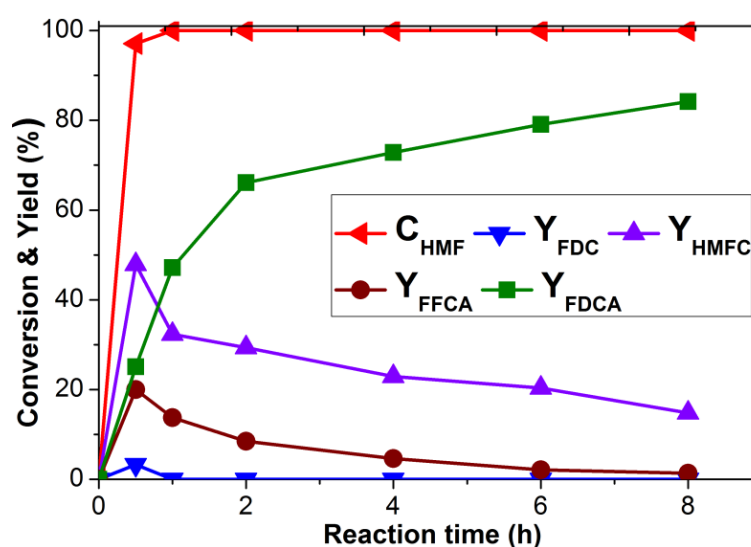
Fig. 4. 11 HMF oxidation and product distribution with reaction time. Reaction conditions: 50°C, pH 13, Pt/HMF molar ratio: 0.1, 10 bar O_2 (g). (Where C = conversion, Y = yield).

Fig. 4. 11 shows the kinetic behavior of HMF oxidation reaction, in particular yield (Y), conversion (C) of HMF and its oxidized intermediate products. About 95% of HMF is converted in less than 30 min of reaction time under pH 13 conditions in the presence of Pt/C catalyst, which indicates that HMF adsorption reaction on Pt surface is very fast. About 50% of the converted HMF is turned into HMFC. This suggests that CHO group reacts relatively faster than the CH_2OH group. And also this behavior indicates that adsorption/reaction of the $-CH_2OH$ group is slow and a rate limiting step for the HMF oxidation under the chosen conditions. 20% of FFCA observed in early reaction time was converted completely in 8h of the reaction time. Fig. 4. 12 shows the sequence of HMF oxidation products.
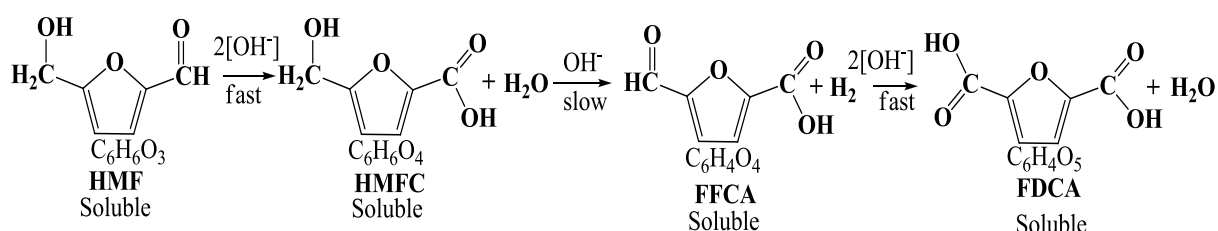
Fig. 4. 12 HMF oxidation reaction pathway at higher pH (pH≥13).

Furthermore, at higher pH (pH≥13), it confirms that the aldehyde moiety of HMF underwent a more rapid oxidation into the carboxylic group relative to the alcoholic group. Therefore HMF initially converts into HMFC, which agreed with findings of Jørgensen et al. for alcohol oxidation [53]. This is also in line with reports that the oxidation of HMF alcohol is slow due to stabilizing electron effects of the furan ring and formyl group, as claimed by Vinke et al. [54]. FDCA yield increases with time by oxidizing both aldehyde and alcohol groups, and 80% FDCA noticed at 8h of reaction time.

4. 3. 4. Effect of pH for HMF oxidation

Effect of pH on HMF oxidation was conducted under similar conditions (section 4.3.2) at pH 1 (0.2M H_2SO_4), pH 6 (H_2O), pH 10 (0.1mM NaOH) and compared with pH 13 (0.1M NaOH).
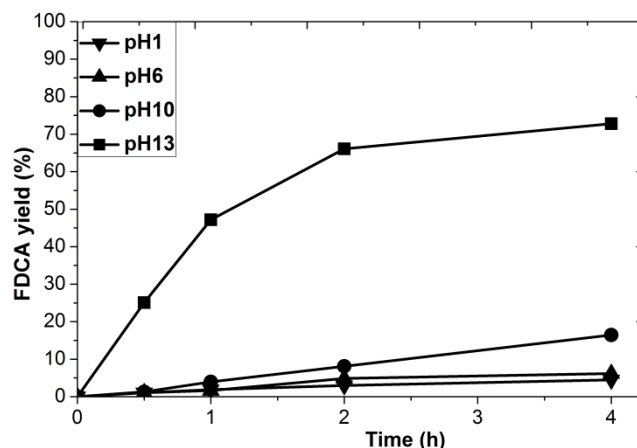
Fig. 4. 13 Effect of pH on FDCA yield from HMF oxidation with reaction time. Reaction conditions: $50^{o}C$, Pt/HMF molar ratio: 0.1, 10 bar O_2.

The formation of FDCA is significantly reduced at lower pH (pH 1 and pH 6). With increase of pH, the formation of FDCA increases and 17% of FDCA was observed at pH 10 in 4h of reaction time. Our interpretation from fig. 4. 13 is that the rate of HMF conversion reaction is low and FDCA inhibition is high at lower pH. Results are in agreement with Verdeguer et al. [37]. FDCA is not completely soluble in aqueous solvent at lower pH (pH$\leq$10). Solubility of FDCA increases with increase of pH, which eventually helps for faster desorption of FDCA from catalyst surface. The product distribution for HMF oxidation and its derivatives were shown in table 4. 3 for 4h of the reaction time.

Table 4. 3 HMF oxidation and product distribution after 4h reaction time (see fig. 4. 14). Reaction conditions: $50^{o}C$, Pt/HMF molar ratio: 0.1, 10 bar O_2.

	Time	C_{HMF}	Y_{FDC}	S_{FDC}	Y_{HMFC}	S_{HMFC}	Y_{FFCA}	S_{FFCA}
	(h)	(%)	(%)	(%)	(%)	(%)	(%)	(%)
pH 1	4	50.21	17.68	35.21	1.53	3.04	14.88	29.64
pH 6	4	56.62	16.25	28.70	2.61	4.60	29.96	52.93
pH 10	4	85.55	8.24	9.63	2.07	2.42	43.41	50.74
pH 13	4	100.00	0.00	0.00	22.91	22.91	4.61	4.61

The rate of HMF conversion increases with an increase in the pH on a Pt metal catalyst. Concentration of [OH]$^-$ influences the oxidation of alcohol and aldehyde functional groups of HMF. The cannizzaro reaction plays an inevitable role to trigger the oxidation of HMF at higher pH. Formation of FDC is more favorable than FDCA at lower pH.
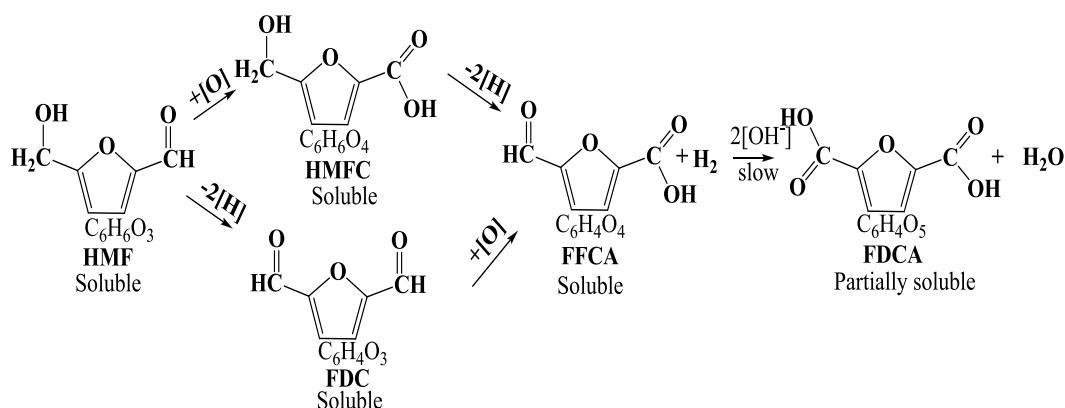
Fig. 4. 14 HMF oxidation reaction pathway at lower pH (pH≤10)

In contrary to higher pH (pH≥13), a different reaction pathway was observed in HMF oxidation at lower pH (pH≤10). In reactions with lower amounts of [OH]⁻ concentration, the yield of the intermediate oxidation products was higher than that of FDCA. In contrast, conversion of HMF decreases with decrease of pH. This may be due to deactivation of Pt by produced carboxylic acid as discussed by Klitgaard et al. [55], who observed deactivation of Au due to carboxylic acid for alcohol oxidation in the absence of [OH]⁻. At the same time, precipitation of formed FDCA onto the Pt surface may also hinder further oxidation of formed oxidative intermediates due to low solubility of FDCA. Therefore, presence of [OH]⁻ is required to achieve faster reaction rates and to get more yield of desired products from HMF oxidation.

4. 3. 5. Effect of oxygen partial pressure

The influence of oxygen partial pressure on HMF oxidation was studied by varying pressure from 1bar, 5bar and 10bar at 50°C.

Initially the rate of reaction for the FDCA yield was similar from 1 to 10 bar. After 1h of reaction time, the effect of pressure influences the FDCA yield. Higher pressure favors higher FDCA yield. This indicates that increased pressure increases the amount of available dissolved oxygen for the HMF oxidation reactions. Same type of pressure influence is observed by Gorbanev et al. [56], Casanova et al. [44] and Pisani et al. [48] for HMF oxidation on supported gold catalyst.
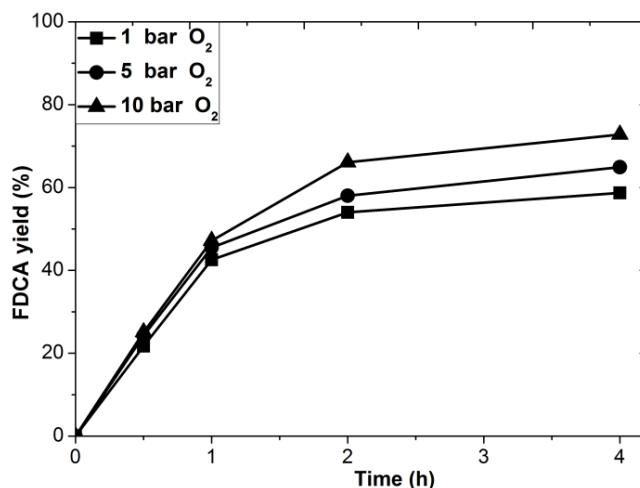
Fig. 4. 15 Effect of oxygen pressure on FDCA yield from HMF oxidation with reaction time. Reaction conditions: $50^{o}C$, pH 13, Pt/HMF molar ratio: 0.1

Table 4. 4 Effect of pH on HMF oxidation and product distribution for 4h reaction time (see fig. 4. 15). Reaction conditions: $50^{o}C$, pH 13, Pt/HMF molar ratio: 0.1, 10 bar O_2.

Pressure	C_{HMF} (%)	Y_{FDC} (%)	Y_{HMFC} (%)	Y_{FFCA} (%)	Y_{FDCA} (%)	Unknowns (%)
1 bar O_2	100	0.51	33.07	6.8	58.72	≤1.00
5 bar O_2	100	0.00	29.02	5.12	64.93	≤1.00
10 bar O_2	100	0.00	22.21	4.61	72.81	≤1.00

Table 4. 4 shows the effect of pressure for HMF oxidation on Pt surface at similar conditions. Effect of pressure is negligible for the HMF conversion. Carbon balance is satisfactory for HMF oxidation reaction at the given conditions with insignificant amount of unknowns. At low pressure, the amount of dissolved oxygen is less, which causes partial oxidation of HMF into intermediates. With increase of pressure, the amount of formed intermediates decreases relatively.

4. 3. 6. Effect of the nature of the metal catalyst

The influence of the catalytically active metal was studied using different supported metal nanoparticle catalysts; in particular Au/TiO$_2$, Ru/C, Rh/C and Pd/C. Their performance was compared with Pt/C. Constant metal/HMF molar ratio was maintained for all metal catalysts and reactions were carried out at similar reaction conditions.
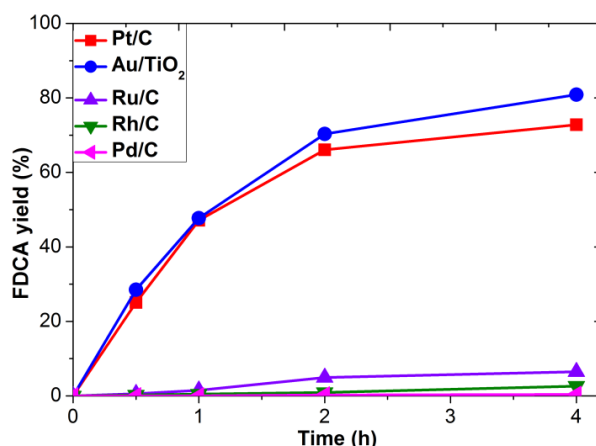
Fig. 4. 16 Effect of catalytically active metal surface on FDCA yield with reaction time. Reaction conditions: $50^{\circ}C$, pH 13, metal/HMF molar ratio: 0.1, 10 bar O_2

From fig. 4. 16 gold catalyst shows superior activity than Pt. Similar effect was observed by Davis et al. [31]. HMF is effectively oxidized on Au surface and yields 80% of FDCA in 4h reaction time at similar reaction conditions. Ru, Rh and Pd show relatively low activity for FDCA formation than Au and Pt surfaces.

Table 4. 5 Effect of catalytically active metal surface on HMF oxidation and product distribution for 4h reaction time. Reaction conditions: $50^{\circ}C$, pH 13, metal/HMF molar ratio: 0.1, 10 bar O_2.

Supported metals	C_{HMF} (%)	Y_{FDC} (%)	Y_{HMFC} (%)	Y_{FFCA} (%)	Y_{FDCA} (%)	Unknowns (%)
Pt/C	100	≤ 1.00	21.91	4.61	72.81	≤ 1.00
Pd/C	54.57	≤ 1.00	10.82	1.12	0.40	42.23
Au/TiO$_2$	100	≤ 2.00	17.77	0.13	80.87	1.23
Ru/C	98.05	7.03	9.93	6.89	6.48	74.75
Rh/C	81.26	≤ 1.00	25.57	33.91	12.62	9.16

Table 4. 5 shows the influence of the type of active metal surface for HMF oxidation reaction under similar conditions. Pt surface is active for HMF conversion into oxidative products such as HMFC, FFCA, and FDCA. The material balance for the reactant and products is satisfactory for Pt catalyzed reaction with less than 1% of unknown products. Even at pH 13 and 4h reaction time, HMF is not completely converted in the case of Pd catalyst. This indicates that the HMF is protected from the degradation. The product distribution for Pd catalyzed HMF oxidation reaction with significant amount of unknowns suggests a different reaction pathway with less selectivity for the desired

products. Au surface shows a superior activity for the HMF oxidative products compared to the Pt surface. In case of Ru catalyzed HMF oxidation reaction, 7% of the FDC was observed, which was in contrast to the other metal surfaces at the given conditions. Ru also appears to follow a different reaction pathway with relatively less amount of oxidative products and significant amount of unknowns. Ru surface contrasts with the Pd surface for the HMF conversion. Here, may be a part of HMF has undergone degradation reaction into humins due to higher pH rather than converting into FDCA. On Rh surface, 81% of HMF is converted into relatively more amount of oxidative intermediates (HMFC, FFCA) than FDCA. This indicates that Rh surface was deactivated due to formed FDCA or strong adsorption of intermediates.

4. 4.   Conclusions

In this chapter, we successfully demonstrated a process based on low temperature liquid-phase heterogeneous catalysis for the production of monomer type molecules for the polymer industry. This partly helps to replace the dependency on petroleum. First, the oxidation of biomass-derived model molecule HMF was studied under mild temperature ($50^{o}C$) and pressure (max. 10 bar O_2) conditions. Aqueous alkaline solvents favored complete oxidation of HMF into FDCA. HMF degradation mechanism was studied in the absence of metal catalyst using in-situ NMR. It has confirmed the loss of HMF at higher pH (≥ 13) by cross-polymerization via cannizzaro reaction. It is also seen that the pH of a reaction has a strong influence on oxidation of alcohol moiety of HMF and $[OH]^-$ influences the HMF oxidation into FDCA. Experimental analysis suggests that at lower pH (≤ 7), the alcoholic group of HMF oxidizes faster than aldehyde moiety on Pt surface, whereas at higher pH (≥ 13), oxidation of alcoholic group appears as the rate limiting step. Low temperatures and basic pH led to the oxidation of both formyl and hydroxyl groups of HMF to FDCA. Using high surface area Pt/C catalysts, 100% of HMF conversion with 80% of FDCA yield was achieved in 8h reaction time at pH13. Increase of partial pressure of molecular oxygen improved FDCA yield slightly. At the given reaction conditions, Au showed better catalytic activity than Pt, Ru, Rh and Pd.

4. 5.   References

1.   Rossini Frederick, D. and J. Mair Beveridge, *Composition of Petroleum*, in *progress in petroleum technology*. 1951, American Chemical Society. p. 334-352.

2.   Frei, H., *Selective Hydrocarbon Oxidation in Zeolites.* Science, 2006. 313(5785): p. 309-310.

3.   Hodnett, B.K., *Heterogeneous Catalytic Oxidation: Fundamental and Technological Aspects of the Selective and Total Oxidation of Organic Compounds*: WILEY.

4.   Corma, A., S. Iborra, and A. Velty, *Chemical Routes for the Transformation of Biomass into Chemicals.* ChemInform, 2007. 38(36): p. no-no.

5.   Gallezot, P., *Catalytic Conversion of Biomass: Challenges and Issues.* ChemSusChem, 2008. 1(8-9): p. 734-737.

6.   Verendel, J.J., T.L. Church, and P.G. Andersson, *ChemInform Abstract: Catalytic One-Pot Production of Small Organics rom Polysaccharides.* ChemInform, 2011. 42(44): p. no-no.

7.   Kamm, B., *Chemical and biochemical generation of carbohydrates from lignocellulose-feedstock (Lupinus nootkatensis)"quantification of glucose.* Chemosphere, 2006. 62(1): p. 97-105.

8.   T. Werpy and G. Petersen, *Top Value Added Chemicals From Biomass Volume I: Results of Screening for Potential Candidates from Sugars and Synthesis Gas* Pacific Northwest National Laboratory (PNNL) and the National Renewable Energy Laboratory (NREL), 2004.

9.   Klemm, D., Cellulose*: Fascinating Biopolymer and Sustainable Raw Material.* Angew. Chem. Int. Ed., 2005. 44(22): p. 3358-3393.

10.   Su, Y., *Single-step conversion of cellulose to 5-hydroxymethylfurfural (HMF), a versatile platform chemical.* Applied Catalysis A: General, 2009. 361(12): p. 117-122.

11.   Rosatella, A.A., 5-*Hydroxymethylfurfural (HMF) as a building block platform: Biological properties, synthesis and synthetic applications.* Green Chem., 2011. 13(4): p. 754-793.

12.   Huber, G.W., S. Iborra, and A. Corma, *Synthesis of Transportation Fuels from Biomass: Chemistry, Catalysts, and Engineering.* Chemical Reviews, 2006. 106(9): p. 4044-4098.

13.   Bicker, M., Dehydration *of d-fructose to hydroxymethylfurfural in sub- and supercritical fluids.* The Journal of Supercritical Fluids, 2005. 36(2): p. 118-126.

14.   Claus, P. and H. Vogel, *The Roll of Chemocatalysis in the Establishment of the Technology Platform "Renewable Resources".* Chemical Engineering & Technology, 2008. 31(5): p. 678-699.

15.   Lichtenthaler, F.W. and S. Peters, *Carbohydrates as green raw materials for the chemical industry.* Comptes Rendus Chimie, 2004. 7(2): p. 65-90.

16.   Moreau, C., M.N. Belgacem, and A. Gandini, *Recent Catalytic Advances in the Chemistry of Substituted Furans from Carbohydrates and in the Ensuing Polymers.* Topics in Catalysis, 2004. 27(1): p. 11-30.

17.   G. J. M. Gruter and F. Dautzenberg, *Method for the manufacture of 5-alkoxymethylfurfural derivatives by reacting a glucose-containing starting material with an alcohol in the presence of a catalytic or sub-stoechiometric amount of acid*, in *Eur. Pat. Appl.* 2007, EP1834950.

18.   West, R.M., Carbon*"carbon bond formation for biomass-derived furfurals and ketones by aldol condensation in a biphasic system.* Journal of Molecular Catalysis A: Chemical, 2008. 296(12): p. 18-27.

19.   Chheda, J.N. and J.A. Dumesic, *An overview of dehydration, aldol-condensation and hydrogenation processes for production of liquid alkanes from biomass-derived carbohydrates.* Catalysis Today, 2007. 123(14): p. 59-70.

20. Simonetti, D.A. and J.A. Dumesic, *Catalytic Strategies for Changing the Energy Content and Achieving C-C Coupling in Biomass-Derived Oxygenated Hydrocarbons.* Chemsuschem, 2008. 1(8-9): p. 725-733.

21. Lilga, M.A.H., Richard T.; Hu, Jianli; White, James F.; Gray, Michel J., *Oxidized Derivatives of Hydroxymethyl Furfural (HMF)*, in *US Patent & Trademark Office*, P.N.N. Laboratory, Editor. 2007, Battelle Memorial Institute: USA.

22. Yang, Z.-Z., A *one-pot approach for conversion of fructose to 2,5-diformylfuran by combination of Fe3O4-SBA-SO3H and K-OMS-2.* Green Chemistry, 2012.

23. Hopkins, K.T., Extended *Aromatic Furan Amidino Derivatives as Anti-Pneumocystis carinii Agents.* Journal of Medicinal Chemistry, 1998. 41(20): p. 3872-3878.

24. Del Poeta, M., Structure-*in vitro activity relationships of pentamidine analogues and dication-substituted bis-benzimidazoles as new antifungal agents.* Antimicrobial Agents and Chemotherapy, 1998. 42(10): p. 2495-2502.

25. Hui, Z. and A. Gandini, *Polymeric schiff bases bearing furan moieties.* European Polymer Journal, 1992. 28(12): p. 1461-1469.

26. Köpnick, H., Polyesters, in *Ullmann's Encyclopedia of Industrial Chemistry.* 2000, Wiley-VCH Verlag GmbH & Co. KGaA.

27. Zuo, X., Liquid *phase oxidation of p-xylene to terephthalic acid at medium-high temperatures: multiple benefits of CO2-expanded liquids.* Green Chemistry, 2010. 12(2): p. 260-267.

28. Fukushima, K.C., Olivier; Lecuyer, Julien M.; Almegren, Hamid A.; Alabdulrahman, Abdullah M.; Alsewailem, Fares D.; McNeil, Melanie A.; Dubois, Philippe; Waymouth, Robert M.; Horn, Hans W.; Rice, Julia E.; Hedrick,; ames L., *Organocatalytic depolymerization of poly(ethylene terephthalate).* Journal of Polymer Science Part A: Polymer Chemistry, 2011. 49(5): p. 1273-1281.

29. Ostapchenko, G.J., *Polyethylene terephthalate articles having desirable adhesion and non-blocking characteristics, and a preparative process therefor* 2005, E. I. du Pont de Nemours and Company: USA.

30. Gandini, A. and M.N. Belgacem, *Recent Contributions to the Preparation of Polymers Derived from Renewable Resources.* Journal of Polymers and the Environment, 2002. 10(3): p. 105-114.

31. Tong, X., Y. Ma, and Y. Li, *Biomass into chemicals: Conversion of sugars to furan derivatives by catalytic processes.* Applied Catalysis A: General, 2010. 385(1-2): p. 1-13.

32. Benecke, H.P., Furanic-*modified amine-based curatives.* 2010, US20100280186: USA.

33. Cottier, L.D., G.; Lewkowski, J.; Skowronski, R., *Oxidation of 5-hydroxymethylfurfural under sonochemical conditions.* Polish Journal of Chemistry, 1994. 68(4): p. 693-698.

34. Amarasekara, A.S., D. Green, and E. McMillan, *Efficient oxidation of 5-hydroxymethylfurfural to 2,5-diformylfuran using Mn(III)-salen catalysts.* Catalysis Communications, 2008. 9(2): p. 286-288.

35. El-Hajj, T., J.-C. Martin, and G. Descotes, *Dérivés de l'hydroxyméthyl-5 furfural. I. Synthése de dérivés du di- et terfuranne.* Journal of Heterocyclic Chemistry, 1983. 20(1): p. 233-235.

36. Van Reijendam, J.W., G.J. Heeres, and M.J. Janssen, *Polyenyl-substituted furans and thiophenes. A study of the electronic spectral.* Tetrahedron, 1970. 26(6): p. 1291-1301.

37. Verdeguer, P., N. Merat, and A. Gaset, *catalytic-oxidation of hmf to 2,5-furandicarboxylic acid.* Journal of Molecular Catalysis, 1993. 85(3): p. 327-344.

38. Partenheimer, W. and Vladimir V. Grushin, *Synthesis of 2,5-Diformylfuran and Furan-2,5-Dicarboxylic Acid by Catalytic Air-Oxidation of 5-Hydroxymethylfurfural. Unexpectedly Selective Aerobic Oxidation of Benzyl Alcohol to Benzaldehyde with Metal=Bromide Catalysts.* Advanced Synthesis & Catalysis, 2001. 343(1): p. 102-111.

39. Cottier, L., ChemInform *Abstract: Ultrasonically Accelerated Syntheses of Furan-2,5-dicarbaldehyde from 5-Hydroxymethyl-2-furfural.* ChemInform, 1995. 26(52): p. no-no.

40. Du, Z., Oxidation *of 5-hydroxymethylfurfural to maleic anhydride with molecular oxygen.* Green Chem., 2011. 13(3): p. 554-557.

41. van Bekkum, H., *Studies on Selective Carbohydrate Oxidation.* Carbohydrates as Organic Raw Materials, ed. F.W. Lichtenthaler. 1991: VCH: Weinham.

42. Cottier, L., Oxidation *of 5-hydroxymethylfurfural and derivatives to furanaldehydes with 2,2,6,6-tetramethylpiperidine oxide radical - co-oxidant pairs.* Journal of Heterocyclic Chemistry, 1995. 32(3): p. 927-930.

43. Saha, B., S. Dutta, and M.M. Abu-Omar, *Aerobic oxidation of 5-hydroxylmethylfurfural with homogeneous and nanoparticulate catalysts.* Catal. Sci. Technol, 2012. 2(1): p. 79-81.

44. Casanova, O., S. Iborra, and A. Corma, *Biomass into Chemicals: Aerobic Oxidation of 5-Hydroxymethyl-2-furfural into 2,5-Furandicarboxylic Acid with Gold Nanoparticle Catalysts.* ChemSusChem, 2009. 2(12): p. 1138-1144.

45. Lilga, M., R. Hallen, and M. Gray, *Production of Oxidized Derivatives of 5-Hydroxymethylfurfural (HMF).* Top. Catal., 2010. 53(15): p. 1264-1269.

46. Boisen, A., Process *integration for the conversion of glucose to 2,5-furandicarboxylic acid.* Chem. Eng. Res. Des., 2009. 87(9): p. 1318-1327.

47. Egeblad, K., Heterogeneous *catalysis for production of value-added chemicals from biomass*, in *Catalysis*, J.J. Spivey and K.M. Dooley, Editors. 2008. p. 13-50.

48. Pasini, T., Selective *oxidation of 5-hydroxymethyl-2-furfural using supported gold-copper nanoparticles.* Green Chem., 2011. 13(8): p. 2091-2099.

49. Davis, S.E., Oxidation *of 5-hydroxymethylfurfural over supported Pt, Pd and Au catalysts.* Catalysis Today, 2011. 160(1): p. 55-60.

50. Kroger, M., U. Prusse, and K.D. Vorlop. *A new approach for the production of 2,5-furandicarboxylic acid by in situ oxidation of 5-hydroxymethylfurfural starting from fructose.* 2000.

51. Carlini, C., Selective *oxidation of 5-hydroxymethyl-2-furaldehyde to furan-2,5-dicarboxaldehyde by catalytic systems based on vanadyl phosphate.* Appl. Catal., B, 2005. 289(2): p. 197-204.

52. Partenheimer, W. and V.V. Grushin, *Synthesis of 2,5-diformylfuran and furan-2,5-dicarboxylic acid by catalytic air-oxidation of 5-hydroxymethylfurfural. Unexpectedly selective aerobic oxidation of benzyl alcohol to benzaldehyde with metal/bromide catalysts.* Advanced Synthesis & Catalysis, 2001. 343(1): p. 102-111.

53. Levenspiel, O., *Chemical Reaction Engineering.* 1999. Third edition.

54. Jørgensen, B., Aerobic *oxidation of aqueous ethanol using heterogeneous gold catalysts: Efficient routes to acetic acid and ethyl acetate.* Journal of Catalysis, 2007. 251(2): p. 332-337.

55. Vinke, P., *On the oxygen tolerance of noble metal catalysts in liquid phase alcohol oxidations the influence of the support on catalyst deactivation*, in *Studies in Surface Science and Catalysis*. 1991, Elsevier. p. 385-394.

56. Klitgaard, S., Aerobic *Oxidation of Alcohols over Gold Catalysts: Role of Acid and Base.* Catalysis Letters, 2008. 126(3): p. 213-217.

57. Gorbanev, Y.Y., Gold-*Catalyzed Aerobic Oxidation of 5-Hydroxymethylfurfural in Water at Ambient Temperature.* Chemsuschem, 2009. 2(7): p. 672-675.

Chapter 5

Heterogeneous Catalytic Hydrogenation of HMF

5.1 Introduction

The products produced by hydrogenation of biomass-derived HMF are sustainable substitutes to replace petroleum-based building blocks [1, 2]. The efficient production of biomass-derived fuels is of technological importance for the transition to a more sustainable future [3, 4]. In this respect, HMF has been identified as a key precursor for the production of chemicals and fuel type molecules (see chapter 3, 4) [5]. Importantly, HMF hydrogenation has a number of attractions as a biofuel. Unlike petroleum derived intermediates, HMF has keto and hydroxyl functionalities that can be hydrogenated into various products [6]. The selective hydrogenation involves addition of hydrogen to C—O of alcoholic group or to C=O of aldehyde group of HMF without changing the furan ring. The complete hydrogenation involves addition of hydrogen to C=C of furan ring [7]. Selective hydrogenation product of HMF is 2, 5-dimethylfuran (DMF) as shown in the fig. 5. 1   DMF has an energy density 40% greater than ethanol, making it comparable to gasoline (petrol) [1, 8].
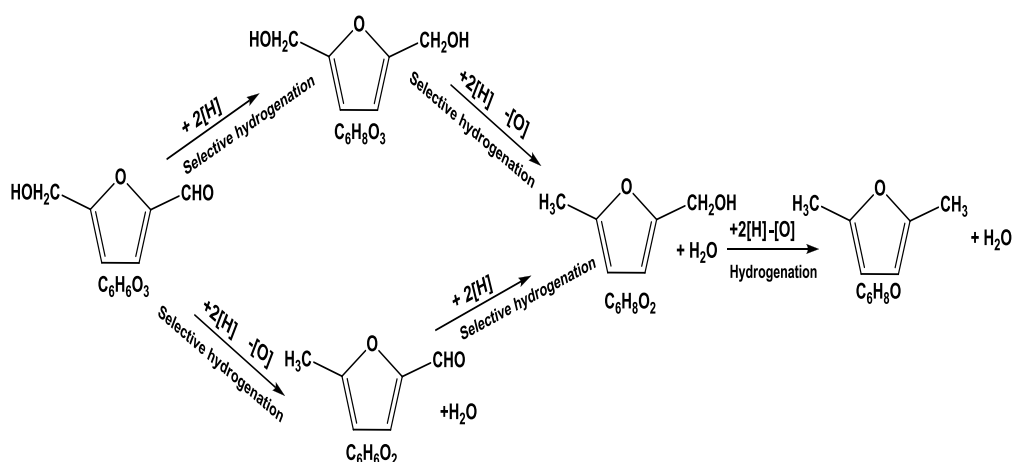
Fig. 5. 1 Selective hydrogenation of HMF.

DMF is attractive as a biofuel due to its ideal boiling point (92–94°C), high energy density (30 kJ/cm^3), and high research octane number (RON=119). Furthermore it is immiscible with water and is easier to blend with gasoline than ethanol [1, 2, 5, 9, 10].

The total hydrogenation product of HMF is dihydroxymethyltetrahydrofuran (DHMTHF), a useful chemical with applications as a solvent, a monomer or precursor to the production of other high-value chemicals [11-13]. For example, DHMTHF can be converted to 1, 6-hexanediol, a valuable chemical used in polymers and specialty chemicals by hydrogenolysis and dehydration reactions as shown in the fig. 5. 2 .
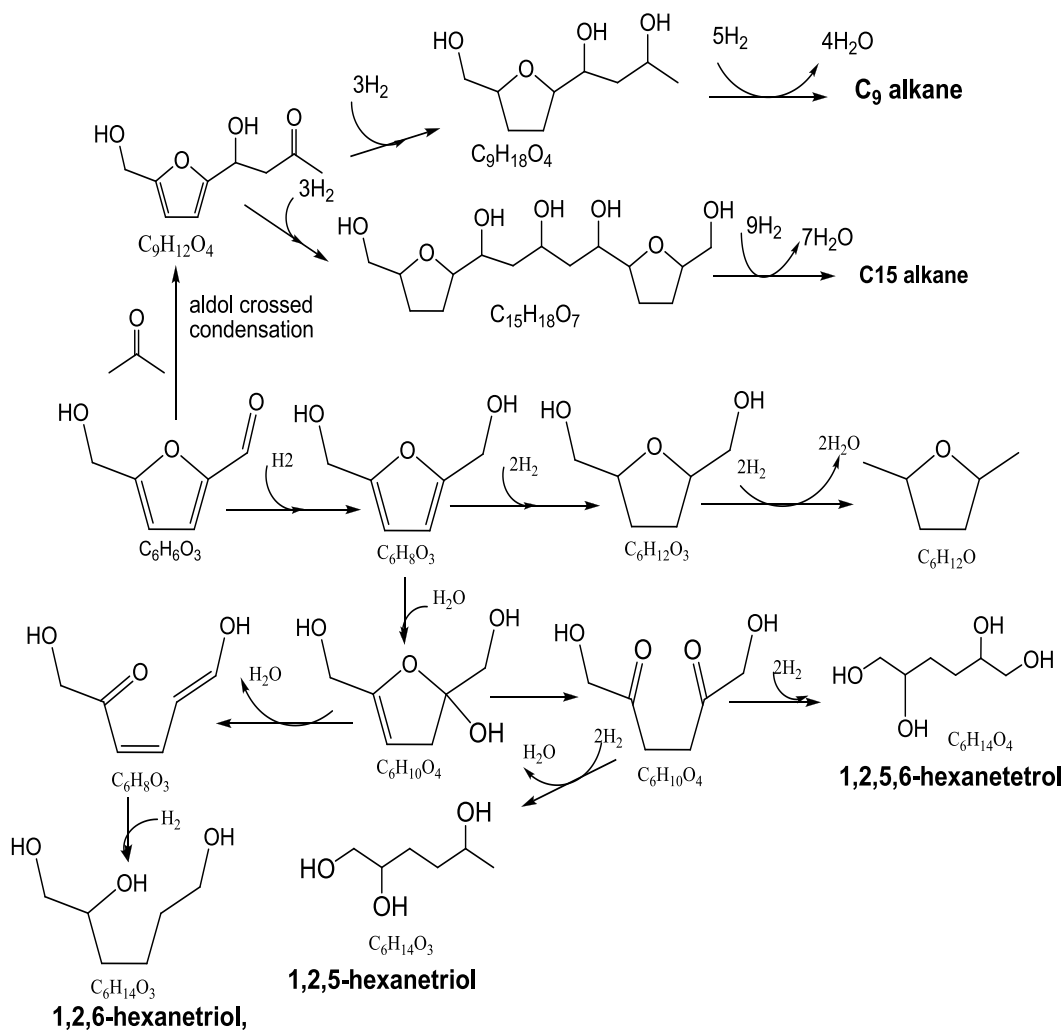
Fig. 5. 2 Total hydrogenation of HMF into DHMTHF and formation of n-alkane and poly-ol by subsequent hydrogenation, hydration and dehydration reactions (based on Huber et al.[11]).

Recently, Roman-Leshkov et al. [1] studied selective catalytic route for the production of DMF from fructose via two-step process. He combined dehydration and hydrogenation reactions to produce DMF in biphasic system. His work is limited to copper–ruthenium (CuRu) catalyst. Binder et al. repeated Dumesic's work in different conditions to produce DMF from fructose [14]. His approach involved production of HMF from fructose with H_2SO_4 as a dehydration catalyst and hydrogenation of HMF

was taken up in 1-butanol with a Cu–Ru/C catalyst. As a result, 32.5% yield of DMF based on d-fructose was obtained. Very recently, Luijkx et al. [12] reported the ether formation in the hydrogenolysis of HMF over a palladium catalyst in 1-propanol. In case of total hydrogenation, quantitative yields in BHF or BHTHF were obtained over conventional hydrogenation catalysts, such as raney nickel with H_2O as solvent at high temperature and under high hydrogen pressure [13, 15-18]. However, effects of different metal catalysts were not well addressed.

5.1.1 Objective of this chapter

The aim of the chapter is to study the liquid-phase hydrogenation of HMF into fuel type DMF molecule. The objectives include selection of suitable reaction conditions and influence of different supported metal catalyst for HMF hydrogenation. To test the activity of a catalyst in terms of product selectivity and yield. Later this study will be compared with electrocatalytic hydrogenation at low temperature.

5.2 Results and Discussions

The hydrogenation of HMF was carried out using molecular hydrogen on the surface of different supported metal catalysts. The reaction was tested in different solvents to understand the pathway of intermediates formation to drive the reaction in the selective hydrogenation way to form desired products. Different heterogeneous metal catalysts such as Ru, Pt, Pd, Rh, Au, Ni, etc supported on carbon and metal oxides were tested for the same reaction.

5.2.1 Selection of Solvent

Solvents are known to have a significant effect on the rate of catalytic hydrogenation. The effect of solvent is attributed to various factors, which include solubility of hydrogen, thermodynamic interaction of solvent with reactant and products, competitive adsorption of solvent, etc. Ru catalyst has been reported to be active and stable for various hydrogenation reactions [1, 14, 18], therefore Ru/C catalyst was used in the initial studies. The solvents employed during hydrogenation of HMF were polar solvents such as water, dimethylacetamide (DMA), dimethyl sulfoxide (DMSO) and 1-butanol. The experiments were conducted using 5% Ru/C catalyst.
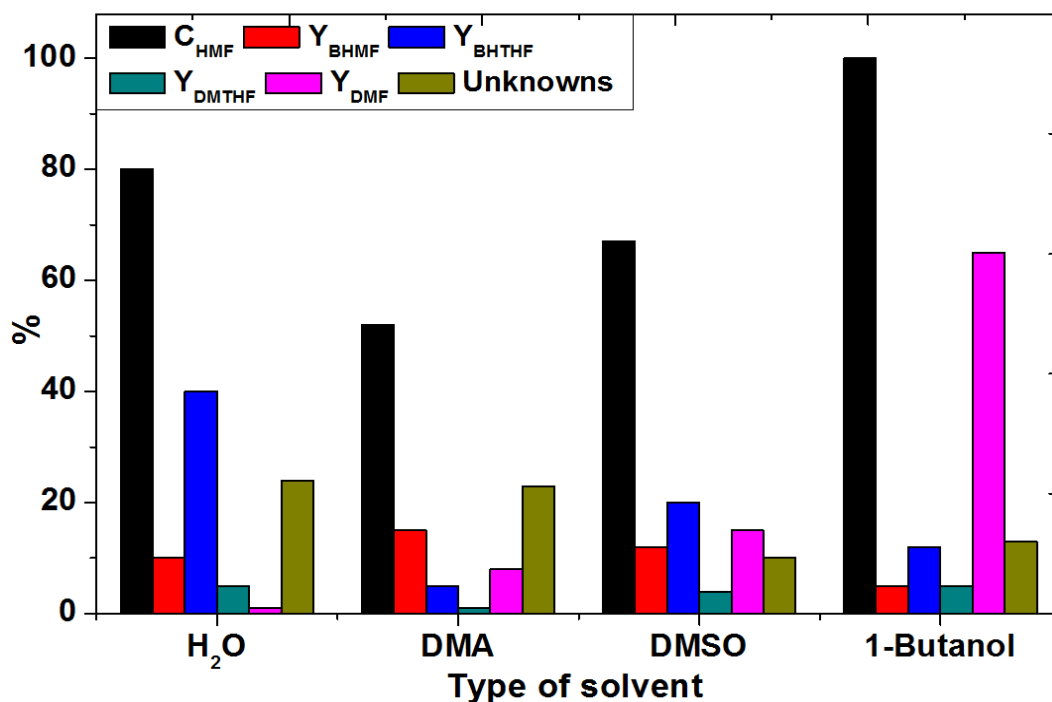
Fig. 5. 3 Effect of solvent on hydrogenation of HMF using Ru/C catalyst. Reaction conditions: 0.1M HMF; 1-butanol;175°C; 10bar H_2; 10h; 1000 rpm, metal/HMF molar ratio: 0.05.

Fig. 5. 3 presents the effect of solvent on HMF hydrogenation using Ru catalyst. At the given conditions, Ru was active to convert HMF in water, but selectivity was low for DMTHF and DMF. The main product was BHMF. Similar type of effect was observed by Alamillo using Ru black catalyst [7]. This study indicates that water was not a suitable solvent for HMF hydrogenation reactions to get the desired product (DMA). Organic solvents such as DMA and DMSO were previously used to produce HMF from fructose (see chapter 3), therefore same type of solvents were tested for HMF hydrogenation. Ru catalyst was active to produce intermediates as shown in the fig. 5. 3. In contrary to other solvents, Ru exhibited more activity for DMF formation in 1-butanol. Therefore, 1-butanol was selected as a suitable solvent to study the effect of supported metal catalyst for HMF hydrogenation.

5.2.2 Effect supported metal catalyst

Studies were conducted to investigate how the selectivity for HMF hydrogenation is affected by different catalytically active metal component. All catalysts were studied using 1-butanol as a solvent. The results are shown in the fig. 5. 4 .
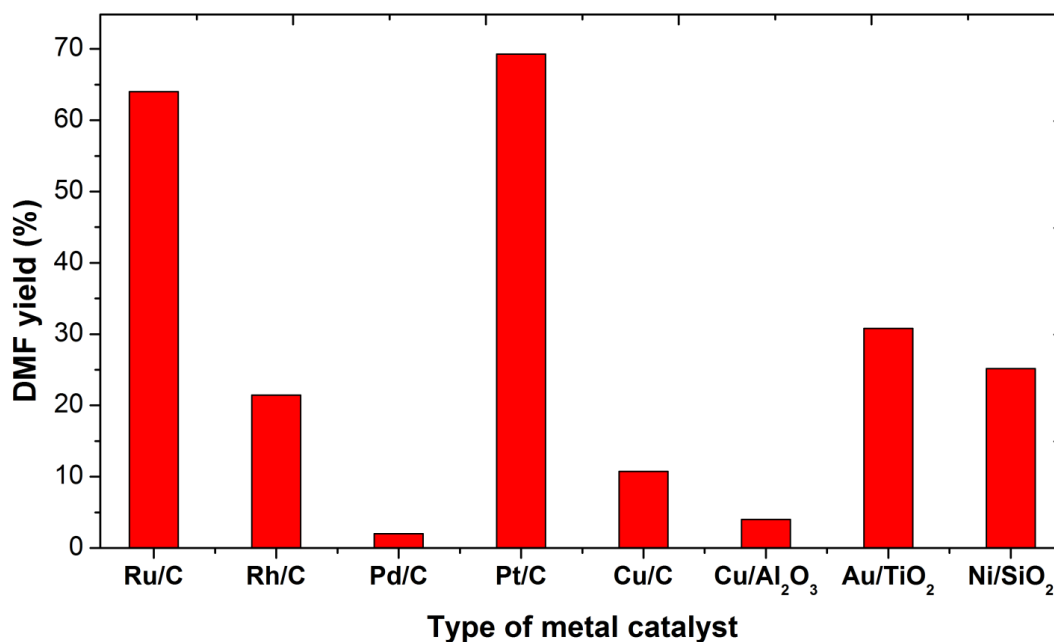
Fig. 5. 4 Hydrogenation of HMF using different catalysts. Conditions:0.1M HMF; 1-butanol;175°C; 10bar H$_2$; 10h; 1000 rpm, metal/HMF molar ratio: 0.05 .

Fig. 5.4 shows hydrogenation of HMF on different supported metal heterogeneous catalysts. All metals were active for the conversion of HMF into intermediates or products. 100% HMF conversion was observed in case of chosen metals. Compared to all metals Pt showed highest activity for the formation of DMF followed by Ru, Au, Ni, Rh, Cu and Pd. As hydrogenation of HMF involved a wide range of products as shown in fig.. 5. 2, combinations of different analytical techniques are required to analyze all products. At present we are not able to detect the complete product spectrum due to lack of proper analytical methods. Based on our existed HPLC method, spectra of the reaction mixture did not reveal significant peaks for unknowns as shown in the fig. 5. 5 , This indicates that the undetected molecules are in the form of insoluble polymers. These polymers may be formed through the loss of formaldehyde from DHMF, followed by furfuryl alcohol polymerization, which is well known from the literature [19, 20 3839 #37 3839 #37].

Fig. 5.5 shows complete product spectrum of HMF hydrogenation on different metals. Black line shows pure HMF signal in 1-buranol solvent. At 8 min retention time, DMF peak was shown.
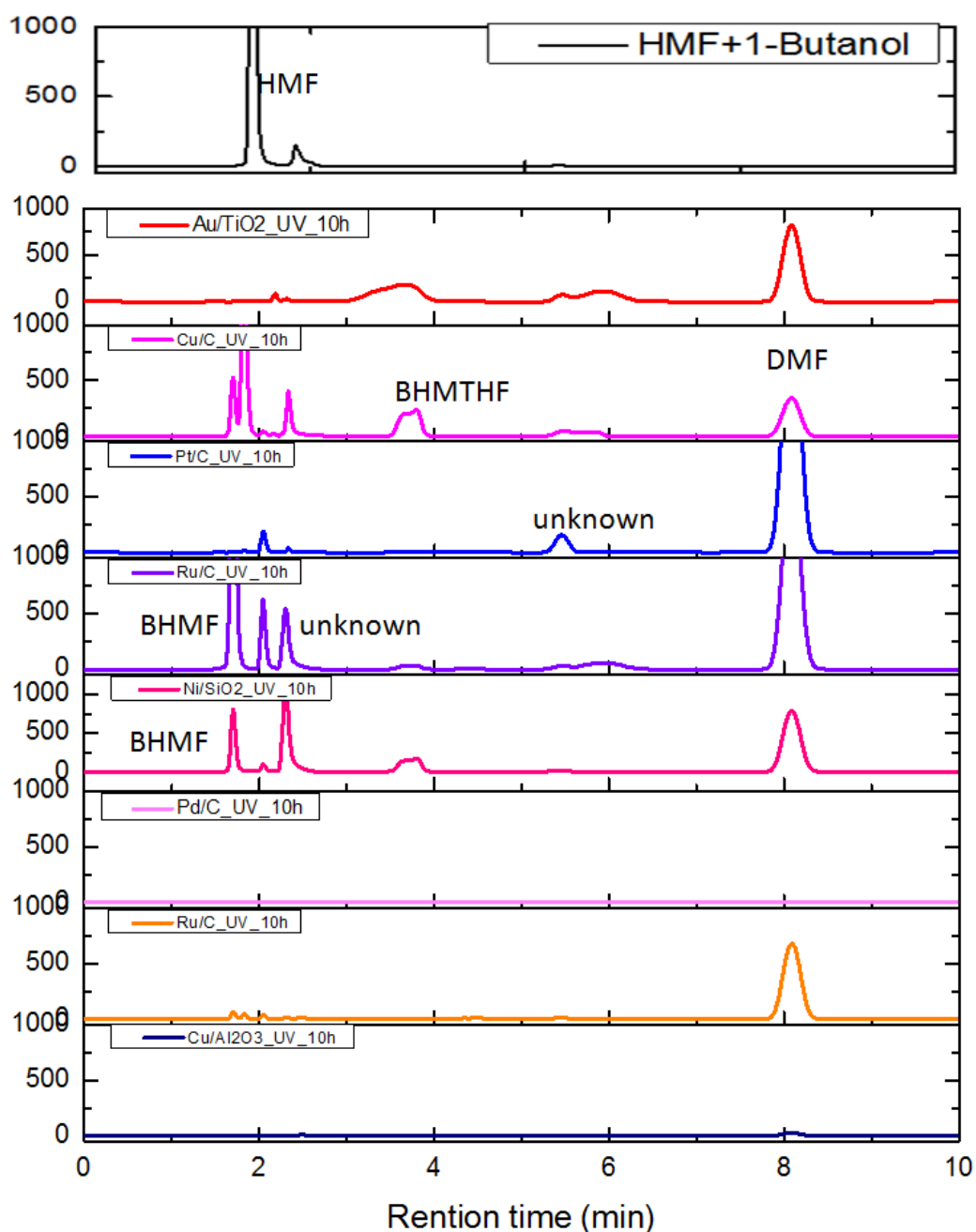
Fig. 5. 5 HPLC spectra for hydrogenation of HMF on different supported metals. Conditions: UV221nm, 0.1M HMF; 1-butanol;175°C; 10bar H_2; 10h; 1000 rpm, metal/HMF molar ratio: 0.05.

Cu/Al$_2$O$_3$ and Pd/C are relatively inactive for DMF formation, but active for conversion of HMF into intermediates (at present unknowns). Whereas Cu/C formed BHMTHF along with BHMF and intermediates. So nature of support also has influence on HMF dehydration reaction. All other metals were active for DMF formation with some percentage of intermediates.

5.3 Conclusions

For the hydrogenation of HMF into DMF the organic synthetic route is superior to the water synthetic route. Pt/C showed a highest activity for selective HMF hydrogenation with 70% of DMF followed by Ru/C > Ni/SiO$_2$ > Au/TiO$_2$ > Rh/C > Cu/Al$_2$O$_3$ > Pd/C. Unidentified products in case of Rh, Ni suggested different reaction pathway. Cu/Al$_2$O$_3$ is less active than Cu/C (due to support effect).

Outlook

Different analytical methods like GC-MS, NMR, etc are required to analyze complete product spectrum. ATR studies will be helpful to understand surface interaction of HMF derivatives with catalyst surface. Detailed kinetic studies are suggested to understand the process better along with a parametric study.

5.4 References

1.   Roman-Leshkov, Yuriy, Barrett, Christopher J., Liu, Zhen Y. and Dumesic, James A., Production of Dimethylfuran for Liquid Fuels from Biomass-Derived Carbohydrates. *Nature*, 2007. 447(7147): p. 982-985.
2.   Shiramizu, Mika and Toste, F. Dean, On the Diels–Alder Approach to Solely Biomass-Derived Polyethylene Terephthalate (Pet): Conversion of 2,5-Dimethylfuran and Acrolein into P-Xylene. *Chemistry – A European Journal*, 2011: p. n/a-n/a.
3.   Sheldon, Roger A., Selective Catalytic Synthesis of Fine Chemicals: Opportunities and Trends. *Journal of Molecular Catalysis A: Chemical*, 1996. 107(13): p. 75-83.
4.   Dutta, Saikat, De, Sudipta and Saha, Basudeb, A Brief Summary of the Synthesis of Polyester Building-Block Chemicals and Biofuels from 5-Hydroxymethylfurfural. *ChemPlusChem.* 77(4): p. 259-272.
5.   Wisniak, Jaime, Hershkowitz, Mordechai and Stein, Shoshanah, Hydrogenation of Xylose over Platinum Group Catalysts. *Product R&D*, 1974. 13(4): p. 232-236.
6.   Chheda, Juben N. and Dumesic, James A., An Overview of Dehydration, Aldol-Condensation and Hydrogenation Processes for Production of Liquid Alkanes from Biomass-Derived Carbohydrates. *Catalysis Today*, 2007. 123(14): p. 59-70.
7.   Alamillo, Ricardo, Tucker, Mark, Chia, Mei, Pagan-Torres, Yomaira and Dumesic, James, The Selective Hydrogenation of Biomass-Derived 5-Hydroxymethylfurfural Using Heterogeneous Catalysts. *Green Chemistry*, 2012.
8.   Chidambaram, Mandan and Bell, Alexis T., A Two-Step Approach for the Catalytic Conversion of Glucose to 2,5-Dimethylfuran in Ionic Liquids. *Green Chemistry*, 2010. 12(7): p. 1253-1262.
9.   Ruppert, Agnieszka M., Weinberg, Kamil and Palkovits, Regina, Hydrogenolysis Goes Bio: From Carbohydrates and Sugar Alcohols to Platform Chemicals. *Angewandte Chemie International Edition.* 51(11): p. 2564-2601.

10. Thananatthanachon, Todsapon and Rauchfuss, Thomas B., Efficient Route to Hydroxymethylfurans from Sugars Via Transfer Hydrogenation. *ChemSusChem*, 2010. 3(10): p. 1139-1141.

11. Lin, Yu-Chuan and Huber, George W., The Critical Role of Heterogeneous Catalysis in Lignocellulosic Biomass Conversion. *Energy & Environmental Science*, 2009. 2(1): p. 68-80.

12. Luijkx, Gerard C. A., Huck, Nina P. M., van Rantwijk, Fred, Maat, Leendert and van Bekkum, Herman, Cheminform Abstract: Ether Formation in the Hydrogenolysis of Hydroxymethylfurfural over Palladium Catalysts in Alcoholic Solution. *ChemInform*, 2009. 40(28): p. no-no.

13. Mehdi, Hasan, Fábos, Viktória, Tuba, Róbert, Bodor, Andrea, Mika, László, and Horváth, István, Integration of Homogeneous and Heterogeneous Catalytic Processes for a Multi-Step Conversion of Biomass: From Sucrose to Levulinic Acid, Γ-Valerolactone, 1,4-Pentanediol, 2-Methyl-Tetrahydrofuran, and Alkanes. *Topics in Catalysis*, 2008. 48(1): p. 49-54.

14. Binder, Joseph B. and Raines, Ronald T., Simple Chemical Transformation of Lignocellulosic Biomass into Furans for Fuels and Chemicals. *Journal of the American Chemical Society*, 2009. 131(5): p. 1979-1985.

15. Hu, Lei, Zhao, Geng, Hao, Weiwei, Tang, Xing, Sun, Yong, Lin, Lu, and Liu, Shijie, Catalytic Conversion of Biomass-Derived Carbohydrates into Fuels and Chemicals Via Furanic Aldehydes. *RSC Advances*, 2012.

16. De, Sudipta, Dutta, Saikat and Saha, Basudeb, One-Pot Conversions of Lignocellulosic and Algal Biomass into Liquid Fuels. *ChemSusChem*, 2012. 5(9): p. 1826-1833.

17. Thananatthanachon, Todsapon and Rauchfuss, Thomas B, Efficient Production of the Liquid Fuel 2,5-Dimethylfuran from Fructose Using Formic Acid as a Reagent. *Angewandte Chemie International Edition*, 2010. 49(37): p. 6616-6618.

18. Gallezot, P., Cerino, P. J., Blanc, B., Flhe, G. and Fuertes, P., Glucose Hydrogenation on Promoted Raney-Nickel Catalysts. *Journal of Catalysis*, 1994. 146(1): p. 93-102.

19. González, Regino, Martínez, Ricardo and Ortíz, Pedro, Polymerization of Furfuryl Alcohol with Trifluoroacetic Acid, 2. The Formation of Difurfuryl Ether. *Die Makromolekulare Chemie, Rapid Communications*, 1992. 13(11): p. 517-523.

20. Bertarione S, Bonino F, Cesano F, Damin A, Scarano D, Zecchina A., Furfuryl Alcohol Polymerization in H-Y Confined Spaces: Reaction Mechanism and Structure of Carbocationic Intermediates. *macromolecules*, 1996, 29, 3839.

Chapter 6

Electrocatalytic Oxidation of HMF

6.1 Introduction

Electrochemical catalysis is an electron transfer across an electrified heterogeneous catalyst interface (electrode), in other words, it is the combination of chemical reaction and heterogeneous electron transfer at an electrode [1]. It differs from chemical reaction in the way of formation of reactive intermediates [2]. During the electrochemical catalysis, electron transfers at the electrode for oxidation and reduction reactions, whereas oxidants or reductants are used for oxidation and reduction reactions in the chemical-catalytic processes [3-6]. Electrocatalysis and heterogeneous catalysis are involved in well-controlled sequences of elementary bond-breaking and bond-making processes and share many common mechanistic principles in the transformation of molecules over supported metal and metal oxide catalysts [7-11]. In general, the current (or electrode reaction rate) is governed by the rates of processes such as mass transfer, electron transfer at the electrode surface, chemical reactions preceding or following the electron transfer and other surface reactions, such as adsorption, desorption as shown in fig. 6. 1.
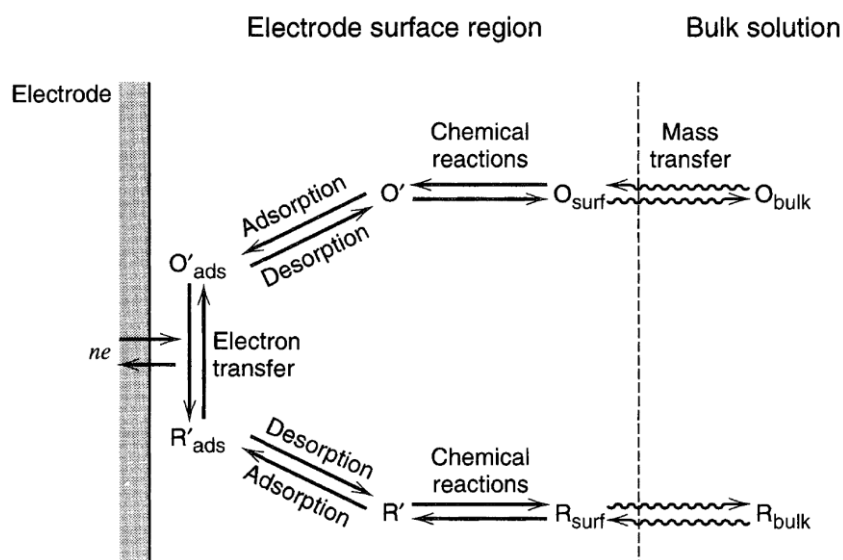
Fig. 6. 1 Electrocatalytic process (source: Bard et. al[12]).

In contrast to heterogeneous catalysis, the driving force of electrochemical reactions is not only controlled by concentration, pressure and temperature, but in addition by the interfacial potential drop (electrode potential) across the interface between electrocatalyst and electrolyte [13].

Electrochemical catalysis is a powerful technique and gains more research attention in recent years in many energy related research areas [14]. In both electrochemical and heterogeneous catalysis, the reactants adsorb on solid metal, diffuses to the surface, breaking some of the reactant bonds, formation of new bonds to form product molecules, which eventually desorbs from metal surface [15-17]. Under open circuit potential (OCP), i.e. in the absence of flow of electrons, electrochemical catalysis shows the similar effect as heterogeneous catalysis at the given conditions. Since electrochemical half cell reactions involve charged species, the interfacial electrode potential affects their Gibbs free energy of reaction ΔG_r. If the half cell process involves an adsorbed intermediate (chemisorption) the electrode potential affects the Gibbs chemisorption energy of that adsorbed intermediates. A change in electrode potential is related to that of the Gibbs free energy of a one-electron reaction process according to equation 6.1.

$$\Delta G_r = -F\Delta E_{electrode} \quad\dots\dots\dots\dots\dots\dots\dots\dots(6.1)$$

Where ΔG_r = Gibbs free energy of reaction or adsorption; n = number of electrons; F = charge on one mole of electrons, 96485 coulombs; E = potential of the electrode; all are at unit activity).

Variations in the chemisorption energies also modify the activation barrier of the elementary reaction. The near-linear relationship between the activation energy E_a and the chemisorption energy of an elementary reaction, ΔE_r (which is directly related to the Gibbs free energy of chemisorption) is referred to as the Brønsted-Evans-Polanyi relationship (BEP) [18]. In effect, the interfacial electrode potential affects the rate of all electrochemical half-cell reactions and hence it is feasible that electrode potentials may be used to manipulate and tune the relative rates of competing electrocatalytic processes [19]. The rate of an electrochemical process is directly related to the product formation rates via Faraday's law [20, 21]. Thus, a change in interfacial potential or current density may be used to selectively control product distributions.

6.1.1 Renewable electrons for water oxidation reactions

Our aim is to use renewable electrons to produce required oxygen for HMF oxidation reactions. The oxygen is available from water according to equations 6.4.

Oxidation $2H_2O \rightarrow 4H^+ + 4e^- + O_2$ $E° = 1.23$ V vs. NHE..........................(6.2)

Reduction $4H^+ + 4e^- \rightarrow 2H_2$ $E° = 0.00$ V vs. NHE..........................(6.3)

Overall $2H_2O \rightarrow 2H_2 + O_2$ $E°cell = +1.23$ V; $\Delta G = 238$ kJ/mol .....(6.4)

These oxidation and reduction steps are pH dependent. Water splitting can be done at higher pH values as well; however the standard potentials (vs NHE) will vary according to the Nernst equation and therefore shift by -59 mV for each pH unit increase. This potential, where equilibrium is established to the thermodynamic standards can be related to Gibbs free energy as shown in equation 6.1.

Therefore, it takes 238 kJ of energy to make one mole of O_2 as calculated by thermodynamics. This energy can be acquired easily from solar or wind electricity. However, in reality no process can be this efficient. The activation energy is associated with high energy transition states that are reached during the electrochemical process of oxygen evolution [3, 4, 22, 23].

6.1.2 Renewable chemicals from HMF oxidation reactions

Carbohydrates represent a well established alternative to fossil fuels as a renewable and economic source of energy and raw materials (see chapter 1). HMF is a versatile intermediate and can be synthesized starting from sucrose, fructose or glucose by dehydration reaction using acid catalyst (see chapter 3). The derivatives of HMF have many applications as starting material for polymer industry and also in macro-cyclic chemistry (chapter 4) [21, 24]. Although HMF is known as an important reactant, intermediate and platform molecule for many chemicals synthesis, its electrochemical properties were scarcely examined. And also, unified principles between heterogeneous catalysis and interfacial electrochemistry of HMF were not discussed in the open literature till date.

Much attention is paid to harvest the sun energy into electricity by using wind, solar and hydropower to lower the use of fossil fuels in electricity production [25]. None of these renewable energy sources can supply carbon atoms to produce organic chemicals to lower our dependency on the petroleum for chemicals. Carbon-containing molecules are found in the renewable biomass and it appears as a real alternative to petroleum. Biomass could potentially serve as a sustainable feedstock for the chemical industry. Renewable biomass chemical catalysis and renewable electricity have coexisted independently. Here we aimed to use direct renewable electrons from sun to transform renewable biomass to develop a sustainable carbon-neutral process in order to produce fuels and high-value chemicals[26, 27] according to the equation 6.5.

Anodic reaction
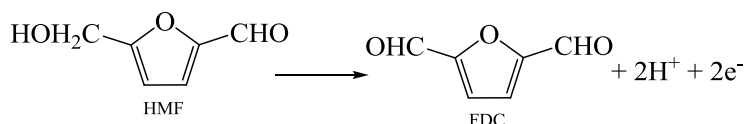
Cathodic counter reaction

$$2H^+ + 2e^- \longrightarrow H_2$$

............................(6.5)

FDC has been used in the synthesis of various useful compounds, including intermediates for pharmaceuticals, antifungal agents, organic conductors, macrocyclic ligands and symmetrical dialdehyde as a monomer in the preparation of new polymeric materials is a relatively unexplored area [22, 28-30].

As per our knowledge very limited literature (2 publications) is available with improper information for HMF anodic oxidation into FDC. Grabowski et al, (1991) published one page report on DC-electrolysis of HMF in a divided H-shaped cell. He applied current density 16mA/cm^2 to oxidize 5mM of HMF for 4 h in 100 ml of 1 M aqueous NaOH using nickel oxide/hydroxide anode and stainless steel cathode at room temperature. He reported 57% FDC yield based on ^{1}H NMR [31]. Skowronski et al, 1996 published 2 page reported using Pt electrode. A current density of 8mA/cm^2 (constant current electrolysis) is applied to a biphasic system of an aqueous solution of inorganic salt and dicholoromethane (organic) in a divided cell at the room temperature. 7% FDC was noticed after 3h of reaction time based on ^{1}H NMR [32].

To the best of our knowledge, the use of electrochemical catalysis in biomass research especially in HMF oxidation has been poorly explored. This is why this chapter focuses

on the oxidation reaction of the biomass-derived model molecule HMF using electro-catalysis. The aim of this study is to investigate and understand the selective conver-sion of the alcohol and aldehyde functional groups into carboxylic groups by keeping furan ring untouched. The influence of important reaction parameters was addressed and the behavior of intermediates with time during the reaction was monitored. The impact of the nature of electrode metal surfaces on the HMF oxidation reaction and its derivatives formation were focused. Apart from the efforts to understand basic mecha-nisms, the need for an electrochemically active material that understands the complex-ity associated with biomass derived molecules conversion continues to increase as their detection poses a challenge for analytical chemistry and liquid chromatography.

6.1.3 Objective of this chapter

The objective of our electrochemical study was to check the general feasibility of elec-trochemical HMF oxidation on the Pt surface and to compare and contrast the hetero-geneous pathway with the electrocatalytic pathway. The product distribution of electro-chemical catalytic oxidation and heterogeneous catalytic oxidation is compared only if the catalytic activity was observed. We are interested in a deeper understanding of the controlling factors of the oxygenating reaction pathways and strive to establish a critical comparison of electrocatalytic and heterogeneously catalyzed reaction conditions. Ul-timately, our goal is the identification of unifying principles between electrocatalysis and heterogeneous catalysis.

6.2 Results and Discussions

Nobel metals such as Pt & Pd and non-noble metal such as Ni were used as electrified catalyst surface. Different solvents were screened to get an appropriate electrolyte. Inorganic salts were used in order to increase the electrolyte conductivity. We assume that these salts have no influence on the conversion reactions. Electrochemical behav-ior of HMF and derivatives on electrified metal surface were discussed. Anodic oxida-tion reactions of HMF on different metal surfaces under different potentials were ad-dressed with qualitative and quantitative information.

6. 2. 1 Selection of electrolyte

As discussed in the chapter 3, organic solvents were better for HMF formation from fructose. Therefore, organic solvents were chosen to prepare electrolyte and inorganic salts were used to increase the conductivity. Initially we screened 2-butanol, acetonitrile (ACN) and dimethyl-acetamide (DMA) as electrolyte with some promising salts $NaClO_4$, $TBAPF_6$, $NH4_F$ and LiF_4 as supporting electrolytes. Our benchmark electrolyte is 1M H_2SO_4 and its conductivity is 24mS/cm. 1M H_2SO_4 electrolyte has negligible resistance for the flow of ions during electrochemical reactions.

Table 6. 1 Conductivity of organic electrolytes with different amounts of inorganic salts

		2-Butanol	CAN	DMA
Without ionic salt	pH at 24°C	3.58	4.2	5.77
	Conductivity at 24°C	0.16 µS/cm	0.72 µS/cm	1.73 µS/cm
$NaClO_4$	0.1g/10mL (0.0816 M)	in soluble	7.62 mS/cm	3.92 mS/cm
	0.5g/10mL (0.40 M)	in soluble	26 mS/cm	13.18 mS/cm
$TBAPF_6$	0.1g/10mL (0.025 M)	in soluble	3.41 mS/cm	1.49 mS/cm
	0.5g/10mL (0.129 M)	in soluble	12.68 mS/cm	17.66 mS/cm
NH_4F	0.1g/10mL (0.27 M)	in soluble	in soluble	in soluble
	0.5g/10mL (1.35 M)	in soluble	NA	NA
LiF_4	0.1g/10mL (0.1 M)	206 µS/cm	7.7 mS/cm	5.4 mS/cm
	0.5g/10mL (0.53 M)	NA	17.97 mS/cm	14.52 mS/cm

 (where $NaClO_4$ = Sodium perchlorate, $TBAPF_6$ = Tetra-n-butylammonium hexafluorophosphate, NH_4F = Ammonium fluoride, LiF_4 = Lithium tetrafluoroborate, ACN = Acetonitrile, DMA = Dimethyl-acetamide)

Table 6. 1 compares the pH and conductivity of different organic electrolytes. The pH of the above selected electrolytes was between 3 and 6. Theses electrolytes will give weak acidic conditions. The selected salts were not soluble in 2-butanol. Except $NaClO_4$, all salts in ACN showed relatively low conductivity. DMA   has also appeared as an inadequate electrolyte due to low conductivity. The disadvantages of these organic electrolytes are poor conductivity, high potentials were required due to internal resistance, may participate directly in electrochemical reaction, decomposes at higher

applied potentials and difficult to produce required oxygen species *in-situ* for oxidation reactions. Apart from conductivity problem, external oxygen needs to be supply for oxidation reactions. Therefore organic electrolytes were not suitable for electrocatalytic oxidation of HMF. Further studies were continued with aqueous electrolytes.

6. 2. 2 Electrocatalytic oxidation of HMF using Pt foil electrode

Platinum is the first choice to study new electrocatalytic reactions. Platinum is more stable against corrosive electrolyte such as strong acidic and basic solutions. So far, Pt represents one of the most efficient catalyst materials for the electrocatalytic oxidation of small organic molecules (CH_3OH, $HCOOH$, etc) [10]. Pt is also efficient for the oxygen evolution from water. Therefore we selected Pt as suitable electrode to explore the HMF conversion reactions.

6.2.2.1 Electrochemical characterization of Pt foil electrode

Cyclic voltammetry (CV) of bare Pt surface was studied in the literature for various applications [33-37]. We repeated CV of our Pt electrode with HMF to characterize its electrochemical behavior. In the beginning, CV of a polycrystalline Pt foil was recorded in different electrolytes (basic, neutral and acidic) at room temperature to understand the electrochemical behavior of HMF.
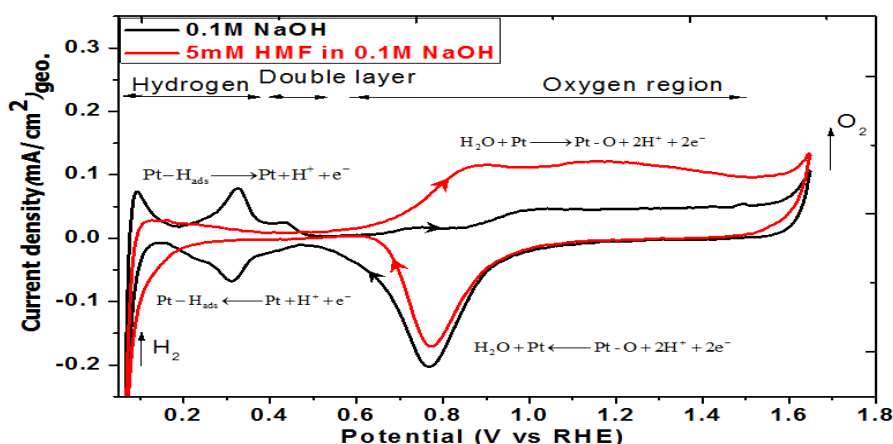
Fig. 6. 2 CV of Pt foil electrode with & without HMF at pH 13. Conditions: 0.1M NaOH electrolyte, scan rate is 50 mV/s, under N_2, room temperature, Pt foil $(4.5cm^2)_{geo.}$ as working electrode (WE), Pt gauze $(12.5cm^2)$ as counter electrode (CE), reversible hydrogen electrode (RHE) as a reference electrode (RE).

The black curve in the fig. 6. 2 shows the behavior of the bare platinum in the support-ing electrolyte without HMF [38]. The observed current-potential behavior in aqueous electrolyte corresponds to the under-potential deposition of atomic hydrogen and oxy-gen layers on the electrode surface. Thermodynamically hydrogen evolution occurs at 0.0V. In the anodic scan direction, the typical hydrogen underpotential deposi-tion/stripping region occurs below 0.5V. The current flow between +0.45V and +0.6V in anodic direction scan is due to electrolytic double layer charge. Above +0.55V, activa-tion begins by water discharge and further oxidation takes place after +0.8V. The oxide formation on Pt at pH 13 is due to specific adsorption of hydroxide anions from water [39,   40].
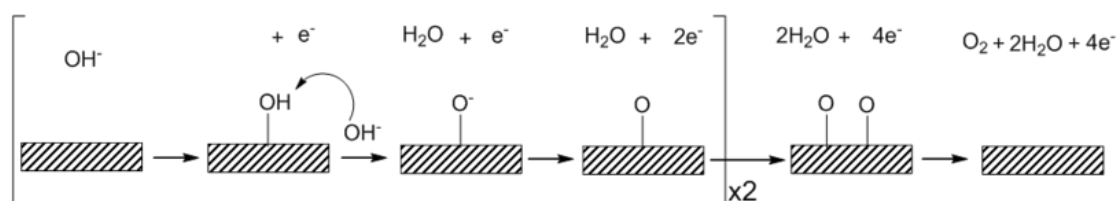
Fig. 6. 3 Illustration of oxygen evolution in basic media

Half-wave potential ($E_{1/2}$) of Pt-OH in 0.1M NaOH is 0.65 V (equation 6.6).

Pt-OH + OH $\leftrightarrow$ Pt-O + H$_2$O + e$^-$ .... (6.6)

 The reversible binding of hydroxide ion coupled to a one electron oxidation is thought to precede a turnover-limiting electrochemical step involving the removal of one proton and one electron to form a surface oxide species as shown in fig.6. 3 [41, 42]. Thermo-dynamically oxygen evolution takes place at 1.23V. Above 1.6 V, oxygen evolution takes place and even at higher potential, a phase of Pt-O may form with thickness more than monolayer.

As the potential sweep was reversed in cathodic direction, oxygen gas surrounding the electrode is reduced at onset potential of +1.0V according to the equation 6.8.

$$Pt\text{-}O + 2H^+ + 2e^- \longleftrightarrow H_2O + Pt$$ .... (6.8)

 At lower potential (< +0.45V) in the cathodic direction, water is reduced into Pt-H as shown in the equation (6.9). More details of water reduction and hydrogen evaluation will be addressed in the chapter 7.

Pt + H$_2$O + e$^-$ $\leftrightarrow$ Pt-H + OH$^-$ .... (6.9)

The summary of electrochemical reaction associated on the surface of bare polycrystalline Pt electrode were reported in the table 6.1.

Table 6. 1 Different potential-related reactions on the bare Pt foil surface [15].

Potential (V vs RHE)	Sweep direction	Surface reaction
0.0 - 0.4 V	Anodic	Hydrogen desorption
0.4 – 0.6 V	Anodic	Double layer
>0.8 V	Anodic	Onset of Pt-O formation
0.8 – 1.1 V	Anodic	Pt-OH & Pt-O monolayer formation
1.1-1.2 V	Anodic	Pt-O bulk formation
>1.23 V	Anodic	Onset of oxygen evolution
1.23 – 0.8 V	Cathodic	Pt-O reduction
0 – 0.4 V	Cathodic	Hydrogen adsorption
≤0.0 V	Cathodic	Hydrogen evolution

Red line in the fig. 6. 2 shows Pt foil electrode surface in the presence of 5mM HMF at pH 13. In the anodic scan direction, under potential desorption of atomic hydrogen (Pt-H_{ad}) peaks disappear compared to the bare Pt foil surface. This behavior was due to the lack of Pt active sites for hydrogen adsorption. From this we assume the adsorption of HMF on the surface of Pt foil at +0V. Therefore the available Pt surface for the hydrogen adsorption reduces as shown in the fig. 6. 4a. As a result no peak appears for hydrogen adsorption and desorption. Similar amount of current was used to charge the double layer between +0.45V and +0.6V. Interestingly, more faradaic current was observed compared to the bare Pt foil electrode at onset potential +0.6V. CV exhibits two shoulders at potential +0.9V and +1.2V and this indicates that there are two reactions taking place. This more faradaic current was attributed due to combination of Pt-OH formation and oxidation of HMF functional groups such as –CH_2OH and –CHO.

It is reasonable to assume that the increase of Pt foil surface potential (after +0.6V), the sitting orientation of HMF on the surface was changed as shown in fig. 6. 4b. In this orientation, HMF facilitates the oxidation of its functional groups selectively without changing the furan ring. At higher anodic potential (> +1.6V), more faradaic current was due to oxygen evaluation and HMF oxidation. At the same time, we assume that the

adsorbed alcoholic group of HMF also oxidizes into aldehyde with the help of reactive oxygen as shown in the fig. 6. 4c.
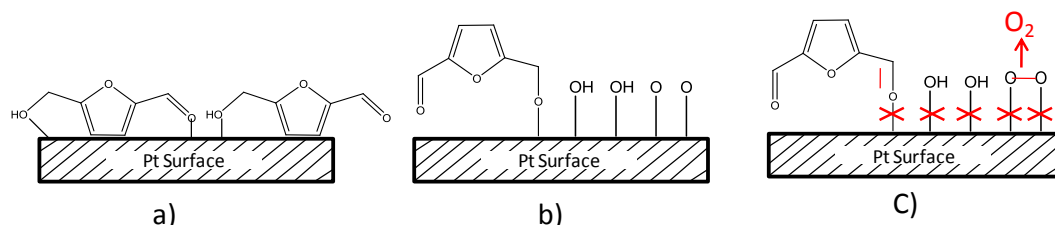
Fig. 6. 4 a) HMF adsorbed on the Pt foil surface at lower potentials (+0V); b) Adsorption of hydroxyl and oxygen ions along with alcoholic group of HMF after +0.6V; c) Evolution of oxygen and oxidation of alcoholic group of HMF at higher potential after +1.6V

In the cathodic scan direction, less faradaic current was observed for Pt-O reduction compared to the bare Pt foil electrode. This effect is due to strong adsorption of HMF oxidative derivatives, which were irreversible type reactions. The early offset potential of Pt-O reduction peak suggests that the surface was occupied by other molecules than atomic oxygen. This observation also supports the disappeared peaks of atomic hydrogen adsorption between the potential +0.4V and +0.2V.
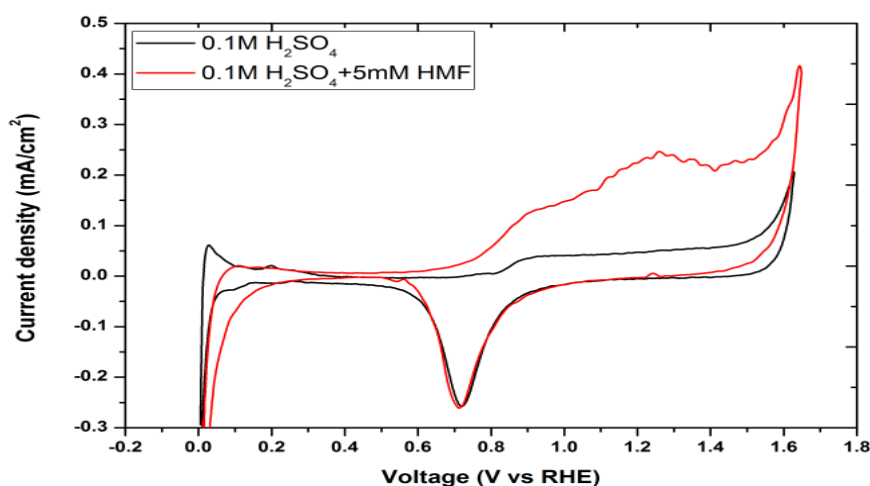
Fig. 6. 5 CV of Pt foil in acidic electrolyte with & without HMF. Conditions: 0.1M H_2SO_4 (pH 1.2), scan rate is 50 mV/s, under N_2, room temperature, WE: Pt foil (4.5cm^2)$_{geo.}$, CE: Pt gauze (12.5cm^2), RE: RHE.

Fig. 6. 5 Black line shows bare Pt foil electrode surface in the acidic electrolyte at pH 1.2. The under potential desorption of hydrogen (H_{upd}) of Pt surface showed relatively smaller peaks compared to alkaline conditions as shown in the fig. 6. 2. This behavior was due to the orientation of crystals of specific metal surface [33, 36, 43]. Although

the onset potential of Pt-OH formation is similar in both electrolytes, the faradaic current for oxide formation in alkaline media exhibited a characteristic peak shape whereas in acidic media current peak was relatively more flat. Half-wave potential 0.1M H_2SO_4 ($E_{1/2}$) of Pt-OH formation is shifted slightly more positive to 0.75V. Oxygen evolution mainly depends on the nature of the electrode surface and pH [7, 44, 45]. Under acidic conditions water binds to the surface with the irreversible removal of one electron and one proton to form a platinum hydroxide as shown in the fig. 6. 6 [46]. Oxygen evolution was observed after +1.45V at the given conditions.
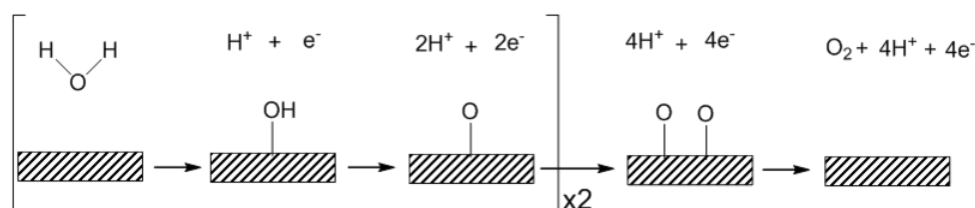
Fig. 6. 6 Illustration oxygen evolution in acidic media.

In the reverse scan towards cathodic direction, Pt-O reduction peak was observed at an onset potential +0.9V similar to Pt foil.

In the presence of HMF, CV showed the increase of faradaic current flow from +0.7V to +1.6V. The more faradaic current flow compared to the bare Pt surface indicates that oxidation of HMF alcoholic and aldehyde groups. As a result an intense peak between +1.2V and +1.4V was observed as shown in the fig. 6. 5. This peak corresponds to the combination of aldehyde group oxidation and formation of Pt-OH. At higher potential oxygen evolution and the oxidation of HMF takes place.

Fig. 6. 7 presents the bare platinum foil CV (black line) in neutral condition. 0.1M NaH_2PO_4 was used to increase the conductivity of electrolyte. In the absence of HMF the platinum surface was polarized between 0V to +1.6V. In the anodic scan direction, bare Pt foil electrode in the neutral electrolyte exhibited different characteristic peaks for H_{upd} compared to the acidic and alkaline electrolytes between the potentials +0V and +0.4V. This observation suggests that effect of electrolyte has an influence on the activation of metal surface and its crystal planes. The current between the potentials +0.4V and +0.75V was used to charge the double layer. The onset potential for Pt-OH and Pt-O formation and for the oxygen evolution were +0.75V and +1.45V respectively. In the reverse scan direction, the onset potential for Pt-O reduction was observed at

+0.9V, which is similar to alkaline and acidic electrolytes. In contrary to alkaline and acidic electrolytes, more characteristic peaks were observed for the hydrogen adsorption in neutral electrolyte between the potentials +0.35V and +0V.
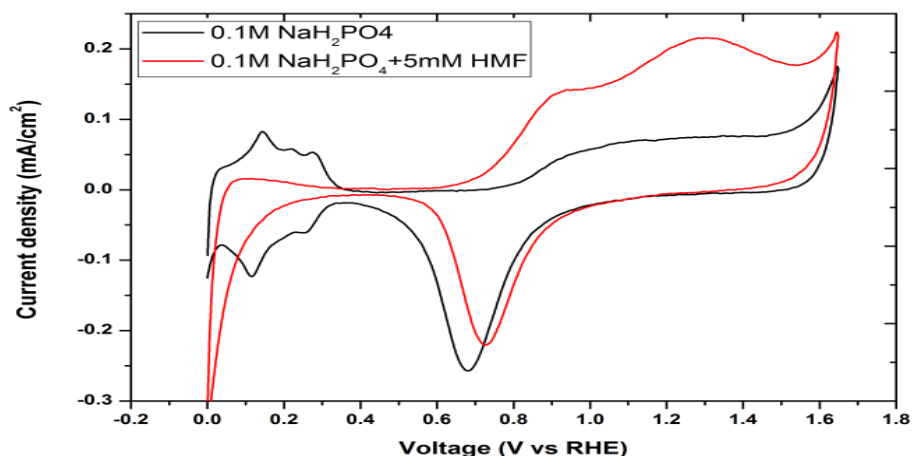
Fig. 6. 7 CV of Pt foil in neutral electrolyte with & without HMF. Conditions: 0.1M NaH_2PO_4 supporting electrolyte, pH 6.4, scan rate is 50 mV/s, under N_2, room temperature, WE: Pt foil $(4.5cm^2)_{geo.}$, CE: Pt gauze $(12.5cm^2)$, RE: RHE.

The red line in the fig. 6. 7 correspond to CV of Pt foil surface in the presence of HMF in the electrolyte at neutral conditions. As observed in acidic and alkaline electrolytes, H_{upd} peaks were blocked by HMF adsorption on Pt foil between the potentials +0V and +0.4V in anodic scan direction. The early faradaic current peaks compared to bare Pt foil for Pt-OH formation and HMF oxidation were observed at onset potential of +0.65V. We believe that the characteristic peaks at the potential +0.9V and +1.3V are corresponding to HMF oxidation. Compared to fig. 6. 2, 6. 5 and 6. 7 the intensity of peak shoulders were more clear. The oxygen evolution was observed after +1.45V along with HMF further oxidation. Compared to acidic conditions, Pt foil surface exhibited different behavior for Pt-O reduction in neutral conditions with early onset potential and less faradaic current. This behavior indicates that HMF adsorption on Pt foil in the acidic electrolyte was relatively weaker than neutral or alkaline electrolytes. The strong adsorption of HMF on Pt foil blocked the hydrogen adsorption between the potentials +0.35V and +0V.

Fig. 6. 2, fig. 6. 5 and fig. 6. 7 clearly expressed that Pt surface has a strong affinity to adsorb HMF at lower potentials (≈0V). At higher potentials (≥0.6V), the functional group of HMF selectively interacts with the platinum surface. The rate of oxidation of particular functional group of HMF depends on the applied potential.

6.2.2.2 CV of HMF functional groups on Pt foil

In order to elucidate more mechanistic electrode surface insights, different HMF type functional groups were characterized using cyclic voltammetry technique. Fig. 6. 8 illustrates CVs of Pt foil electrode at pH 13 with different functional groups on the furan ring. Furan ring was adsorbed on the Pt electrode surface (H_{upd} disappeared) and showed the characteristic peak shoulders at 1.2 V as shown in the fig. 6. 8a. It was also observed that after the potential +1.4V, the faradaic current was exhibited due to oxygen evolution without adsorption of furan ring. This observation was supported by Pt-O reduction peak at +0.7V. In the presence or in the absence of furan, Pt electrode exhibited same faradaic current for Pt-O, which means Pt surface was completely occupied by atomic oxygen and not by furan. Similarly hydroxymethylfuran (-CH$_2$OH), furfural (-CHO) and FDCA (-COOH) were characterised on the Pt foil electrode and showed slightly different behavior as shown in the fig. 6. 8b, 6. 8c and 6. 8d respectively.
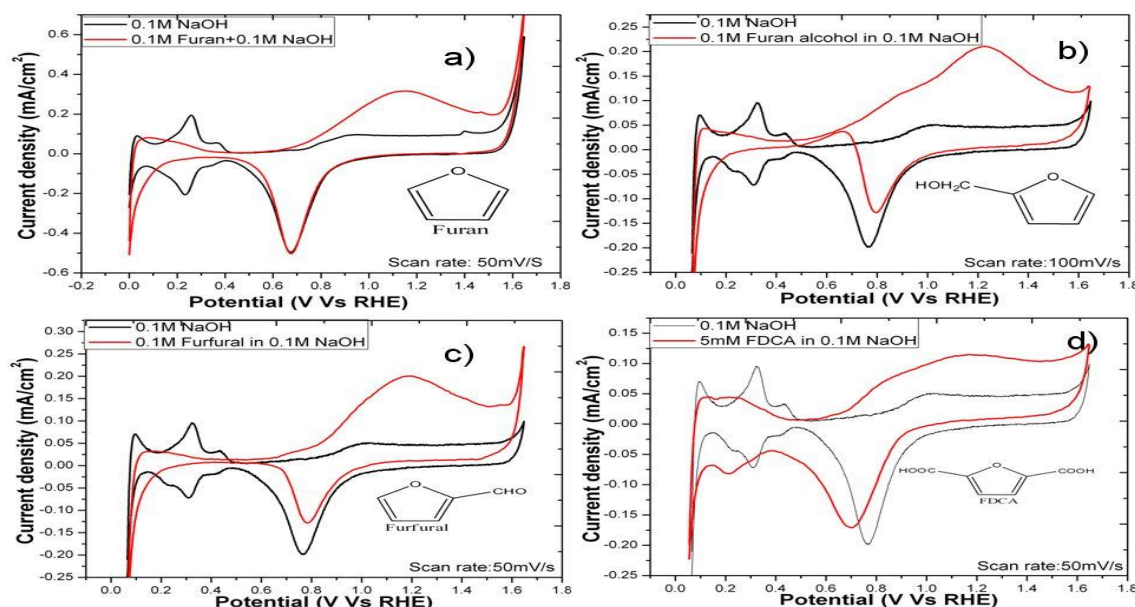
Fig. 6. 8 CV of Pt foil electrode with different possible HMF derivatives with C-C bond cleavage a) furan b) hydroxymethylfuran c) furan d) furandicarboxylic acid. Conditions: at pH13, scan rate is 50 mV/s, under N$_2$, room temperature, WE: Pt foil (4.5cm^2)$_{geo.}$, CE: Pt gauze (12.5cm^2), RE: RHE.

The functional groups of these molecules were adsorbed/occupied on Pt foil surface at higher potential (> +1.4V) and resulted different Pt-O reduction peaks based on their adsorption strength. This observation is also in agreement with fig. 6. 4c. Fig. 6. 8b gives the evidence that alcoholic group oxidises around +0.9V (overlap shoulder) with

early onset potential at +0.55V. Whereas, the peak corresponding to the aldehyde group may be beneath the furan ring peak at +1.2V as shown in the fig. 6. 8c. It is also observed that missing shoulder at +0.9V was due to the absence of -CH$_2$OH functional group. Furan ring with acid group (in the absence of alcoholic and aldehyde group) was shown in figure 6. 8d. Interestingly, acidic group of furan doesn't have any characteristic peak, but a significant alcoholic group peak was missed at +0.9V. This concludes that furan don't have any characteristic peak except broader peak between +0.7 to +1.6V. Therefore cyclic voltammetry technique has limited applications to understand the product distribution of HMF derivatives electrochemically.

From the chapter 4, it was concluded that HMF is unstable in strong basic conditions in the absence of metal catalyst surface. So, basic conditions (≥pH13) are not suitable to study electrocatalytic oxidation due to self degradation of HMF. At the same time, complete oxidation of HMF is difficult at neutral and lower pH due to the lack of OH$^-$ ions. Therefore we have chosen weak basic conditions (pH10) in order to study the HMF oxidation using electrochemical catalysis. HMF was relatively stable in pH10 electrolyte and NaClO$_4$ makes the electrolyte more conductive.

6.2.2.3 Electrocatalytic oxidation of HMF

Constant current density was applied to the electrode, and the potential variation is followed as a function of time. Chronopotentiometry was carried out by applying various current densities in electrochemical system (see section 2.10) to HMF at pH10. For HMF oxidation, the value of the current was controlled across the electrode and the variation of potential with time was registered as shown in fig.6. 9.

Fig. 6. 9 shows the behavior of the electrode surface potential with the time at applied current density under N$_2$ and room temperature. The surface potential increases with the increase of the current density. At low current density, the applied electrons were used to charge the double layer and to defuse from the surface.
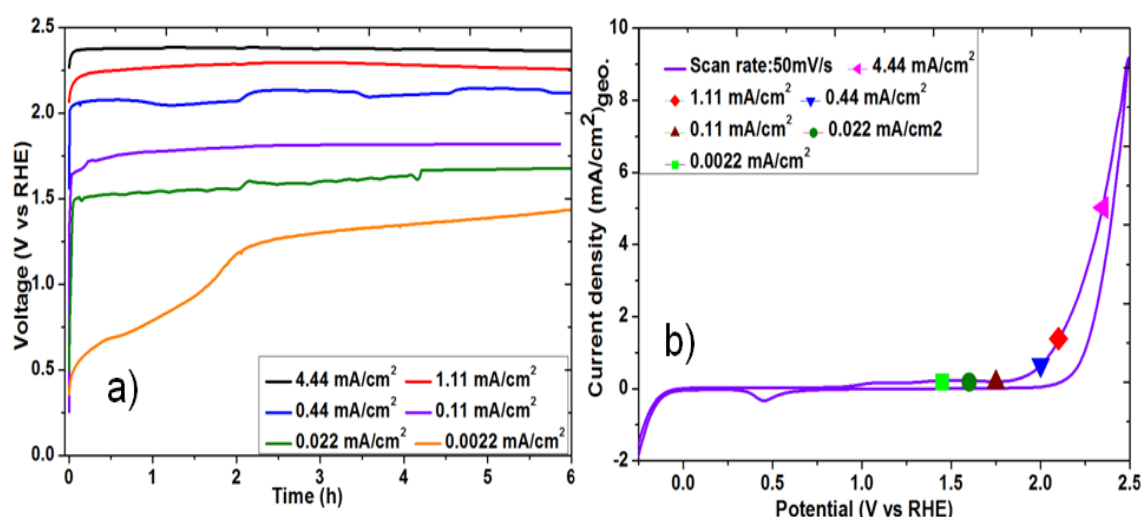
Fig. 6. 9 a) Surface potential of Pt electrode at different current densities b)Location of observed potentials against giving current density in the CV of Pt. Conditions: (0.3M $NaClO_4$ + 10mM NaOH) supporting electrolyte, pH 10, scan rate is 50 mV/s, under N_2, room temperature, magnetic stirring, WE: Pt foil $(4.5cm^2)_{geo.}$, CE: Pt gauze $(12.5cm^2)$, RE: RHE.

Fig. 6. 9a when there is no electrode reaction, the entire current is a non-faradaic charging current. A current step applied to an electrode provokes a change in its potential. The flux of electrons is used to first charge the double layer, and then for the faradaic reactions. Neglecting the capacitive current, the potential at a planar electrode is approximately constant until the end of the total consumption of the electro-active species in the neighborhood of the electrode. That transition time is negligible if the current density is higher. This also keeps the electrode potential higher. With the further increase of current density the electrode potential may increase rapidly and destroy the electrode and electrolyte. The higher potential, where electrolyte was decomposed is called as limiting potential of specific electrolyte and the corresponding current is called as limiting current. Position of observed potential against current density was located in CV of Pt foil as shown in fig. 6. 9b. The applied potential (≥2.2V) corresponds to the higher current density in the region of oxygen evolution. In this region more oxygen evolution takes place due to water splitting reaction. The potential corresponding to the lower current densities are in the region of Pt-OH, Pt-O formation.

Fig. 6. 11 shows the effect of applied current density on product distribution of anodic oxidation of HMF. At lower applied current density, the surface potential of electrode was also relatively low and affects the HMF conversion as shown (green color) in fig. 6. 11 . From fig. 6. 10, HMF conversion was possible from the potential +0.6V, but the conversion is very low and difficult to analyse in HPLC.
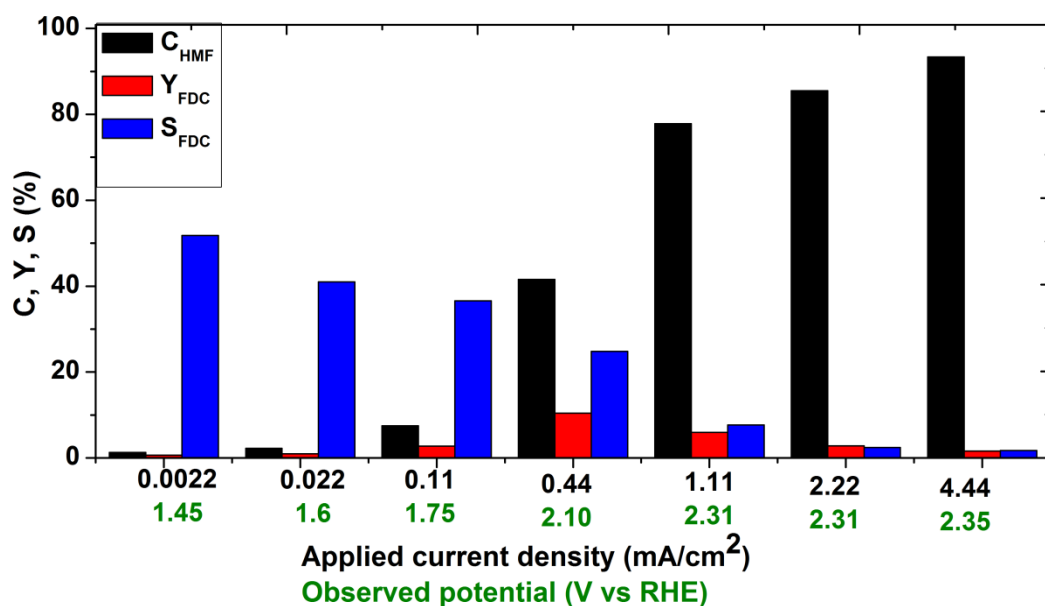
Fig. 6. 11 Product distribution of HMF anodic oxidation at different surface potentials at 6h. Conditions: (0.3M NaClO$_4$ + 10mM NaOH) supporting electrolyte, 5mM HMF, pH 10, scan rate is 50 mV/s, magnetic stirring, under N$_2$, room temperature, WE: Pt foil (4.5cm^2)$_{geo.}$, CE: Pt gauze (12.5cm^2), RE: RHE.

The HMF conversion is increased with the increase of current density from 3.5% with 0.0022mA/cm^2 to 93.38% with 4.44mA/cm^2. Whereas, the yield of FDC is increased with the increase of current density till 0.44mA/cm^2 and decreased with further increase of current density. The selectivity was relatively more at low current densities but decreased drastically at higher current density.

To find out the efficiency of applied current for the conversion of HMF into FDC, faradaic efficiency was calculated according to the faradays law (see section 2.10). Faradaic efficiency is the charge altered at the electrode to the total charge as per faraday's law.
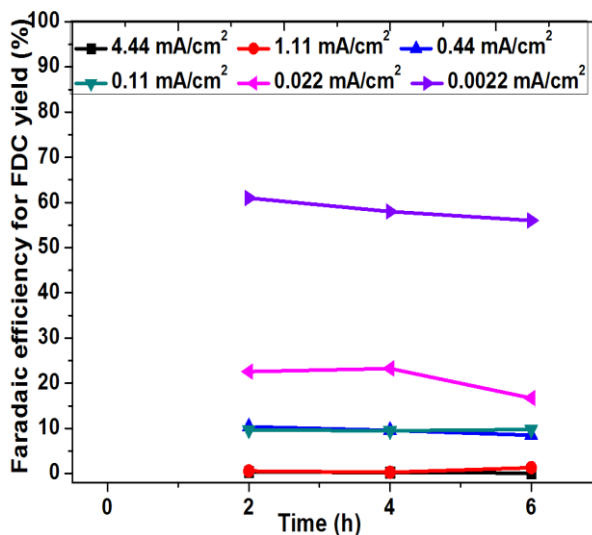
Fig. 6. 12 Faradaic efficiency for FDC yield.

Fig. 6. 12 shows the faradic efficiency for FDC yield with time for a different applied current density. At higher current densities (4.44, 1.11 mA/cm^2) the faradic efficiency was less than 1%, which means that the applied current is used for some other elec-

110

trode reactions. The applied current was used for competing reactions, which are occurring at higher potential for instance oxygen evolution (equation 6.10).

$$4\ OH^-(aq) \rightarrow O_2(g) + 2H_2O(l) + 4e^- \qquad \ldots\ldots\ldots\ldots\ldots\ldots(6.10)$$

At these current densities the selective oxidation reaction was low or electrolyte itself is destroyed. Whereas at lower current densities the faradaic efficiency was higher and with less competitive reactions, but it takes longer reaction time to get required amount of product.

Therefore, 0.44mA/cm^2 current density was chosen as an optimum current density with 41% HMF conversion, 10% yield of FDC with 25% selectivity in 6 h of reaction time. Using optimized current density the anodic oxidation reaction of HMF was investigated further.
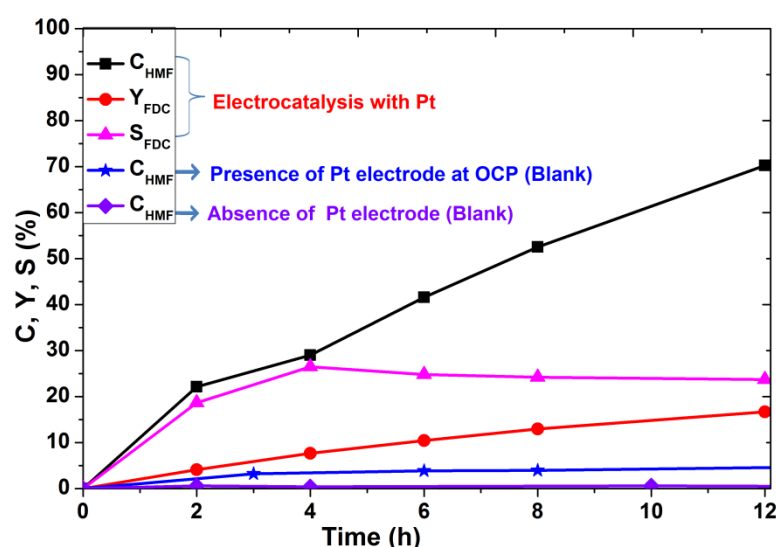
Fig. 6. 13 Kinetics of electrocatalytic oxidation of HMF along with blank tests using *Pt* foil at 0.44mA/cm^2 current density, 25°C under N$_2$. Conditions: (0.3M NaClO$_4$ + 10mM NaOH) supporting electrolyte, pH 10, 5mM HMF, magnetic stirring, under N$_2$, room temperature, WE: Pt foil (4.5cm^2)$_{geo.}$, CE: Pt gauze (12.5cm^2), RE: RHE. Where C= Conversion, Y=Yield, S=Selectivity.

Fig.6. 13 shows "blank" tests for HMF stability with similar conditions as that of electrocatalysis at pH 10 using Pt foil (4.5cm^2)$_{geo}$ in the absence of current density (i,e at OCP). The electrolyte is stable at 12h of reaction time without loss of HMF. This condition was similar to heterogeneous catalysis with pure unsupported Pt metal with very low surface area (4.5cm^2). This data confirms that there is no significant product formation using low surface area heterogeneous unsupported metal catalyst. Then

chronopotentiometry was carried out by applying 0.44mA/cm^2 current densities in electrochemical system to 5mM HMF in pH10 electrolyte. In case of Pt the yield of desired oxidative product FDC increases to 18% and conversion of HMF to 70% with reaction time of 12h. The selectivity of FDC increased to 29% and then decreased to 20%.

High surface area electrocatalyst prepared using 46.7% Pt/vulcan (see section 2.4.2) was tested using continuous flow reactor (see section 2.2.3.2) and observed 28% FDC with 80% HMF conversion at 2mA applied current (galvanostatic).

6.2.2.4 Comparison of electro-catalysis with heterogeneous catalysis
A comparative analysis of heterogeneous catalysis and electrochemical catalysis was carried on Platinum surface as shown fig. 6. 14.
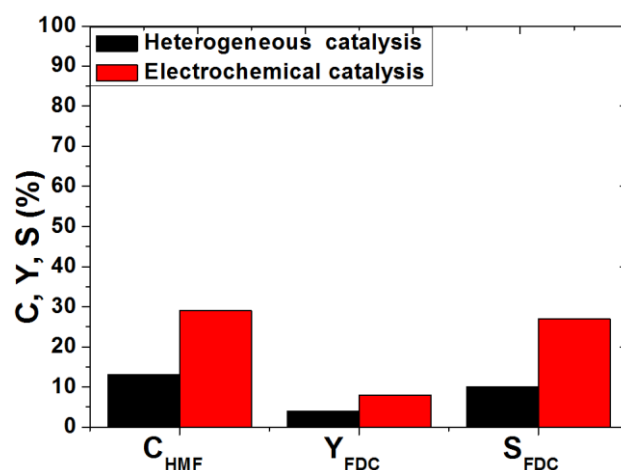
Fig. 6. 14 comparison of heterogeneous catalytic and electrocatalytic HMF oxidation on Platinum surface. Heterogeneous catalysis conditions: Pt/C (150m^2/g), 1 bar O$_2$, 25°C,4h, pH10, Pt/HMF molar ratio: 0.1; Electrocatalytic conditions: Pt foil (4.5cm^2)$_{geo.}$, magnetic stirring.

Fig. 6. 14 compares high surface area platinum at heterogeneous catalytic conditions with low surface area platinum electrode at 0.44mA/cm^2 current density. Electrochemical catalytic reactions clearly showed superior activity towards HMF oxidation into FDC at pH10.

6. 2. 3 Electrocatalytic oxidation of HMF using Pd foil electrode

Palladium is one of the most important materials due to its unique catalytic activities towards various reactions of technological significance. Therefore Pd was chosen to test its electrocatalytic activity towards HMF oxidation.

6. 2.3. 1. Electrochemical characterization of Pd foil
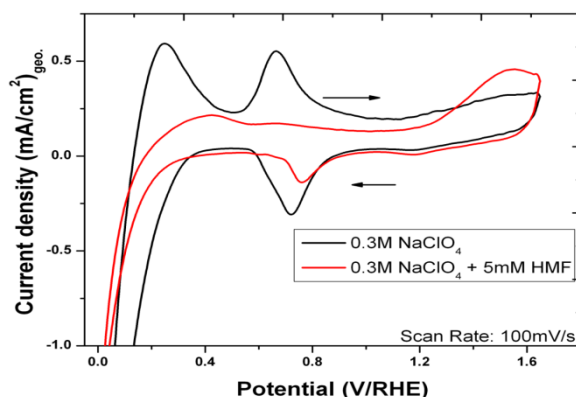
Fig. 6. 15 CV of Pd electrode with and without HMF in pH10 electrolyte. Conditions: scan rate 50mV/s, (0.3M $NaClO_4$ + 10mM NaOH) supporting electrolyte, pH 10, under N_2, room temperature, WE: Pd foil (4.5cm^2) $_{geo.}$ CE: Pt gauze (12.5cm^2), RE: RHE.

Cyclic voltammetry studies were conducted to characterize the electrocatalytic activity of Pd foil electrode at pH 10 conditions with and without HMF as shown in fig. 6. 15. In the case of bare Pd metal (black line), hydrogen adsorption/desorption was observed between +0.1V and +0.3V in the anodic direction. It is also seen that Pd electro-oxidation commences at +0.75V, while in the cathodic scan the oxides reduction starts at +0.85V and with a peak at a potential of +0.7V. The cathodic current observed at E< +0.35V is attributed to hydrogen evolution. All these phenomena agree with the documented literature[3, 47]. Pd was not active when compared with the Pt surface for oxygen evolution at the potential ≥ +1.23V. In the presence of HMF (red line), the Pd foil surface exhibited different behavior. The surface of Pd was fully adsorbed/occupied by HMF. The faradaic current for Pd-O reduction was relatively low compared to bare Pd foil electrode. It also suggests that the adsorption of HMF on the surface of Pd was very strong and preventing Pd-O formation. At higher potential insignificant amount of faradaic current flow indicates that Pd was not electrochemically active for water oxidation and HMF conversion.

6. 2.3. 2. Electrocatalytic oxidation of HMF

Pd electrode was used for electrochemical catalytic oxidation of HMF using pH10 electrolyte at room temperature under nitrogen atmosphere. "Blank" conditions were tested in the absence and in the presence of Pd electrode at open circuit potential (OCP).

Chronopotentiometry (CP) technique was used to apply optimized current density 0.44mA/cm² (discussed in section 6.2.2.3 for Pt electrode).
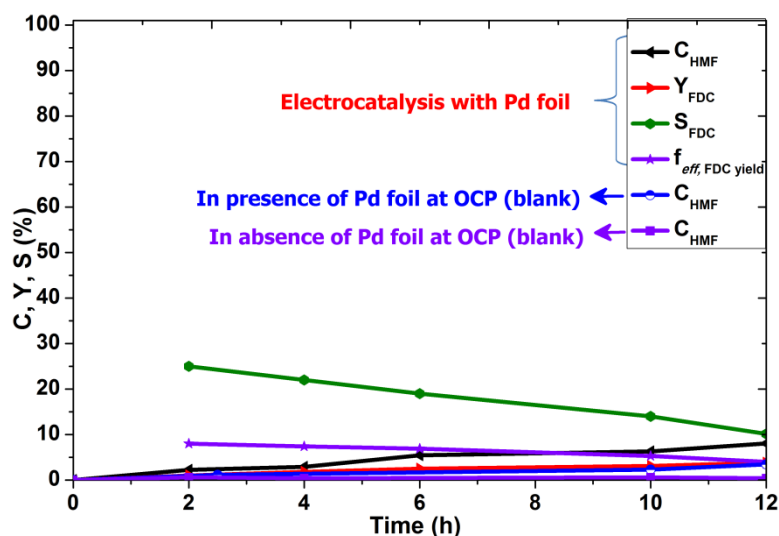
Fig. 6. 16 Time resolved kinetics of HMF oxidation using Pd foil electrode. Conditions: (0.3M NaClO$_4$ + 10mM NaOH) supporting electrolyte, 5mM HMF, pH 10, applied current density 0.44 mA/cm^2, observed surface potential +1.9V, under N$_2$, room temperature, magnetic stirring, WE: Pd foil (4.5cm^2)$_{geo.}$, CE: Pt gauze (12.5cm^2), RE: RHE.

Fig. 6. 16 demonstrated HMF conversion in "blank" conditions in the presence and in the absence of Pd electrode at OCP. An insignificant amount of HMF conversion was noticed at 12h of reaction time at OCP. These results were in agreement with Pt electrode (fig. 6. 13) at OCP conditions. So in the absence of electrified potential surface, Pd surface was not active to oxidize HMF. Whereas different results were observed when constant current density under similar conditions was applied. Initially, the rate of HMF conversion was slow till 4h (black line). The HMF conversion is increased slowly with reaction time and 8% was observed at 12h. The FDC yield is increased to 4% at 12h of reaction time (red line), but the selectivity and faradaic efficiencies of FDC are decreased from 25% and 8% to 10% and 4% respectively.

6. 2.3. 3. Effect of external temperature and O$_2$ on HMF oxidation

In contrast to Pt, Pd electrode surface was not active for the oxidation of HMF. Therefore, we studied the effect of external operating parameter such as temperature in order to improve the Pd electrode surface activity. The temperature of electrolyte was increased to 50°C. It is also observed (from fig. 6. 15) that the Pd electrode was not active for oxygen evolution reaction compared to Pt electrode at a given potential (+1.9V). Oxygen evolution was an important consecutive reaction, where required oxy-

gen molecules for HMF oxidation were generated *in-situ*. Hence, molecular oxygen gas was circulated over the surface of Pd electrode to find out limiting rate of HMF electrocatalytic oxidation.
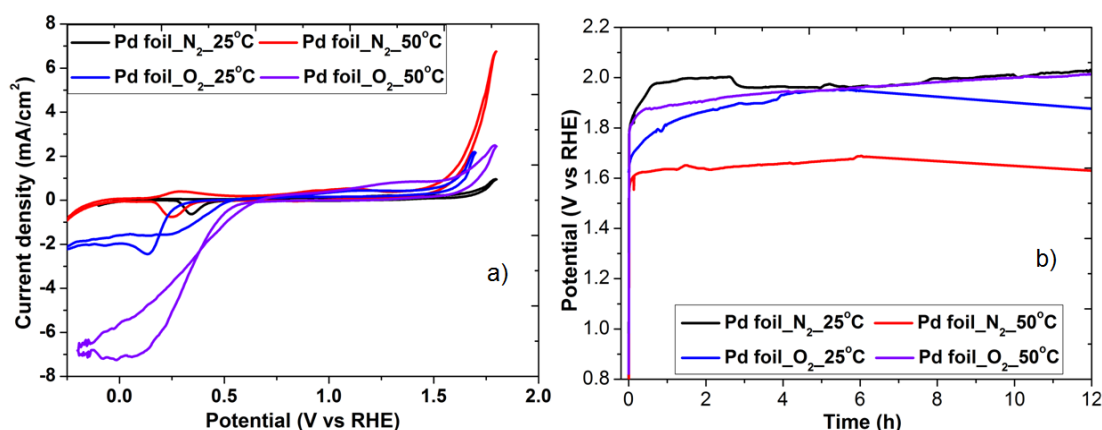
Fig. 6. 17 a) CVs of Pd electrode surface; b) CPs (potential vs time) at applied current density (0.44mA/cm²) for HMF oxidation at 25°C and 50°C under N_2 and O_2. Conditions: (0.3M $NaClO_4$ + 10mM NaOH) supporting electrolyte, pH 10, scan rate is 50 mV/s, magnetic stirring, WE: Pd foil (4.5cm^2)$_{geo.}$, CE: Pt gauze (12.5cm^2), RE: RHE.

In fig. 6. 17 Oxygen evolution starts after 1.5V RHE. Temperature has an influence on electrocatalytic activity of Pd, where the oxygen evaluation peak has shifted to a lower potential (0.4V or less) at 50°C. The effect of temperature on electrode potential will be discussed in the section 6.2.4.3. Supply of external oxygen showed a negative effect for the oxygen evolution rate. More faradaic current was observed during cathodic scan due to reduction of external supplied oxygen into H_2O.
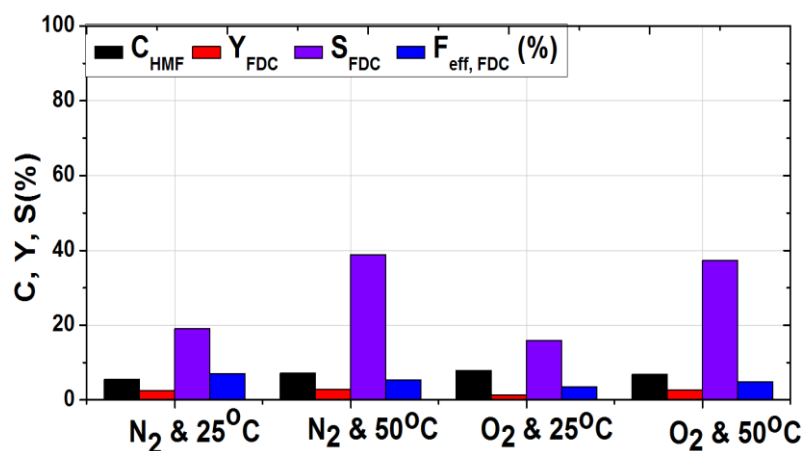
Fig. 6. 18 Production distribution of HMF oxidation on the Palladium surface at a different temperatures and gas environment. Conditions: (0.3M $NaClO_4$ + 10mM NaOH) supporting electrolyte, pH 10, scan rate is 50 mV/s, under N_2, room temperature, magnetic stirring, WE: Pd foil (4.5cm^2)$_{geo.}$, CE: Pt gauze (12.5cm^2), RE: RHE.

In case of nitrogen atmosphere, increase in the temperature from 25°C to 50°C decreases the HMF conversion slightly as shown in the fig. 6. 18. FDC yields are almost comparable. The FDC selectivity has improved significantly (doubled) and this may be due to less surface potential. Whereas, faradaic efficiency decreased slightly. Supply of external oxygen has not influenced the electrocatalytic HMF oxidation reaction at low temperature (25°C).

In case of oxygen atmosphere, the activity of Pd foil electrode increased for FDC yield with the increase of temperature from 25°C to 50°C. Faradaic efficiency improved slightly.

Therefore, bare Pd foil electrode exhibited relatively low electrocatalytic activity for HMF oxidation compared to Pt foil electrode. Similar type of results were observed in case of heterogeneously catalysed HMF oxidation using 5% Pd/C (see section 4.3.6).

6. 2. 4 Electrocatalytic oxidation of HMF using Ni foil electrode

A polycrystalline Ni foil electrode $(4.5cm^2)_{geo.}$ was used to study the electrocatalytic conversion of HMF on Ni surface. Ni foil electrode was electrochemically characterized at pH 13 and pH 10 with and without HMF in the electrolyte. HMF oxidation reactions were carried out at an optimised current density $0.44mA/cm^2$ (section 6. 2. 2) to know the kinetic behavior. Effects of current density, external temperature and oxygen supply on HMF oxidation reactions were studied.

6. 2.4. 1. Electrochemical characterization of Ni foil

In the fig. 6. 19a, the black line shows CV of bare Ni foil scanned between 0V and +1.6V at pH 13. At higher alkaline conditions (pH 13), Ni (0) changed to Ni(II) at +0.06V as shown in equation 6.11. The Ni(II) may exist in both α-Ni(OH)$_2$ and β- Ni(OH)$_2$.

$$Ni + 2OH^- \longleftrightarrow Ni(OH)_2 + 2e^- \qquad ......(6.11)$$
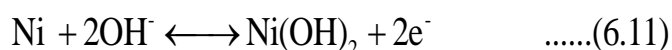
In the anodic scan direction, the plateau region from +0.06V to +1.05 V corresponds to double layer capacitive behavior.
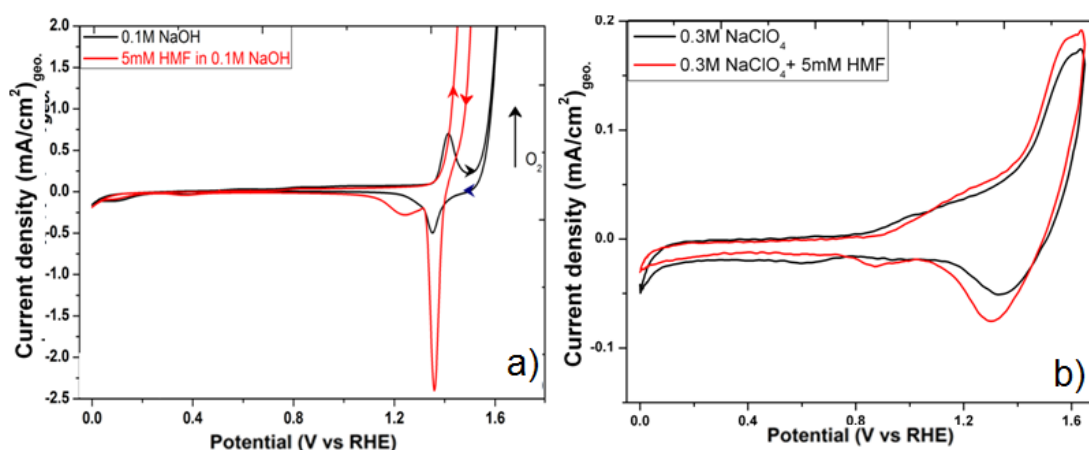
Fig. 6. 19 CV of Ni foil electrode with and without HMF. a) Electrolyte (0.1M NaOH) at pH 13; b) Electrolyte (0.3M NaClO$_4$ + 10mM NaOH) at pH 10. Conditions: scan rate is 50 mV/s, under N$_2$, room temperature, CE: Pt gauze (12.5cm^2), RE: RHE.

The peak region from +1.05 to +1.6 V corresponds to the faradaic charge transfer reaction. The redox peaks were due to the proton insertion and de-insertion reaction of Ni (II) transformation to Ni (III) as shown in equation 6.12 [48, 49]. This phenomenon was well documented in the studies for Ni electrode rechargeable batteries [50, 51].

$$Ni(OH)_2 \longleftrightarrow NiOOH + H^+ + e^- \quad ......(6.12)$$

At higher potential values (> +1.4 V), a huge anodic current was observed. This current was mainly attributed due to the oxygen evolution as shown in equation 6.13.

$$Ni(OH)_2 + 2OH^- \longleftrightarrow Ni\text{-}O_2 + 4H^+ + 2e^- \quad ......(6.13)$$
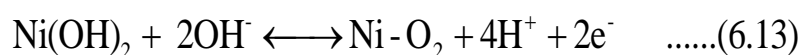
It is important to note that the variation of the potential of Ni from its standard value is due to the variation of pH.

In fig. 6. 19a, the red line shows CV of Ni foil in the presence of HMF. Surprisingly, Ni (III) was super- active for HMF conversion with huge faradaic current at +1.41V. This behavior was in contrast with Pt (fig. 6. 2) surface, where HMF conversion occurs mainly in oxygen evolution region. It was also observed that Ni(III) surface dominates the Ni(iV) transformation in the presence of HMF. The peak at +1.45V corresponds to both HMF oxidation and oxygen evolution reactions. Interestingly, in the reverse scan, oxidized HMF was reduced with large faradic current on Ni(III) surface. From this be-

havior, we assume that the formation of –CH$_2$OH from CHO is reversible reaction as shown in the fig. 6. 20 .
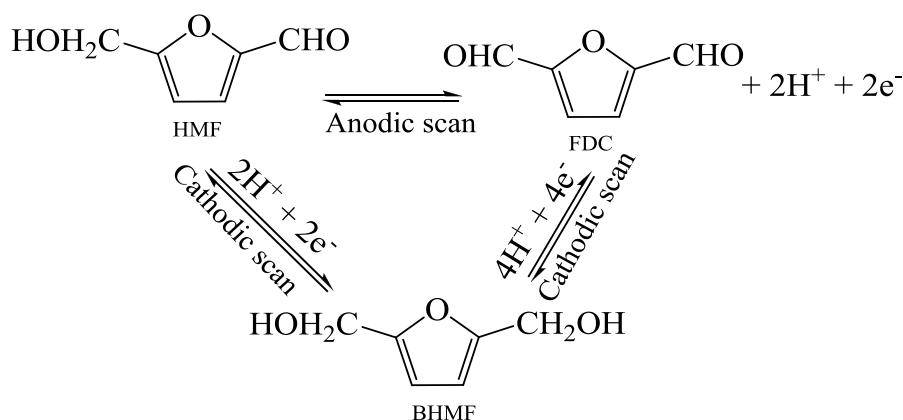
Fig. 6. 20 Reversible behavior of HMF on Ni surface

The electrocatalytic activity of Ni foil was drastically decreased at pH 10 as shown in fig.6. 19b. The rate of transformation of Ni (II) to Ni(III) was slow with less faradaic current. The corresponding redox peaks were shown between the potential region +0.85V and +1.6V. The activity of nickel surface was relatively more due to HMF redox reactions, which was matched with the observations of fig. 6. 19a and fig. 6. 20 . Therefore, it was concluded that the concentration of [OH]$^-$ influences the activity of Ni electrode for both HMF oxidation and oxygen evolution reactions. The higher pH favours the formation of Ni (III) surface, which was more active for HMF conversion reactions.

6. 2.4. 2. Electrocatalytic oxidation of HMF using Ni foil

Initially, the optimised current density for FDC yield (on Pt electrode) 0.44mA/cm^2 was used to study the electrocatalytic activity of Ni foil electrode for HMF oxidation at pH 10.

Fig. 6. 21 shows time resolved kinetic information for HMF oxidation using Ni foil electrode and blank reactions for HMF stability at pH 10. In the absence of nickel electrode, HMF was a stable at 12h under OCP conditions. An insignificant amount of HMF conversion was observed in the presence of nickel electrode under OCP conditions. As observed in case of Pt (fig. 6. 13) and Pd (fig. 6. 16) electoral catalysis, Ni foil electrode

also exhibited its electrocatalytic activity for HMF oxidation. The rate of HMF conversion is increased with the reaction time and 34% was observed at 12h.
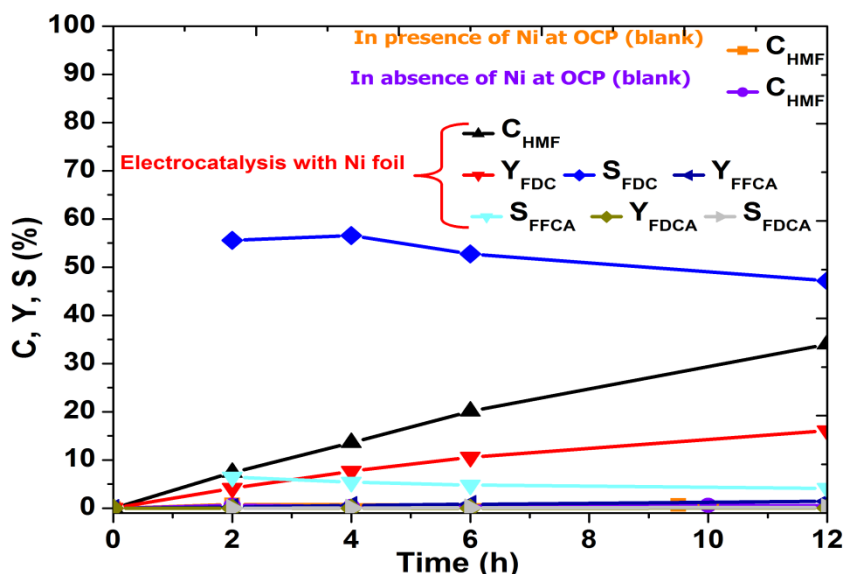
Fig. 6. 21 HMF oxidation on Ni foil electrode against reaction time and blank reactions. Conditions: (0.3M $NaClO_4$ + 10mM NaOH) supporting electrolyte, pH 10, 5mM HMF, magnetic stirring, under N_2, room temperature, WE: Ni foil $(4.5cm^2)_{geo.}$, CE: Pt gauze $(12.5cm^2)$, RE: RHE. Where C= Conversion, Y=Yield, S=Selectivity.

In comparison to HMF conversion, the FDC yield also increased to 16% at 12h of reaction time. In contrast to Pt (fig. 6. 13) and Pd (fig. 6. 16) foil electrodes, Ni foil electrode showed highest selectivity for FDC yield (50%) as shown in the fig. 6. 21 (blue line). Further oxidation of HMF into derivatives such as FFCA, FDCA were observed. 1.5% yield of FFCA with 5% selectivity was observed. ≤ 1% of FDCA yield was detected. The super activity of Ni electrode was due to Ni (III). At the applied current density the observed surface potential was +1.95V, where Ni (II) in $Ni(OH)_2$ transformed to Ni (III) in NiOOH as per equation 6.12. Nickel oxyhydroxide (NiOOH) involved in the reaction oxidized CH_2OH of HMF into CHO of HMF and further oxidized to COOH of HMF.

6. 2.4. 3. Effect of external temperature and O_2 on HMF oxidation

Similar to the section 6.2.3.3, the influence of external temperature on the surface potential and HMF oxidation reaction were studied on nickel electrode. The optimized current density for FDC yield $(0.44mA/cm^2)$ was applied to Ni electrode. The anodic oxidation of 5mM HMF was carried out in an electrochemical cell by varying the tem-

perature and reaction environment. Fig. 6. 22 shows CV and CP behavior of nickel surface at different reaction conditions such as nitrogen & oxygen atmosphere and at 25°C & 50°C.
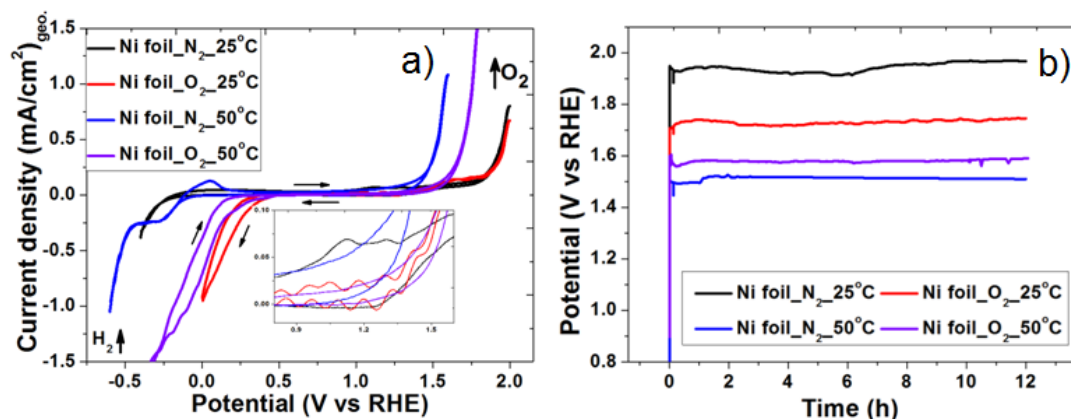
Fig. 6. 22 a) CVs of Ni surface for electrocatalytic oxidation of HMF at a different reaction conditions. b) Ni surface potentials with the reaction time at applied for the current density (0 .44 mA/cm^2) at different reaction conditions. Conditions: (0.3M NaClO$_4$ + 10mM NaOH) supporting electrolyte, pH 10, scan rate is 50 mV/s, under N$_2$, room temperature, WE: Ni foil (4.5cm^2)$_{geo.}$, CE: Pt gauze (12.5cm^2), RE: RHE.

Fig. 6. 22a shows HMF electrocatalytic oxidation on Ni electrode in pH10 electrolyte. With the increase in the temperature from 25°C to 50°C, the surface potential is shifted to less positive, where a strong anodic faradaic current was observed. The faradaic current for oxygen evolution was observed at +1.8V and +1.4V at the electrolyte temperature 25°C and 50°C respectively as shown in figure Fig.6. 22b. The shift in the surface potential could be explained with the help of Nernst equation (6.14)

$$E_{electrode} = E^o{}_{electrode} + \frac{RT}{nF} \ln \frac{a_{O_2}{}^{1/2}}{a_{H_2O} a_{H^+}{}^2} \ldots\ldots\ldots\ldots\ldots(6.14)$$

From the equation 6.14, standard electrode potential decreases with the increase in the temperature.

In the case of external oxygen circulation over Ni electrode, potential shift to left side was observed with the increase of temperature. With the increase of temperature from 25°C to 50°C the electrode potential was shifted from +1.75V to +1.6V.
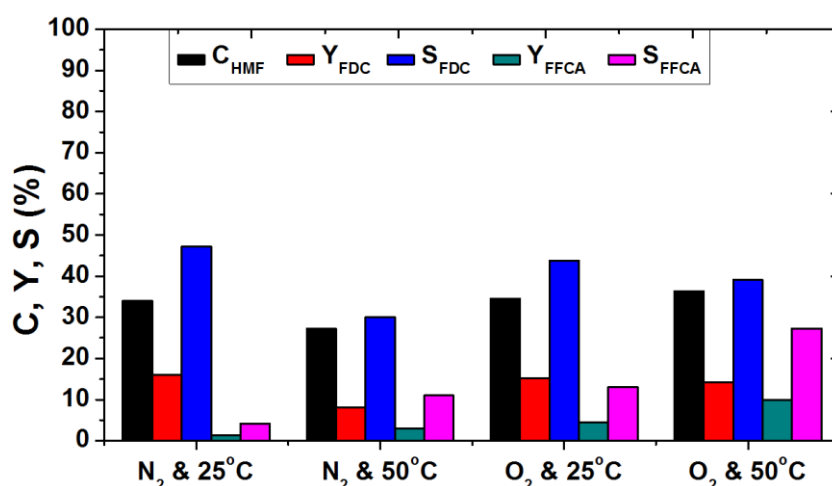
Fig. 6. 23 Product distribution of HMF oxidation on Ni surface at different reaction conditions over 12h of reaction time at pH 10 electrolyte. Conditions: (0.3M $NaClO_4$ + 10mM NaOH) supporting electrolyte, pH 10, magnetic stirring, under N_2, room temperature, WE: Ni foil $(4.5cm^2)_{geo.}$, CE: Pt gauze ($12.5cm^2$), RE: RHE.

Fig. 6. 23 shows the electrocatalytic activity of Ni surface for HMF oxidation at different reaction conditions. In case of nitrogen atmosphere the HMF conversion was decreased with increase of temperature from 25°C to 50°C. This is due to the decrease of +0.4V surface potential. The yield of FDC was also decreased with the decrease of potential. Interestingly the formation of the intermediate FFCA was increased with the decrease of potential at 50°C. The increase of temperature favours the formation of intermediates or further oxidation. In the case of oxygen atmosphere, similar trend was observed. The supply of external oxygen was not influenced by the product distribution. Therefore the required oxygen generated *in-situ* by electrocatalysis of water was sufficient to oxidize HMF using electrified surface.

6. 2.4. 4. Effect of current density on HMF oxidation

Fig. 6. 24 shows the influence of different current densities for HMF oxidation on the Ni surface. With the increase of surface potential from +1.75V to +2V, HMF conversion increases from 9% to 63% along with the increase of FDC yield from 6% to 24%. In contrary to platinum surface, Ni electrode showed different behavior with the increase of surface potential. And also it was noticed that with the increase of potential, further oxidative intermediates were shown up. When nickel surface was compared to the platinum surface, nickel appears as a promising electrocatalytic for the oxidation of HMF.
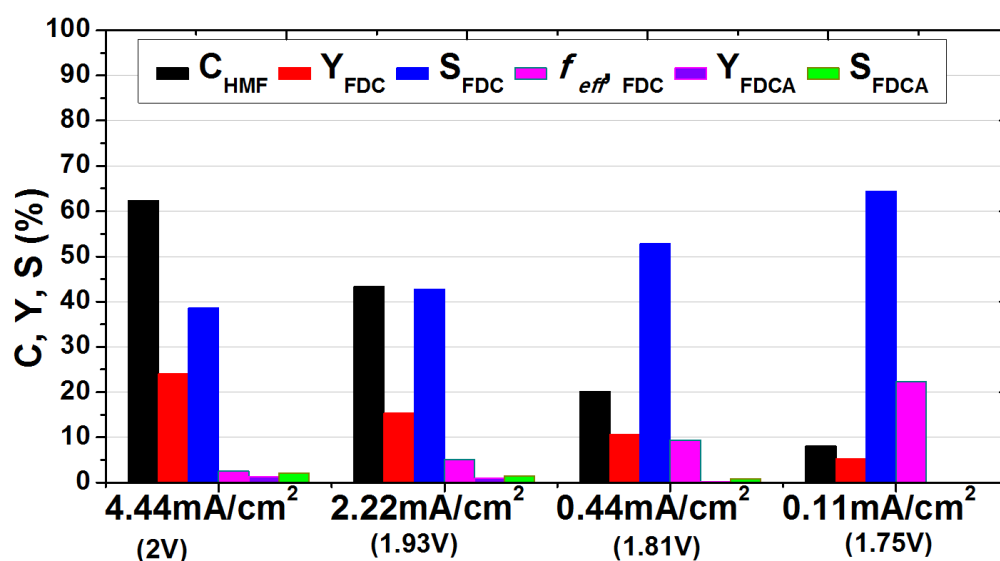
Fig. 6. 24 Influence of different current density (corresponding potential) on the nickel surface for HMF oxidation in pH10 electrolyte under nitrogen atmosphere and room temperature. Conditions: (0.3M $NaClO_4$ + 10mM NaOH) supporting electrolyte, 5mM HMF, 6h, pH 10, magnetic stirring, under N_2, room temperature, WE: Ni foil (4.5cm^2)$_{geo.}$, CE: Pt gauze (12.5cm^2), RE: RHE. Where C=Conversion; Y=Yield; S=Selectivity; f_{eff}=faradaic efficiency.

6. 2. 5 Comparison of Pt, Pd and Ni electrodes activity for HMF oxidation
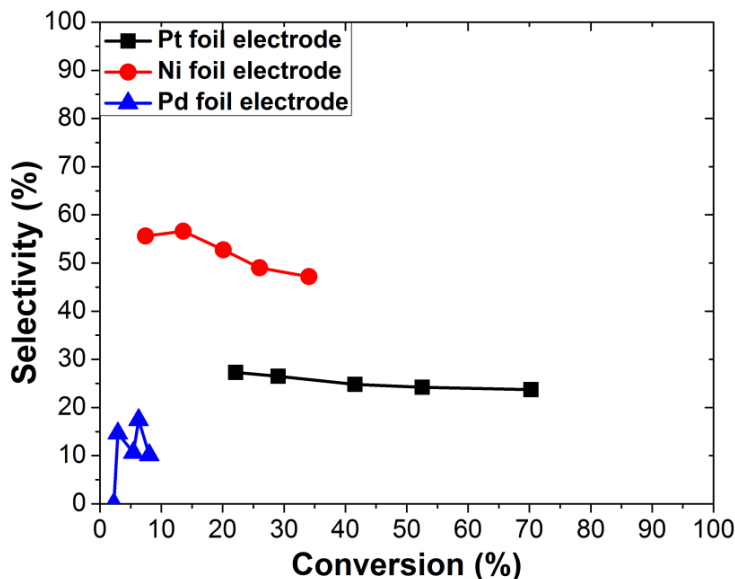
Fig. 6. 25 Comparison of electrocatalytic activity of Pt, Pd and Ni for FDC formation from HMF. Conditions: (0.3M $NaClO_4$ + 10mM NaOH) supporting electrolyte, pH 10, magnetic stirring, under N_2, room temperature, WE: metal foil (4.5cm^2)$_{geo.}$, CE: Pt gauze (12.5cm^2), RE: RHE.

Fig. 6. 25 comparatively Ni surface appeared as the promising electro catalyst for HMF oxidation into FDC. Unlike Pt and Pd foil electrodes, significant electrocatalytic activity for HMF oxidation was showed Ni foil electrode.

6.3 Conclusions

Electrocatalytic oxidation was successfully demonstrated for biomass-derived HMF under mild conditions. It is promising and appears as potential technology for the future in order to produce variety of chemicals and polymers and to reduce the dependency on petroleum-based derivatives. For the first time in the open literature, we systematically studied different options of HMF oxidation using different electrocatalytic surfaces. The conditions used in this process are environmentally friendly and hazardous free.

Noble metals such as platinum, palladium and non noble metals such as nickel are selected to study the electrochemical electrocatalytic behavior of HMF oxidation reactions. Organic electrolytes were not selected for HMF oxidation due to the low conductivity. HMF alone was not stable at a higher pH (basic conditions), so not suitable to use as a electrolyte for slow electrochemical reactions

Anodic oxidation of HMF was studied on different metal foil electrodes by applying chronopotentiometric techniques. Noble metals such as platinum, palladium and non noble metals such as nickel were selected to study the electrochemical electrocatalytic HMF oxidation reactions. HMF alone was not stable at a higher pH (basic conditions). Platinum electrode was examined extensively at different pHs and reaction conditions to know electrocatalytic activity for HMF oxidation. Product distribution was qualified and quantified using LC-MS. A mapping of different current densities/operating potentials on platinum surface in terms of FDC yield and selectivity was addressed in detail. The current density was optimized to 0.44mA/cm^2 to get higher FDC yield from HMF oxidation.

Interestingly, Ni electrode showed higher activity for FDC selectivity compared to Pt and Pd. Use of external temperature reduced the standard potential of electrode.

Outlook

DFT calculations are required to get total energy changes during the oxidation reactions. Developing a continuous process by combining heterogeneous and electrochemical catalysis for biomass derived sugars into valuable chemicals would be advised.

6.4 References

1. Zhao, S.-F., *Influences of the operative parameters and the nature of the substrate on the electrocarboxylation of benzophenones.* Journal of Electroanalytical Chemistry, 2012. 664(0): p. 105-110.

2. da Silva, A.P., *Homogeneous electro-mediated reduction of unsaturated compounds using Ni and Fe as mediators in DMF.* Tetrahedron, 2006. 62(23): p. 5435-5440.

3. Rigano, P.M., C. Mayer, and T. Chierchie, *Structural investigation of the initial stages of copper electrodeposition on polycrystalline and single crystal palladium electrodes.* Electrochimica Acta, 1990. 35(7): p. 1189-1194.

4. Sakellaropoulos, G.P. and S.H. Langer, *Electrocatalysis; selective electrogenerative reduction of organic halides.* Journal of Catalysis, 1976. 44(1): p. 25-39.

5. Santana, D.S., *Electrocatalytic hydrogenation of organic compounds using current density gradient and sacrificial anode of nickel.* Tetrahedron Letters, 2003. 44(25): p. 4725-4727.

6. Santana, D.S., *Electrocatalytic hydrogenation of organic compounds using a nickel sacrificial anode.* Journal of Electroanalytical Chemistry, 2004. 569(1): p. 71-78.

7. Skoplyak, O., M.A. Barteau, and J.G. Chen, *Enhancing H2 and CO Production from Glycerol Using Bimetallic Surfaces.* ChemSusChem, 2008. 1(6): p. 524-526.

8. Smil, V., *Energy at the crossroads. Paper presented at OECD Global Science Forum, 17-18 May 2006, Paris.* 2006.

9. Vilar, M., J.L. Oliveira, and M. Navarro, *Investigation of the hydrogenation reactivity of some organic substrates using an electrocatalytic method.* Applied Catalysis A: General, 2010. 372(1): p. 1-7.

10. Xie, S.-W., et al., *Comparison of Alcohol Electrooxidation on Pt and Pd Electrodes in Alkaline Medium.* International Journal of Electrochemical Science, 2011. 6(4): p. 882 - 888.

11. Yei, L.H.E., B. Beden, and C. Lamy, *Electrocatalytic oxidation of glucose at platinum in alkaline medium: on the role of temperature.* Journal of Electroanalytical Chemistry and Interfacial Electrochemistry, 1988. 246(2): p. 349-362.

12. Bard, A.J. and L. Faulkner, *Electrochemical methods fundamentals and applications.* 2001: John Wiley & Sons, Inc.

13. Vayenas, C.G., *Non-faradaic electrochemical modification of catalytic activity: A status report.* Catalysis Today, 1992. 11(3): p. 303-438.

14. Nilges, P., *Electrochemistry for biofuel generation: Electrochemical conversion of levulinic acid to octane.* Energy Environ. Sci., 2012. 5(1): p. 5231-5235.

15. Arvia, A.J., R.C. Salvarezza, and W.E. Triaca, *Noble Metal Surfaces and Electrocatalysis. Review and Perspectives.* Journal of New Materials for Electrochemical Systems 2004. 7: p. 133-143.

16. Bai, Y., *Electrochemical oxidation of ethanol on Pt-ZrO2/C catalyst.* Electrochemistry Communications, 2005. 7(11): p. 1087-1090.

17. Bannari, A., *Mathematical modeling of the kinetics of phenol electrocatalytic hydrogenation over supported Pdâ€"alumina catalyst.* Applied Catalysis A: General, 2008. 345(1): p. 28-42.

18. Logadottir, A., *The Brønsted–Evans–Polanyi Relation and the Volcano Plot for AmmoniaSynthesis over Transition Metal Catalysts.* Journal of Catalysis, 2001. 197(2): p. 229-231.

19. Hammer, B., J.K. NÃ¸rskov, and H.K. Bruce C. Gates, *Theoretical surface science and catalysisâ€"calculations and concepts*, in *Advances in Catalysis*. 2000, Academic Press. p. 71-129.

20. Koper, M.T.M., *Introductory Lecture Electrocatalysis: theory and experiment at the interface.* Faraday Discussions, 2009. 140: p. 11-24.

21. Li, L.-H., W.-D. Zhang, and J.-S. Ye, *Electrocatalytic Oxidation of Glucose at Carbon Nanotubes Supported PtRu Nanoparticles and Its Detection.* Electroanalysis, 2008. 20(20): p. 2212-2216.

22. Oliveira, M.C.F., *Study of the hypophosphite effect on the electrochemical reduction of nitrobenzene on Ni.* Electrochimica Acta, 2003. 48(13): p. 1829-1835.

23. Parpot, P., *Electrochemical investigations of the oxidation–reduction of furfural in aqueous medium: Application to electrosynthesis.* Electrochimica Acta, 2004. 49(3): p. 397-403.

24. Li, Z., *Mild electrocatalytic hydrogenation and hydrodeoxygenation of bio-oil derived phenolic compounds using ruthenium supported on activated carbon cloth.* Green Chemistry, 2012, 14(9): p. 2540-2549.

25. Morton, O., *Solar energy: A new day dawning Silicon Valley sunrise.* Nature, 2006. 443(7107): p. 19-22.

26. Skowronski, R., et al., *ChemInform Abstract: Selective Anodic Oxidation of 5-Hydroxymethylfurfural.* ChemInform, 1997. 28(15): p. no-no.

27. Vuyyuru, K.R. and P. Strasser, *Oxidation of biomass derived 5-hydroxymethylfurfural using heterogeneous and electrochemical catalysis.* Catalysis Today, 2012.

28. Musau, R.M. and R.M. Munavu, *The preparation of 5-hydroxymethyl-2-furaldehyde (HMF) from d-fructose in the presence of DMSO.* Biomass, 1987. 13(1): p. 67-74.

29. Otsuka, K., K. Suga, and I. Yamanaka, *Electrochemical enhancement of oxidative coupling of methane over LiCl-doped NiO using stabilized zirconia electrolyte.* Catalysis Letters, 1988. 1(12): p. 423-428.

30. Park, S.-M., N.C. Chen, and N. Doddapaneni, *Electrochemical Oxidation of Ethanol in Aqueous Carbonate Solutions.* Journal of The Electrochemical Society, 1995. 142(1): p. 40-45.

31. Grabowski, G., J. Lewkowski, and R. Skowronski, *The electrochemical oxidation of 5-hydroxymethylfurfural with the nickel oxide/hydroxide electrode.* Electrochimica Acta, 1991. 36(13): p. 1995-1995.

32. Skowronski, R., et al., *Selective anodic oxidation of 5-hydroxymethylfurfural* Synthesis 1996: p. 1291-1292.

33. Casella, I.G., M. Gatta, and M. Contursi, *Oxidation of sugar acids on polycrystalline platinum and gold electrodes modified with adsorbed bismuth oxide adlayers.* Journal of Electroanalytical Chemistry, 2004. 561: p. 103-111.

34. Jaksic, M.M., B. Johansen, and R. Tunold, *Electrochemical behaviour of platinum in alkaline and acidic solutions of heavy and regular water.* International Journal of Hydrogen Energy, 1993. 18(10): p. 817-837.

35. Gootzen, J.F.E., *The electrocatalytic reduction of NO3 on Pt, Pd and Pt + Pd electrodes activated with Ge.* Journal of Electroanalytical Chemistry, 1997. 434(1-2): p. 171-183.

36. Colmati, F., *Surface structure effects on the electrochemical oxidation of ethanol on platinum single crystal electrodes.* Faraday Discussions, 2009. 140: p. 379-397.

37. El-deab, M.S., *Electrocatalytic Oxidation of Methanol at γ -MnOOH Nanorods Modified Pt Electrodes.* International Journal of Electrochemical Science, 2009. 4: p. 1329-1338.

38. Hamann, C.H., *Electrochemistry, 2007, p. 262*.

39. Tarasevich, M.R., A. Sadkowski, and E. Yeager, *"Kinetics and mechanisms of electrode processes," in Comprehensive Treatise of Electrochemistry,* , ed. J.O.M.B. B. E. Conway, E. Yeager, S. U. M. Khanand, and R. E. White. Vol. 7. 1983: Plenum Press, New York.

40.   Gasteiger, H.A. and P.N. Ross, *Oxygen Reduction on Platinum Low-Index Single-Crystal Surfaces in Alkaline Solution: Rotating Ring DiskPt(hkl) Studies.* The Journal of Physical Chemistry, 1996. 100(16): p. 6715-6721.

41.   Birss, V.I., Damjanovic, A., and Hudson, P. G. J. Electrochem. Soc. 1986, 133, 1621.

42.   Zeng, D.Z.P.i.E.a.C.S.

43.   Aoun, S.B., *Electrocatalytic oxidation of sugars on silver-UPD single crystal gold electrodes in alkaline solutions.* Electrochemistry Communications, 2003. 5(4): p. 317-320.

44.   Dabo, P., *Selective electrocatalytic hydrogenation of 2-cyclohexen-1-one to cyclohexanone.* Electrochimica Acta, 1997. 42(9): p. 1457-1459.

45.   Li, Z., *Aqueous electrocatalytic hydrogenation of furfural using a sacrificial anode.* Electrochimica Acta, 2012. 64(0): p. 87-93.

46.   Conway, B.E.a.L., T. C. Langmuir 1990, 6, 268– 276.

47.   Correia, A.N., *Active surface area determination of Pd-Si alloys by H-adsorption.* Electrochimica Acta, 1997. 42(3): p. 493-495.

48.   Rudnik, E., K. Kokoszka, and J. Lapsa, *Comparative studies on the electroless deposition of Ni-P, Co-P and their composites with SiC particles.* Surface and Coatings Technology, 2008. 202(12): p. 2584-2590.

49.   Palaniappa, M., G.V. Babu, and K. Balasubramanian, *Electroless nickel-phosphorus plating on graphite powder.* Materials Science and Engineering: A, 2007. 471(1-2): p. 165-168.

50.   Hameed, R.M.A. and K.M. El-Khatib, *Ni-P and Ni-Cu-P modified carbon catalysts for methanol electro-oxidation in KOH solution.* International Journal of Hydrogen Energy. In Press, Corrected Proof.

51.   Jayalakshmi, M., M. Mohan Rao, and K.-B. Kim, *Effect of Particle Size on the Electrochemical Capacitance of a-Ni(OH)2 in Alkali Solutions.* International Journal of Electrochemical Science, 2010. 1: p. 324-333.

Chapter 7

Electrocatalytic Reduction of HMF

7.1 Introduction

Industrial hydrogenation reactions of petroleum related-compounds are usually performed at higher pressure of hydrogen (e.g. 50 – 200 bars) and high temperatures [1, 2]. In general, high-temperatures (> 250°C) are required in order to hydrogenate the C=C bond of petroleum platform molecules [3]. The supply of energy for high temperature and hydrogen for high pressure are generally considered as main barriers for the success of future biomass conversion technologies [4, 5]. Also, huge demand for hydrogen is anticipated in the future to convert carbon dioxide into chemicals [6-9]. Therefore it is desirable to perform hydrogenation reactions under relatively moderate temperature conditions and without employment of molecular hydrogen [10]. In our current proposed concept, the required hydrogen is produced *in-situ* from the cathodic hydrogen evolution half cell reaction (HER) of the water electrolysis and hence saves the energy to make, store and deliver hydrogen to the reactor.

The hydrogen evolution reaction (HER) is perhaps the most studied electrochemical reaction and is of importance for applications ranging from electro-deposition and corrosion of metals to energy storage via H_2 production [11-14]. The hydrogen evolution reaction is a reaction where two protons and two electrons combine to form hydrogen. The reaction in acidic electrolyte is given by:

$$2H^+ + 2e^- \leftrightarrow H_2 \qquad \text{..................... (7.1)}$$

While the process in alkaline environments is given by

$$H_2O + 2e^- \leftrightarrow H_2 + 2\ OH^- \qquad \text{.............................. (7.2)}$$

Different reaction paths have been proposed, the initial reaction where a proton and an electron react to form an adsorbed hydrogen atom is called the Volmer reaction:

$$H^+ + e^- \leftrightarrow H_{ad} \qquad \text{...................... (7.3)}$$

This reaction step can then be followed by the Tafel reaction [15], where two adsorbed H atoms react associatively followed by desorption of molecular hydrogen and desorbs continuation

$$2H_{ad} \leftrightarrow H_2 \qquad\qquad ……………………….. (7.4)$$

or the Heyrovsky reaction which is an Eley-Reidel type reaction, where a proton and an electron react directly with an adsorbed atomic H atom to form hydrogen [15].

$$H_{ad} + H^+ + e^- \leftrightarrow H_2 \qquad\qquad ……………………….(7.5)$$
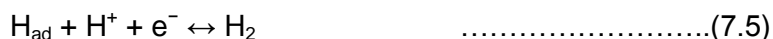
The exact reaction path is not always simple to deduce and it has for instance been found that the same material can exhibit different HER reaction paths. Pt is known as the most active catalyst for the HER and is commonly used in fuel cell for the catalysis, both of hydrogen oxidation and oxygen reduction [16]. Interestingly, Pt is the most well-known catalyst for methanol oxidation. However, there is no evidence that HMF is hydrogenated to BHMF or BHMTHF under electrochemical conditions at the room temperature. The general hydrogenation mechanism mentioned in the heterogeneous catalysis literature is that the adsorbed hydrogen on active Pt or Ru under high H_2 pressure hydrogenates the C=O bond stabilizing HMF ring to its hydrogenated alcohol form, i.e. BHMF. The inactivity of Pt and Ru during electrocatalytic hydrogenation might be due to the kinetics of hydrogen evolution (Eq. 7.4 or 7.5).

Compared to traditional heterogeneous catalytic hydrogenation processes, the electrocatalytic processes are performed under mild conditions (ambient temperature and pressure), avoiding the use of molecular H_2 [1, 17]. Due to the co-production of hydrogen, careful selection of the electrocatalyst as well as the applied potential/current is important in order to obtain high yield and selectivity towards BHMF. The over potential for water reduction and the adsorption of HMF depend strongly on the nature of the catalyst interface.
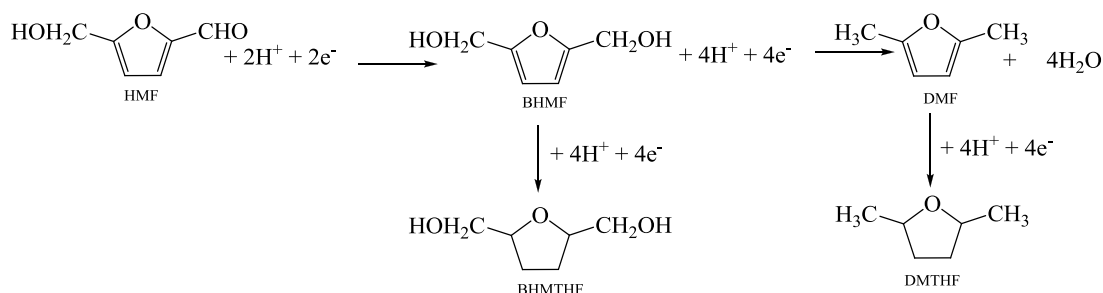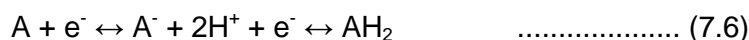

Fig. 7. 1 Reaction pathway of the electrocatalytic hydrogenation of HMF

Till date, the electrocatalytic HMF hydrogenation to BHMF or DMF has not been reported in the literature (fig.7. 1). A fundamental understanding of the reactions relation between electrocatalyst structure and electrocatalytic reduction activity is largely absent. Detailed work regarding the selective HMF electroreduction voltammetry has probably not been reported due to existing technical limitations regarding the online analysis of products.

An important difference between the heterogeneous chemical catalytic and electro catalytic reduction process is the way how atomic hydrogen is supplied [18]. Heterogeneous catalytic process requires externally supplied hydrogen gas and splits molecular hydrogen into atomic hydrogen by surface adsorption [13, 19, 20], while electrocatalytic hydrogenation reduces water or hydronium ions to form atomic hydrogen *in-situ* on the catalytic cathode surface using external electrons [21]. Electrochemical hydrogenation of C=C (e.g C=C of HMF = A) compounds ($A + 2H \leftrightarrow AH_2$) in general can occur via three types of mechanisms [22, 23].

Direct electron transfer (decoupled electron and proton transfer)

$$A + e^- \leftrightarrow A^- + 2H^+ + e^- \leftrightarrow AH_2 \qquad \text{.................... (7.6)}$$

Catalytic hydrogenation

$$A + 2H_{ads} \leftrightarrow AH_2 \qquad \text{………………. (7.7)}$$

Electrocatalytic hydrogenation (coupled proton and electron transfer)

$$A + 2H^+ + 2 e^- \leftrightarrow AH_2 \qquad \text{…….…………. (7.8)}$$

The direct electron transfer mechanism (Equation 7.6) is generally believed to occur over materials with high HER overpotentials, such as Hg, Bi, Sn and Cd [24]. These materials have very low surface coverage of hydrogen. So reduction of unsaturated compounds occurs via the production of a radical cation intermediate, which is subsequently reacted to form the saturated organic compound [25, 26].

The catalytic and electrocatalytic hydrogenation mechanisms involve the reaction of adsorbed unsaturated compounds with either adsorbed hydrogen atoms (Equation 7.7) or protons (Equation 7.8), respectively. One difference between these two reaction pathways is the effect that the electron transfer in Equation 7.9 has on the characteris-

tic rate equation [26]. The catalytic hydrogenation rate expression involves the surface coverage of the HMF (θ_{HMF}) and hydrogen (θ_{H}^{+}) reactants [27].

$$Rate = k\theta_{HMF}{}^{a}\ \theta_{H^{+}}{}^{b}$$ ………………. (7.8)

The rate expression for the direct and electrocatalytic pathway incorporates an exponential term (Butler Volmer) to account for the potential dependence of the electron transfer [5].

$$Rate = k\theta_{HMF}{}^{a}\ \theta_{H^{+}}{}^{b}\exp(\frac{\alpha FV}{RT})$$ ……………….. (7.9)

where V is the applied potential, k is the reaction rate constant, and a and b are the orders of reaction. The implication from the electrochemical pathway is that an applied potential will have the effect of increasing the reaction rate [22, 27]. Nevertheless, the chemisorption of the organic and hydrogen reactants may also depend on the applied potential, which will likewise affect the rate [23, 28, 29].

HMF is fairly soluble in all types of solvents such as aqueous, organic and ionic liquids. Whereas electrocatalytic reduction derivatives of HMF such as BHMF, DMF are fuel type molecules and are not soluble in many of organic solvents. The desired product DMF is not miscible with the water, which makes this molecule more attractive for fuel.

7. 1. 1. Objective of the chapter

This chapter aims to explore novel electrocatalytic approaches to convert abundant, inexpensive lignocellulosic biomass-derived HMF into liquid biofuels (electrobiofuels) type molecule in electrocatalytic cell reactors. Our current focus is to study electrocatalytic hydrogenation of HMF on different electrified metal surfaces and compare their activity and selectivity towards reduced reaction products qualitatively and quantitatively.

7.2 Results and Discussions

Electrocatalysts such as platinum, palladium, copper and nickel were selected to carry out electrocatalytic reduction of HMF. Before going to test their electrocatalytic activity

for HMF reduction, the characterization studies were conducted using cyclic voltammetry.

7.2.1. Cyclic voltammetry of electrocatalyst surface

Copper and nickel were not stable in acidic conditions (1M H_2SO_4). Copper forms copper sulphate and nickel forms nickel sulphate. HMF was not stable in strongly basic conditions. Therefore pH 10 electrolyte (as used in the chapter 6) was chosen to understand the electrochemical characteristics of each metal electrocatalytic hydrogenation reactions. Selected metals were stable at pH 10 conditions.

Fig. 7. 2 shows the voltammograms of different foils in a cathodic potential window in the absence of HMF (so called "blank" solution). The metals showed characteristic differences in their onset potential and activity towards the hydrogen evolution reaction. No other surface electrochemical process could be discerned on any of the metal electrodes. The increase of cathodic current observed in the blank experiment is attributed to the evolution of H_2. Here all catalysts in fig. 7. 2 show different onset potential for H_2 evolution in the absence of HMF. The results clearly indicate that the formation of chemisorbed hydrogen and molecular H_2 is strongly dependent on the surface adsorption properties of the catalyst.
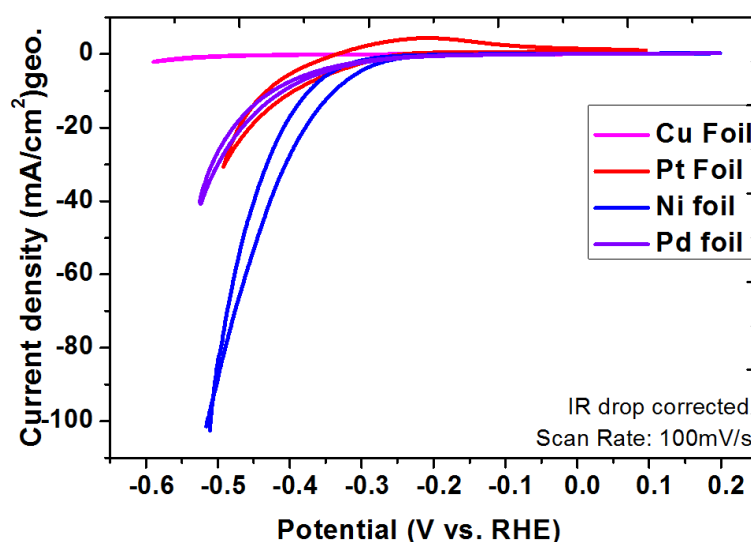
Fig. 7. 2 CV of bare Pt, Pd, Cu and Ni foils at negative potentials for cathodic reactions. Conditions: (0.3M $NaClO_4$ + 10mM NaOH) supporting electrolyte, pH 10, in the absence of HMF, scan rate is 100 mV/s, under N_2, room temperature, WE: metal foil $(4.5cm^2)_{geo.}$, CE: Pt gauze $(12.5cm^2)$, RE: RHE.

Copper clearly showed less activity towards hydrogen evolution and hence required more cathodic potentials. Pt and Pd showed a similar activity for the hydrogen evolu-

tion reactions. Compared to other metals nickel showed higher electrochemical activity for the production of hydrogen from water at lower potential. Therefore at given conditions nickel electrode appears as a promising electrode for HMF reduction reactions and will generate required hydrogen by splitting water.

All these metals were then tested in the presence of HMF to understand their electrochemical behavior. All metals exhibited similar type of CVs without any characteristic peak relating to HMF reduction reaction. So HMF appeared to be not electrochemically active at negative electrode potentials. We assumed from section 6.2.2.1 that HMF ring (C=C) and functional groups (CH_2OH and CHO) adsorb on the metal surface at lower potential (≈0V) and participate in the hydrogenation reactions by using *in-situ* generated hydrogen. Therefore, negative potentials were applied to all metals in order to study the electrocatalytic reduction of HMF. The product distribution was analyzed using HPLC.

7.2.2. Electrocatalytic reduction of HMF

Electrocatalytic hydrogenation of HMF was carried out in a biphasic system, which contains conducting aqueous electrolyte and organic solvent to trap products. Constant current density was applied to different metal surfaces under similar conditions and product distribution was monitored.
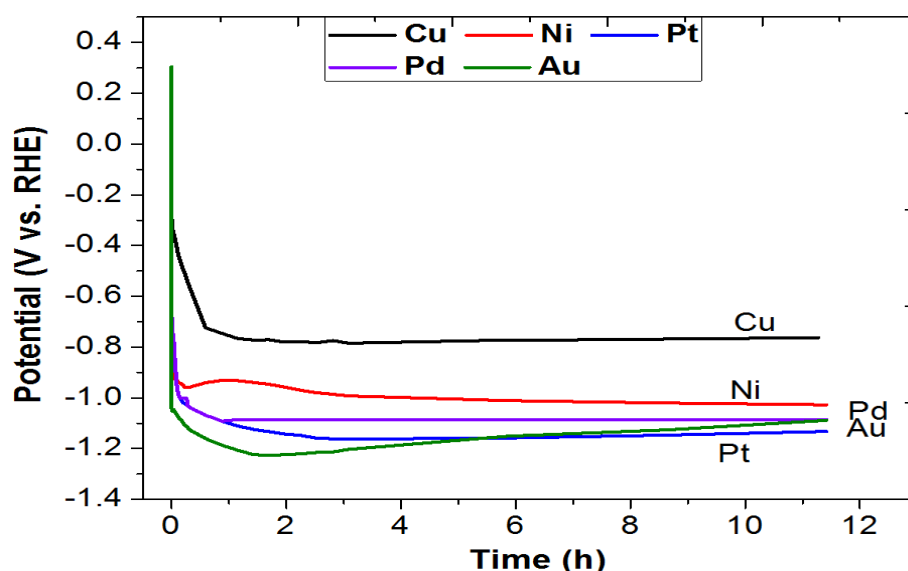

Fig. 7. 3 Chronopotentiometry profiles (E vs. t) of different metal surfaces under applied current density -2.22mA/cm^2 for HMF electrocatalytic hydrogenation. Conditions: (0.3M NaClO$_4$ + 10mM NaOH) supporting electrolyte, pH 10, 1-butanol organic phase, 5mM HMF, magnetic

stirring, under N_2, room temperature, WE: metal foil $(4.5cm^2)_{geo.}$, CE: Pt gauze $(12.5cm^2)$, RE: RHE.

Fig. 7. 3 Presents the interfacial electrode potential of each metal foil for an applied constant current density to hydrogenate HMF. Pt, Au, Pd exhibited comparable electrode potentials for a given current density, whereas Cu exhibited a somewhat higher cathodic over potential. Ni electrode surface potential was in between Cu and Pd. This observation was consistent with the relative hydrogen evolution reactivity. Pt and Pd were able to meet the current condition at a less cathodic over potential.
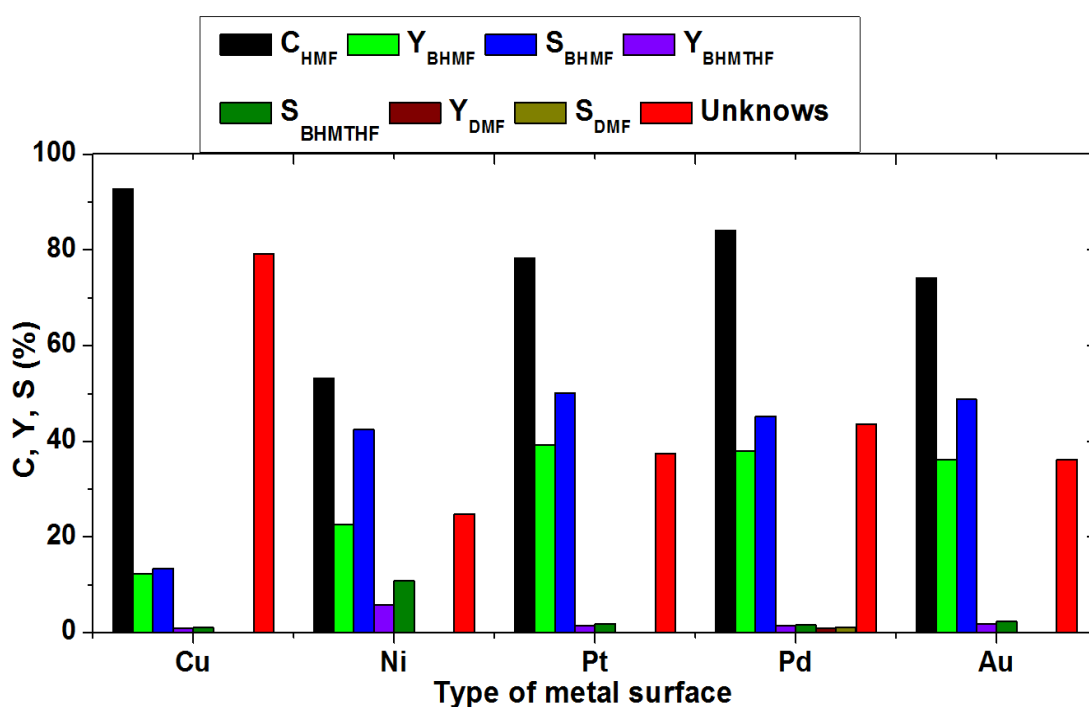
Fig. 7. 4 Electrocatalytic hydrogenation of HMF over 12h of reaction time on different metal surfaces; reaction conditions: biphasic system ((50ml of 0.3NaClO4+10mM NaOH in H_2O) + 20ml 1-butanol)), pH10, -2.22mA/cm^2 current density applied; N_2 atmosphere; magnetic stirring; Pt gaze counter electrode, RHE reference electrode (where C= conversion, Y= yield, S= selectivity).

Fig. 7. 4 Demonstrates the product distribution of HMF electrocatalytic hydrogenation at 12h of reaction time at applied current density -2.22mA/cm^2. Cu surface was more active for HMF conversion followed by Pd, Pt, Au and Ni. The formation of BHMF was higher on Pt, Pd, Au surfaces compared to the Cu. Effect of each metal electrode on HMF electrocatalytic hydrogenation will be discussed separately in the next sections with the help of the supporting information fig. 7. 7. Reactants, products and unknown

molecules were detected using UV as shown in the fig. 7. 7a-e. Both products and un-knowns were not active for refractive index detector.

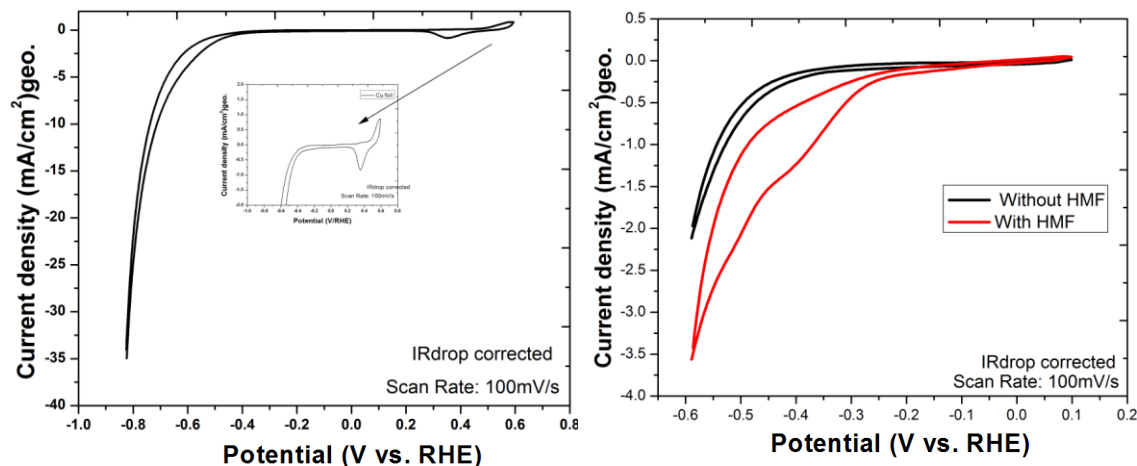### 7.2.3. Cu foil electrode surface

Fig. 7. 5 CV of Cu surface in pH 10 electrolyte a) bare Cu surface without HMF b) Cu surface with and without HMF. Conditions: (0.3M NaClO4 + 10mM NaOH) supporting electrolyte, pH 10, scan rate is 100 mV/s, under N_2, room temperature, CE: Pt gauze (12.5cm^2), RE: RHE.

Fig. 7. 5a Shows the current potential behavior of Cu metal electrode between +0.2V and +0.7V. An anodic electrochemical redox wave possibly associated with the oxida-tion of Cu^0 to higher oxidation states was detected at +0.6V in the anodic scan and reduced to Cu^0 during cathodic scan. Therefore, it is reasonable to assume that Cu surface remained in the oxidation state Cu^0 during HMF electrocatalytic hydrogenation reactions below ≤+0.2V. Fig. 7. 5b indicates a significant change in the faradaic current flow in the presence of HMF than in blank HMF free electrolyte. This was likely due to HMF adsorption on the Cu surface. Compared to Pt and Ni electrodes (fig. 7. 6 , Cu exhibited more faradaic current in the presence of HMF. From this observation, we can conclude that the presence of HMF inhibits hydrogen evolution, presumably by adsorb-ing onto the electrode surface. Fig. 7. 4 suggests that at the given current density Cu exhibited higher electrocatalytic activity for HMF conversion, but with a low selectivity for BHMF compared to other electrodes. This is mainly due to the formation of other byproducts. Fig. 7. 7a supports same conclusions that there was a formation of some unknown compounds and unable to detect with existed analytical methods.

7.2.4. Pt & Ni foil electrodes
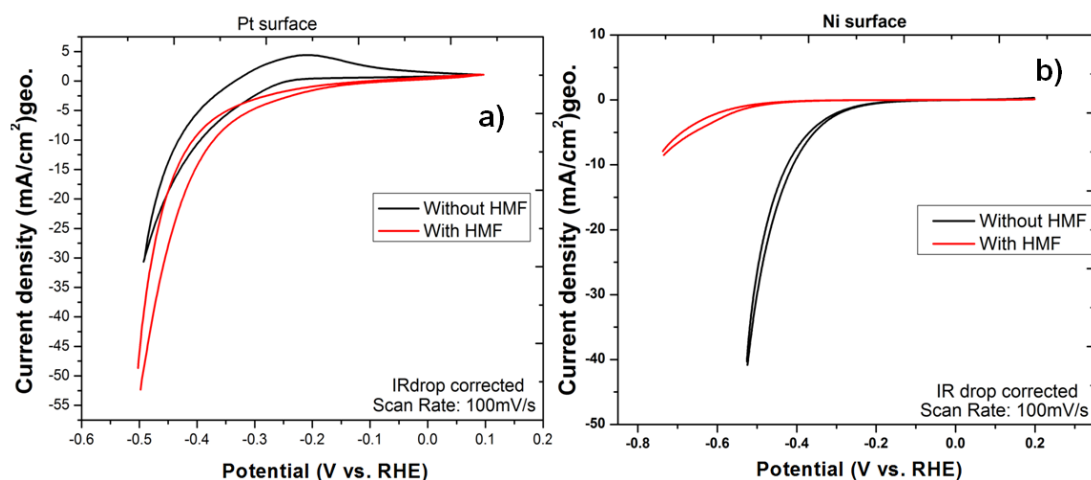
Fig. 7. 6 CV of Pt and Ni foil electrode with & without HMF. Conditions: (0.3M NaClO4 + 10mM NaOH) supporting electrolyte, pH 10, scan rate is 100 mV/s, under N_2, room temperature, CE: Pt gauze (12.5cm^2), RE: RHE.
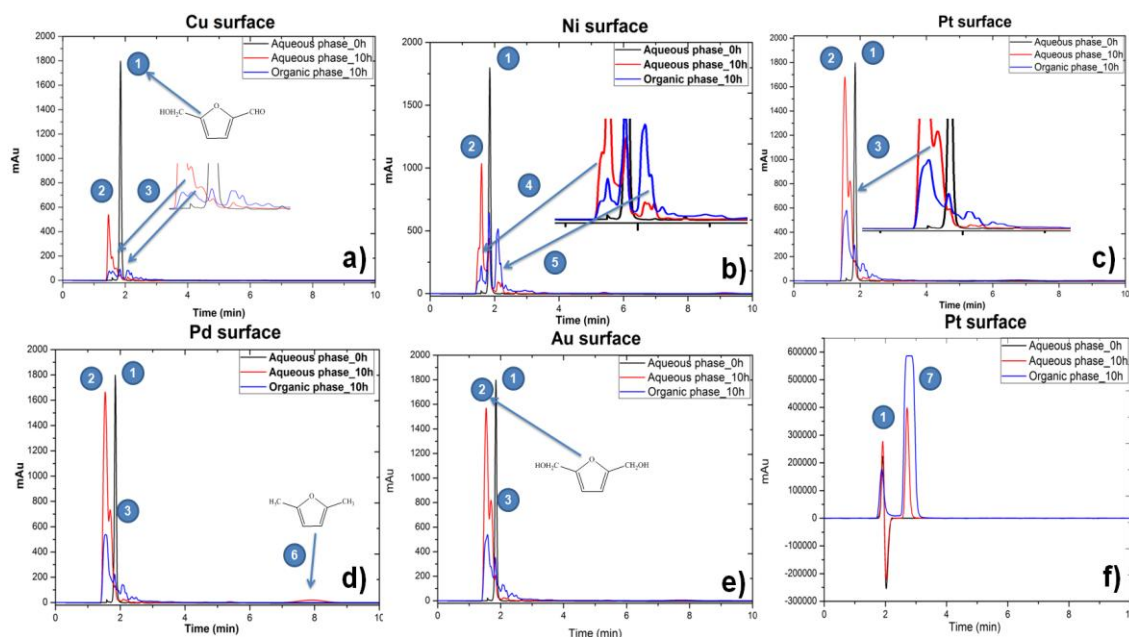
Fig. 7. 7 HPLC chromatograms of HMF electrocatalytic hydrogenation on different metal surfaces; a), b), c), d), e) UV spectrum of product distribution on Cu, Ni, Pt, Pd, Au respectively and f) RI spectrum. Reaction conditions: 5mM HMF; pH10 (0.3M NaClO$_4$+10mMNaOH in 50ml H$_2$O) as aqueous phase; 20ml of 1-butanol. As organic phase; 2.22mA/cm^2 current density; room temperature; N$_2$ atmosphere; magnetic stirring. 1-HMF, 2-BHMF, 3-unknown, 4-unknown, 5-BHMTHF, 6-DMF, 7-solvent (1-butanol).

In contrast to the other metals, the onset potential for hydrogen evolution reaction on platinum group metals is less negative (close to -0.1 V) as shown in fig. 7. 6 . Similar to

Cu electrode (fig. 7. 5), more faradaic current was observed in the presence of HMF than bare Pt electrode. Fig. 7. 4 shows electrocatalytic activity of Pt for HMF hydrogenation, where Pt exhibited highest selectivity for BHMF. Insignificant amount of the total hydrogenation product (BHMTHF) was observed. Like Ni electrode Pt also produced similar type of unknown-3 as shown in fig. 7. 7c.

Fig. 7. 6 b shows that the cathodic current on Ni increases from ca. -0.2 V in the absence of HMF. In contrast to all metals, more negative (-0.6V) onset potential was observed in case of Ni in the presence of HMF, which indicates that HMF was possibly adsorbed on the surface of the Ni foil and hence delayed the reduction of hydrogen. Fig. 7. 4 presents electrocatalytic activity of nickel for HMF hydrogenation. Unlike other metal electrodes, Ni exhibited a stark catalytic activity towards the production of BHMTHF (a valuable biomass derived fuel-additive). A different type of unknown-4 product was observed as shown in the fig. 7. 7b. Although Raney-typed Ni catalysts are widely applied for heterogeneous hydrogenation reactions in industry, previous reports emphasize that Ni shows hardly any electrocatalytic activity for glucose reduction to s-orbitol [12, 30]. However, at the applied current (10 mA/ cm^2) or potential (< -1 V vs. RHE) in these works will yield 25% BHMF and 5% BHMTHF.

7.2.5. Pd & Au foil electrodes

Similarly, Pd and Au metal electrodes were tested for the electrocatalytic activity for HMF hydrogenation under similar conditions. Pt and Au showed comparable electrocatalytic activity for the production of BHMF as shown in the fig.7. 4. Pd was not active compared to Pt and Ni for the oxidation of HMF (see chapter 6), but the same Pd exhibited more catalytic activity than Ni electrode. Interestingly, a weak signal was observed for the formation of most wanted product, DMF (a potential biomass derived fuel) as shown in fig. 7. 7d. Au is also electrocatalytically active for the hydrogenation of HMF into BHMF as shown in the fig. 7. 4 and fig. 7. 7e.

7.3 Conclusions

Electrocatalytic hydrogenation of HMF was accomplished using an electrochemical cell at a constant current. This study demonstrates the viability and significance of the hypothesis in this thesis of using renewable electrons for renewable biomass conversion

at low temperature and ambient pressure without using external hydrogen. The main barrier of hydrogen for future chemical industry can be overcome by using electro catalysis of water and required chemicals and fuels can be generated from renewable lignocellulosic biomass. This study opens door for new research directions.

Electrocatalytic activity of different metal foil electrodes were tested for hydrogenation of HMF. The activity of metal electrodes was discussed in detail qualitatively and qualitatively using CV. Cu electrode was active for HMF conversion, but exhibited lowest selectivity than other metals for desirable products. Au and Pt showed comparable activity for the formation of BHMF. Ni and Pd exhibited more activity towards formation of further hydrogenated products. 5% of BHTHF was observed on the Ni foil electrode. Interestingly, an activity was showed for the formation of DMF. Apart from other products and unknowns, the electrocatalytic activity for the formation of BHMF by different metal electrodes is Pt > Pd > Au > Ni > Cu.

Outlook

Detailed investigations are required in order to get more insights of electrode surface in terms of selectivity and conversion. Design, synthesis, and characterization of metallic nanostructures with controlled size, shape, composition, structure, and morphology as efficient electrocatalysts are critical for electrocatalytic processing of biomass derived HMF to increase the selectivity. Designing of continuous process will increase the productivity and reduce the cost.

7.4 References

1.   Corma, A. and P. Serna, *Chemoselective Hydrogenation of Nitro Compounds with Supported Gold Catalysts.* Science, 2006. 313(5785): p. 332-334.
2.   Teschner, D., et al., *The Roles of Subsurface Carbon and Hydrogen in Palladium-Catalyzed Alkyne Hydrogenation.* Science, 2008. 320(5872): p. 86-89.
3.   Vispute, T.P., et al., *Renewable Chemical Commodity Feedstocks from Integrated Catalytic Processing of Pyrolysis Oils.* Science, 2010. 330(6008): p. 1222-1227.
4.   Rosatella, A.A., et al., *5-Hydroxymethylfurfural (HMF) as a building block platform: Biological properties, synthesis and synthetic applications.* Green Chemistry, 2012. 13(4): p. 754-793.
5.   Beck., F., *Electrochemical and catalytic hydrogenation: common features and dierences. .* International Chemical Engineering, 1979. 19(1): p. 1-11.
6.   Centi, G. and S. Perathoner, *Opportunities and prospects in the chemical recycling of carbon dioxide to fuels.* Catalysis Today, 2009. 148(3-4): p. 191-205.

7.   *Chapter 8 Hydrogen Energy: The Future?*, in *Hydrogen Energy: Challenges and Prospects*. 2008, The Royal Society of Chemistry. p. 275-295.

8.   *Chapter 14 Energy-Renewable and Clean*, in *Nano-Society: Pushing the Boundaries of Technology*. 2009, The Royal Society of Chemistry. p. 223-234.

9.   Derwent, R., R.E. Hester, and R.M. Harrison, *Global warming consequences of a future hydrogen economy*, in *Transport and the Environment*. 2004, The Royal Society of Chemistry. p. 25-34.

10.   *Chapter 4 Solar Hydrogen Utilization*, in *Solar Hydrogen: Fuel of the Future*, The Royal Society of Chemistry. p. 119-154.

11.   Bannari, A., et al., *Mathematical modeling of the kinetics of phenol electrocatalytic hydrogenation over supported Pd-alumina catalyst.* Applied Catalysis A: General, 2008. 345(1): p. 28-42.

12.   Bin Kassim, A., C.L. Rice, and A.T. Kuhn, *Formation of sorbitol by cathodic reduction of glucose.* Journal of Applied Electrochemistry, 1981. 11(2): p. 261-267.

13.   Kaneco, S., et al., *Electrochemical Reduction of Carbon Dioxide to Hydrocarbons with High Faradaic Efficiency in LiOH/Methanol.* The Journal of Physical Chemistry B, 1999. 103(35): p. 7456-7460.

14.   Sakellaropoulos, G.P. and S.H. Langer, *Electrocatalysis; selective electrogenerative reduction of organic halides.* Journal of Catalysis, 1976. 44(1): p. 25-39.

15.   Hamann, C.H., *Electrochemistry, 2007.*

16.   Hasché, F., M. Oezaslan, and P. Strasser, *Activity, Stability, and Degradation Mechanisms of Dealloyed PtCu3 and PtCo3 Nanoparticle Fuel Cell Catalysts.* ChemCatChem, 2011. 3(11): p. 1805-1813.

17.   Li, Z., et al., *Aqueous electrocatalytic hydrogenation of furfural using a sacrificial anode.* Electrochimica Acta, 2012. 64(0): p. 87-93.

18.   Li, Z., et al., *Mild electrocatalytic hydrogenation and hydrodeoxygenation of bio-oil derived phenolic compounds using ruthenium supported on activated carbon cloth.* Green Chemistry, 2012 14(9): p. 2540-2549.

19.   Koper, M.T.M., *Introductory Lecture Electrocatalysis: theory and experiment at the interface.* Faraday Discussions, 2009. 140: p. 11-24.

20.   Lan, Y.-C., et al., *Electroreduction of dibromobenzenes on silver electrode in the presence of CO2.* Journal of Electroanalytical Chemistry. 664(0): p. 33-38.

21.   Tountian, D., et al., *Effect of support conductivity of catalytic powder on electrocatalytic hydrogenation of phenol.* Journal of Applied Electrochemistry, 2009. 39(3): p. 411-419.

22.   Vilar, M.r., J.L. Oliveira, and M. Navarro, *Investigation of the hydrogenation reactivity of some organic substrates using an electrocatalytic method.* Applied Catalysis A: General. 372(1): p. 1-7.

23.   Robin, D., et al., *The electrocatalytic hydrogenation of fused poly cyclic aromatic compounds at Raney nickel electrodes: the influence of catalyst activation and electrolysis conditions.* Canadian Journal of Chemistry, 1990. 68(7): p. 1218-1227.

24.   Analogies, C.L.W., *Between Electrolytic and Chemical Methods of Reduction. Experiments with Sorbic Acid. Remarks on Mechanism. Transactions of* Transactions of The Electrochemical Society 1939. 75: p. 353.

25.   Lyons, M.E.G. and M.P. Brandon, *Redox switching and oxygen evolution electrocatalysis in polymeric iron oxyhydroxide films.* Physical Chemistry Chemical Physics, 2009. 11(13): p. 2203-2217.

26.   Bond, G.C., G. Webb, and a.A.T.K. M.D. Birkett, *The catalytic hydrogenation of organic compounds: a comparison between the gas-phase, liquid-phase, and electrochemical routes.* RSC Publishing, 1983: p. 61-89.

27.   Zhao, S.-F., et al., *Influences of the operative parameters and the nature of the substrate on the electrocarboxylation of benzophenones.* Journal of Electroanalytical Chemistry. 664(0): p. 105-110.

28.   Byrne, M.a.K., A.T. , *Electro-catalytic reduction of ethylene on platinum and ruthenium. .* Journal of the Chemical Society, Faraday Transactions 1: Physical Chemistry in Condensed Phases,, 1972. 68: p. 355-368.

29.   Mahdavi, B., J.M. Chapuzet, and J. Lessard, *The electrocatalytic hydrogenation of phenanthrene at raney nickel electrodes: the effect of periodic current control.* Electrochimica Acta, 1993. 38(10): p. 1377-1380.

30.   bin Kassim, A., C.L. Rice, and A.T. Kuhn, *Cathodic reduction of glucose.* Journal of the Chemical Society, Faraday Transactions 1: Physical Chemistry in Condensed Phases, 1981. 77(3): p. 683-695.

*This page was left intentionally blank*

Chapter 8

Conclusions and Outlook

This thesis addressed chemical transformation of biomass derived model molecules using heterogeneous catalysis and electrochemical catalysis. In chapter 3, cellulosic derived fructose was converted into the valuable platform molecule HMF via dehydration reaction. Initially, dehydration reactions were repeated as per literature using liquid acid catalyst and different solvents were screened to select favorable reaction conditions. Cross polymerization of fructose into humins was observed in the aqueous solvents as cited in the literature. To minimize the formation of humins, organic solvents were used for fructose dehydration into HMF. The DMSO solvent showed catalytic activity in (absence of acid catalyst) "blank" runs for fructose dehydration. DMA appeared as a suitable solvent for fructose dehydration with negligible amount of humins formation; it is economically cheaper to use in industry as well. Different solid acid catalysts such as sulfonated zirconia, sulfonated silica, sulfated titania, sulfonated SBA-15 were synthesized using different sulfonic acid group linkers such as cholosulfonic acid, benzenesulfonic acid, (3-Mercaptopropyl)trimethoxysilane (MPTMS) and (3-((3-(trimethoxysilyl)-propyl)thio)-propane-1-sulfonic acid) (TESAS). These catalysts were tested for fructose dehydration into HMF and compared with the commercially available solid acid catalysts such as amberlyst-15, p-toluenesulfonic acid. 38% HMF selectivity and 100% fructose conversion was achieved using sulfonated zirconia. Sulfonated zirconia has appeared as a potential support for bi-functional catalyst to impregnate both acid groups and active metals to run dehydration and oxidation reactions in one pot. Hydroxyl groups on the surface of the support influence the covalent attachment of acid groups and subsequently play a role in the dehydration reactions. The reactive centers of MPTMS and TESAS linkers supported on SBA-15 have flexibility to move sulfonic acid group freely during the reaction similar to the homogeneous catalysts. At the same time these have the advantage of recyclability like heterogeneous catalysts. 70% HMF selectivity was noticed in case of TESAS on SBA-15 and exhibited catalytic activity up to 4 recycles. Temperature has a strong influence on fructose dehydration into HMF.

Chapter 4 focused on the heterogeneous chemical catalytic oxidation of HMF. Reactions were carried out in the temperature and pressure controlled autoclave reactor using molecular oxygen as oxidant. *in-situ* NMR study on HMF degradation mechanism

at higher pH (pH≥13) in the absence of a metal catalyst confirmed the loss of HMF due to cross-polymerization of HMF (humins) via cannizzaro reaction. Reaction pathways were proposed based on different reaction conditions. It is also seen that the pH of a reaction has a strong influence on oxidation of alcohol moiety of HMF. Concentration of $[OH]^-$ influences the HMF oxidation into FDCA. Using high surface area ($150m^2/g$) Pt/C catalyst, 100% of HMF conversion with 80% of FDCA yield was achieved in 8h at mild temperature (50^oC). Influence of pH was addressed with quantitative and qualitative information of reaction products as shown in the fig. 8.1.
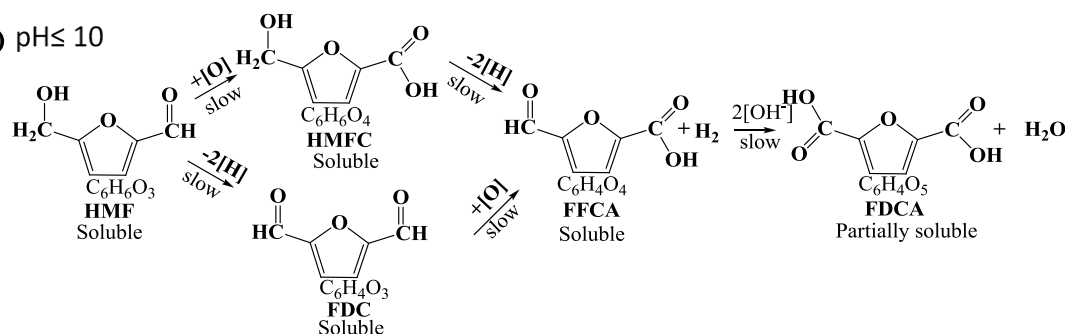
a) pH≥13
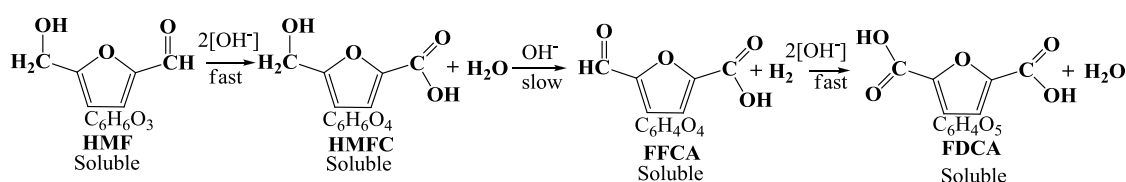
b) pH≤ 10

Fig. 8. 1 Influence of pH on HMF reaction pathway.

HMF was converted into FDCA at a higher pH (pH≥13) with less amounts of intermediates and converted into FDC at a lower pH (pH≤10). Experimental analysis suggests that at lower pH (≤7), the alcoholic group of HMF oxidizes faster than aldehyde moiety on Pt surface, whereas at higher pH (≥13), oxidation of alcoholic group appears as the rate limiting step. Low temperatures and basic pH led to the oxidation of both formyl and hydroxyl groups of HMF to FDCA. Effect of different metal surfaces was addressed on HMF oxidation into FDCA at pH 13. An order of reactivity was observed following: Au/TiO$_2$ > Pt/C > Ru/C > Rh/C > Pd/C. In case of Ru and Rh, more intermediates such as HMFC and FFCA were observed. Pd was inactive for HMF oxidation and followed a different reaction pathway with unknown products.

Chapter 5 focused on HMF hydrogenation using heterogeneous catalyst. HMF hydrogenation reactions were carried out using molecular hydrogen. Different solvents were tested for HMF hydrogenation on Ru surface. Total hydrogenation of HMF into

dimethyltetrahydrofuran (DMTHF) was observed in aqueous solvents. Selective hydrogenation of HMF into DMF was achieved using 1-butanol as a solvent. Effect of different metal surfaces was studied under selected conditions. Under similar conditions, Pt/C showed highest activity with 75% of DMF yield followed by Ru/C > Ni/SiO$_2$ > Au/TiO$_2$ > Rh/C > Cu/Al$_2$O$_3$ > Pd/C.

In the chapter 6, electrocatalytic oxidation of HMF was addressed for the first time in detail with quantitative and qualitative results. Electrocatalytic reactions have an added advantage over heterogeneous catalytic reactions in terms of additional operating parameters like interfacial potential. The required oxygen for oxidation reactions was generated *in-situ* by electrocatalytic water splitting. Initial understanding of electrochemical behavior of different HMF derivatives was characterized in different solvents such as acidic, basic, neutral and organic using cyclic voltammetry. Organic electrolytes are not suitable for HMF oxidation due to less conductivity. Anodic oxidation of HMF was studied using different metal foil electrodes. Chronopotentiometric techniques were used to change the electrode surface potential by applying constant current density. Noble metals such as platinum, palladium and non noble metals such as nickel were selected to study the electrochemical electrocatalytic HMF oxidation reactions. HMF alone was not stable at a higher pH (basic conditions). Platinum electrode was examined extensively at different pHs and reaction conditions to know electrocatalytic activity for HMF oxidation. A mapping of different current densities/operating potentials on platinum surface and its associated FDC yield & selectivity were performed. The current density was optimized to 0.44mA/cm^2 to get optimal FDC yield from HMF oxidation. A comparative analysis of heterogeneous catalysis and electrochemical catalysis was carried, for instance on Pt surface is shown fig. 8.2.

Fig.8.2 compares high surface area platinum at heterogeneous catalytic conditions with low surface area platinum electrode at 0.44mA/cm^2 current density. Electrochemical catalytic reactions clearly showed superior activity towards HMF oxidation into FDC in terms of higher yield and selectivity at pH10.
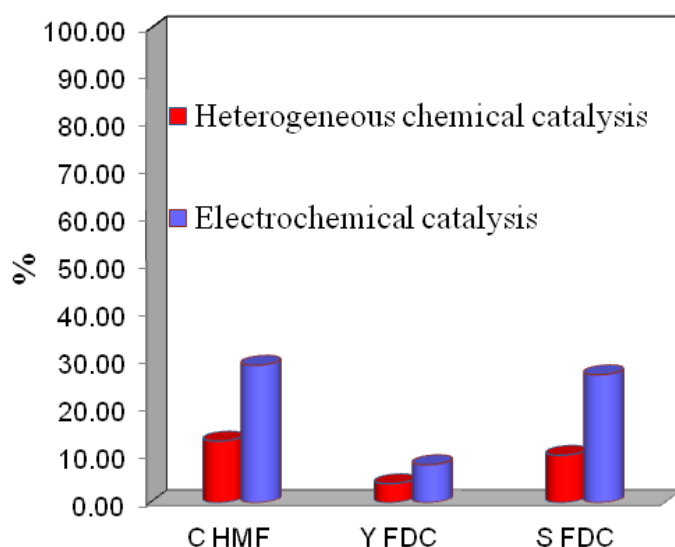
Fig. 8. 2 comparison of heterogeneous catalytic and electrocatalytic HMF oxidation on Platinum surface. Heterogeneous catalysis conditions: Pt/C ($150 m^2/g$), 1 bar O_2, 25^oC,4h, pH10, Pt/HMF molar ratio: 0.1. Electrocatalytic conditions: Pt foil (4.5cm2)geo. surface area, 1 bar N_2 , 25^oC,4h, pH 10, $0.44 mA/cm^2$ current density. (Where C= Conversion, Y=Yield, S=Selectivity).

In contrary to Pt electrode, relatively low electrocatalytic activity towards HMF oxidation was observed on Pd electrode surface. Increase in the electrolyte temperature helped to improve the electrocatalytic activity of palladium for HMF oxidation. Not much influence was observed by circulating oxygen in order to influence its activity. Interestingly, Ni appeared as a promising electrocatalyst with higher activity for HMF oxidation into FDC comparison with Pt and Pd as shown in fig.8.3.
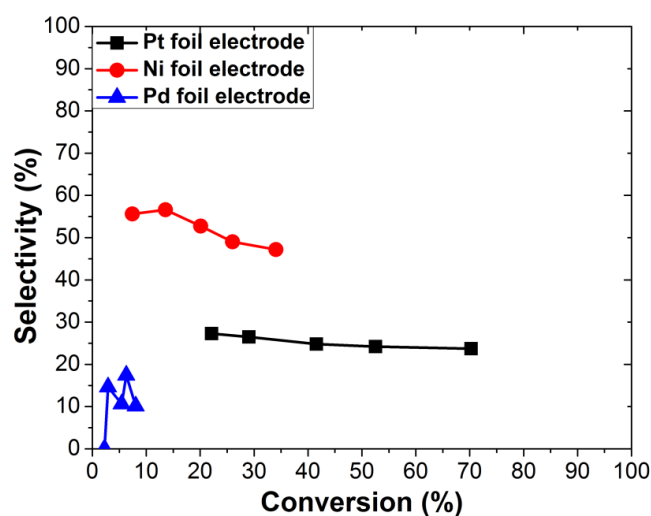

Fig. 8. 3 Comparison of electrocatalytic activity of Pt, Pd and Ni for FDC formation from HMF. Conditions: (0.3M $NaClO_4$ + 10mM NaOH) supporting electrolyte, pH 10, scan rate is 50 mV/s, under N_2, room temperature, CE: Pt gauze ($12.5cm^2$), RE: RHE.

Increase in the current density (>0.44mA/cm^2) on Pt electrode resulted less FDC formation, whereas higher FDC formation along with FFCA and FDCA was observed on Ni electrode.

Chapter 7 focused on electrocatalytic hydrogenation of HMF at negative potentials. Electrocatalytic hydrogenation of HMF was studied on different metal electrode surfaces using a biphasic solvent. The activity of metal electrodes was discussed in detail qualitatively and quantitatively using CV. 38% of BHMF was observed from HMF hydrogenation using Pt surface at 2.22mA/cm2 current density. Ni and Pd exhibited more activity towards formation of further hydrogenated products. The electrocatalytic activity for the formation of BHMF by different metal electrodes is Pt > Pd > Au > Ni > Cu.
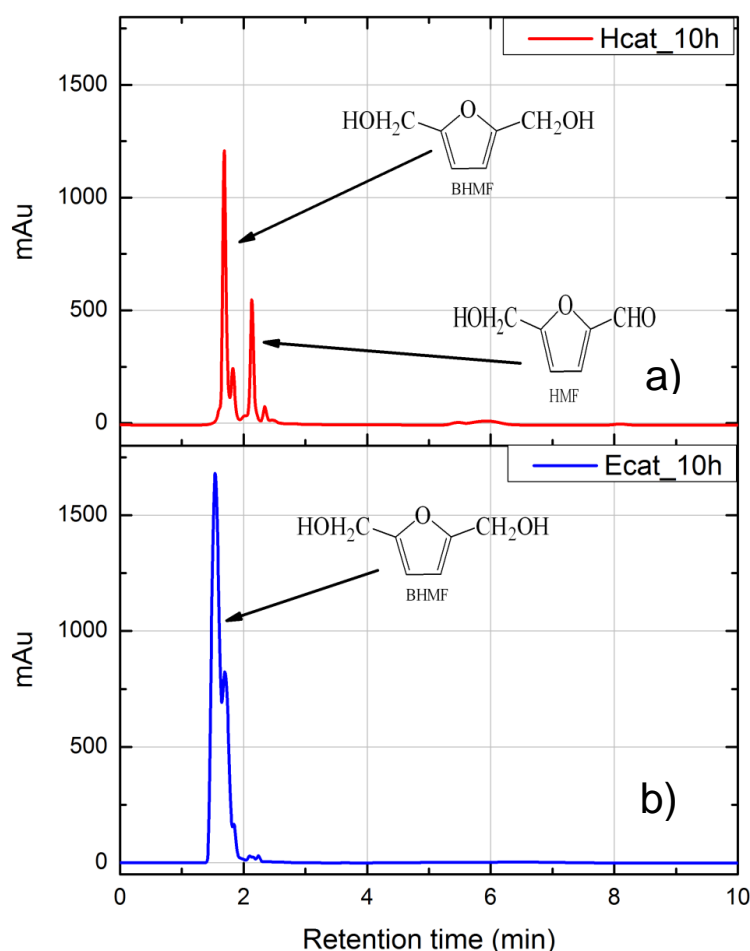

Fig. 8. 4 Comparison of heterogeneous catalysis and Electrocatalysis for hydrogenation of HMF. a) Conditions: a) Heterogeneous catalysis: Pt/C (150m^2/g),0.1M HMF; water; 175°C; 10bar H$_2$; 10h; 1000 rpm, Metal/HMF molar ratio: 0.05; b) Electrochemical catalysis: Pt foil (4.5cm^2)$_{geo.}$, (50ml of 0.3NaClO$_4$+10mM NaOH in H$_2$O), pH10, -2.22mA/cm^2 current density applied; N$_2$ atmosphere; magnetic stirring; Pt gaze counter electrode, RHE reference electrode.

Fig. 8.4 shows superior activity of electrocatalysis for hydrogenation of HMF over heterogeneous catalysis. HMF is converted completely in electrocatalysis than heterogeneous catalysis. Formation of BMBF is also higher using electrocatalysis.
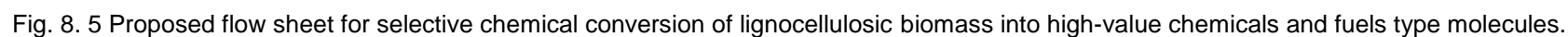
Outlook

The rapidly growing field of HMF synthesis from carbohydrates holds a great promise for the future. The field, however, is still immature and a number of issues need to be investigated in detail in the continuous search for realistic large-scale processes. Future research should target an economic analysis of the potential processes.

In case of fructose dehydration, intense investigations are required to control leaching of acid groups from solid surface. More sophisticated characterization studies were required to find out the amount of surface acidity and surface structure.

In case of heterogeneous catalytic oxidation and hydrogenation reactions of HMF, development of mixed metal catalysts are required in order to mix non-noble metals to reduce the cost of the catalyst. Detailed kinetic investigations are required along with modeling of reactions in order to scale up. Continuous processes are required to optimize the production cost of polymer based chemicals (e.g FDCA) and fuel type molecules (e.g. DMF).

In case of electrocatalytic oxidation and hydrogenation reactions, more investigations are required to understand adsorption mechanism of HMF conversion on the potential surface of electrode using sophisticated spectroscopic techniques such as ATR, etc. DFT calculations are required to get total energy changes during the oxidation and hydrogenation reactions. Developing a continuous process by combining heterogeneous and electrochemical catalysis for biomass derived sugars into valuable chemicals would be advised.

Finally our experimental results may aid to develop a process to get valuable chemicals and fuels from lignocellulosic biomass as shown in fig. 8.5.

Fig. 8. 5 Proposed flow sheet for selective chemical conversion of lignocellulosic biomass into high-value chemicals and fuels type molecules.

Appendix

1. Instrument: LC-MS (liquid chromatography in combination with mass spectrometry) from Agilent 1200 series

Major components of LC:

Agilent 1200 Series LC with

Name	Part No	S.No
Variable Wavelength Detector	G1314B	DE71365676
Refractive Index Detector	G1362A	DE00960016
Binary Pump	G1312A	DE63061986
Thermostatted Column Compartment (TCC)	G1316A	DE90377551
Standard Autosamplers (ALS)	G1329A	DE64774893
Micro Vacuum Degasser	G1379B	JP82012248

2.   Major components of MS:
Multimode source. ESI (electrospray ionization), APCI (atmospheric-pressure chemical ionization)

3. Frequent maintenance required:

Binary pump: Pump A & Pump B, some internal parts of pump, inlet & outlet valves, tubes

Auto sampler: Needle, needle seat, switching valve, UV lamp after 1-2 years depending on usage , Multimode source cleaning daily, weekly, Nebulizer needle, Cleaning of conductive capillary, Change of inlet filter of MSD, Change of switching valve of MSD

4.   Column used for separating the compounds
Organic acid column from Klaus Ziemer GmbH, Agilent Zorbax XDB C-18 from Agilent

5.   Qualification of pure compounds: (direct to MSD)
HMF (positive polarity)

6.   Quantification of compounds
Retention time of particular compound depends on method conditions like Flow rate Temperature of column, Size of the column, And sensitivity of a compound depends on UV wavelength & size of the column.

7.   Method development for Ion exchange column.

Size: 8mm dia & 300mm length. It mainly consists of organic acid column consists of a highly crosslinked, sulfonated polystyrene-divinylbenzene gel in the hydrogen form.

Currently optimized method conditionds:

Method name: MSD&UV265.M

Column: Ion Exchange (Organic Acid) Column [300*8 mm]

Injection Volume: 10 µL, Flow rate: 1mL/min, Mobile phase: 0.1% formic acid in water (Isocratic), Temp: 60 C, Pressure:141 barg, Detectors: VWD (265nm) & MSD-ESI
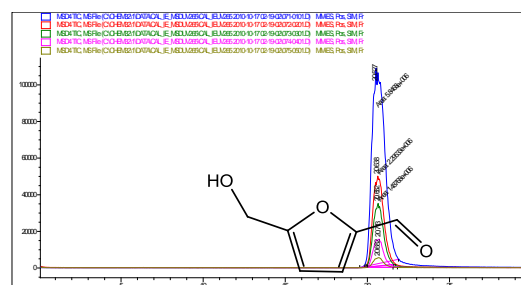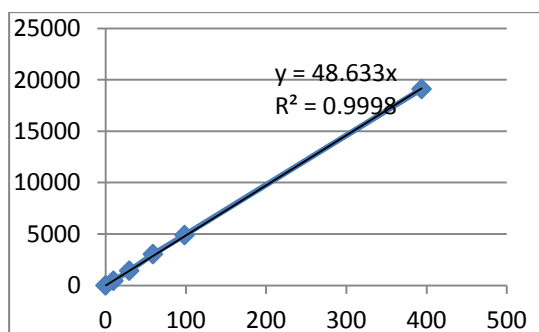
Spary Chamber settings:

Drying gas flow rate: 12L/min

Nebulizer Press. : 40psig
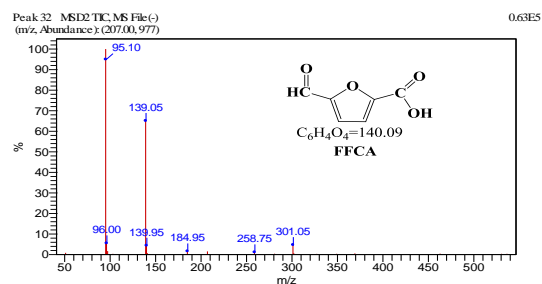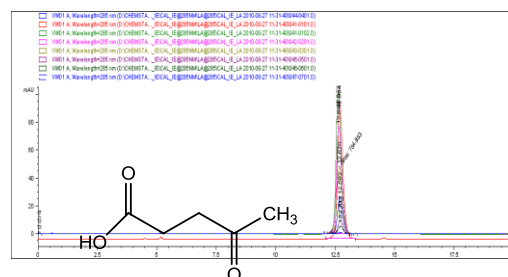
Drying gas temp. : 350 C

Vaporizer temp: 250 C

	pos.	neg.
Capillary Voltage:	1000 V	2500 V
Corona :	2	4
Charging Voltage:	2000 V	2000 V
Fragmentor	60V	60V
Gain	1	1
Dwell	76	76

8. Calibration for HMF

149

9. FDC UV at 265nm

$y = 33.551x$
$R^2 = 0.9993$

Peak 32   MSD2 TIC, MS File (-)
(m/z, Abundance): (207.00, 977)   0.63E5

$C_6H_4O_4 = 140.09$
FFCA
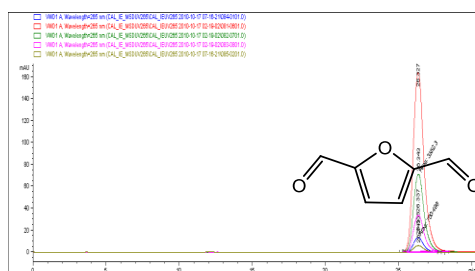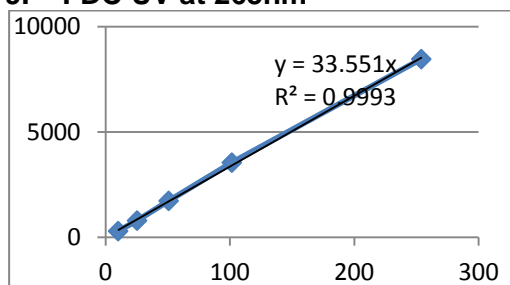
Mass spectrum of FFCA; m/z =139 (M-H);

Fragmented ion = loss of CO2 (44) = 95

(m/z)

10. FDCA

$y = 83.206x$
$R^2 = 0.9982$

11. LA UV 265nm

UV LA@285 $y = 0.0709x$
$R^2 = 0.9998$

Area (mAU)

Amount (µg/mL)
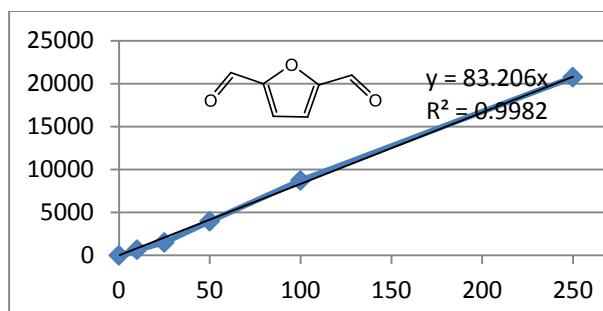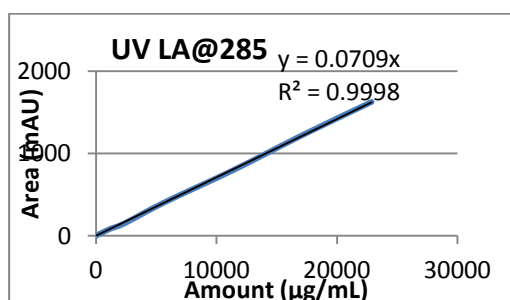
Curriculum Vitae

Personal Details

Name	**Koteswara Rao Vuyyuru**
Date of birth	25.06.1984
Place of birth	Peddavaram, India
Nationality	Indian

Educational Qualifications

08/2009 - 11/2012	Ph.D Thesis Technische Universität Berlin, Germany Prof. Dr. Peter Strasser (supervisor, TU Berlin), Prof. Dr. Robert Schlögl (co-supervisor, FHI Berlin)
06/2006 - 05/2008	Master (Research) in Chemical Engineering Indian Institute of Technology (IIT) Delhi, New Delhi, India Prof. Dr. V. V. Krishnan (supervisor), Prof. Dr. K. K. Pant(co-supervisor), Prof. Dr. K. D. P. Nigam(co-supervisor)
07/2002 - 05/2006	Bachelor of Technology (B.Tech) in Chemical Engineering Acharya Nagarjuna University, India Prof. Dr. Mohan Rao (supervisor), Prof. Dr. N. Rama Gopal (co-supervisor)
06/1999 - 04/2002	Intermediate Education M.S.Reddy Jr.College, Andhra Pradesh, India
06/1996 - 04/1999	Secondary Education A.P.R.School, Tadikonda, Andhra Pradesh, India
06/1989 – 04/1996	Elementary Education S.J.A.U.P School, Kanagala, Andhra Pradesh, India

Professional Experience

06/2008 – 05/2009	ACME Tele Power Ltd., Gurgaon, India Deputy Manager, Research & Development, Competency Center for Energy Technologies

Scholastic Achievements

06/2009 – 09/2012	Fellow of Berlin International Graduate School of Natural Sciences and Engineering (BIG-NSE), Berlin, Germany
06/2009 – 09/2012	Member of Cluster of Excellence "Unifying Concepts in Catalysis", funded by the German Research Foundation (DFG)

08/2012	Invitation by BASF to participate in the *BASF International Summer Course-2012*, 14th – 24th Aug 2012, Ludwigshafen, Germany
06/2011	Scholarship by European Federation of Catalysis Societies to participation in the summer school on ''Material and Energy from Sun'', 20th – 23rd June 2011, Roldue Abbey, Netherlands

Publications

- K. R. Vuyyuru, P. Strasser, Oxidation of biomass derived 5-hydroxymethylfurfural using heterogeneous and electrochemical catalysis, *Catalysis Today*, in press

-

- K. R. Vuyyuru, P. Strasser, Electrocatalytic conversion of biomass into high-value chemicals & fuels using renewable electrical energy, (to be submitted to *Angewandte Chemie International Edition)*

- Reiche S, Kunkes E, Mansor N, Zhao X. C, Vuyyuru, K. R, Villa A, Tessonnier J, Su D, Behrens M, Strasser P, and Schlögl R, Comparison of Heterogeneous Catalysts in the Dehydration of Fructose to HMF (submitted to *ChemCatChem*)

- K. R. Vuyyuru, P. Strasser, Anodic oxidation of biomass into chemicals using electrochemical catalysis (to be submitted to *Energy & Environmental Science*)

- K. R. Vuyyuru, P. Strasser, Selective hydrogenation of hydroxymethylfurfural into dimethylfurfural, (under submission to *ACS Catalysis*)

- K. R. Vuyyuru, K. K. Pant, V. V. Krishnan, K. D. P. Nigam, Recovery of nickel from spent industrial catalysts using chelating agents, *Industrial & engineering chemistry research*, 49 (2010) 2014 – 2024

Technical Conferences

- K. R. Vuyyuru, P. Strasser, **Oral presentation** on Conversion of cellulosic biomass into high-value chemicals: a perspective of heterogeneous & electrochemical catalysis, Catbior 2011 - 1st International congress on catalysis for biorefineries, 2nd - 5th October 2011, Torremolinos – Málaga, Spain

- K. R. Vuyyuru, M. Gliech, P. Strasser, **Oral presentation** on Applications of heterogeneous catalysis for biomass conversion, International symposium on relations between homogeneous and heterogeneous catalysis, 11th - 16th September 2011, Berlin, Germany

- K. R. Vuyyuru, P. Strasser, **Summer school** on the utilization of biomass for the production of chemicals or fuels - The concept of biorefinery comes into operation, 18th -24th September 2011, Castro Marina, Italy

- K. R. Vuyyuru, P. Strasser, **Poster presentation** on Electrocatalytic oxidation of 5-hydroxymethylfurfural (HMF) using solar energy, 19th European biomass conference and exhibition, 6th -10th June 2011, ICC Berlin, Germany